Universität Potsdam
Institute of Earth and Environmental Science

Hydrological processes in the Vietnamese Mekong Delta: Insights from stable water isotopes and monitoring data analysis

Cumulative dissertation
for the degree of “doctor rerum naturalium” (Dr. rer. nat.)
in Hydrology

submitted to the Faculty of Science
at the University of Potsdam, Germany

prepared at the Section Hydrology
of the German Research Centre for Geosciences (GFZ)

by
Nguyen Le Duy

Potsdam, April 08, 2022

First supervisor Prof. Dr. Bruno Merz
Second supervisor Prof. Dr. Markus Weiler
Mentor Dr. Heiko Apel

First reviewer Prof. Dr. Bruno Merz
Second reviewer Prof. Dr. Markus Weiler
Third reviewer Prof. Dr. Markus Disse

Examination board members
Prof. Dr. Sascha Oswald
Prof. Dr. Bruno Merz
Prof. Dr. Markus Weiler
Prof. Dr. Markus Disse
Prof. Dr. Michael Kühn
Prof. Dr. Andreas Güntner

Published online on the
Publication Server of the University of Potsdam:
https://doi.org/10.25932/publishup-60260
https://nbn-resolving.org/urn:nbn:de:kobv:517-opus4-602607

Declaration of originality

I hereby declare that this dissertation has not been presented to any University for examination, neither in Germany nor in another country.

I certify that the work contains no material which has been accepted for the award of any other degree, in any university or other tertiary institution and, to the best of my knowledge and belief, contains no material previously published or written by another person, except where due reference has been made in the text.

I also officially ensure, that the printed version as submitted by me fully confirms with the digital version. I agree that the digital version will be used to subject the dissertation to plagiarism examination.

Melbourne, January 21, 2022

Nguyen Le Duy

Acknowledgements

The present thesis was conducted in the Section Hydrology of Helmholtz Centre Potsdam, GFZ German Research Centre for Geosciences. Financial supports from NaWaM-DAAD scholarship program (funded by the German Academic Exchange Service) and the joint German-Vietnamese Catch-Mekong project (funded by the German Ministry of Education and Research BMBF and the Vietnamese Ministry of Science and Technology MOST) are gratefully acknowledged. Many thanks to my home institute, Southern Institute of Water Resource Research (SIWRR), for the agreement on my doctoral study. I express my gratitude to all those institutions.

First of all, I would like to thank my primary supervisors, Prof. Bruno Merz and Dr. Heiko Apel. I have been fortunate to have supervisors who give me the encouragement and freedom to explore on my own. Special thanks to Heiko for always supporting my ideas and research directions. Thanks Bruno for your valuable guidance, enthusiasm, and supports throughout my study period. I also want to thank my second supervisor, Prof. Markus Weiler, for helpful comments on the second manuscript and the dissertation.

I am grateful to Dr. Ingo Heidbüchel, Dr. Nguyen Viet Dung, and Dr. Hanno Meyer for the cooperation in the work, as well as the insightful comments and feedbacks during my study progress. All of you provide me with valuable expertise on water isotopes, transit-time modelling and statistical analysis, as well as helpful advice on writing scientific papers, and many encouragements.

I would like to thank all co-authors of the papers collected in this thesis for many constructive discussions and their agreement on my research. I am also indebted to the staff at An Long station for water sampling and the laboratory of the Alfred-Wegener-Institute in Potsdam for analysing isotope samples.

I am also thankful to the Helmholtz Centre Potsdam for the excellent working atmosphere. I would especially like to thank the Welcome Center Potsdam and all colleagues at the section Hydrology, to name a few, Roumiana Zimmer, Heiko Thoss, Knut Günther for supporting and helping me in any kind of requests.

My thanks go to Nguyen V.K. Triet, Tran Tuan Anh, Do Thi Chinh, Tran Duc Long, as well as, Marvin Reich, Stefan Lüdtke, and Eva-Styliani Steirou who have been amazing friends and great sources of emotional support on the long roads of a PhD. We together have a memorable time in Germany.

And last but not least, this work is dedicated to my family. Gửi bố mẹ kính yêu của con, tất cả các thành tựu học vấn con đạt được ngày hôm nay đều nhờ vào công sức dạy dỗ của bố mẹ. Con rất biết ơn bố mẹ hai bên đã luôn ủng hộ, động viên, và giúp đỡ gia đình con trong suốt thời gian làm nghiên cứu sinh. Gửi bà xã yêu dấu và các con, cảm ơn em và con đã luôn ở bên cạnh anh trong suốt giai đoạn khó khăn này. Mãi yêu em và các con!

Table of contents

List of Tables

List of Figures

Summary

Understanding hydrological processes is of fundamental importance for the Vietnamese national food security and the livelihood of the population in the Vietnamese Mekong Delta (VMD). As a consequence of sparse data in this region, however, hydrologic processes, such as the controlling processes of precipitation, the interaction between surface and groundwater, and groundwater dynamics, have not been thoroughly studied. The lack of this knowledge may negatively impact the long-term strategic planning for sustainable groundwater resources management and may result in insufficient groundwater recharge and freshwater scarcity. It is essential to develop useful methods for a better understanding of hydrological processes in such data-sparse regions. The goal of this dissertation is to advance methodologies that can improve the understanding of fundamental hydrological processes in the VMD, based on the analyses of stable water isotopes and monitoring data. The thesis mainly focuses on the controlling processes of precipitation, the mechanism of surface–groundwater interaction, and the groundwater dynamics. These processes have not been fully addressed in the VMD so far. The thesis is based on statistical analyses of the isotopic data of Global Network of Isotopes in Precipitation (GNIP), of meteorological and hydrological data from Vietnamese agencies, and of the stable water isotopes and monitoring data collected as part of this work.

First, the controlling processes of precipitation were quantified by the combination of trajectory analysis, multi-factor linear regression, and relative importance analysis (hereafter, a model-based statistical approach). The validity of this approach is confirmed by similar, but mainly qualitative results obtained in other studies. The total variation in precipitation isotopes ($\delta^{18}O$ and $\delta^{2}H$) can be better explained by multiple linear regression (up to 80%) than single-factor linear regression (30%). The relative importance analysis indicates that atmospheric moisture regimes control precipitation isotopes rather than local climatic conditions. The most crucial factor is the upstream rainfall along the trajectories of air mass movement. However, the influences of regional and local climatic factors vary in importance over the seasons. The developed model-based statistical approach is a robust tool for the interpretation of precipitation isotopes and could also be applied to understand the controlling processes of precipitation in other regions.

Second, the concept of the two-component lumped-parameter model (LPM) in conjunction with stable water isotopes was applied to examine the surface–groundwater interaction in the VMD. A calibration framework was also set up to evaluate the behaviour, parameter identifiability, and uncertainties of two-component LPMs. The modelling results provided insights on the subsurface flow conditions, the recharge contributions, and the spatial variation of groundwater transit time. The subsurface flow conditions at the study site can be best represented by the linear-piston flow distribution. The contributions of the recharge sources change with distance to the river. The mean transit time (mTT) of riverbank infiltration increases with the length of the horizontal flow path and

the decreasing gradient between river and groundwater. River water infiltrates horizontally mainly via the highly permeable aquifer, resulting in short mTTs (<40 weeks) for locations close to the river (<200 m). The vertical infiltration from precipitation takes place primarily via a low-permeable overlying aquitard, resulting in considerably longer mTTs (>80 weeks). Notably, the transit time of precipitation infiltration is independent of the distance to the river. All these results are hydrologically plausible and could be quantified by the presented method for the first time. This study indicates that the highly complex mechanism of surface–groundwater interaction at riverbank infiltration systems can be conceptualized by exploiting two-component LPMs. It is illustrated that the model concept can be used as a tool to investigate the hydrological functioning of mixing processes and the flow path of multiple water components in riverbank infiltration systems.

Lastly, a suite of time series analysis approaches was applied to examine the groundwater dynamics in the VMD. The assessment was focused on the time-variant trends of groundwater levels (GWLs), the groundwater memory effect (representing the time that an aquifer holds water), and the hydraulic response between surface water and multi-layer alluvial aquifers. The analysis indicates that the aquifers act as low-pass filters to reduce the high-frequency signals in the GWL variations, and limit the recharge to the deep groundwater. The groundwater abstraction has exceeded groundwater recharge between 1997 and 2017, leading to the decline of groundwater levels (0.01-0.55 m/year) in all considered aquifers in the VMD. The memory effect varies according to the geographical location, being shorter in shallow aquifers and flood-prone areas and longer in deep aquifers and coastal regions. Groundwater depth, season, and location primarily control the variation of the response time between the river and alluvial aquifers. These findings are important contributions to the hydrogeological literature of a little-known groundwater system in an alluvial setting. It is suggested that time series analysis can be used as an efficient tool to understand groundwater systems where resources are insufficient to develop a physical-based groundwater model.

This doctoral thesis demonstrates that important aspects of hydrological processes can be understood by statistical analysis of stable water isotope and monitoring data. The approaches developed in this thesis can be easily transferred to regions in similar tropical environments, particularly those in alluvial settings. The results of the thesis can be used as a baseline for future isotope-based studies and contribute to the hydrogeological literature of little-known groundwater systems in the VMD.

Zusammenfassung

Ein fundiertes Verständnis der hydrologischen Prozesse im vietnamesischen Mekong Delta (VMD) ist von grundlegender Bedeutung für den Lebensunterhalt der Bevölkerung im Mekong Delta, und darüber hinaus auch für die nationale Ernährungssicherheit. Aufgrund des Fehlens einer belastbaren Datenbasis konnten bislang eine Reihe von wichtigen hydrologischen Prozessen nur unzureichend untersucht und quantifiziert werden. Dazu zählen unter anderem die Analyse des Ursprungs des Niederschlages im Delta, die Interaktion zwischen Oberflächen- und Grundwasser, sowie die Grundwasserdynamik. Diese Lücken im Wissensstand verhindern eine solide datenbasierte Wasserwirtschaftsplanung, was unter Berücksichtigung der derzeitigen Trends mittelfristig zu weiter fallenden Grundwasserständen und Wasserknappheit führen wird. Daher ist es von großer Bedeutung, Methoden und Werkzeuge zu entwickeln, die auch unter der bestehenden Datenknappheit belastbare quantitative Ergebnisse für eine nachhaltige Wasserbewirtschaftung liefern können. Das Ziel dieser Dissertation ist es, solche Methoden zu entwickeln und zu testen, um grundlegende hydrologische Prozesse im VMD besser verstehen und quantifizieren zu können. Hierzu werden die existierenden Messdaten sowie im Rahmen dieser Arbeit gesammelte Daten zum Gehalt an stabilen Wasserisotopen verwendet. Mit Hilfe dieser Daten wurden folgende Prozesse untersucht:

1. Der Ursprung und die Fraktionierung des Niederschlages im VMD.
2. Die Interaktion zwischen Oberflächen- und Grundwasser mit einem besonderen Fokus auf die ufernahen Gebiete.
3. Die großflächige Dynamik in den verschiedenen Grundwasserleitern der letzten Jahrzehnte.

Die Prozesse, die den Ursprung und die Verteilung des Niederschlagsbestimmen, wurden mittels einer Kombination aus Isotopendaten, Trajektorienanalyse, multifaktorieller Regression, und relativer Wichtigkeitsanalyse untersucht. Diese Kombination ist nachfolgend „modelbasierter statistischer Ansatz“ betitelt. Hierbei wurde festgestellt, dass die Varianz im Isotopengehalt des Niederschlags ($\delta^{18}O$ and $\delta^{2}H$) mit der multifaktoriellen Regression zu 80% erklärt werden konnte, was im Vergleich zu einer einfachen Regression mit 30% erklärter Varianz eine deutliche Verbesserung darstellt. Die Wichtigkeitsanalyse ergab zudem, dass großskalige atmosphärische Feuchtigkeitsverteilungen einen weitaus größeren Einfluss auf die Isotopenverteilung im Niederschlag haben, als lokale klimatische Bedingungen im VMD. Der hierbei wichtigste Faktor ist die Regenmenge entlang der Trajektorien der Luftmassenbewegungen. Die Wichtigkeit der Faktoren variiert jedoch saisonal zwischen Regen- und Trockenzeit. Der in dieser Dissertation entwickelte modelbasierte statistische Ansatz ist ein robustes Werkzeug zur Analyse und Interpretation der Isotopenverteilung im Niederschlag, der auch auf ähnliche Fragestellungen in andere Regionen übertragbar ist.

Im zweiten Teil der Dissertation wurden Zweikomponentenmodelle (LPM) in Verbindung mit Isotopenmessungen im Niederschlag, Oberflächen- und Grundwasser verwendet, um die Interaktion zwischen Oberflächen- und Grundwasser qualitativ und quantitativ zu beschreiben. Verschiedene Modellansätze wurden hierbei in einem automatischen Kalibrieransatz getestet, und deren Unsicherheit bestimmt. Hierbei hat sich das lineare Kolbenfließmodell (linear piston flow model) als das am besten geeignetste herausgestellt. Die Modellierungsergebnisse ermöglichten daraufhin eine modellbasierte Abschätzung der Grundwasserschwankungen und -flüsse, der Grundwasserneubildung und der räumlichen Variabilität der Grundwasserlaufzeiten. Hierbei zeigte sich, dass Grundwasserneubildung und deren Quellen räumlich variabel ist, und sich mit zunehmender Entfernung vom Fluss die Neubildung von primär Uferinfiltration hin zu Neubildung durch Niederschläge ändert. Analog dazu erhöhen sich die Grundwasserlaufzeiten mit der Länge der horizontalen Fließwege (= Entfernung vom Vorfluter) und mit sinkendem Gradienten zwischen Grundwasserstand und Wasserstand im Fluss. Flusswasser infiltriert über das Flussufer in den wasserleitenden Aquifer, mit mittleren Transferzeiten (mTT) von < 40 Wochen für Bereiche mit weniger als 200 m Entfernung zum Fluss. In größeren Entfernungen findet die Neubildung im Wesentlichen durch Versickerung von Regenwaser statt. Da der betrachtete holozäne Grundwasserleiter mit einer schwerdurchlässigen Deckschicht überlagert ist, liegen die mTT in diesen Bereichen mit > 80 Wochen wesentlich höher. Es konnte mit dieser Studie gezeigt werden, dass die komplexe Interaktion zwischen Grund- und Oberflächenwasser mittels eines konzeptionellen Modells in Verbindung mit aus Wasserproben bestimmten Isotopendaten konzeptionalisiert und quantifiziert werden kann. Der Ansatz empfiehlt sich daher als Werkzeug für die Untersuchung der Mischungsprozesse der Ufer- und Regenwasserinfiltration, sowie der Fließwege des Grundwassers in ähnlichen Gebieten.

Im letzten Teil der Dissertation wurden Trends in den Grundwasserständen im gesamtem VMD untersucht. Hierzu wurde eine Reihe von Methoden zur Zeitreihenanalyse angewandt. Der Fokus der Untersuchungen lag auf zeitvariablen Trends in den Grundwasserständen, der Wasserspeicherdauer (memory effect), und der hydraulischen Reaktionszeit zwischen dem Oberflächenwasser und den verschiedenen Aquiferen im VMD. Die Analyse ergab, dass die verschiedenen Schichten von Aquiferen und Aquitarden wie ein Tiefpassfilter auf die hydraulischen Signale des Oberflächenwassers wirken, was wiederum die Grundwasserneubildung in den tieferen Aquiferen stark reduziert. Die Zeitreihenanalyse ergab, dass die Entnahmemengen an Grundwasser insbesondere in den tieferen, stark genutzten Aquiferen die Neubildung im gesamten Analysezeitraum 1997 – 2017 überschritten hat. Dies führte zu Absenkung des Grundwasserspiegels von 0.01 – 0.55 m pro Jahr in den verschiedenen Aquiferen des VMD. Die Speicherdauer variiert zwischen den verschiedenen Regionen und Aquiferen des VMD. In den flacheren Aquiferen und in der Region mit tiefen Überflutungen während der Hochwassersaison sind die Speicherdauern kürzer, während sie in den tieferen Aquiferen und in den küstennahen Regionen wesentlich länger sind. Die Reaktionszeit variiert ebenfalls im Raum, wobei die wichtigsten Einflussfaktoren der Abstand des Grundwasserspiegels zur Oberfläche, die Saison und die Lage, hier besonders die Entfernung zum Fluss oder der Küste, sind. Diese qualitativen wie quantitativen Ergebnisse fügen

wichtige und wesentlich Erkenntnisse zum Wissensstand über das Grundwasser im VMD hinzu. Die verwendeten Methoden empfehlen sich darüber hinaus für die Analyse von Grundwasserdynamiken in alluvialen Aquifersystemen im Generellen, wenn Daten und Ressourcen für ein physisches numerisches Grundwassermodell fehlen.

Die vorliegende Dissertation zeigt, dass wichtige hydrologische Prozesse auch über statistische Analysen von Mess- und Isotopendaten quantitativ analysiert werden können. Die Ergebnisse stellen eine Basisanalyse der Grundwasserdynamik und der sie beeinflussenden Prozesse im VMD dar, und sollten in weiteren Studien ausgebaut werden. Die Analyse der Isotopendaten liefert darüber hinaus die Basislinie für hydrologische Analysen mit stabilen Isotopen im VMD und aufgrund der ähnlichen klimatischen und geografischen Lage auch für weite Teile Südostasiens. Die entwickelten Methodenkombinationen können aufgrund ihrer generellen Natur auch problemlos auf andere tropische Regionen, insbesondere solche mit alluvialen Aquiferen, übertragen werden.

Chapter 1 General introduction

1.1 Background

The Vietnamese Mekong Delta (VMD) is located in the southern tip of Vietnam and covers an area of 3.9 million ha. The delta has a multi-layer alluvial basin structure, of which the plain is divided by a dense network of rivers, human-made channels and waterways. It is the home of more than 17 million people who mainly live in rural areas and depend on agriculture or aquaculture as their primary source of income (Renaud and Kuenzer, 2012). Food production has significantly increased in the VMD since the mid-1990s and become the leading sector in the export industry of Vietnam. The delta contributes approximately 50% of the national food production and 85% of the annual rice export (GSO, 2016), positioning Vietnam as one of the largest rice exporters in the world.

Water resources management is a crucial driver for the socio-economic development in the VMD. Despite the improvements in agricultural systems and the rapid economic growth in the region, farmers and communities directly depend on water resources for their livelihoods and daily subsistence. The delta is globally seen as one of the key hotspots of climate change related risks due to its exposure to floods, salinization and potential sea-level rise (Birkmann et al., 2012). The hydraulic constructions (e.g., dykes and sluice gates systems) have been rapidly developed to improve food production (Tri, 2012). Groundwater exploitation has also increased as a result of urbanization and industrial development (Danh and Khai, 2015). These human activities have a direct impact on hydrological manipulation, placing the VMD on many water-related challenges (Renaud and Kuenzer, 2012). Therefore, a thorough understanding of hydrological processes is one of the prerequisites for sustainable development in the delta.

Many reports on the hydrology of the VMD have been recently published, with the majority of the studies dealing with the dynamics of surface water as well as the associated sedimentation and salinity intrusion. Studies on climatic or sub-surface flow processes are, however, rare. The hydrologic and hydraulic features denoting the increasing trends in water level (Dang et al., 2016; Fujihara et al., 2016), floodplain hydrology (Apel et al., 2012; Hung et al., 2012), the flood dynamics (Dung et al., 2011; Dang et al., 2016; Triet et al., 2017), sedimentation (Kummu and Varis, 2007; Hung et al., 2014b; Hung et al., 2014a; Manh et al., 2014; Darby et al., 2016; Tu et al., 2019), and salinity intrusion (Nguyen and Savenije, 2006; Toan, 2014; Renaud et al., 2015; Smajgl et al., 2015; Eslami et al., 2019) have been well studied. Based on large-scale hydrological and hydraulic modelling (e.g., Dung et al., 2011), the dynamics of future food (e.g., Triet et al., 2020) and future sediment (e.g., Manh et al., 2015) can be projected. Also, the impacts of upstream hydropower dams, climate change and sea-level rise on food security, hydrological alterations, and coastal erosion have been quantified for the VMD (e.g., Wassmann et al., 2004; Lauri et al., 2012; Arias et al., 2014; Anthony et al., 2015; Dang et al., 2018).

In contrast to the numerous hydrological studies, studies on groundwater dynamics have been limited. Most of the groundwater studies have targeted local areas (e.g., provinces or cities) rather than the whole delta. These studies have mainly focused on groundwater recharge sources (Ho et al., 1991; An et al., 2014), the arsenic contamination of aquifers (e.g., Shinkai et al., 2007; Buschmann et al., 2008; Kocar et al., 2008; Erban et al., 2013; Huang et al., 2016), groundwater quality (e.g., Wilbers et al., 2014; An et al., 2018; Tran et al., 2019). At the larger scale, groundwater has been reported to be considerably controlled by the river system (Wagner et al., 2012) and closely connected to the surface water in the floodplains (Kazama et al., 2007). The recently large-scale groundwater exploitation for socio-economic and industrial development has been proposed as the primary driver of groundwater depletion (Ha et al., 2015) and land subsidence (Minderhoud et al., 2017) in the VMD. However, information on the declining groundwater levels (e.g., Wagner et al., 2012; Erban et al., 2014) or the surface water – groundwater interaction based on numerical modelling (e.g., Vermeulen et al., 2013; Shrestha et al., 2016; Hung Van et al., 2019) has been scarce. The mechanism of flow conditions in the groundwater system of the VMD remains poorly understood due to the complexity of the hydrogeological subsurface system (Wagner et al., 2012) and the sparsity of groundwater level and lithological data (Johnston and Kummu, 2012).

Environmental isotopes as tracers have become an effective tool to understand different hydrological processes (Clark and Fritz, 1997; McGuire and McDonnell, 2008; Kendall and McDonnell, 2012). In paleoclimate-reconstruction studies, stable isotopes ($\delta^{18}O$ and $\delta^{2}H$) offer the possibility to identify the sources of precipitation and the contribution of regional and local climatic parameters (Gat, 1996). In the Asian monsoon region, the isotopic signature of precipitation has been found to correlate with large-scale climatic parameters such as sea surface temperature and relative humidity of the air masses (Dansgaard, 1964; Merlivat and Jouzel, 1979; Clark and Fritz, 1997; Lachniet, 2009), ENSO (Ichiyanagi and Yamanaka, 2005; Tan, 2014; Yang et al., 2016) and the vertical wind shear index (Vuille et al., 2005). Furthermore, tracer application can be used to gain insights in hydrological processes such as streamflow generation (e.g. Kendall and Caldwell, 1998), and in rainfall-runoff studies (e.g. Genereux and Hooper, 1998). In catchment hydrology, analyzing water isotopes within the hydrological cycle can provide valuable information on the water budget and the runoff generation (e.g., McGuffie and Henderson-Sellers, 2004; Fekete et al., 2006; Bowen et al., 2011), as well as enable a quantitative separation of individual water components (e.g., Weiler et al., 2003b; Wenninger et al., 2010; Klaus and McDonnell, 2013; Klaus et al., 2014). In groundwater studies, time-domain tracers have frequently been used to examine recharge pattern (McGuire and McDonnell, 2008) and groundwater transit time (Małoszewski and Zuber, 1982). For example, tracer application can reveal the origin of groundwater (Weyhenmeyer et al., 2002; Blasch and Bryson, 2007), the groundwater-surface water interactions (Stichler et al., 1986; Stichler et al., 2008), subsurface flow conditions (McGuire

et al., 2002), groundwater mixing processes (Stewart and Thomas, 2008), groundwater transport (Maloszewski et al., 2002; Kabeya et al., 2007; Stewart et al., 2007), and recharge mechanisms (Koeniger et al., 2016). Hence, tracer-based studies promise to close knowledge gaps on hydrological processes in the VMD.

1.2 Motivation

To the best of the author's knowledge, there is no long-term sampling campaign that provides high-resolution isotopic measurements to generate a basic dataset for isotope-based studies in the VMD. Most of the isotope-based studies in this region (e.g., Ho et al., 1991; Kabeya et al., 2008; An et al., 2014; An et al., 2018) are based on low isotopic data quality, thus the results are stained with high uncertainty. Therefore, it is highly recommended to set up pilot areas for isotopic data generation and the installation of long-term gauging station. Based on these datasets, baseline isotopic studies can be conducted. For example, the local meteoric water line or the groundwater transit time of a focused region can be estimated and used as reference baselines for the whole VMD.

Regarding the choice of methodological tools, although hydrological modelling using mathematical simulation can provide a wealth of results, it is not always straightforward to develop and calibrate a numerical model, due to missing data and limited resources to set up or run a numerical model (Johnston and Kummu, 2012). Statistical analyses can often provide invaluable insights into the temporal and spatial dynamics of hydrological processes with much less effort, given sufficient data availability. In groundwater studies, statistical-based analysis (e.g., time series model) can, to a certain extent, be of greater value than numerical groundwater models (Bakker and Schaars, 2019). It can be used to clean up the data, identify the major stresses on the aquifer, determine the most important processes that affect flow in the aquifer, and give an indication of the sub-surface flow conditions. Therefore, it is surely worthwhile to develop statistic- and isotope-based approaches to enhance the understanding of hydrological processes in the VMD.

1.3 Aims and scope of the study

This thesis used a statistical multi-method approach based on the analyses of long-term isotope measurement and hydrometric monitoring data to gain insights into hydrological processes in the VMD. The main objective is to advance existing methodologies that can improve the understanding of (1) the controlling processes of precipitation, (2) the mechanism of surface–groundwater interaction, and (3) the groundwater dynamics in the VMD. The study area was selected because knowledge about these processes is lacking, but required for a sustainable use of groundwater resources. The VMD can be seen representative for an alluvial and density populated tropical delta, and the results could thus be transferred to a certain extent. To address

the main objectives, this work developed methodologies to answer the following research questions:

1. Where do the moisture sources of precipitation in the VMD origin from? (Chapter 2)

2. Which factors control the precipitation isotopes in the VMD? (Chapter 2)

3. What are the subsurface flow conditions in riverbank infiltration areas in the VMD? (Chapter 3)

4. What is the level of infiltration of river water and precipitation to shallow groundwater and their age variations in riverbank areas in the VMD? (Chapter 3)

5. What changes in groundwater levels in the VMD can be detected over the last two decades? (Chapter 4)

6. What is the length of groundwater memory effect (the time that an aquifer holds water) in the VMD? (Chapter 4)

7. What is the response of alluvial aquifers to surface water in the VMD? (Chapter 4)

Based on these research questions, this thesis applied the following methodologies:

- A model-based statistical approach to identify the potential moisture sources of precipitation (Question 1) and factors controlling the precipitation isotopes (Question 2) in the VMD.
- A concept of two-component lumped parameter models to examine the subsurface flow conditions (Question 3), the infiltration of river water and precipitation to shallow groundwater, and their age variations (Question 4) in riverbank areas in the VMD.
- Time-series analysis (e.g., trend analysis, correlation analysis, moving-window approach) to evaluate the trend of groundwater levels (Question 5), the memory effect of groundwater (Question 6), and the hydraulic response between surface water and alluvial aquifers (Question 7) in the VMD.

1.4 Features of the study area

The VMD covers an area of 3.9 million hectares between 8.5–11.5 ºN and 104.5–106.8 ºE (Figure 2.1). Located in a tropical monsoon region, the climate of the VMD has a distinct seasonality with two seasons: the rainy season (May to November) resulting from the flow of moisture from the Indian Ocean and Western North-Pacific Ocean accounting for approximately 80-90% of the annual rainfall (Tri, 2012), and the dry season (December to April) controlled by high-pressure systems over the Asian continent (Wang et al., 2001). Precipitation from the Indian monsoon is forced by the convective heat sources over the Bay of Bengal (Wang et al., 2001) and arrives earlier than precipitation from the Western North-Pacific monsoon (Delgado et al., 2012), forced by a convective heat source over the South China Sea – Philippine Sea. The average annual rainfall is

1400-2200 mm, characterized by an uneven distribution, both spatially and temporally (Renaud and Kuenzer, 2012; GSO, 2016).

The annual average temperature is 27°C with the small interannual variability of about 1°C. Monthly variation of temperature throughout the year is between 25°C and 29°C. The annual relative humidity ranges from 82% to 85%, with a seasonal variation of 80% to 88% during the rainy season and 77% to 83% during the dry season. The mean annual evaporation is 984 mm with a significant difference between the rainy season and the dry season. The monthly evaporation rate ranges from 67 to 80 mm and 76 to 109 mm in the dry and rainy season, respectively. Daily sunshine duration is about 8.7 to 9.6 hours in the dry season and 5.5 to 5.9 hours in the rainy season (Renaud and Kuenzer, 2012; GSO, 2016).

The delta has an extremely low mean elevation (~0.8m above sea level) (Minderhoud et al., 2019). During the flood season (July-November), 35–50% of the delta is flooded, mainly by river discharge exceeding bank level. The resulting inundation reaches depths of up to 4.0 m for 3 to 6 months (Toan, 2014), constituting inundation areas that recharge water to alluvial aquifers. These inundation areas cover a territory of approximately 2.0 million hectares in the northern part of the VMD (Triet et al., 2017).

The subsurface structure and hydrogeological units in the VMD are classified according to their geological formation: the Holocene, the Pleistocene, the Pliocene, and the Miocene aquifer systems. The multi-layered aquifer system in the delta has an alluvial basin structure, forming by sediment deposited during transgression and regression events around 6,000–5,000 yr BP (Lap Nguyen et al., 2000). The deepest area of the basement is located below the Mekong and Bassac Rivers and rises to the Northeast, North, and Northwest borders (Anderson, 1978). These age units can be sub-divided into eight hydrogeological aquifer systems (Wagner et al., 2012), including Holocene (qh), Upper Pleistocene (qp_3), Middle Pleistocene (qp_{2-3}), Lower Pleistocene (qp_1), Middle Pliocene (n_2^2), Lower Pliocene (n_2^1), Upper Miocene (n_1^3), and Middle Miocene (n_1^{2-3}). Each unit consists of two layers: (i) a low-permeable aquitard layer composed of silt and clay; and (ii) a high-permeable aquifer layer composed of fine to coarse sand and gravel.

1.5 Monitoring and sampling campaigns

The Plain of Reeds in VMD (Figure 3.1) is chosen as a pilot area for the monitoring and sampling campaigns. For the sampling campaigns, the study site An Long in the Plain of Reeds (Figure 3.1) was selected, primarily considering logistic constraints. This area was already covered by the WISDOM project carried out by GFZ Potsdam for many years. Six field campaigns in the VMD were carried out between 2015 and 2018 to collect water samples for isotope analysis. The isotopic data covered by the WISDOM project between 2009 and 2014 were also collected. The result of water samples is shown in Table 3.1.

The stable isotope samples were analyzed at the Alfred-Wegener-Institute (AWI) in Potsdam, Germany. All samples were stored in 30 mL plastic sample bottles with tight screw caps and kept in the dark before the isotopic analysis to avoid evaporation effects. The measurements were performed with a Finnigan MAT Delta-S mass spectrometer using equilibration techniques to determine the ratio of stable oxygen ($^{18}O/^{16}O$) and hydrogen ($^{2}H/^{1}H$) isotopes. Analytical results were reported as $\delta^{2}H$ and $\delta^{18}O$ (‰, relative to Vienna Standard Mean Ocean Water - VSMOW) with internal 1σ errors of less than 0.8‰ for $\delta^{2}H$ and 0.1‰ for $\delta^{18}O$. The detailed measuring procedure is described in Meyer et al. (2000).

Additionally, surface and groundwater levels were recorded every 15 min by automatic pressure sensors (HOBO U20 Fresh Water Level Data Logger). The duration of monitoring was from June 2015 to December 2017. A terrestrial survey was carried out in 2016 to put the recorded water groundwater level measurements into the context of the river water levels at the gauge in An Long.

1.6 Thesis outline and author contribution

The thesis has five chapters, including three journal articles, to present the major findings of this doctoral study. The manuscripts were reformatted to form a cumulative dissertation to answer the research questions. All manuscripts are the result of the collaboration between the author of this thesis (Nguyen Le Duy) and several co-authors (initials). The following paragraph highlights the contribution of authors in each manuscript.

Chapter 1 provides a general introduction to the thesis.

Chapter 2: What controls the stable isotope composition of precipitation in the Mekong Delta? A model-based statistical approach

Author: Nguyen Le Duy, Ingo Heidbüchel, Hanno Meyer, Bruno Merz, and Heiko Apel

Journal: Hydrology and Earth System Sciences (HESS).

NLD contributed to Conceptualization, Methodology, Resources, Software, Visualization, Writing - original draft; HM supported data analyses; all authors (NLD, IH, HA, BM and HM) contributed to the interpretation of Results and finalizing the paper.

This chapter developed a model-based statistical approach to identify the factors controlling the precipitation sources and distribution in the VMD. The assessment was based on the dataset of climatic parameters (daily precipitation, temperature, relative humidity) and stable precipitation isotopes ($\delta^{18}O$ and $\delta^{2}H$) between 2014 and 2015. Back trajectory modelling by HYSPLIT model was computed to investigate the seasonal variations of moisture sources. Multi-factor linear regression analysis was applied to examine the influence of local and regional meteorological factors on precipitation isotopes. Lastly, relative importance analysis was utilised to quantify the

power of individual predictors in the linear regression. The approach was evaluated for the reliable interpretation of precipitation isotopes in the VMD and a potential pathway for improved reconstruction of paleoclimates based on isotopic records.

Chapter 3: Identification of groundwater mean transit times of precipitation and riverbank infiltration by two-component lumped parameter models

Author: Nguyen Le Duy, Nguyen Viet Dung, Ingo Heidbüchel, Hanno Meyer, Markus Weiler, Bruno Merz, and Heiko Apel

Journal: Hydrological Processes.

NLD contributed to Conceptualization, Methodology, Resources, Software, Visualization, Writing - original draft; HM supported data analyses; NVD and IH supported Methodology and Software; IH, HA, BM and MW discussed the Results, revised the full text. All authors contributed to finalizing the paper.

This chapter examined a novel concept of two-component lumped parameter models (LPMs) that were inversely solved using $\delta^{18}O$ records. The model concept was tested to quantify the mixing processes, the contribution of river and precipitation components to shallow groundwater, and their age variations in the riverbank infiltration areas. Six transit time distributions, including the exponential, linear, exponential-piston flow, linear-piston flow, advection-dispersion, and the gamma model were tested. It was assumed that the best-suited TTD could describe the subsurface flow conditions in the study site. Monte Carlo solution was applied to find the best parameter sets of a model. The generalized likelihood uncertainty estimation (GLUE) method was used to quantify the uncertainty of model predictions. Three model set-ups were also defined to get deeper insights into the model behaviour, parameter identifiability, and uncertainties. The uncertainty analysis was attributed to (1) the modified input functions, (2) the mass balance analysis, and (3) the assumed nonstationary or steady-state conditions during the calibration. The findings on the subsurface flow conditions, the recharge contributions, and the transit time of river and precipitation infiltration were used to develop a conceptual mechanism of surface–groundwater interaction for riverbank infiltration in the VMD.

Chapter 4: Groundwater Dynamics in the Vietnamese Mekong Delta: Trends, Memory Effects, and Response Times

Author: Nguyen Le Duy, Nguyen Van Khanh Triet, Nguyen Viet Dung, Tran Tuan Anh, Nguyen Thi Ha, Ingo Heidbüchel, Bruno Merz, and Heiko Apel

Journal: Journal of Hydrology – Regional Studies.

NLD contributed to Conceptualization, Methodology, Software, Visualization, Writing - original draft; NVKT, TTA and NTH contributed to Resources and Visualization; NVD supported

Methodology and Software; IH, HA, BM contributed to the interpretation of Results and Discussions.

This chapter evaluated the usefulness of time series techniques to investigate groundwater dynamics. The assessment was based on an update set of groundwater level data (1996-2017) which has not been published beforehand. Variabilities of GWL trends, the groundwater memory effect, and the response of alluvial aquifers to surface water were quantified on the basis of this dataset for the VMD. A trend analysis and a moving-window approach were applied to evaluate the time-variant trends of groundwater level over the last two decades. Auto-correlation was used to identify the groundwater memory effect, and moving-window cross-correlation analysis was applied to quantify the response time between aquifers and surface water. This chapter highlighted the usefulness of time-series techniques for a better understanding of groundwater behaviours in alluvial settings. Findings in this chapter also contribute useful information on the potential recharge and the conceptualization of groundwater system that are essential for groundwater resources management in the VMD.

Chapter 5 summarizes the main findings from individual chapters and discusses them concerning the overall aim of the thesis. It also suggests the methodological implications and limitations that should be considered to gain insights into the hydrological process in similar settings. This chapter ends with concluding remarks for the doctoral study.

Chapter 2 What controls the stable isotope composition of precipitation in the Mekong Delta? A model-based statistical approach

This chapter has been published as:

Duy, N.L., Heidbüchel, I., Meyer, H., Merz, B., Apel, H., 2018. What controls the stable isotope composition of precipitation in the Mekong Delta? A model-based statistical approach. Hydrology and Earth System Sciences, 22(2): 1239-1262. DOI: https://doi.org/10.5194/hess-22-1239-2018

Abstract

This study analyzes the influence of local and regional climatic factors on the stable isotopic composition of rainfall in the Vietnamese Mekong Delta (VMD) as part of the Asian monsoon region. It is based on 1.5 years of weekly rainfall samples. In a first step, the isotopic composition of the samples is analyzed by local meteoric water lines (LMWL) and single-factor linear correlations. Additionally, the contribution of several regional and local factors is quantified by multiple linear regression (MLR) of all possible factor combinations and by relative importance analysis. This approach is novel for the interpretation of isotopic records and enables an objective quantification of the explained variance in isotopic records for individual factors. In this study, the local factors are extracted from local climate records, while the regional factors are derived from atmospheric backward trajectories of water particles. The regional factors, i.e. precipitation, temperature, relative humidity and the length of backward trajectories, are combined with equivalent local climatic parameters to explain the response variables $\delta^{18}O$, $\delta^{2}H$, and d-excess of precipitation at the station of measurement.

The results indicate that (i) MLR can much better explain the isotopic variation of precipitation (R^2 = 0.8) compared to single-factor linear regression (R^2 = 0.3); (ii) the isotopic variation in precipitation is controlled dominantly by regional moisture regimes (~70%) compared to local climatic conditions (~30%); (iii) the most important climatic parameter during the rainy season is the precipitation amount along the trajectories of air mass movement; (iv) the influence of local precipitation amount and temperature is not significant during the early rainy season, unlike the regional precipitation amount effect; (v) secondary fractionation processes (e.g. sub-cloud evaporation) can be identified through the d-excess and take place mainly in the dry season, either locally for $\delta^{18}O$ and $\delta^{2}H$, or along the air mass trajectories for d-excess. The analysis shows that regional and local factors vary in importance over the seasons and that the source regions and transport pathways, and particularly the climatic conditions along the pathways have a large influence on the isotopic composition of rainfall. While the general results have been reported

qualitatively in previous studies (proving the validity of the approach), the proposed method provides quantitative estimates of the controlling factors, both for the whole data set and for distinct seasons. Therefore, it is argued that the approach constitutes an advancement in the statistical analysis of isotopic records in rainfall that can supplement or precede more complex studies utilizing atmospheric models. Due to its relative simplicity, the method can be easily transferred to other regions, or extended with other factors.

The results illustrate that the interpretation of the isotopic composition of precipitation as a recorder of local climatic conditions, as for example performed for paleorecords of water isotopes, may not be adequate in the Southern part of the Indochinese Peninsula, and likely neither in other regions affected by monsoon processes. However, the presented approach could open a pathway towards better and seasonally differentiated reconstruction of paleoclimates based on isotopic records.

2.1 Introduction

Precipitation is typically composed of regional contributions, where atmospheric moisture has been transported over large distances, and local contributions, where the moisture has been provided by evapotranspiration within the close vicinity. Understanding the sources of precipitation and their relative contribution is critical for basin-wide water balance studies (Ingraham, 1998). Stable isotopes ($\delta^{18}O$ and $\delta^{2}H$) offer the possibility to identify the sources of precipitation and to quantify the contribution of regional and local sources (Gat, 1996). Furthermore, they can be used to investigate hydrological processes such as mechanisms responsible for streamflow generation (e.g. Kendall and Caldwell, 1998), in groundwater studies (e.g. Gonfiantini et al., 1998) and rainfall-runoff studies (e.g. Genereux and Hooper, 1998).

Isotopic variation in precipitation has been correlated with climatic parameters such as precipitation amount, air temperature, and air mass history (Dansgaard, 1964; Rozanski et al., 1992; Gat, 1996), termed amount effect, temperature effect (Dansgaard, 1964), and circulation effect (Tan, 2009; Tan, 2014), respectively. The circulation effect describes the changes in isotopic composition in precipitation because of air moisture originating from different areas of the ocean.

Delineating the present-day relationship between climatic factors and stable isotope variation in precipitation can also help to understand past climatic conditions at regional and global scales. However, the factors controlling isotopic variation of precipitation are numerous and complex; hence a better understanding of the climatic influences on isotopic values would improve the use of precipitation isotopes as a proxy to reconstruct paleoclimates (Yang et al., 2016).

In the Asian monsoon region, the isotopic signature of precipitation has been found to correlate with large-scale climatic parameters such as sea surface temperature and relative humidity of the air masses (Dansgaard, 1964; Merlivat and Jouzel, 1979; Clark and Fritz, 1997; Lachniet, 2009),

ENSO (Ichiyanagi and Yamanaka, 2005; Tan, 2014; Yang et al., 2016) and the vertical wind shear index (Vuille et al., 2005). Other processes were also identified as relevant for monsoon regions: distillation during vapor transport (Araguás-Araguás et al., 1998; Yoshimura et al., 2003; Vuille et al., 2005; Dayem et al., 2010; Lee et al., 2012; Liu et al., 2014), re-evaporation and rain-vapor interactions (Risi et al., 2008b; Chakraborty et al., 2016).

Relations between climate and water isotopes have been analyzed by univariate statistical regression methods (e.g. Araguás-Araguás et al., 1998; Bowen, 2008), isotope-enabled global climate models (GCMs) (Yoshimura et al., 2008; Risi et al., 2010b; Yoshimura et al., 2014; Okazaki and Yoshimura, 2017), isotope-incorporated Lagrangian models (Pfahl and Wernli, 2008; Sodemann et al., 2008), or the combination of GCMs (or Lagrangian models) with statistical analysis (Vuille et al., 2003; Vuille et al., 2005; LeGrande and Schmidt, 2009; Tindall et al., 2009; Ishizaki et al., 2012; Conroy et al., 2013). Statistical models are not able to explain the actual processes causing a phenomenon (e.g., the physical controls of isotope variations in precipitation), in contrast to the physical model representation of the processes like e.g. GCMs or Lagrangian models. They can, however, detect the results of a process, and thus help to identify the responsible processes. Both approaches, statistical and physical models, have their advantages and disadvantages and hence coexist supplementing each other. We argue that taking into consideration the limitations and benefits of both statistical and physical models can enhance their power to interpret the relations between climate and water isotopes.

As illustrated in previous studies (e.g. Noone and Simmonds, 2002) and discussed in Sturm et al. (2010), the inherent limitations of empirical (or statistical) climate reconstructions from precipitation isotopes can lead to incorrect paleoclimate reconstructions. A significant limitation is the assumption that a single climatic factor controls the isotopic signal and that the stationary relationship (e.g., between temperature and $\delta^{18}O$) remains valid over the entire proxy record. This mono-factorial relationship does not consider the interplay of different climatic factors and is possibly biased. Another limitation is the assumption of a constant precipitation source or similar isotopic signatures of different moisture sources throughout the study period when using only local parameters (e.g., local precipitation) to interpret precipitation isotopes. In real cases, these assumptions are rarely fulfilled and often unrealistic because of the changes in seasonality and atmospheric circulation patterns. This is particularly true in those parts of the Asian monsoon region located in the transition zone between the Indian and Western North-Pacific monsoons, where precipitation originates from both the Indian and Pacific Oceans (Delgado et al., 2012). The isotopic signatures of air masses arising from the Indian Ocean differ considerably from those of the Pacific Ocean, where the average $\delta^{18}O$ of the latter is about 2.5‰ more negative (Araguás-Araguás et al., 1998). Seasonally varying sources of precipitation have also been observed in China (Tan, 2014, and references therein), India (e.g. Breitenbach et al., 2010; Chakraborty et al., 2016),

Korea (Lee et al., 2003), Thailand (Ishizaki et al., 2012), and elsewhere (Araguás-Araguás et al., 1998).

Additionally, many studies have presented evidence that large-scale monsoon circulation is the primary driver of variations in precipitation isotopes instead of local controls (e.g., local precipitation amount or temperature) in some parts of the Asian monsoon region. This evidence has been found at different temporal scales including daily isotopic variability (Yoshimura et al., 2003; Yoshimura et al., 2008), seasonal isotopic variability (Araguás-Araguás et al., 1998; Kurita et al., 2009; Dayem et al., 2010; Peng et al., 2010; Baker et al., 2015), and/or interannual isotopic variability (Vuille et al., 2005; LeGrande and Schmidt, 2009; Ishizaki et al., 2012; Tan, 2014; Kurita et al., 2015). This means that the isotopic composition of rainfall cannot be described adequately by mono-factorial statistical approaches. Quantitative multi-factorial statistical studies of the isotopic composition are, however, rare. Only Ishizaki et al. (2012) present a multi-factorial analysis, which is limited to two factors (local precipitation amount and distillation of the moisture along its transport trajectories). To our best knowledge, there is no study considering the interplay of several local and regional factors available quantitatively, whereas the need for a simultaneous consideration of local and regional factors for the explanation of isotopic signatures has already been formulated in other studies (Johnson and Ingram, 2004). Therefore, a quantitative multi-factorial statistical approach is developed in this study, utilizing Multiple Linear Regression (MLR) and Relative Factor Importance Analysis to determine the most important drivers of isotopic composition in rainfall and their individual contributions.

We hypothesize that using multiple factors in a single linear model can explain a more significant share of the observed variance in isotopic composition, compared to mono-factorial analyses. Furthermore, we also hypothesize that through importance analysis of the factors considered in the MLR models the most important factors can be identified and their contribution quantified, thus enabling a better process understanding. Such a multi-factorial statistical method could also be applied in paleoclimate studies, separating and quantifying the impacts of local and regional factors on the isotopic composition of local precipitation (Sturm et al., 2010), thus overcoming the shortcomings of single factor analysis. The advantages of the statistical models are their simplicity and ease of interpretation, in contrast to complex circulation models (e.g. GCMs), which can also distinguish between local and regional drivers, but which require more extensive expertise and are more difficult to interpret. Circulation models can simulate the fractionation processes along the transport pathways of water in the atmosphere, but they cannot be used in a straightforward way to extract the impact of dominant factors and weight their relative importance for the variability of the observed isotopic signal. For this statistical techniques are required, in order to quantify the correlation between observed isotopic signal variability and regional climate change patterns (Sturm et al., 2010). Thus using statistical models straight away might be an attractive

alternative to obtain first indications about the dominant processes controlling the isotopic composition of rainfall, both for contemporary and paleoclimate studies.

This study uses the Vietnamese Mekong Delta (VMD) as a test case, for which isotopic data in precipitation has been collected for the first time. The rainfall samples ($\delta^{18}O$ and $\delta^{2}H$) were collected comparatively frequently (bi-weekly to weekly) over a period of 18 months. This dataset enables a better analysis of the temporal dynamics of the isotopic composition as compared to the typical monthly Global Network of Isotopes in Precipitation (GNIP) data (IAEA/WMO, 2016). The sampled data was used to test the proposed approach for the identification and quantification of the controls on the isotopic variation of precipitation.

2.2 Study area

The study area, the Plain of Reeds (Figure 2.1), is located in the northern part of the Vietnamese Mekong Delta (VMD), between latitudes 10°42’7"N to 10°48’9"N and longitudes 105°22’45"E to 105°33’54"E. With an area of 697,000 ha, it accounts for 17.7% of the total area of the VMD. About 95% of the Plain of Reeds is primarily used for rice paddy, but also vegetable cultivating, shrimp and fish farming (Hung et al., 2014b). The average elevation ranges from 1-4 m above sea level.

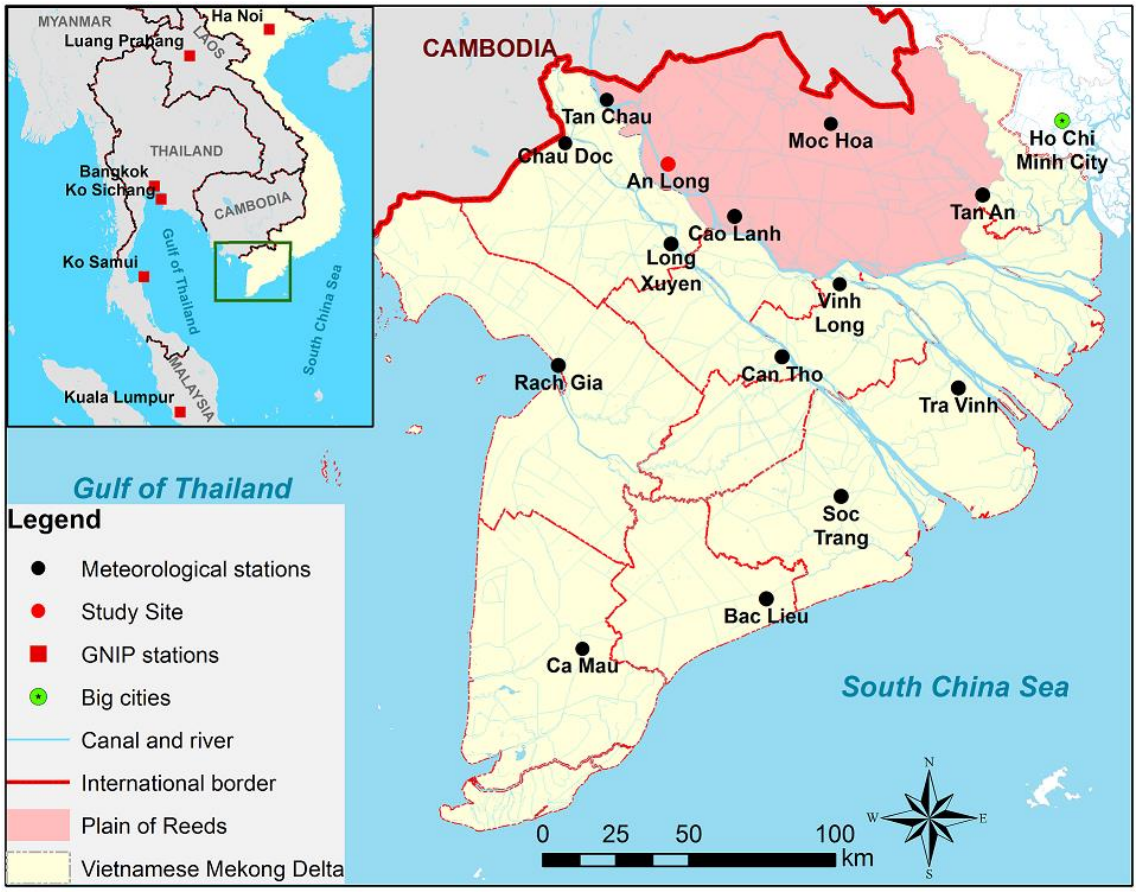

Figure 2.1: Sampling and monitoring sites in the study area

Located in a tropical monsoon region, the climate of the VMD has a distinct seasonality with two seasons: the rainy season (May to November) resulting from the flow of moisture from the Indian Ocean and Western North-Pacific Ocean accounting for approximately 80-90% of the annual rainfall (Tri, 2012), and the dry season (December to April) controlled by high-pressure systems over the Asian continent (Wang et al., 2001). Precipitation from the Indian monsoon is forced by the convective heat sources over the Bay of Bengal (Wang et al., 2001) and arrives earlier than precipitation from the Western North-Pacific monsoon (Delgado et al., 2012), forced by a convective heat source over the South China Sea – Philippine Sea. The average annual rainfall is 1400-2200 mm, characterized by an uneven distribution, both spatially and temporally (Renaud and Kuenzer, 2012; GSO, 2016).

The local climate of An Long is described by data from Cao Lanh station. Cao Lanh is the closest national meteorological station to An Long with continuous climate records, located approximately 37 km Southeast of An Long. It is assumed that the climatic conditions of An Long and Cao Lanh are similar. The proximity of the two locations without any orographic obstacles in between, the same elevation, and the similar geographical setting (flat topography, located at the Eastern bank of the Mekong river) justify this assumption.

The two distinct seasons were defined by the monthly precipitation amounts and the monthly number of days with precipitation recorded at Cao Lanh (Figure 2.2). The dry season is set as the months with rainfall amount smaller than the overall average (blue line in Figure 2.2), and a monthly number of days with precipitation smaller than the overall average (red line in Figure 2.2). All other months are included in the rainy season. The definition used here is mainly developed for the local climatic conditions, the problem to be solved, and the data available. Other definitions could cause some data points to be assigned to the other season. However, those data points will most likely be from the transition period from one season to the other, i.e., other definitions would affect samples that have the least explanatory value for the actual dry and wet seasons. The data indicates that the rainy season in 2014 lasted from May to November, and in 2015 from June to November. The dry season is thus defined from December 2014 to May 2015 and starts again in December 2015. The study period was somewhat dry with an annual rainfall of 985 mm compared to the long-term average of 1550 mm at the station Cao Lanh. This anomaly needs to be considered in the interpretation of the results.

The annual average temperature is 27°C with the small inter-annual variability of about 1°C. Variation of temperature throughout the year is small with monthly averages in the range of 25°C to 29°C (Figure 2.3). The average annual relative humidity ranges from 82% to 85%, with a seasonal variation of 80% to 88% during the rainy season and 77% to 83% during the dry season (Figure 2.3). The mean annual evaporation is 984 mm with a significant difference between the rainy season and the dry season. The monthly evaporation rate ranges from 67 to 80 mm and from 76 to 109 mm in the rainy and dry season, respectively. Daily sunshine duration is about 8.7 to 9.6

hours in the dry season and 5.5 to 5.9 hours in the rainy season (Renaud and Kuenzer, 2012; GSO, 2016).

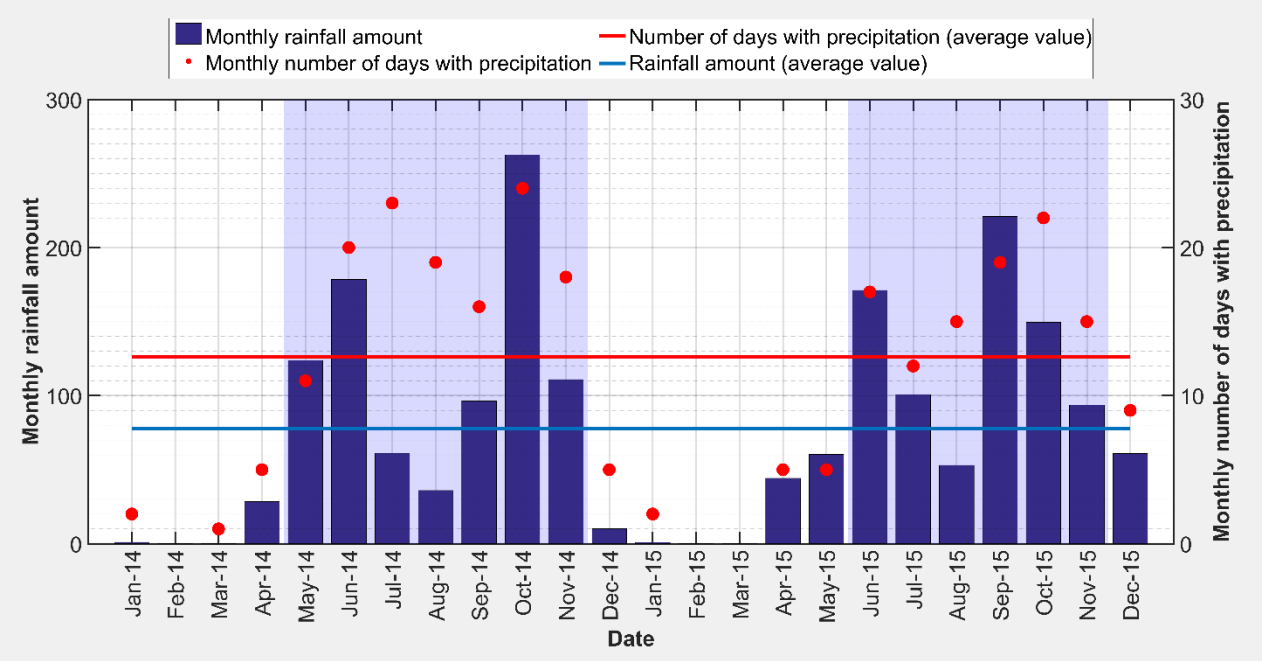

Figure 2.2: Monthly precipitation (mm) and a monthly number of days with precipitation for Cao Lanh station. Light blue background indicates rainy season.

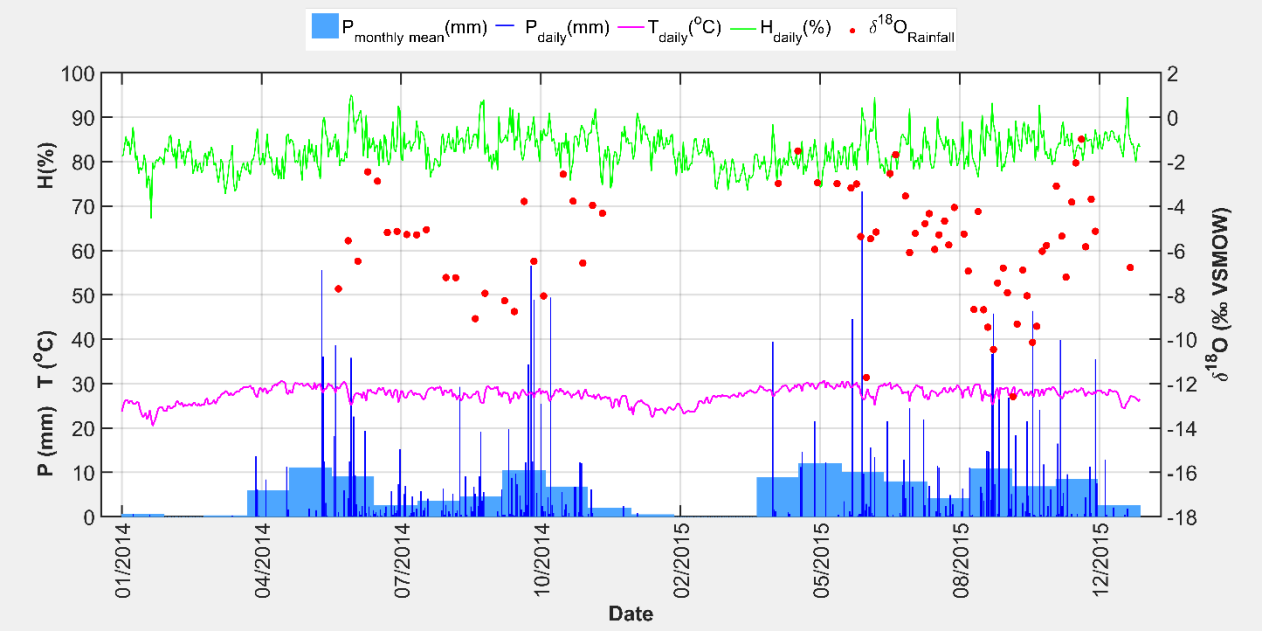

Figure 2.3: Climate data from the Cao Lanh meteorological station for the study period. Daily temperature (T) is given together with monthly and daily precipitation (P) and daily relative humidity (H). Weekly and bi-weekly $\delta^{18}O$ (‰ VSMOW) values of rainwater are presented as red circles.

2.3 Methodology

An overview of the methodology is given in Figure 2.4. For the derivation of local factors relevant for the isotopic composition of precipitation climate data from the nearby meteorological station of Cao Lanh were collected (section 2.3.1). At the test location, precipitation samples were analyzed for their isotopic composition (section 2.3.2 and 2.3.3). Local meteoric water lines (LMWL) were derived from the isotopic data (section 2.3.4). The regional factors were derived from atmospheric back trajectory modeling (section 2.3.5). All possible combinations of local and regional predictors were included in multiple linear regressions, and their ability to explain the observed variance of the isotopic composition of precipitation was determined with performance statistics (MLR, section 2.3.6). Finally, the influence of the different factors on the explained variance of isotopic composition was determined by relative importance analysis (section 2.3.7).

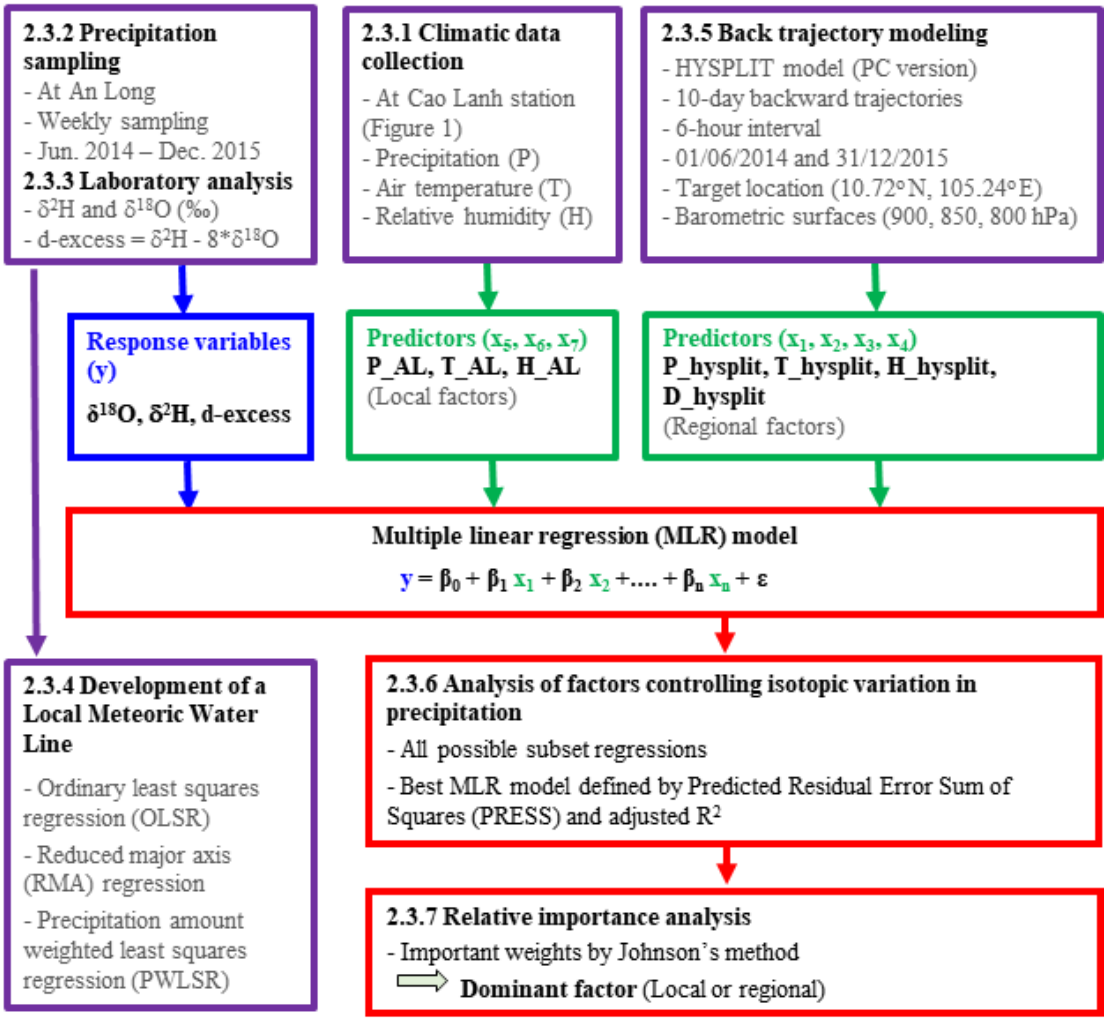

Figure 2.4: Methodology used in the study. Local precipitation (P_AL), air temperature (T_AL), and relative humidity (H_AL) at An Long. Precipitation amount (P_hysplit), mean temperature (T_hysplit) and relative humidity (H_hysplit) along the transport pathways, and the length of backward trajectories (D_hysplit).

2.3.1 Climatic and isotopic data collection

Daily precipitation, air temperature, and relative humidity were obtained from the National Centre for Hydro-Meteorological Forecasting (NCHMF) of Vietnam at Cao Lanh for the period 2012-2015. Long-term (more than 30 years) climatic data at this station was provided by SIWRP (2014). Precipitation isotopic data from six selected GNIP stations (IAEA/WMO, 2016) located in the Indochinese Peninsula (Figure 2.1) was collected for comparison with the isotopic data sampled in this study in order to investigate regional similarities or differences in isotope composition in rainfall in SE-Asia. This was tested by the Levene test (Levene, 1960) for equality of variances of the isotopic data of the different stations, and the comparison of Local Meteoric Water Lines.

2.3.2 Precipitation sampling at An Long

Precipitation at An Long in the Plain of Reeds (Figure 2.1) was sampled on a weekly basis between June 2014 and May 2015 and twice a week between June 2015 and December 2015. The rain collector was a dip-in sampler type as described in the guidelines of the IAEA technical procedure for precipitation sampling (IAEA, 2014). It consists of a 5 L accumulation glass bottle fitted with a vertical 14 cm diameter plastic funnel that reaches almost to the bottom to prevent evaporative losses, and a pressure equilibration plastic tube (2 mm in diameter and 15 m in length) to minimize evaporation. All collected samples were stored in 30 mL plastic sample bottles with tight screw caps to avoid evaporation effects. Between collection and laboratory analysis, the samples were stored in the dark.

2.3.3 Isotopic laboratory analysis

All stable isotope samples were analyzed at the laboratory of the Alfred-Wegener-Institute (AWI) in Potsdam, Germany. The measurements were performed with a Finnigan MAT Delta-S mass spectrometer using equilibration techniques to determine the ratio of stable oxygen (18O/16O) and hydrogen (2H/1H) isotopes. Analytical results were reported as δ^2H and $\delta^{18}O$ (‰, relative to Vienna Standard Mean Ocean Water - VSMOW) with internal 1σ errors of better than 0.8‰ and 0.1‰ for δ^2H and $\delta^{18}O$, respectively. The measuring procedure is described in detail in Meyer et al. (2000). The deuterium excess (d-excess) was calculated following Equation 2.1 (Dansgaard, 1964):

$$\text{d-excess} = \delta^2H - 8*\delta^{18}O \quad (2.1)$$

2.3.4 Development of local meteoric water lines

Local meteoric water lines (LMWL) were derived by least-squares regression of $\delta^{18}O$ against δ^2H values of the samples. The quality of fit of the LMWLs was evaluated based on the coefficient of

determination R^2 (also referred to as explained variance), the standard error SE, and the statistical significance value (p-value). The regression model indicates a good fit to the data when R^2 is close to 1.0, the standard error is small in relation to the magnitude of the data, and the p-value is smaller than 0.0001 (Helsel and Hirsch, 2002). The slope and intercept of LMWL of An Long were compared to those of GNIP stations to put the data from An Long in a regional context.

2.3.5 Back trajectory modeling

The potential locations of atmospheric moisture sources and the direction of the air mass causing precipitation before reaching An Long station were investigated via back-trajectory analysis. This investigation was performed using the PC Windows-based HYSPLIT (Hybrid Single Particle Lagrangian Integrated Trajectory) model developed by NOAA (National Oceanic and Atmospheric Administration) at the Air Resources Laboratory (ARL) (www.arl.noaa.gov/HYSPLIT_info.php). The model builds on the Lagrangian approach, using a moving frame of reference for the advection and diffusion calculation as the air parcels move from their initial location (Draxler and Rolph, 2003; Stein et al., 2015).

The 1^ox1^o climatic dataset generated by the global data assimilation system (GDAS) was used as input to the HYSPLIT model. 10-day backward trajectory analysis was performed every 6 hours between 01-JUN-2014 and 31-DEC-2015 at the sampling site (10.72^{o}N, 105.24^{o}E) for three levels at 1000, 1500, and 2000 m above ground (corresponding to barometric surfaces of approximately 900, 850, and 800 hPa). These barometric surfaces were chosen because the 850-hPa vorticity is highly indicative of the strength of the boundary layer moisture convergence and rainfall in regions away from the equator (Wang et al., 2001), hence rainfall is expected to mostly originate from these altitudes. Consequently, the combination of 800 hPa and 850 hPa barometric surfaces accounts for the fact that rainfall is expected to mostly originate between 1500 and 2000 m above ground level. Correspondingly, the combination of the barometric surfaces of 800, 850 and 900 hPa means that rainfall is expected to mostly originate between 1000 and 2000 m above ground level. In total, 6948 backward trajectories were computed. The HYSPLIT outputs, i.e., precipitation, temperature, relative humidity along the backward trajectories, and the length of trajectories (the distance of moisture sources travelled), were used as regional factors potentially controlling the variation of the isotopic composition of precipitation at An Long. Accumulated precipitation, mean values of temperature and humidity of the hourly HYSPLIT output were calculated along the trajectory, as well as the length of the trajectory. All these factors were used as predictors in the MLR.

A cluster analysis of a large number of trajectories arriving at the study site was applied to group similar trajectories and thus source regions, in order to better interpret the trajectories and to confirm the accuracy of the trajectory analysis. More information about the HYSPLIT cluster analysis can be found at https://ready.arl.noaa.gov/documents/Tutorial/html/.

2.3.6 Analysis of factors controlling isotopic variation in precipitation

Multiple linear regression (MLR) was used to assess how the isotopic variation in precipitation is related to regional and local controlling factors. As indicators of regional factors the output of the HYSPLIT model was used consisting of the accumulated precipitation amount along the transport pathways (hereafter P_hysplit), mean temperature (T_hysplit) and mean relative humidity (H_hysplit) along the trajectory, and the distance of moisture sources travelled within the time frame of 10 days (D_hysplit). The local climatic factors are weekly precipitation amount (P_AL) at An Long station, and weekly mean air temperature (T_AL) and weekly mean relative humidity (H_AL) taken from the nearby Cao Lanh station during the sampling period. These seven predictors were related to isotopic values ($\delta^{18}O$, $\delta^{2}H$, and d-excess) defined as response variables in the MLR. Pearson linear correlation coefficients were computed to show inter-correlations between response and predictor variables and then used to determine the importance of predictors in the MLR.

All possible subset regression models consisting of all possible combinations of predictors (2^7-1 = 127 models) were applied separately for $\delta^{18}O$, $\delta^{2}H$ and d-excess. The coefficient of determination R^2 for the MLR was calculated for each subset regression. The goodness of each MLR model was evaluated based on the Prediction Residual Error Sum of Squares (PRESS) (Eq. 2.2) and adjusted R^2 (R_a^2) (Eq. 2.3) (Helsel and Hirsch, 2002).

$$PRESS = \sum_{i=1}^{n} {e_{(i)}}^2 \tag{2.2}$$

$$R_a^2 = R^2 - (1 - R^2)\frac{p}{(n - p - 1)} \tag{2.3}$$

In Equation 2.2, the PRESS residuals are defined as $e_{(i)} = y_i - \hat{y}_{(i)}$ where $\hat{y}_{(i)}$ is the regression estimate of y_i based on a regression equation computed leaving out the i^{th} observation. The process is repeated for all n observations. The selection of best models with PRESS is equivalent to a leave-one-out cross-validation, which tests the regression models for robustness and reduces the chances of model over-fitting, i.e., the chances of finding spurious regression models that provide good results for the given combination of factors and selected period only.

In Equation 2.3, p is the total number of predictors in the MLR model and n is the number of observations. The statistical significance of all linear regression was evaluated based on the p-value for the F-test as part of a one-way ANOVA analysis. A good MLR model is thus characterized by:

(i) PRESS approaching zero,

(ii) Adjusted R^2 (R^2_a) approaching 1.0,

(iii) a p-value smaller than 0.0001.

For each response variable, six pressure layers (800 hPa, 850 hPa, 900 hPa, and mean values of their combinations) and 10 durations of backward trajectories (from 1-day to 10-day backward) were used. The different pressure levels and combinations were chosen to tackle the inherent uncertainty regarding the pressure levels from which the rainfall actually stems. Similarly, various durations of the trajectories were chosen in order to avoid fixing the a-priori unknown travel time of precipitation reaching An Long. Overall, this resulted in 7620 MLR models for each response variable $\delta^{18}O$, $\delta^{2}H$ and d-excess (6 pressure levels times 10 trajectory durations times 127 predictor sets). The best MLR model was then identified by the smallest PRESS value (Eq. 2.2). Furthermore, the goodness of fit of the MLR models was characterized based on the adjusted R^2 values.

2.3.7 Relative importance analysis

Relative importance analysis determines the proportion of the variance explained by the individual predictors in the regression. However, this is difficult when predictors are correlated, since multicollinearity can lead to a high sensitivity of regression coefficients caused by small changes in the model. This means that the importance can strongly shift from one predictor to another well correlated one if the data set is changed even only slightly. The leave-one-out cross-validation may be particularly vulnerable to this effect.

While several methods such as zero-order bivariate correlation (e.g. Pearson correlation), standardized regression weights (β weights), structure coefficient (the correlation between an observed predictor and the predicted criterion scores), or all possible subsets regression can be applied to interpret and understand the contributions of predictors playing in forming regression effects, these traditional estimates of importance fail to appropriately partition variance to the various predictors when they are correlated (Tonidandel and LeBreton, 2011). In response, two useful techniques for interpreting a regression equation and for quantifying predictor importance are available: dominance analysis (Budescu, 1993) and relative weight analysis (Johnson, 2000), which has been developed for more accurately quantifying the power of predictors when they are correlated. Both these methods are advantageous over traditional measures of importance (LeBreton et al., 2007). Although both these methods yield qualitatively similar results, Johnson ‘s relative weight analysis is much more computationally efficient, especially with large numbers (>10) of predictors (Johnson, 2000). For a review of approaches to estimate predictor importance, readers are referred to Tonidandel and LeBreton (2011); Kraha et al. (2012).

Because of its computational efficiency the relative weight analysis (Johnson, 2000) was applied in this study to quantify the proportion of the variance explained by the individual regression factors in the MLR, and thus identifies the dominant controls on the isotopic composition of rainfall. Specifically, relative weight analysis approximates the relative importance of a set of predictors by creating a set of variables that are highly related to the original set of variables but are uncorrelated with each other. The response variable is then regressed on the uncorrelated set of predictors to approximate the relative weight of the original set of predictors, defined as the relative contribution of each predictor to R^2. Relative weights of correlated predictors are therefore analogous to squared standardized regression coefficients when predictors are uncorrelated. Details are given in Johnson (2000) and Tonidandel et al. (2009). In this study, relative weights were also reported as percentages of the regression R^2.

2.4 Results and discussion

2.4.1 Variability of moisture sources

Single backward trajectory computations by the HYSPLIT model are not definite, but can contain quite some uncertainty. The horizontal uncertainty of the trajectory calculations by HYSPLIT has been estimated to be 10–20 % of the travel distance (Draxler and Hess, 1998). Errors in trajectory calculation computed from analyzed wind fields seem to be typically in the order of 20% of the distance travelled (Stohl, 1998). However, the statistical analysis of a large number of trajectories arriving at a study site would increase the accuracy of the trajectory analysis (Cabello et al., 2008). In this study, several quality control measures were applied, as recommended in Stohl (1998), to increase confidence in the HYSPLIT-generated back trajectories and to improve the validity of the air mass history. Firstly, trajectories were computed for three pressure levels (900, 850, and 800 hPa). Similar origins of atmospheric moisture for these pressure levels suggest that resolution errors and atmospheric shearing instabilities are negligible, which increases the confidence in the results. Secondly, we use the shortest possible integration time step (i.e., one hour) and a small value for the parameter TRATIO (0.25), which is the fraction of a grid cell that a trajectory is permitted to transit in one advection time step. Smaller values of TRATIO help to minimize the trajectory computation error using the HYSPLIT model. Thirdly, the statistical analysis of a large number of trajectories (e.g., trajectory cluster analysis) arriving at the study site was applied to confirm the accuracy of the trajectory analysis. The trajectory cluster analysis is conducted by the HYSPLIT model to group trajectories with similar pathways. The cluster analysis merges these trajectories that are near each other and represents those clusters by their mean trajectory. Differences between trajectories within a cluster are minimized while differences between clusters are maximized. Computationally, trajectories are combined to decrease the number of clusters until the total spatial variance (TSV) starts to increase significantly. This occurs when

disparate clusters are combined. This number of clusters is then selected as the optimal cluster number for sorting and combining similar trajectories.

Figure 2.5 shows back-calculated trajectories of atmospheric moisture prior to rainy days at An Long for the sampling period from June 2014 to December 2015. Left and right panels show the results of 850 hPa trajectories for 2014 and 2015, and the upper, middle, and lower panels show the results for the early (June – September) and late (October – November) rainy season and dry season (December – May), respectively. Figure 2.6 shows the spatial distribution of vapour trajectories (cluster means) for precipitation days at An Long for 3 barometric surfaces (800, 850, 900 hPa) between June 2014 and December 2015, and the change in total spatial variance (TVS) for different cluster numbers. The TSV was used to identify the optimum number of clusters. The similarity of back-calculated trajectories (Figure 2.1) and trajectory cluster analysis (Figure 2.6) at three barometric surfaces (900, 850, and 800 hPa) illustrates that the trajectories and thus the source regions do not differ between different atmospheric layers. This indicates a barotropic atmosphere, with the consequence that it is unlikely that the selection of the pressure layer for the HYSPLIT trajectories modifies the results of the MLR significantly.

Figure 2.5 and Figure 2.6 demonstrate that the dry-season precipitation (from December to May) in the Plain of Reeds mainly originates from the moisture sources of the Asian continental air masses and the oceanic air masses carried by the equatorial easterlies. Whereas during the rainy season (from June to November) air masses travel a longer distance over the tropical Indian Ocean (from June to September) and the South Pacific Ocean (October to November).

These findings for An Long agree with the general characterization of monsoonal circulation and precipitation over the Southeast Asia region, with moisture from the Indian Ocean dominating during the initial stage of monsoon evolution, and the Pacific Ocean dominating in the later stages. This indicates that the HYSPLIT model provides valid trajectories to be used in the MLR.

The mean $\delta^{18}O$ values for the 5 clusters are noted in Figure 2.6 (in blue). The mean cluster values are similar for the three pressure levels. Also, the mean values of the two clusters from the Indian Ocean, as well as the two clusters from the Pacific, are similar. For a fingerprinting one also has to consider the variation of the values within the clusters, which partly overlap. This means that the $\delta^{18}O$ values of precipitation in the Mekong Delta cannot be used to uniquely identify the origin of the trajectory. However, they provide a coarse indication of their origin.

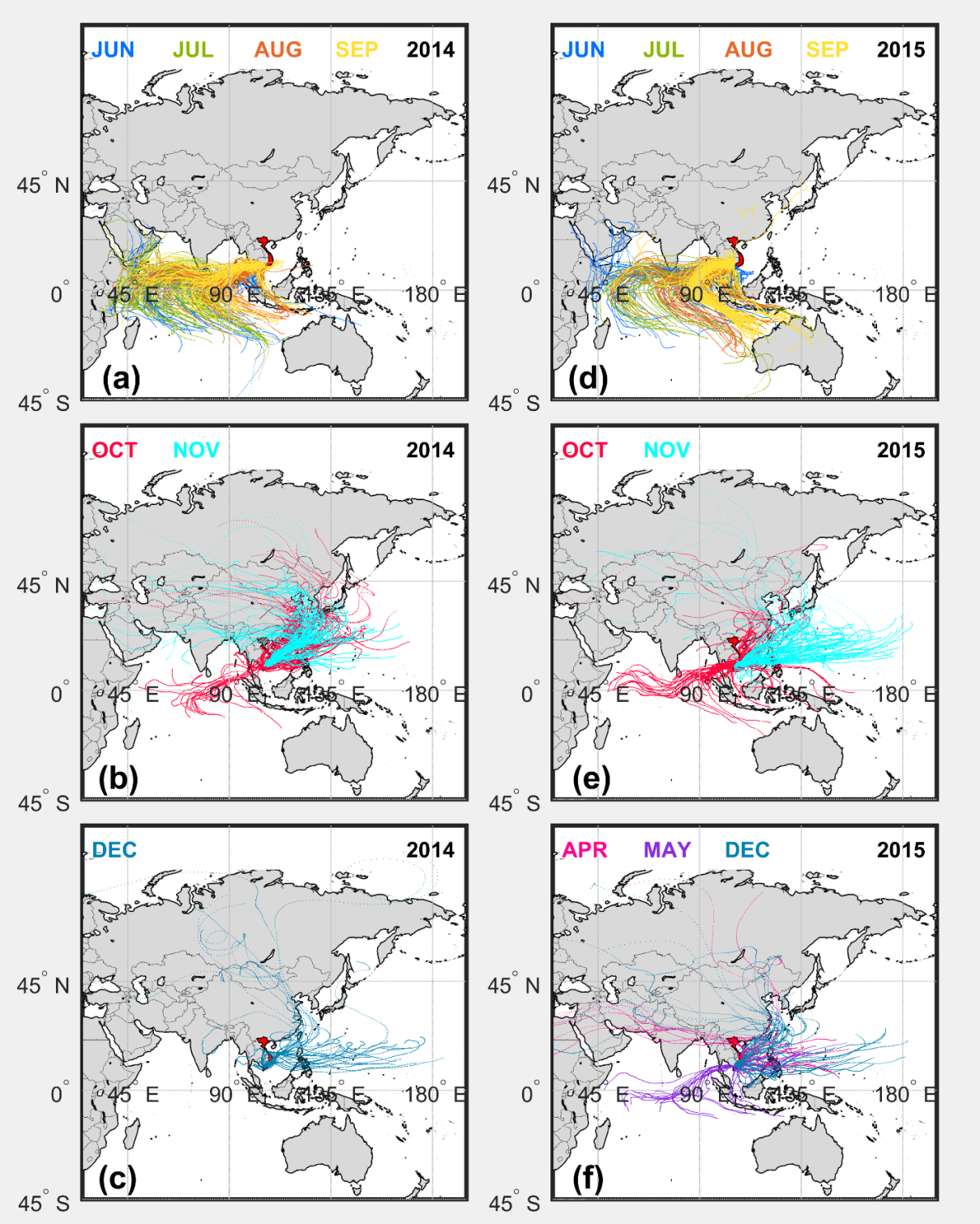

Figure 2.5: Back-trajectories indicating potential moisture sources of precipitation (plotted only for days with precipitation) at An Long station for the barometric surfaces at 850 hPa between June 2014 and December 2015. Left panels show the results for 2014, right panels for 2015; top row (a, d) early rainy season (June – September), middle row (b, e) late rainy season (October – November), bottom row (c, f) dry season (December – May). In January, February and March 2015 no rainfall was recorded.

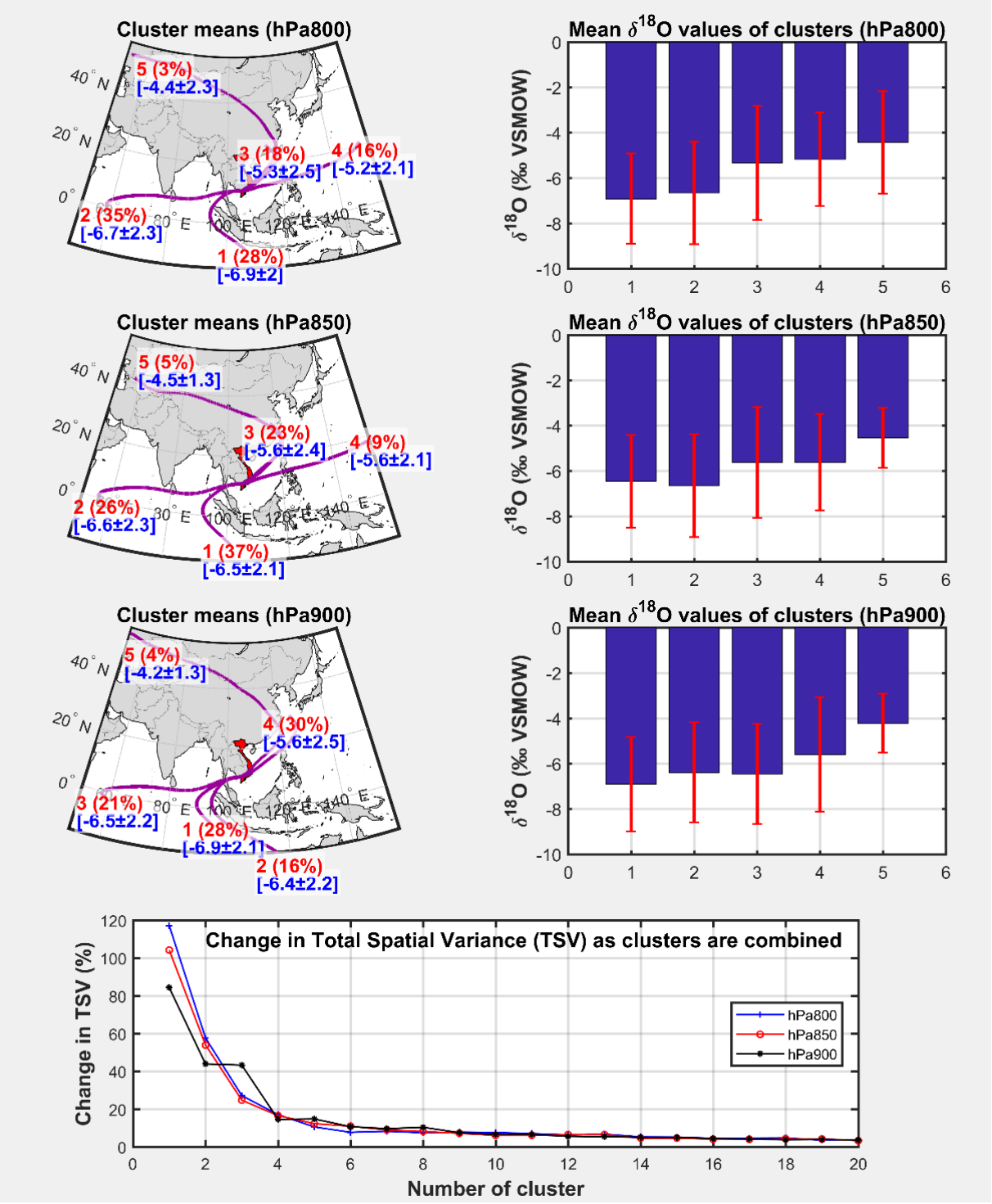

Figure 2.6: Spatial distribution of vapor trajectories (cluster means) for precipitation days at An Long for 3 barometric surfaces (800, 850, 900 hPa) between June 2014 and December 2015, and change in total spatial variance (TVS) for different cluster numbers. The TSV was used to identify the optimum number of clusters (hereby 5 clusters). Red texts indicate the cluster number (1-5) and the percent of all trajectories assigned to each of the five clusters. Blue texts and bar charts indicate the mean $\delta^{18}O$ values for each cluster plus/minus the standard deviation of each cluster.

2.4.2 Isotopic composition of precipitation

2.4.2.1 Meteoric water lines

The ordinary least squares linear regression (OLSR) of 74 pairs of $\delta^{18}O$ and $\delta^{2}H$ values at An Long yield the following LMWL for the Plain of Reeds:

$\delta^{2}H = (7.56 \pm 0.11) * \delta^{18}O + (7.26 \pm 0.67)$

(SE = 2.26; $r^2 = 0.99$; $p < 0.0001$; n = 74)

The numbers in brackets indicate the estimates of slope and intercept plus/minus the standard deviation, indicating the parameter uncertainty. The regression is stable against different regression techniques, as shown in the Appendix A1.

The close fit of all considered regressions indicates a very good linear relationship between $\delta^{18}O$ and $\delta^{2}H$ in the study. On large temporal scales, a good linear relationship between $\delta^{18}O$ and $\delta^{2}H$ is usually observed at sites where secondary fractionation processes, e.g. sub-cloud evaporation, are insignificant (Crawford et al., 2014). The LMWL for An Long is slightly different from the global meteoric water line (GMWL; defined by $\delta^{2}H = 8*\delta^{18}O + 10$ (Craig, 1961) (Figure 2.7) and the LMWLs derived for six selected GNIP stations (IAEA/WMO, 2016) located in the Indochinese Peninsula (Table 2.1). The small difference in slope between the LMWL compared to that of GMWL, and the distribution of isotope values along the GMWL indicate that evaporative isotopic enrichment during rainfall is not significant. However, the less positive intercepts of the LMWL (<10‰) may reflect smaller kinetic effects during evaporation (Ingraham, 1998) over the Mekong Delta compared to the worldwide average.

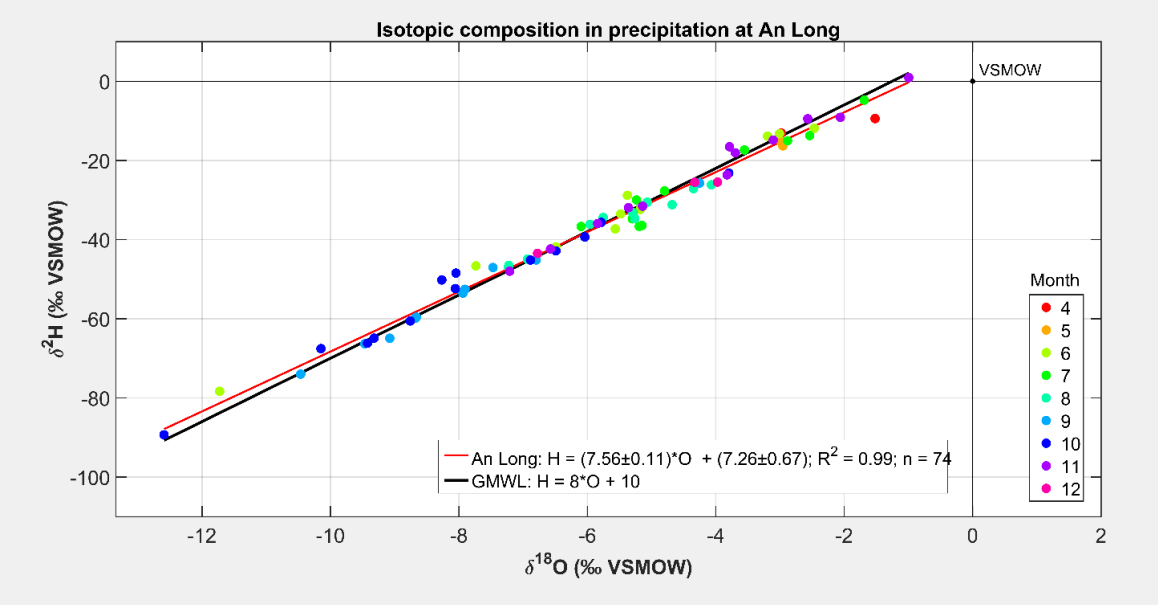

Figure 2.7: The LMWL of An Long in comparison to the GMWL

Table 2.1. Isotopic composition of precipitation at An Long and six selected GNIP stations throughout the Indochinese Peninsula.

Station Name	Location	Country	AL	P	T	Period	$\delta^{18}O$		$\delta^{2}H$		d-excess	LMWL (OLSR)		LMWL (RMA)		LMWL (PWLSR)	
				(mm)	(°C)		WM	M	WM	M	WM	S	Int.	S	Int.	S	Int.
An Long	105.24 °E - 10.72 °N	Vietnam	2	985* (1550)	27.4* (27.2)	06.2014 - 12.2015	-6.4 ±1.5	-5.8 ±2.5	-40.9 ±11.5	-36.2 ±18.7	10.4 ±1.8	7.56 ±0.11	7.26 ±0.67	7.61 ±0.11	7.58 ±0.67	7.61 ±0.11	7.87 ±0.73
Hanoi **	105.84 °E - 21.02 °N	Vietnam	10	1659 ±257	24.8 ±0.5	2004 - 2007	-8.8 ±0.7	-5.9 ±0.5	-56.9 ±4.2	-33.8 ±3.6	13.5 ±1.5	7.91 ±0.10	12.45 ±1.25	7.99 ±0.18	12.90 ±1.22	7.77 ±0.21	10.92 ±1.91
Bangkok **	100.50 °E - 13.73 °N	Thailand	2	1558 ±314	28.5 ±0.6	1968 - 2015	-6.5 ±1.0	-5.2 ±1.0	-42.6 ±7.6	-33.2 ±7.2	9.4 ±1.6	7.35 ±0.04	5.36 ±0.47	7.53 ±0.08	6.29 ±0.47	7.68 ±0.07	7.25 ±0.49
Ko Samui **	100.03 °E - 09.28 °N	Thailand	7	1265 ±611	27.9 ±0.2	1979 - 1983	-5.8 ±1.4	-4.8 ±0.9	-28.8 ±7.1	-24.1 ±4.4	10.8 ±0.0	7.18 ±0.10	6.89 ±1.20	7.30 ±0.25	7.41 ±1.16	7.45 ±0.25	7.89 ±1.26
Ko Sichang **	100.80 °E - 13.17 °N	Thailand	26	877 ±320	27.9 ±0.6	1983 - 1995	-6.2 ±0.6	-6.2 ±1.1	-39.3 ±5.1	-39.7 ±8.8	10.2 ±0.6	7.62 ±0.06	7.61 ±1.15	7.72 ±0.18	8.16 ±1.12	7.77 ±0.23	8.65 ±1.44
Luang Prabang **	102.13 °E - 19.88 °N	Lao PDR	305	1228 ±178	25.7 ±0.7	1961 - 1967	-7.8 ±1.2	-6.7 ±0.3	-54.2 ±7.6	-45.9 ±0.9	8.4 ±1.9	7.90 ±0.13	7.97 ±2.00	8.01 ±0.27	8.70 ±1.93	7.80 ±0.28	7.52 ±2.29
Kuala Lumpur **	101.68 °E - 03.13 °N	Malaysia	26	1801 ±787	-	1993 - 2012	-7.3 ±0.8	-7.0 ±0.7	-46.6 ±7.7	-45.1 ±6.8	11.8 ±4.1	7.63 ±0.07	8.10 ±1.93	8.26 ±0.26	12.53 ±1.92	7.73 ±0.29	8.95 ±2.24

Note:

* Measured at An Long in 2015; numbers in parentheses show mean values of long-term measurements at Cao Lanh;

** Data are from https://nucleus.iaea.org/wiser/gnip.php (IAEA/WMO, 2016);

P: annual precipitation (mm/year); T: average temperature (°C); AL: altitude (meter above sea level); WM: weighted mean value; M: mean value; S: slope; Int.: intercept. [a] RMA: reduced major axis regression; [b] PWLSR: precipitation amount weighted least squares regression.

2.4.2.2 Seasonal variation and spatial homogeneity of isotope composition

The 74 precipitation samples at An Long showed that $\delta^{18}O$ ranges between -12.6‰ and -1.0‰, with an arithmetic mean value and standard deviation of -5.8‰ ± 2.5‰, and $\delta^{2}H$ ranges between -89.3‰ and 0.9‰, with an arithmetic mean value and standard deviation of -36.2‰ ± 18.7‰. Generally, less negative isotopic values are observed in the dry-season precipitation samples. The most negative values occur in the second half of the rainy season (September and October), whereas the least negative values are observed in the late dry season in April and May (Figure 2.7 and Figure 2.8). This shows that the isotopic composition of precipitation at An Long station exhibits marked seasonal variations, which in turn indicates different dominant moisture sources and/or processes in the different seasons. A comparison of the seasonal variation of $\delta^{18}O$ with the short-term (2014-2015) and long-term (1968-2015) monthly averages of Bangkok (Figure 2.8) reveals very similar seasonality, both in terms of timing and magnitude. The small differences between $\delta^{18}O$ for An Long and Bangkok are likely caused by the exceptional low rainfall in the study period compared to the long-term monthly values, particularly during May and July. But considering the similarity of the isotopic signatures and general factors controlling stable isotopic composition of precipitation between the two stations, i.e. annual rainfall amount, air temperature, altitude and latitude (Dansgaard, 1964; Ingraham, 1998), it can be concluded that the isotopic variations of An Long and Bangkok follow the same dynamics and controls, both on an annual and seasonal scale. Moreover, the overall similarity suggests an important role of regional or larger-scale controls on An Long precipitation isotope ratios.

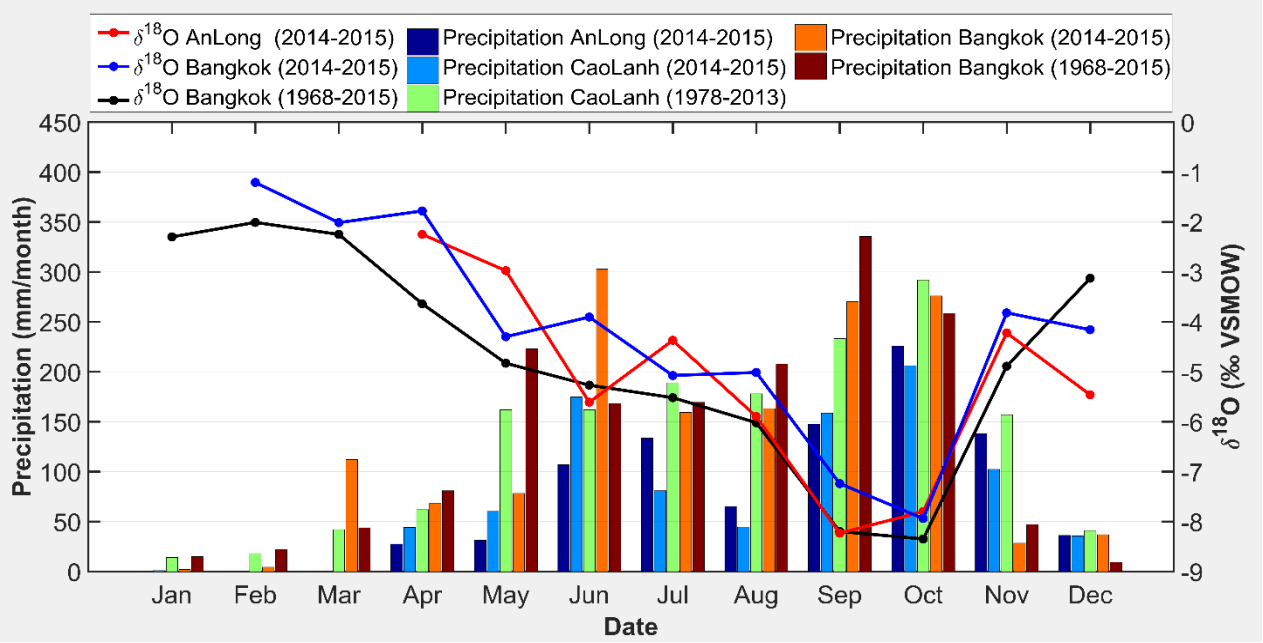

Figure 2.8: Seasonal variation of the average monthly precipitation for An Long and Cao Lanh and $\delta^{18}O$ values of precipitation for An Long (for the period of observation (red)) and Bangkok (both for the period of observation (blue) and the long-term mean (black)).

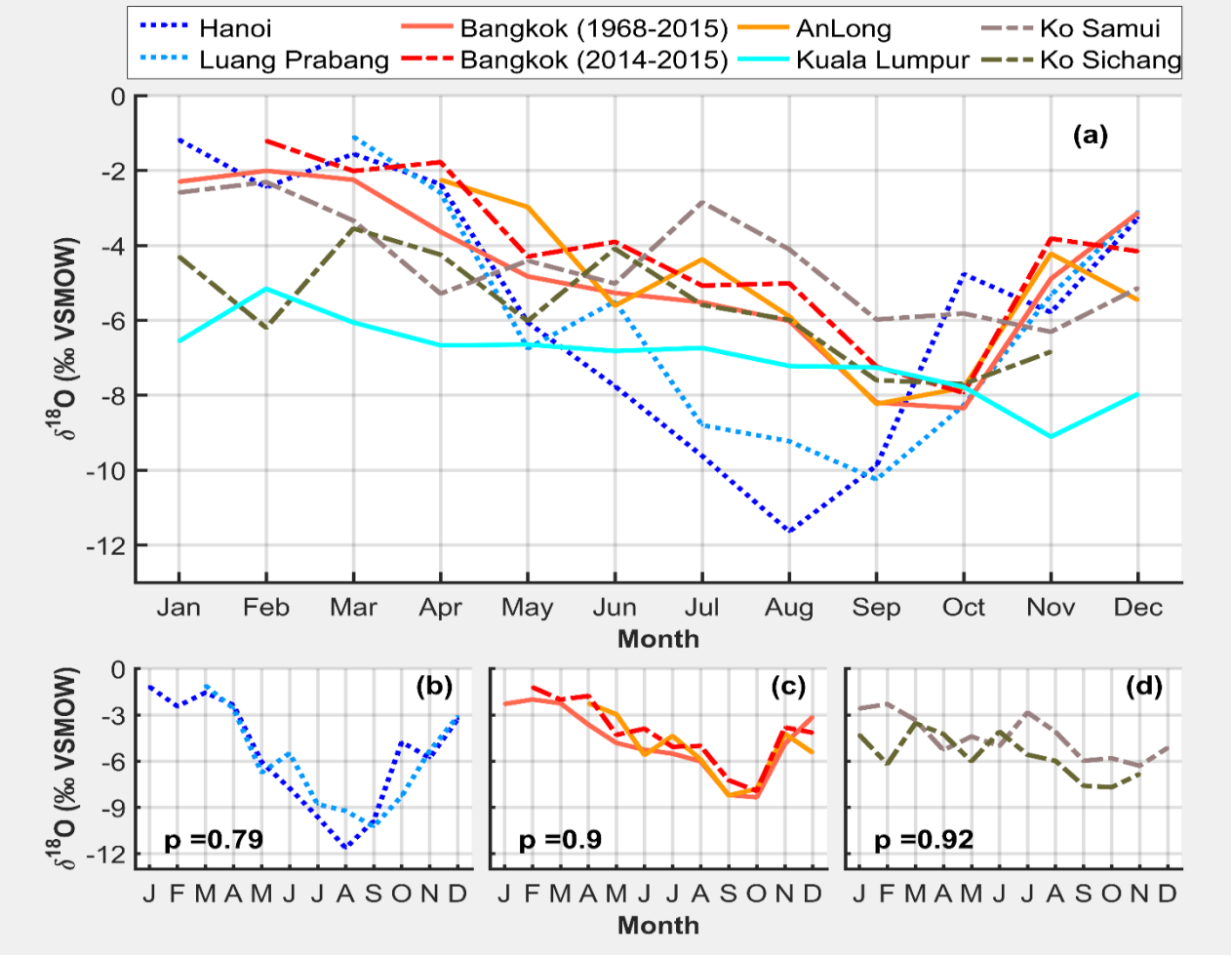

Figure 2.9: Seasonal monthly mean $\delta^{18}O$ values for An Long and GNIP data from the Indochinese Peninsula. The data is grouped according to similar variability tested with the Levene test. The p-values given in (b) to (d) are the test statistics. High values indicate similar variance. The time series of Bangkok is plotted for short-term (2014-2015) and long-term (1968-2015) periods.

In order to test the representativeness of the An Long data for a wider area, the variability of the monthly mean $\delta^{18}O$ data of An Long was compared to the available GNIP data of the Indochinese Peninsula (Table 2.1). As shown in Figure 2.9, the test results in four distinct groups of data series with similar variances: the Northern part of the Indochinese Peninsula (Hanoi and Luang Prabang), the Southern part of the Indochinese Peninsula (Bangkok and An Long), the islands in the Gulf of Thailand (Ko Samui and Ko Sichang), and finally Kuala Lumpur showing only little seasonal variability. The Northern and Southern parts of the Indochinese Peninsula generally show a similar seasonal behavior with a distinct higher depletion during the rainy season, but in the Northern part the highest depletion is one month earlier (August) than in the Southern part, and the magnitude of the depletion is larger. The seasonal $\delta^{18}O$ variability in precipitation on the islands is much lower than on the stations located on the continent. This is likely due to the maritime setting and could indicate a continental effect in the data of the mainland stations. In addition,

the short-term time series of Bangkok and An Long (i.e., 2014-2015) show similar variances, resulting in a highly significant Levene test statistic of 0.98. The variation of the short-term time series of Bangkok and An Long is also very similar to the long-term time series, again shown by a highly significant Levene test statistic of 0.90. This indicates that the variability of the isotopic signature of the An Long time series is almost identical to the one from Bangkok. In summary, the analyzed GNIP data suggests that the data and results from this study are likely to be representative of the Southern continental part of the Indochinese Peninsula.

2.4.3 Factors controlling isotopic composition of precipitation

Prior to the MLR, the correlation of the predictors was analyzed (Table 2.2). The absolute values of the correlation coefficients between local (P_AL, T_AL, H_AL) and regional (P_hysplit, T_hysplit, H_hysplit, D_hysplit) climatic parameters are relatively small and mostly not significant ($|r| < 0.4$, Table 2.2b). However, the correlation coefficients between regional predictors are in most cases high and significant (Table 2.2c). Highest correlations are found between temperature and humidity for local factors, and between humidity and precipitation for regional factors. Interestingly, the correlation between P_AL and H_AL is quite low. This indicates that the local precipitation is influenced by other factors than local humidity (which is rather uniform throughout the year), as e.g. large-scale circulation. The correlation between the predictors underlines the necessity to consider multicollinearity when investigating how the predictors control the response variables $\delta^{18}O$ and $\delta^{2}H$.

2.4.3.1 Local factors and isotopic composition in precipitation

Typically, in tropical regions subject to a monsoon climate the correlation between $\delta^{18}O$ and $\delta^{2}H$ values of precipitation and air temperature is virtually non-existent, whereas a strong relation between $\delta^{18}O$ and amount of precipitation has been observed (Rozanski et al., 1992; Araguás-Araguás et al., 1998). Our data show that the correlation of local precipitation amount (P_AL) and local temperature (T_AL) with isotopic values ($\delta^{18}O$ and $\delta^{2}H$) are both low ($|r| < 0.45$, Table 2.2a). This suggests that $\delta^{18}O$ and $\delta^{2}H$ variation is neither dominated by local precipitation amount nor by local temperature during the sampling period. This lack of a significant correlation ($|r| < 0.5$) between $\delta^{18}O$ and local rainfall amount was also observed in other regions affected by the Asian monsoon climate such as Bangkok, Hong Kong, New Delhi (Ishizaki et al., 2012), and Cherrapunji, India (Breitenbach et al., 2010). This again supports the statement that $\delta^{18}O$ may not be an adequate proxy for local climatic conditions (e.g., temperature or rainfall amount) in the Asian monsoon region (Aggarwal et al., 2004; Vuille et al., 2005).

Secondary fractionation processes such as sub-cloud evaporation or secondary evaporation from open water bodies tend to decrease d-excess in the residual rainwater (Stewart, 1975) and enrich it in the heavy isotopes (Guan et al., 2013). The negative correlation of humidity (H_AL) with $\delta^{18}O$ and $\delta^{2}H$ ($r = -0.53$, Table 2.2a) combined with a positive correlation with d-excess ($r = 0.2$, Table

2.2a), indicates that some secondary fractionation processes (Risi et al., 2008b; Crawford et al., 2017) may occur during some months at An Long. To examine in which month secondary fractionation processes are likely significant, amount-weighted mean and arithmetic mean, for both $\delta^{18}O$ and d-excess are compared. The rationale is that if secondary fractionation processes are important (with the assumption that the moisture sources of different events within the month are the same), the arithmetic mean should have a $\delta^{18}O$ value that is more enriched in heavy isotopes, and a much smaller d-excess than the weighted mean (Guan et al., 2013). Figure 2.10 shows that secondary fractionation processes may take place mainly during the dry season, in December 2014, and in April, May and November 2015, because in these months a) less negative $\delta^{18}O$ values and lower d-excess values compared to the overall arithmetic mean are observed, while at the same time the monthly arithmetic means are higher for $\delta^{18}O$, and lower for d-excess compared to the monthly weighted means.

Table 2.2: Pairwise correlation coefficients between regional factors (P_hysplit, T_hysplit, H_hysplit, D_hysplit) and local factors (P_AL, T_AL, H_AL) and stable isotopic values ($\delta^{18}O$, $\delta^{2}H$, and d-excess). Bold and italic numbers denote significance at the 0.01 and 0.05 level (2-tailed), respectively. The meteorological data are aggregated to weekly values corresponding to the precipitation sampling at An Long.

(a)	P_hysplit	H_hysplit	T_hysplit	D_hysplit	P_AL	H_AL	T_AL	Isotopic values vs. Regional and Local factors
δ 18O	-0.74	-0.45	-0.38	0.24	-0.34	-0.53	0.45	
δ 2H	-0.76	-0.47	-0.39	0.20	-0.32	-0.53	0.45	
d-excess	0.18	0.04	0.07	-0.36	0.27	0.20	-0.15	
(b)	P_hysplit	H_hysplit	T_hysplit	D_hysplit	Regional factors vs. Local factors			
P_AL	0.13	0.23	0.04	0.03				
H_AL	0.38	0.17	0.21	0.10				
T_AL	-0.21	0.05	0.17	-0.33				
(c)	P_hysplit	H_hysplit	T_hysplit	D_hysplit	Regional factors vs. Regional factors			
P_hysplit	1							
H_hysplit	0.77	1						
T_hysplit	0.59	0.67	1					
D_hysplit	-0.10	-0.17	-0.49	1				
(d)	P_AL	H_AL	T_AL	Local factors vs. Local factors				
P_AL	1							
H_AL	0.20	1						
T_AL	-0.14	-0.78	1					

To further corroborate this finding, linear regression was performed for different seasons to derive seasonal LMWL's and relations between local humidity and $\delta^{18}O$ and d-excess. Table 2.3 suggests that secondary fractionation processes are likely to take place in the dry season between December 2014 and May 2015. This is depicted by a slope of lower than 8 (slope = 6.9) for the dry season, the slightly negative correlation between $\delta^{18}O$ and local relative humidity, and the markedly positive correlation between humidity and d-excess. This is a distinctly different behavior compared to the rainy season as a whole, but also for the first (early monsoon) and second (late monsoon) parts of the rainy season. In summary, these findings indicate that secondary fractionation processes influence the isotopic composition of precipitation primarily in the dry season, which is characterized by lower humidity and higher temperature in the Plain of Reeds. While this conclusion is plausible due to the climatic conditions and low rainfall amounts, one has to consider the low number of rainfall samples during the dry season, which associates some uncertainty to this analysis.

Table 2.3: Results of the linear regression analysis between local relative humidity (H_AL) and isotopic values at An Long. Regressions that are statistically significant at the 0.05 level are marked in bold.

	Linear regression line	r	R2	p-value	n	Period
δ^2H - $\delta^{18}O$	δ2H = 7.56*δ18O+7.26	0.99	0.99	< 0.001	74	full year
	δ2H = 7.62*δ18O+7.74	0.99	0.99	< 0.001	67	rainy season (Jun-Nov)
	δ2H = 7.58*δ18O+7.21	0.99	0.98	< 0.001	42	early monsoon (Jun-Sep)
	δ2H = 7.68*δ18O+8.6	0.99	0.99	< 0.001	25	late monsoon (Oct-Nov)
	δ2H = 6.9*δ18O+3.98	0.98	0.96	< 0.001	7	dry season (Dec-May)
$\delta^{18}O$ - Humidity	δ18O = -0.51*H_AL+36.05	-0.53	0.28	< 0.001	74	full year
	δ18O = -0.46*H_AL+32.09	-0.47	0.22	< 0.001	67	rainy season (Jun-Nov)
	δ18O = -0.33*H_AL+21.84	-0.42	0.17	0.006	42	early monsoon (Jun-Sep)
	δ18O = -0.83*H_AL+63.12	-0.61	0.37	0.001	25	late monsoon (Oct-Nov)
	δ18O = -0.56*H_AL+41.34	-0.88	0.77	0.010	7	dry season (Dec-May)
d-excess - Humidity	d-excess = 0.2*H_AL-6.36	0.20	0.04	0.090	74	full year
	d-excess = 0.13*H_AL-0.46	0.13	0.02	0.301	67	rainy season (Jun-Nov)
	d-excess = 0.18*H_AL-5.35	0.21	0.04	0.211	42	early monsoon (Jun-Sep)
	d-excess = -0.08*H_AL+17.44	-0.07	0.01	0.734	25	late monsoon (Oct-Nov)
	d-excess = 0.34*H_AL-19.42	0.31	0.10	0.455	7	dry season (Dec-May)

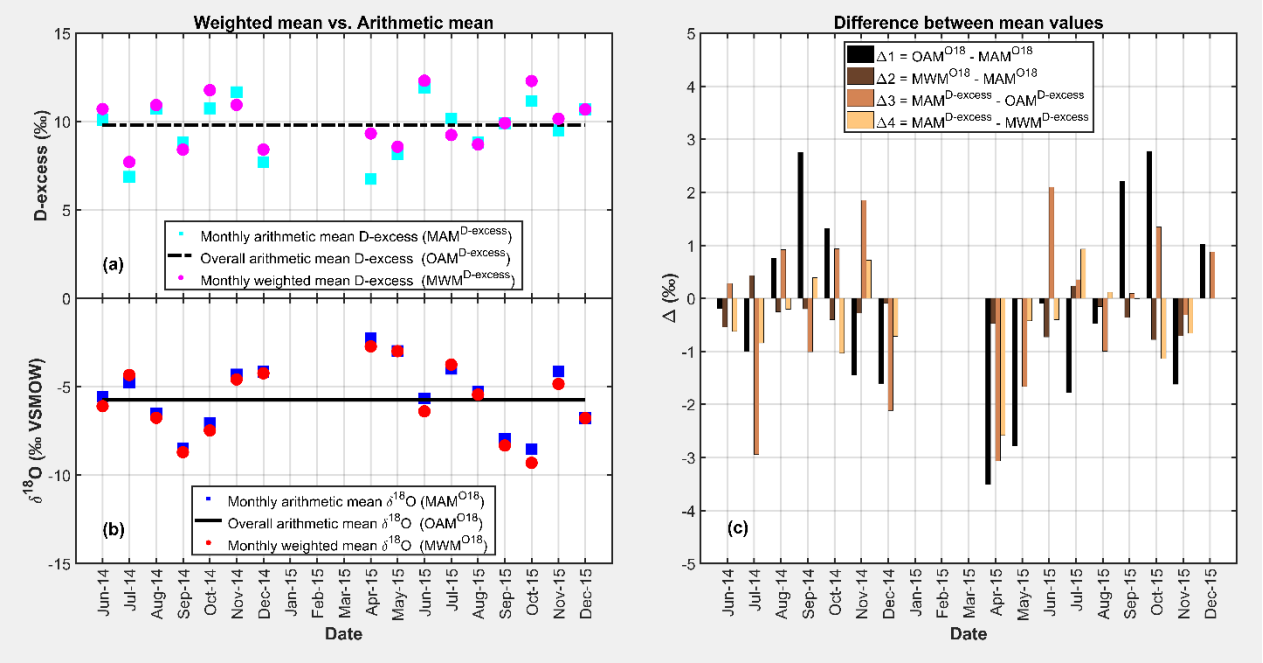

Figure 2.10: Monthly arithmetic mean (MAM) versus overall arithmetic mean (OAM), and monthly arithmetic mean (MAM) versus monthly amount-weighted mean (MWM) for d-excess (a) and $\delta^{18}O$ (b) at An Long during the sampling period June 2014 to December 2015. The difference between these mean values (c) including $\Delta^1 = OAM^{18O} - MAM^{18O}$, $\Delta^2 = MWM^{18O} - MAM^{18O}$ for $\delta^{18}O$, and $\Delta^3 = MAM^{Dexcess} – OAM^{Dexcess}$, $\Delta^4 = MAM^{Dexcess} – MWM^{Dexcess}$ for d-excess are shown to examine in which month secondary fractionation processes are likely significant (defined by all values of Δ in that month smaller than zero).

2.4.3.2 Regional factors and isotopic composition of precipitation

In comparison to other regional and local parameters, the precipitation amount along the transport pathways of moisture sources (P_hysplit) shows the strongest correlation with $\delta^{18}O$ and $\delta^{2}H$ as depicted by a correlation coefficient of -0.76 (Table 2.2a). Other predictors show weaker correlations with $|r| < 0.55$. This, however, does not exclude that these predictors do have some predictive power for the isotopic composition of precipitation in An Long when used in combination with other predictors. Although $\delta^{18}O$ and $\delta^{2}H$ are rather well correlated with some climatic parameters, d-excess (which is a function of both) is not well correlated. This is because of the relative difference of the variation of $\delta^{18}O$ and d-excess, which is expressed by a low correlation coefficient between two these variables (r = -0.44). The weak correlation between d-excess and all climatic parameters ($|r|<0.36$) indicates that the selected predictors (i.e., selected climatic parameters) are not sufficient to explain the processes responsible for the variability of the d-excess. On a global scale, drivers controlling d-excess variation are likely sea surface temperature or near-surface relative humidity of moisture sources (Pfahl and Wernli, 2008; Uemura et al., 2008; Pfahl and Sodemann, 2014), which are not considered in this study. In tropical areas, a major contribution to the seasonal variation in d-excess can be convective processes, e.g.

re-evaporation and rain–vapor interactions (Risi et al., 2008a; Risi et al., 2010a), or the influence of large-scale processes, e.g. conditions at the vapor source, convection and recycling of moisture along trajectories (Landais et al., 2010). A complete investigation of factors controlling d-excess in precipitation is thus not possible by the presented study design and selected predictors. However, some conclusions about the factors controlling the d-excess can be obtained with the presented method, see below.

2.4.4 MLR and relative importance analysis

The results of the MLR with all predictor combinations indicate that $\delta^{18}O$ signal in precipitation at An Long is best explained by moisture sources of 5-day backward trajectories (Figure 2.11). The MLRs using the predictors of these trajectories produces the lowest PRESS and highest R^2 values, indicating that about 80% of the variability of precipitation $\delta^{18}O$ (Figure 2.11) and $\delta^{2}H$ (not shown) at An Long can be explained by the best MLR model. However, the explained variance differs only slightly between the different pressure levels used. The best performance regarding the lowest PRESS value was obtained by the mean backward trajectories of the 800 hPa and 850h Pa levels.

Contrary to $\delta^{18}O$ and $\delta^{2}H$, the MLR fails to explain the variation of d-excess over the whole study period to a large extent, with a maximal R^2 of 0.3 (Figure 2.11). This indicates that the climatic parameters used in our MLR models have an only little impact on the annual d-excess variation, which corroborates the findings of the linear correlation analysis in section 4.3.2.

In the next step, the importance of the MLR predictors was analyzed. Figure 2.12 shows the results applying Johnson's relative weight analysis for the best performing MLR models, i.e. using the mean of the 800 hPa and 850 hPa 5-day backward trajectories. In general, the predictive power of the MLR models increases with increasing number of predictors.

The results indicate that regional factors are always more important than local factors if the R^2 value is above 0.5. The local factors dominate only in MLR models with low performance, or when no regional factors are used as predictors. This is also highlighted by the sum ratio line (black line in Figure 2.12), defined as the fraction of R^2 explained by regional factors normalized to the overall R^2. In the best MLR model (124^{th} model) with the lowest PRESS value and an R^2 of 0.80, which is equivalent to an explained variance of 80%, the regional factors explain 56% of the absolute $\delta^{18}O$ variance (which is equivalent to 70% relative to R^2 = 0.80), while local factors explain only 24% (30% relative to R^2 = 0.80). This result agrees with the two-factor analysis of Ishizaki et al. (2012) who stated that distillation during transport from source regions is the dominant contributor to inter-annual variability of $\delta^{18}O$ precipitation in Bangkok, Bombay, and Hong Kong, accounting for 70%, 60% and 70% relative to the overall explained variance, while the amount of local precipitation contributed the remaining 27%, 33%, and 25% of the explained variance, respectively.

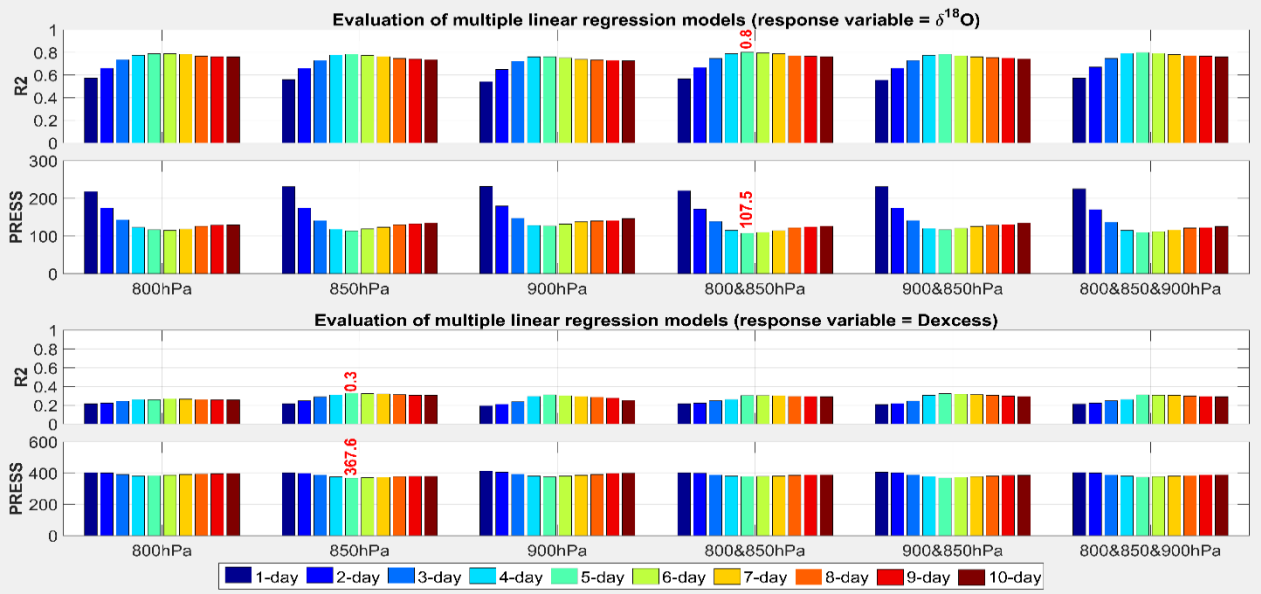

Figure 2.11: Evaluation of multiple linear regression (MLR) models applied for $\delta^{18}O$ and d-excess as response variables for different pressure levels used for three HYSPLIT backward trajectories and their combinations (mean values of the different levels). The best MLR model is marked with red text.

In all models where precipitation amount along transport pathways from moisture source regions (P_hysplit) is included, this factor explains the highest proportion of R^2, which is always at least double and up to triple of the explained variance of other factors (Figure 2.12). In turn, the absence of P_hysplit as a predictor in the MLR model considerably decreases the R^2, indicating that P_hysplit is the most dominant factor. In the best MLR model (124^{th} model) the most important predictor is P_hysplit, explaining 47% of the total $\delta^{18}O$ variance (partial $R^2 = 0.47$, Figure 2.12). The second dominant factor is T_AL, accounting for 21% of the explained the total variance. The remaining factors account for less than 13% of the $\delta^{18}O$ variance. This result indicates that the regional amount effect is a dominant process in controlling isotopic variation, whereas the local amount effect is not important in the VMD. Similar findings are reported for other regions in Asia (e.g. Rozanski et al., 1992; Araguás-Araguás et al., 1998). The local temperature T_AL, however, can be regarded as a modulating factor for the isotopic composition on top of P_hysplit.

In a next step, the predictor importance analysis is performed for different seasons, to analyze if seasonal differences in the dominating factors for the isotopic composition exist, as the correlation analysis of local factors and isotopic composition suggests (section 4.3.1). The samples were split into dry season and rainy season subsets, for which the MLR was applied individually. The definition of the seasons follows the analysis in section 2.2, i.e., the dry season lasts from December to May. However, due to the low number of samples during this period, the dry season samples were taken from mid-November to mid-June in order to increase the sample number, thus enabling a more robust MLR fitting. This selection can be justified: Because the delineation

of the dry and wet season above is based on monthly data, the "sharp" distinction between the rainy and dry season is forced by the temporal resolution of the data used. In reality, the transition between rainy and dry season is somewhat gradual. Thus the delineation between the rainy and dry season should rather be regarded as fuzzy. Using data from the last two weeks of November and the first two weeks of June can be seen as one way to consider this.

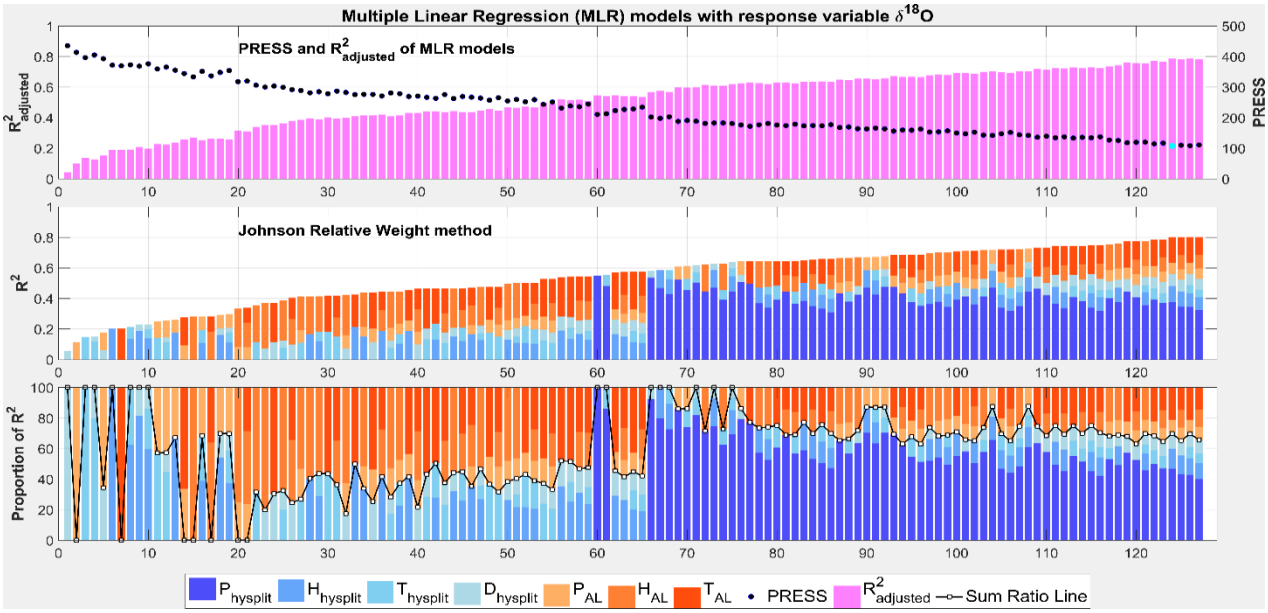

Figure 2.12: MLR with response variable $\delta^{18}O$ and relative importance analysis applied for all possible subsets. The 127 MLR models are sorted according to their R^2 values in ascendant order. Colors represent the relative contribution (in %) of the predictors. The sum ratio line separates the contribution of local (in red and orange) and regional (in blue) factors. PRESS and adjusted R^2 values indicate the quality of the MLR model. The best MLR model depicted by the lowest PRESS (model 124, highlighted by the cyan dot) explains 80% of the $\delta^{18}O$ variation (R^2 = 0.8).

Furthermore, the rainy season was subdivided according to the different moisture source regions shown in section 2.4.1: the Indian Ocean, dominating during the initial and high stage of the Indian monsoon from June to September/mid-October, and the South China Sea – Philippine Sea and the North-West Pacific Ocean from October to May during the late rainy and dry seasons, with some contribution from continental Asia (Figure 2.5). In order to test if the factors have different importance caused by different source regions during the rainy season, the MLR models and relative importance analysis were applied for these two time periods in addition to the dry season. The number of samples for the different subsets was 42, 18 and 14 for the early rainy season, late rainy season and dry season, respectively. This reduced number of data points need to be considered when interpreting the results of the seasonal MLR analysis, because the degrees of freedom of the regression (i.e. the difference between the number of data points and the number of predictors) are getting rather small, particularly for the dry season.

Figure 2.13 shows the results of the MLR and importance analysis for the three seasonal subsets for $\delta^{18}O$. The sorting of the models is the same as in Figure 2.12. On a first glance, the results for the rainy season subsets (Figure 2.13a, b) are quite similar to each other and to the overall data set. The best performing model in terms of the lowest PRESS value is in all cases the model 124. However, in terms of R^2, the performance of the early rainy season is somewhat lower compared to the overall data set, while for the late rainy season it is significantly better, with $R^2 = 0.96$. This increase in explained variance is caused by an increased contribution of the regional factors. In the late rainy season, the regional factors alone contribute 76% to the overall R^2 of 0.96 of the best PRESS model, which equals 79% of the explained variance (Table 2.4). The final best models (both for annual and seasonal analyses) are presented in

Table 2.5.

Table 2.4: Explained variance (partial R^2) of regional and local factors of the best MLR model according to the PRESS value. The first value indicates the absolute partial R^2, the second value the relative contribution to the overall explained variance.

	Whole period	Early rainy season	Late rainy season	Dry season
Regional factors	0.56 | 70%	0.51 | 68%	0.76 | 79%	0.14 | 22%
Local factors	0.24 | 30%	0.24 | 32%	0.20 | 21%	0.51 | 78%
Total	0.80 | 100%	0.75 | 100%	0.96 | 100%	0.65 | 100%

This is a much larger contribution compared to the partial R^2 values of 56% and 51% for the whole data set and the early rainy season, respectively. The increase stems from a more significant importance of the other regional factors H_hysplit and/or T_hysplit. While their contribution to the whole data set and the early rainy period is rather low and P_hysplit dominates the contribution of the regional factors, it is raised to about 30% in the late rainy season, either individually or in combination. For the best PRESS model marked with the cyan dot in Figure 2.13b, T_hysplit contributes 27% to the overall R^2 of 0.96. It indicates that temperature and humidity play a more significant role in the isotopic fractionation along the trajectories of water stemming from the North-West Pacific/South China Sea and continental Asia compared to water originating from the Indian Ocean during the boreal summer months. The broad regional and thus climatic heterogeneity of water sources during the late rainy season offers a plausible explanation for this result. The source regions during this period are located in oceans and continental areas of higher latitudes outside the tropics, where vast climatic differences may occur during the transport along the trajectories. Therefore, fractionation processes caused not only by the rainfall amount but also evaporation and condensation are likely to have a significant effect on the final isotopic composition of rainfall reaching An Long during this period. This climatic variability along the transport pathways is much more substantial compared to the low climatic variability of the tropical Indian Ocean source region, where the rainfall during the early rainy seasons originates.

An entirely different picture reveals the MLR fitting and importance analysis for the dry seasons shown in Figure 2.13c. While the overall performance in terms of R^2 is comparable to the early rainy season, the importance of the local and regional factors is very different from the other seasons. For the dry season, the local factors dominate. In the best performing MLR model with the lowest PRESS value (cyan dot in Figure 2.13c), T_AL contributes 78% of the explained variance. Similar results are obtained for almost all of the MLR models. For the models with $R^2 > 0.5$, T_AL is the most important factor, followed by P_AL and H_AL with similar importance. The regional factors do not contribute more than 22% of the explained variance, if $R^2 > 0.6$. This finding corroborates the assumed higher importance of secondary fractionation processes during the dry season in the VMD, as already hypothesized in section 4.3.1. However, in combination with other predictors, T_AL seems to be a better predictor of the secondary fractionation processes compared to H_AL, which was used in 4.3.1. As T_AL and H_AL are closely correlated (Table 2.2), the findings of section 4.3.1 and the MLR of the dry season presented in this section agree well. With regard to the low degrees of freedom for the dry season MLR models, it can be stated that this consistent high importance of the local factors in various MLR models reduces the uncertainty of this analysis stemming from the low number of data points to some extent.

The MLR modeling of δ^2H shows very similar results to $\delta^{18}O$ leading to the same conclusions (see Appendix A2). The MLR modeling of seasonal d-excess also shows an improved fit for the late rainy and dry seasons (see Appendix A3), while for the early rainy season the results are not as satisfying as for the whole dataset. In contrast to $\delta^{18}O$ and δ^2H, regional factors explain the bulk of the d-excess variance also for the dry season. Among the regional factors, P_hysplit has the lowest importance for d-excess, while the others factors T_hysplit, H_hysplit, and D_hysplit explain about 65% of the best R^2 of 0.66. This is also a distinctively different result compared to $\delta^{18}O$ and δ^2H, where P_hysplit always dominated the regional factor contribution. The remaining explained variance stems mainly from the local precipitation P_AL, with some contribution of T_AL. This finding is in line with the rationale outlined in section 4.3.1, that evaporation along the transport pathway decreases the d-excess (Stewart, 1975). This effect is much more variable during the late rainy and dry season due to the transport pathways from higher latitudes, as compared to the rather uniform climatic conditions along the transport pathways during the rainy season, as already argued in the previous paragraph for the late rainy season results of $\delta^{18}O$. Particularly the water stemming from continental Asia is very likely prone to evaporation and thus changes in d-excess along its transport pathways as it crosses some semi-arid areas (e.g. Tibet, Mongolia, cf. Figure 2.5). This means in summary that the MLR and relative importance analysis of d-excess for the late rainy and dry season corroborate the hypothesis that secondary fractionation processes caused by evaporation are relevant during the dry season, respectively for rainfall stemming from the Pacific region and continental Asia. However, for $\delta^{18}O$ and $\delta^{18}H$ local factors describing evaporation are more critical, while for d-excess regional factors and thus evaporation processes

along the transport pathways dominate. But again, the low number of data points for the dry season needs to be taken into account for the interpretation of the results. Although the results are similar over a wide range of different MLR models corroborating the findings, and although the mechanism explaining the results are plausible, the results for the dry seasons still contain some uncertainty stemming from the low data volume.

Table 2.5: The final best models (both for annual and seasonal analyses) for $\delta^{18}O$, $\delta^{2}H$, and d-excess as the response variable in MLR.

	Multiple Linear Regression (MLR) models	R2	R2 adjust	p-value	n	Period
$\delta^{18}O$	$\delta^{18}O$ = (-0.116)*P_hysplit + (-0.033)*P_AL + (0.118)*H_hysplit + (1.043)*T_AL + (0.078)*D_hysplit - 40.64	0.80	0.79	1.9E-22	74	full year
	$\delta^{18}O$ = (-0.101)*P_hysplit + (-0.041)*P_AL + (0.311)*T_hysplit + (1.128)*T_AL + (0.104)*D_hysplit - 41.42	0.75	0.72	4.3E-10	42	early monsoon (Jun-Sep)
	$\delta^{18}O$ = (-0.113)*P_hysplit + (-0.018)*P_AL + (0.461)*H_AL + (-0.404)*T_hysplit + (1.603)*T_AL - 77.59	0.96	0.94	7.1E-08	18	late monsoon (Oct-Nov)
	$\delta^{18}O$ = (-0.369)*T_hysplit + (2.493)*T_AL - 68.43	0.65	0.58	3.3E-03	14	dry season (Dec-May)
$\delta^{2}H$	$\delta^{2}H$ = (-0.894)*P_hysplit + (-0.224)*P_AL + (0.826)*H_hysplit + (7.744)*T_AL + (0.513)*D_hysplit - 289.23	0.79	0.78	5.9E-22	74	full year
	$\delta^{2}H$ = (-0.792)*P_hysplit + (-0.313)*P_AL + (2.220)*T_hysplit + (8.390)*T_AL + (0.679)*D_hysplit - 295.19	0.74	0.71	9.4E-10	42	early monsoon (Jun-Sep)
	$\delta^{2}H$ = (-0.914)*P_hysplit + (-0.094)*P_AL + (3.045)*H_AL + (-2.615)*T_hysplit + (12.044)*T_AL - 547.97	0.97	0.95	1.7E-08	18	late monsoon (Oct-Nov)
	δ2H = (-3.446)*T_hysplit + (19.923)*T_AL - 529.90	0.67	0.61	2.2E-03	14	dry season (Dec-May)
d-excess	d-excess = (0.034)*P_hysplit + (0.029)*P_AL + (0.206)*H_AL + (-0.421)*T_hysplit + (-0.148)*D_hysplit + 3.05	0.33	0.28	4.2E-05	74	full year
	d-excess = (0.346)*H_AL + (-0.311)*T_hysplit + (-0.162)*D_hysplit - 8.00	0.38	0.33	3.7E-04	42	early monsoon (Jun-Sep)
	d-excess = (0.049)*P_AL + (-0.532)*H_AL + (-1.989)*T_AL + (-0.228)*D_hysplit + 113.98	0.65	0.54	6.0E-03	18	late monsoon (Oct-Nov)
	d-excess = (0.105)*P_AL + (-0.300)*H_hysplit + (1.013)*T_AL + (0.202)*D_hysplit - 6.41	0.66	0.51	3.1E-02	14	dry season (Dec-May)

The MLR modeling of δ^2H shows very similar results to $\delta^{18}O$ leading to the same conclusions (see Appendix A2). The MLR modeling of seasonal d-excess also shows an improved fit for the late rainy and dry seasons (see Appendix A3), while for the early rainy season the results are not as satisfying as for the whole dataset. In contrast to $\delta^{18}O$ and δ^2H, regional factors explain the bulk of the d-excess variance also for the dry season. Among the regional factors, P_hysplit has the lowest importance for d-excess, while the others factors T_hysplit, H_hysplit, and D_hysplit explain about 65% of the best R^2 of 0.66. This is also a distinctively different result compared to $\delta^{18}O$ and δ^2H, where P_hysplit always dominated the regional factor contribution. The remaining explained variance stems mainly from the local precipitation P_AL, with some contribution of T_AL. This finding is in line with the rationale outlined in section 4.3.1, that evaporation along the transport pathway decreases the d-excess (Stewart, 1975). This effect is much more variable during the late rainy and dry season due to the transport pathways from higher latitudes, as compared to the rather uniform climatic conditions along the transport pathways during the rainy season, as already argued in the previous paragraph for the late rainy season results of $\delta^{18}O$. Particularly the water stemming from continental Asia is very likely prone to evaporation and thus changes in d-excess along its transport pathways as it crosses some semi-arid areas (e.g. Tibet, Mongolia, cf. Figure 2.5). This means in summary that the MLR and relative importance analysis of d-excess for the late rainy and dry season corroborate the hypothesis that secondary fractionation processes caused by evaporation are relevant during the dry season, respectively for rainfall stemming from the Pacific region and continental Asia. However, for $\delta^{18}O$ and $\delta^{18}H$ local factors describing evaporation are more critical, while for d-excess regional factors and thus evaporation processes along the transport pathways dominate. But again, the low number of data points for the dry season needs to be taken into account for the interpretation of the results. Although the results are similar over a wide range of different MLR models corroborating the findings, and although the mechanism explaining the results are plausible, the results for the dry seasons still contain some uncertainty stemming from the low data volume.

Nevertheless, it can be stated that applying all possible subset regression, MLR models can much better explain the isotopic variation in rainfall compared to approaches considering only one predictor, i.e., a simple correlation analysis. Moreover, the associated relative importance analysis enables the identification of the dominant factors, thus offering interpretation aids for the identification of the processes responsible for the isotopic signature of local rainfall. The presented analysis illustrates that the investigation of dominant factors controlling isotopic composition in precipitation with simple correlation analyses may lead to wrong conclusions, particularly when predictors are correlated. Additionally, MLR is able to consider the combination of different local and regional factors, thus enabling a better identification and interpretation of the manifold processes controlling the isotopic composition of rainfall.

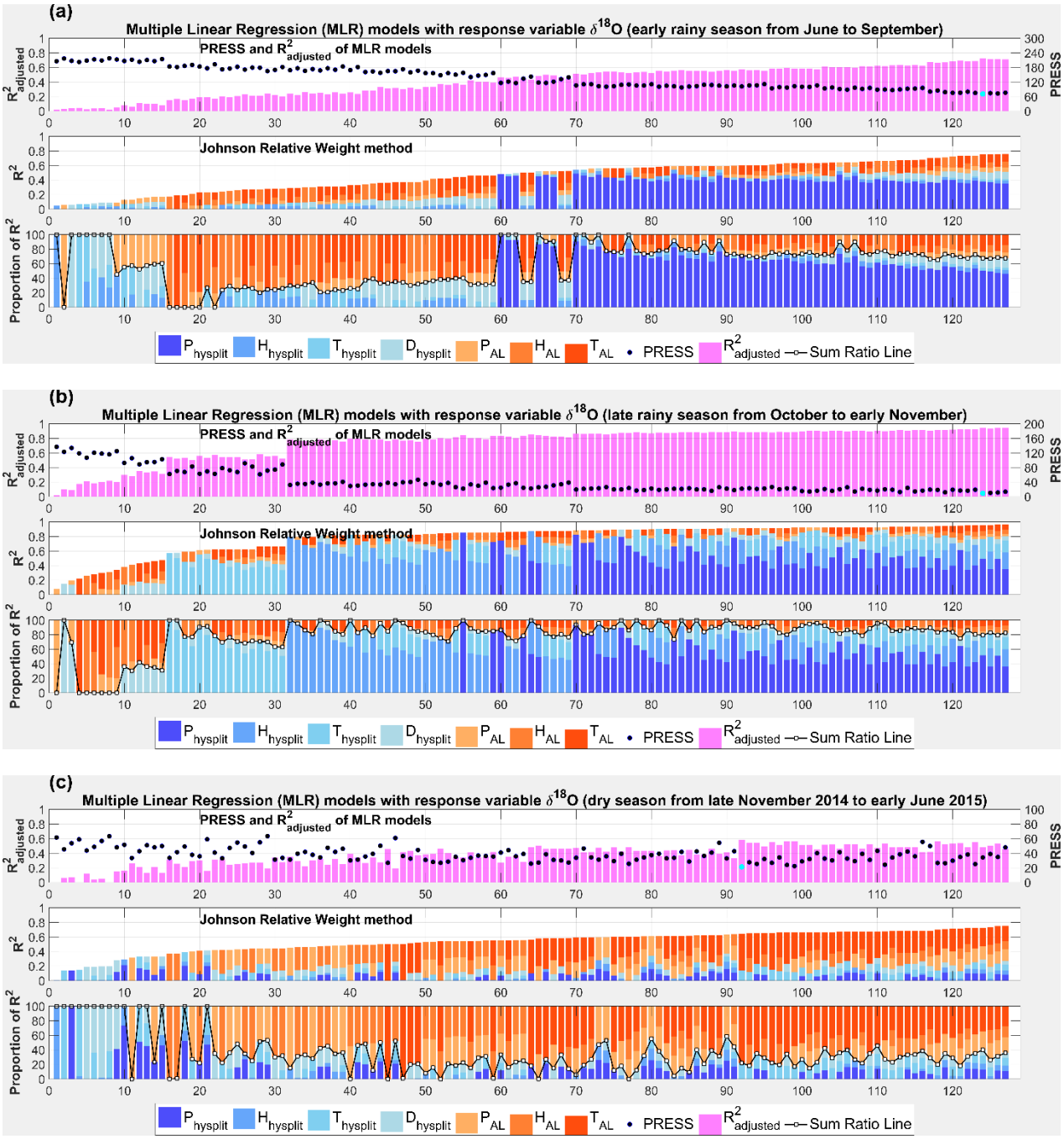

Figure 2.13: MLR with response variable $\delta^{18}O$ and relative importance analysis applied for all possible subsets (127 MLR models) for different seasons: a) early monsoon from June to September, b) late monsoon from October to mid-November, and c) the dry season from mid-November to mid-June.

2.5 Conclusions

This study analyzes the influence of local and regional meteorological factors on the isotopic composition of precipitation, expressed as $\delta^{18}O$, $\delta^{2}H$, and d-excess, in the Vietnamese Mekong Delta (VMD). For this purpose, rainfall samples were taken on a weekly to bi-weekly basis for 1.5 years at An Long in the North-Eastern part of the VMD, and analyzed for stable water isotopes. The regional factors potentially influencing isotopic composition were derived by back-tracing of water particles up to 10 days from the target location using the HYSPLIT model, while the local factors were derived from local climate records. The influence of the different factors on the isotopic condition was quantified by multiple linear regression (MLR) of all factor combinations combined with relative importance analysis. This method is novel for the interpretation of isotopic records of rainfall and opens a pathway for a better understanding of the controlling processes with a rather simple statistical method.

The MLR showed that up to 80% of the total variation of $\delta^{18}O$ could be explained by linear combinations of the selected factors. Similar results are obtained for $\delta^{2}H$. Contrary to this, only about 30% of the total variation of the d-excess can be explained by the selected factors, if the whole data series is used. General considerations regarding the controls of d-excess in tropical areas suggest that additional factors, like sea surface temperatures of the source region, need to be taken into account for an improved modeling of d-excess variation by MLR.

The study showed that local climatic factors, specifically rainfall amount and temperature, play a minor role in controlling the isotopic composition of the rainfall at An Long. However, there is evidence that sub-cloud evaporation has a small but notable effect during the dry season. Regional factors, on the contrary, dominate the isotopic composition of rainfall at An Long. 70% of the explained variance, i.e., a partial R^2 of up to 0.56, can be attributed to regional factors, among which precipitation amount along the transport pathway can explain most of the variance. The remaining 30% of the explained variance is attributed to local factors, among which the temperature plays the most important role. These findings indicate that local secondary fractionation processes like sub-cloud evaporation play a small additional role for the isotopic composition, which is otherwise dominated by the rainout along the transport pathway of the precipitation.

Furthermore, the analysis of transport durations implies that the moisture-producing precipitation reaching An Long travels about 4-6 days from its source, as the best regression results are obtained for these travel durations. For longer travel durations the explained variability of the regression decreases, suggesting that the moisture is recycled, i.e., precipitated and evaporated again, when the travel time exceeds six days.

If the data set is divided into seasonal subsets defined by precipitation amount and water source regions, the MLR and importance analysis enables a better identification of factors and thus

processes controlling the isotopic composition in the different seasons. For the late rainy and dry seasons (i.e., October to May), the importance of regional (late rainy season) and local (dry season) factors increases, respectively, compared to the overall dominating factor P_hysplit. Because of this the explained variance is raised, particularly for the late rainy season. The source regions (Pacific ocean and continental Asia) and the associated transport pathways as well as local processes are more critical for the late rainy and dry season, indicating that secondary fractionation processes by evaporation, either along the pathway (for d-excess) or locally (for $\delta^{18}O$ and $\delta^{2}H$), are more important than the amount effect, which is dominant during the Indian monsoon (early rainy season) period. This is reasonable, because moisture transported to the Mekong Delta from the Pacific region and continental Asia passes through different climatic regimes, compared to the more uniform climatic conditions along the pathway from the Indian Ocean during the Indian summer monsoon.

In summary, it can be concluded that the proposed approach, consisting of simultaneous testing of all possible factors by MLR combined with relative importance analysis, is able to detect the relevant factors controlling the isotopic composition of rainfall as well as their individual contributions. If applied to seasonal data subsets, the predictions can be improved, and the seasonal differences in controlling factors and processes can be identified. The validity of the approach is confirmed by similar, but mainly qualitative results obtained in other studies. The comparable results provide a strong indication that the method is able to identify the dominant factors responsible for the isotopic composition of rainfall records. In contrast to previous studies, the presented approach and results provide, however, a quantitative assessment of the impact of different factors, and thus information about the dominant processes of isotopic fractionation. It can support the interpretation of processes responsible for observed patterns of isotopic composition. The rather simple approach can, of course, not provide detailed information about atmospheric dynamics, but it offers a relatively simple and easy to apply approach supplementing or preceding more complex studies of isotopic composition with circulation models. Due to the simplicity, the method can be easily applied to investigate factors controlling isotopic composition in precipitation at any given study area around the world without the requirement of setting up and in-depth knowledge about running complex numerical atmospheric circulation models. Furthermore, the approach is easily reproducible and contains a rigorous quantitative analysis of the interplay of different driving factors. The analysis can easily be extended to other factors and processes of importance, e.g. in order to capture the d-excess particularly better by including sea surface temperatures at the source regions. However, a sufficient number of data points (multiple times of the number of predictors) is required to obtain robust regression results.

The similarity of isotopic signatures and their variability over Southeast Asia, as well as similar general climatic conditions, allows the conclusion that the findings are representative for a larger area. Particularly the similarity of the variability of the monthly isotopic composition of rainfall,

and climatic conditions of the VMD and Bangkok suggests that the results are representative for the whole Mekong Delta, and possibly for large areas of the southern tip of the continental Indochinese Peninsula.

The results have direct implications for the interpretation of paleorecords of stable water isotopes in terms of past climate conditions for Southeast Asia. This study shows that the factors controlling the isotopic signature of precipitation are changing between and even within seasons, and that regional factors have substantial impacts on the local isotopic composition of rainfall. This needs to be considered in the reconstruction of past climates based on isotopic records: for the presented study area $\delta^{18}O$ and $\delta^{2}H$ values are likely to be representative of the local climatic conditions during the dry season. However, regional factors dominate during most of the rainy season receiving the bulk of the total annual rainfall. In this case, reconstructions of past climates based on paleo isotopic records would have to be carefully interpreted. The proposed approach might open a pathway for an improved reconstruction of paleoclimates based on isotopic records. It may e.g. be used for identifying suitable variables to improve the performance of proxy data assimilation in paleoclimate reconstruction by circulation models. Moreover, assuming that the general circulation is stable over the period considered in paleoclimate reconstruction, which is reasonable for e.g. the Holocene, the presented findings can be used to infer moisture source regions and the strength of the two monsoonal regimes influencing SE-Asia from paleo isotopic records.

Chapter 3 Identification of groundwater mean transit times of precipitation and riverbank infiltration by two-component lumped parameter models

This chapter has been published as:

Le Duy, N., Dung, N. V., Heidbüchel, I., Meyer, H., Weiler, M., Merz, B., & Apel, H. (2019). Identification of groundwater mean transit times of precipitation and riverbank infiltration by two-component lumped parameter models. Hydrological Processes, 33(24), 3098-3118. DOI: https://doi.org/10.1002/hyp.13549

Abstract

Groundwater transit time is an essential hydrologic metric for groundwater resources management. However, especially in tropical environments, studies on the transit time distribution (TTD) of groundwater infiltration and its corresponding mean transit time (mTT) have been extremely limited due to data sparsity. In this study, we primarily use stable isotopes to examine the TTDs and their mTTs of both vertical and horizontal infiltration at a riverbank infiltration area in the Vietnamese Mekong Delta (VMD), representative of the tropical climate in Asian monsoon regions. Precipitation, river water, groundwater, and local ponding surface water were sampled for 3 to 9 years and analysed for stable isotopes ($\delta^{18}O$ and $\delta^{2}H$), providing a unique data set of stable isotope records for a tropical region. We quantified the contribution that the two sources contributed to the local shallow groundwater by a novel concept of two-component lumped parameter models (LPMs) that are solved using $\delta^{18}O$ records.

The study illustrates that two-component LPMs, in conjunction with hydrological and isotopic measurements, are able to identify subsurface flow conditions and water mixing at riverbank infiltration systems. However, the predictive skill and the reliability of the models decrease for locations farther from the river, where recharge by precipitation dominates, and a low-permeable aquitard layer above the highly permeable aquifer is present. This specific setting impairs the identifiability of model parameters. For river infiltration, short mTTs (<40 weeks) were determined for sites closer to the river (<200 m), whereas for the precipitation infiltration, the mTTs were longer (>80 weeks) and independent of the distance to the river.

The results not only enhance the understanding of the groundwater recharge dynamics in the VMD but also suggest that the highly complex mechanisms of surface–groundwater interaction can be conceptualized by exploiting two-component LPMs in general. The model concept could thus be a powerful tool for better understanding both the hydrological functioning of mixing processes and the movement of different water components in riverbank infiltration systems.

3.1 Introduction

Environmental isotopes have been used commonly to identify the dynamics of groundwater systems. Environmental isotope techniques can provide insights into the origin of water (Maloszewski, 2000), the interaction between surface and groundwater (e.g., Stichler et al., 1986; Stichler et al., 2008), subsurface flow conditions (McGuire et al., 2002), fundamental mixing processes (Stewart and Thomas, 2008), water transport (e.g., Maloszewski et al., 2002; Kabeya et al., 2007; Stewart et al., 2007), and recharge mechanisms (Koeniger et al., 2016) in the subsurface system. Given that the hydraulic properties of aquifers are poorly known and spatially variable, environmental tracer methods can provide more accurate groundwater flow velocities and recharge rates than traditional hydraulic methods (Cook and Böhlke, 2000). For example, numerical flow models can over- or underestimate the flow velocity depending on the aquifer thickness, the hydraulic conductivity, and the effective porosity (Zuber et al., 2011).

The groundwater transit time is an essential hydrologic metric that integrates the variety of subsurface flow paths, storage capacities, and mixing processes in the groundwater system. The mean transit time (mTT) describes the average time that water particles spend traveling through a system (McGuire and McDonnell, 2006), and the transit time distribution (TTD) describes the whole spectrum of transit times of those water particles transported through the system (Maloszewski, 2000). Knowledge of the TTD and its corresponding mTT is essential for groundwater resources management, for example, when installing groundwater extraction systems for water supply (Hiscock and Grischek, 2002), calibrating numerical groundwater transport models (Bethke and Johnson, 2008), evaluating the security of drinking water supplies (e.g., Darling et al., 2005; Eberts et al., 2012), or understanding the sources of contamination (e.g., Morgenstern et al., 2015).

Most mTT estimation methods are based on the lumped parameter model (LPM), pioneered by Małoszewski and Zuber (1982). The LPM does not require detailed hydrological information and thus can be used for initial investigations of little known systems (Mook and Rozanski, 2000) where data are insufficient, e.g., in developing countries or ungauged basins (McGuire and McDonnell, 2006). It is based on a lumped convolution integral (a black-box model), in which an input signal is related to a specific transfer function (or a TTD) to obtain an appropriate output signal. A common assumption for the application of LPM is the time-invariance of TTDs (see Maloszewski and Zuber, 1996; McGuire and McDonnell, 2006). Assuming steady-state conditions, LPMs can be set up to determine the best-fit TTD and mTT for the best representation of the local subsurface flow conditions (Maloszewski and Zuber, 1996). In reality, however, many systems are dynamic and stationary conditions hardly ever met (Rinaldo et al., 2011). LPMs can be applied in a moving-window approach (e.g., Hrachowitz et al., 2009) to estimate the time-variant transit times and examine the nonstationary of TTDs (e.g., Hrachowitz et al., 2010; Heidbüchel et al., 2012; Tetzlaff et al., 2014; Birkel et al., 2016).

Despite the long history and high potential of hydrological applications (Leibundgut et al., 2011), studies on mTT in tropical environments are still rare (Birkel et al., 2016; Mosquera et al., 2016), mainly due to financial constraints and data sparsity (Bonell and Bruijnzeel, 2005). Moreover, most of these studies have focused on water transit times in African (e.g., Jacobs et al., 2018), Australian (e.g., Lamontagne et al., 2015; Duvert et al., 2016), and/or Central and Latin American regions (e.g., Roa-García and Weiler, 2010; Muñoz-Villers and McDonnell, 2012; Timbe et al., 2014; Farrick and Branfireun, 2015; Timbe et al., 2015; Birkel et al., 2016; Mosquera et al., 2016; Muñoz-Villers et al., 2016). To our best knowledge, groundwater transit times from stable isotopes have never been quantified in Asian Monsoon regions.

Groundwater modeling in the Vietnamese Mekong Delta (VMD) was pioneered by Haskoning B.V., DWRPIS (Boehmer, 2000) who set up a regional groundwater model. The author pointed out that groundwater recharge in most of the delta ranges from 0.01 to 1 mm/d and is dominated by (i) infiltration of precipitation and irrigation water, (ii) downward leakage through the semi-permeable layers of the Holocene aquifer, and (iii) seepage from rivers, streams, and lakes. The water balance analysis suggested that recharge from rainfall and irrigation is significant (for the Plain of Reeds; see Figure 3.1) and slightly (for the whole VMD) smaller than that from the Mekong river branches and the canal system. Also, the hydraulic connection between shallow and deep groundwater is insignificant, except for the dune area along the coast of the eastern VMD (Boehmer, 2000).

Although groundwater has been determined to be closely linked to surface water in the Mekong floodplains (Kazama et al., 2007; Raksmey et al., 2009) or significantly controlled by rivers and tributaries (Wagner et al., 2012), groundwater modeling is still challenging due to the sparsity of groundwater data (Johnston and Kummu, 2012). Recent modeling studies have focused on understanding groundwater dynamics (Nuber et al., 2009; Vermeulen et al., 2013; Nam et al., 2017) and on evaluating land subsidence (Minderhoud et al., 2017). Despite the high demand on groundwater resources (Wagner et al., 2012) for household and industrial consumption (Danh and Khai, 2015), surface-groundwater interaction and groundwater recharge have not been sufficiently quantified (Thu, 2017). Instead, there has been considerable interest in the arsenic contamination of groundwater (Stanger et al., 2005; Shinkai et al., 2007; Buschmann et al., 2008; Kocar et al., 2008; Erban et al., 2013; Merola et al., 2015) and general groundwater quality (Hoang et al., 2010; Wilbers et al., 2014; Le Luu, 2017; An et al., 2018) in the VMD. Also, tracer-based groundwater studies have primarily focused on qualitative aspects such as tracing the groundwater recharge sources (e.g., Ho et al., 1991; An et al., 2014; Thu, 2017; An et al., 2018). In other parts of the Mekong Delta, groundwater studies estimated the sources of recharge affected by evaporation, for example, from the wetland and ponds to the shallow groundwater in Cambodia (e.g., Lawson et al., 2013; Lawson et al., 2016; Richards et al., 2018).

In this study, we primarily used stable isotope ($\delta^{18}O$) time series to identify the mTTs of shallow groundwater and the optimized TTDs best describing the subsurface flow conditions when applying the two-component LPMs. The Plain of Reeds, serving as the seepage area for groundwater infiltration in the northwest region of the VMD (Boehmer, 2000), was chosen as a pilot area. For the sampling campaigns, the study site An Long in the Plain of Reeds (Figure 3.1) was selected, primarily considering logistic constraints. Although this area may not be representative for the entire Mekong Delta, the site is likely indicative of the general nature of the near-stream subsurface flow dynamics because of the low variation of lithology and topography (Nguyen et al., 2000) throughout the region. The information on subsurface mixing processes, the preferred flow pathways, and the transit times of water infiltration at riverbank areas resulting from long-term isotopic records could enhance the understanding of the groundwater dynamics as well as groundwater vulnerabilities in the VMD.

The general objective of this work was to test the applicability of two-component LPMs to examine TTDs and their mTTs in a riverbank infiltration system where two distinct water components are present. Our specific objectives were to (i) identify the dominant TTDs that best describe the subsurface flow conditions, (ii) quantify the subsurface mixing processes and the time-variant mTTs of water near the river bank, and (iii) determine the uncertainty associated with parameter identification and model performance.

3.2 Study area

The study area is located in the Plain of Reeds, in the VMD between latitudes 10°42’7"N to 10°48’9"N and longitudes 105°22’45"E to 105°33’54"E (Figure 3.1). The average elevation ranges from 1-4 m above sea level. The average annual rainfall is 1400-2200 mm, characterized by a distinct seasonal distribution (Renaud and Kuenzer, 2012; GSO, 2016). The annual average temperature is 27°C with monthly averages ranging from 25°C to 29°C. The annual average relative humidity ranges from 77% to 88%. The monthly evaporation rate ranges from 67 to 80 mm and 76 to 109 mm in the rainy and dry season, respectively (Renaud and Kuenzer, 2012; GSO, 2016).

The hydrogeological units in the VMD are classified according to their geological formation: the Holocene, the Pleistocene, the Pliocene, and the Miocene aquifer systems. At the study site, the target aquifer is the Holocene sediment sequence. It is characterized by the uppermost layer of silt and clay (low-permeable aquitard), overlying a layer of fine to coarse sands (high-permeable aquifer). The average depths of aquitard and aquifer are approximately less than 11 m and 30 m below ground level, respectively (Wagner et al., 2012; Minderhoud et al., 2017). The grain sizes defined for clay, silt, fine and coarse sand, and fine gravel are 1-4 µm, 4-63 µm, 63 µm–2 mm, and 2-8 mm, respectively (Wentworth, 1922). The hydraulic conductivity of aquitard and aquifer are 0.02-0.2 m/day (for silt and clay) and 12-200 m/day (for fine to coarse sands), respectively

(Boehmer, 2000). The effective porosity of clay and sand layers are 0.5 and 0.2, respectively (Benner et al., 2008).

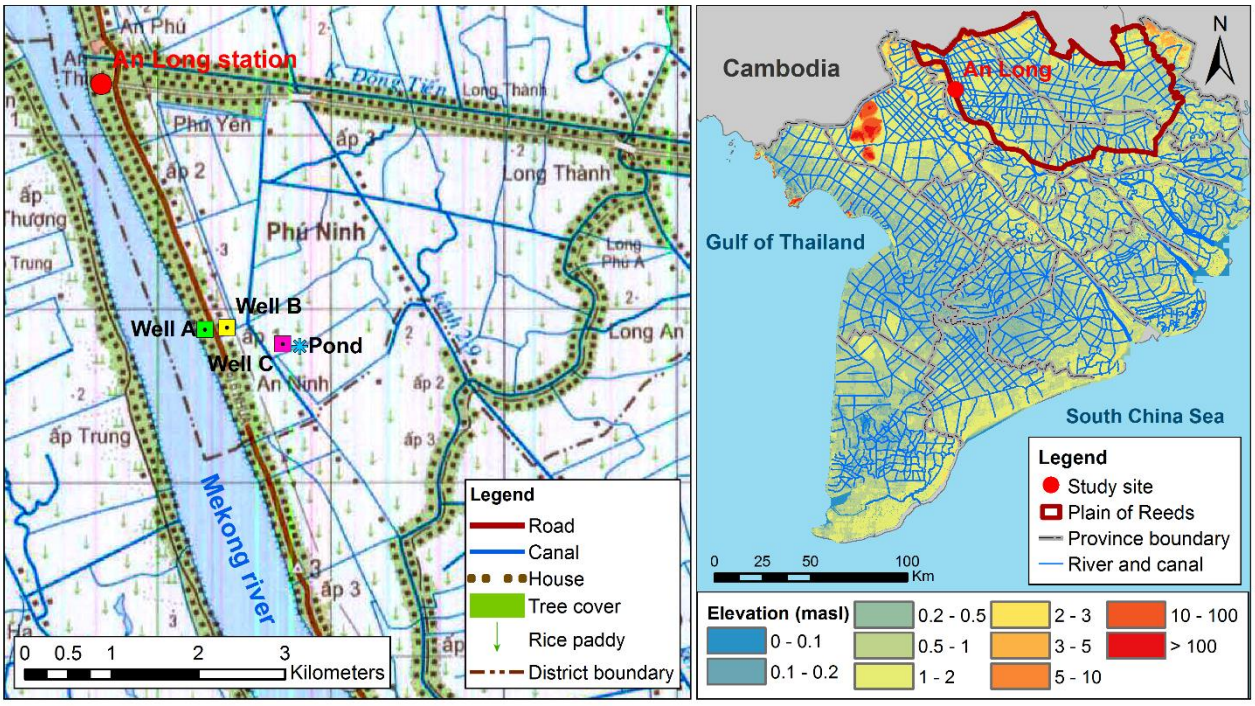

Figure 3.1: The Plain of Reeds in the Vietnamese Mekong Delta (right) and the study site (zoomed in) of An Long (left). The screening depths of Wells A, B, and C are 15, 12, and 14 m, respectively. The distance from Wells A, B, and C to the Mekong river is 140, 190, and 660 m, respectively. The pond with an area of approximately 500 m^2 and a depth of 2 m is used for fish farming. The distances from the pond to Well C and the Mekong river are around 40 and 700 m, respectively.

3.3 Methods

3.3.1 Water sampling and isotopic analysis

Precipitation and river water were sampled at An Long station. Groundwater was sampled at three wells (A, B, C) closed to the AnLong station and the Mekong river (Figure 3.1). The distances from Well A, Well B, and Well C to the Mekong river are 140 m, 190 m, and 660 m, respectively. The screening depths of these wells are 15 m, 12 m, and 14 m, respectively. These wells are used for household water supply only. Following the classification of aquifer systems by Wagner et al. (2012), the groundwater samples were collected from the Holocene aquifer and representative of the shallow groundwater in the VMD. A pond, located 700 m away from the Mekong river and used for fish farming, was included to provide information about the isotopic fractionation of local surface water by evaporation, characteristic for the floodplains during the monsoonal floods. The total number of samples and the schedule of water sampling are summarized in Table 3.1.

To avoid evaporation effects, we stored the collected samples in 30 mL plastic sample bottles with tight screw caps and kept all samples in the dark before the laboratory analysis. The stable isotope samples were analyzed at the Alfred-Wegener-Institute (AWI) in Potsdam, Germany. The measurements were performed with a Finnigan MAT Delta-S mass spectrometer using equilibration techniques to determine the ratio of stable oxygen ($^{18}O/^{16}O$) and hydrogen ($^{2}H/^{1}H$) isotopes. Analytical results were reported as $\delta^{2}H$ and $\delta^{18}O$ (‰, relative to Vienna Standard Mean Ocean Water - VSMOW) with internal 1σ errors of less than 0.8‰ for $\delta^{2}H$ and 0.1‰ for $\delta^{18}O$. The detailed measuring procedure is described in Meyer et al. (2000).

Table 3.1: Water sampling at An Long

	Period	Frequency	Number of samples
Precipitation	06.2014 – 06.2015	weekly	155
	06.2015 – 07.2017	sub-weekly	
River water	01.2009 – 05.2010	fortnightly	737
	06.2010 – 07.2017	sub-weekly	
Well A	06.2014 – 07.2017	weekly	157
Well B	06.2014 – 07.2017	weekly	157
Well C	06.2014 – 07.2017	weekly	157
Pond water	03.2016 – 12.2016	weekly	42

3.3.2 Hydrological measurements

Groundwater and river water levels were recorded every 15 min between June 2015 and July 2017 by pressure sensors (HOBO U20 Fresh Water Level Data Logger). River water levels were monitored at An Long station, about 2 km upstream of the wells. Groundwater levels were observed at two additional monitoring wells screened at a depth of 15 m below ground level, in order to avoid disturbance of the level records by water extraction. The first monitoring well was installed between Well A and Well B, and another one was located between Well C and the pond (Figure 3.1). The distance from the first and second monitoring wells to Well A and Well C are 20 m and 25 m, respectively. Sediment samples taken during the installation of these monitoring wells indicated that the upper aquitard layer (from 8 to 10 m below ground level) is dominated by clay and silty clay, while the aquifer layer below consists mainly of coarse sand. A terrestrial survey was carried out in June 2016 to reference all recorded water level measurements to the gauge at An Long, a national water level monitoring station. All water levels are reported as meters above sea level.

3.3.3 Two-component lumped parameter models

LPMs are based on the lumped convolution integral approach (Małoszewski and Zuber, 1982) to transform the tracer input signal (C_{in}) into the tracer output signal (C_{out}), considering a distribution

of transit times according to a transfer function. Stewart and McDonnell (1991) introduced a more robust approximation by adding flow weights (w) to the isotopic composition of the input so that the outflow composition reflects the mass flux of tracer leaving the system (McGuire and McDonnell, 2006)

$$C_{out}(t) = \frac{\int_0^\infty C_{in}(t-\tau)w(t-\tau)g(\tau)d\tau}{\int_0^\infty w(t-\tau)g(\tau)d\tau} \quad (3.1)$$

where τ is the transit time, t is the time of exit from the system, and (t − τ) represents the time of entry into the system; C_{in} and C_{out} are the input and output tracer signature, respectively; $g(\tau)$ is the transfer function representing the assumed TTD of the subsurface flow system. This modification is more flexible than other recharge adjustment techniques (e.g., Grabczak et al., 1984; Maloszewski and Zuber, 1996) as the weighting term w(t) can include any appropriate factor such as rainfall rates, throughfall rates, or effective rainfall (McGuire and McDonnell, 2006).

The recharge sources of shallow groundwater in the VMD are mainly river water and precipitation (Ho et al., 1991; Boehmer, 2000; Wagner et al., 2012). The output isotopic composition ($\delta^{18}O$) thus stems from the water of two different sources with likely different transit times. Therefore, the two-component LPMs were chosen for transit time modeling. We excluded a deep groundwater component because the connection between shallow and deep groundwater is insignificant (Ho et al., 1991; Boehmer, 2000; An et al., 2014). During the calibration, integrated parameters were adjusted to fit the measured isotopic records for each investigated well, following Weiler et al. (2003a). The model was re-written in a modified two-component convolution equation:

$$C_{Well}(\mathrm{t}) = p\frac{\int_0^\infty C_{inR}(t-\tau)w_R(t-\tau)g_R(\tau)d\tau}{\int_0^\infty w_R(t-\tau)g_R(\tau)d\tau} + (1-p)\frac{\int_0^\infty C_{inP}(t-\tau)w_P(t-\tau)g_P(\tau)d\tau}{\int_0^\infty w_P(t-\tau)g_P(\tau)d\tau} \quad (3.2)$$

where C_{inR}, C_{inP} is the input tracer signature of the river and precipitation infiltration, respectively; C_{Well} is the output tracer signature of an investigated well; $g_R(\tau)$, $g_P(\tau)$ are TTD functions of the river and precipitation infiltration, respectively; p and (1-p) are the fractions of the river and precipitation infiltration in the investigated well, respectively; the weighting terms w_R, w_P are defined as follows:

$$w_{Ri} = \frac{N\alpha_i^R Q_i}{\sum_{i=1}^N \alpha_i^R Q_i} \quad (3.3)$$

$$w_{Pi} = \frac{N\alpha_i^P P_i}{\sum_{i=1}^N \alpha_i^P P_i} \quad (3.4)$$

where

(i) N is number of measurements; Q_i is river discharge (m^3/s); P_i is rainfall amount at An Long station (mm);

(ii) river infiltration coefficient: $\alpha^R = 1$ and $\alpha^R = 0$ for periods when the river water level is higher (losing streams) and lower (gaining streams) than the groundwater level, respectively. In this sense, $\alpha^R = 1$ (or $\alpha^R = 0$) indicates mass flux (or no mass flux) of tracer infiltrated from the river to a well;

(iii) precipitation infiltration coefficient: $\alpha^P = 1$ for months with precipitation infiltration (months in the rainy season), and $\alpha^P = 0$ for months without precipitation infiltration (dry season). We assumed that rainfall infiltrating to the shallow groundwater in the dry season is not significant due to the thickness (~9 m) of the upper low-permeable aquitard (see Section 3.2) and the small rainfall amount during the dry season.

The fractions of the river (*p*) and precipitation (1-*p*) infiltration in each well can be derived by a linear mixing equation using long-term averages:

$$p = \frac{\overline{C_{well}} - \overline{C_{inP}}}{\overline{C_{inR}} - \overline{C_{inP}}} \tag{3.5}$$

where $\overline{C_{well}}$ is the mean $\delta^{18}O$ value of the investigated well; $\overline{C_{inR}}$ and $\overline{C_{inP}}$ are the weighted mean $\delta^{18}O$ values of river and precipitation infiltration (weighted by the weighting terms w_R and w_P, respectively).

3.3.4 Selection and combination of transit time distributions

We tested six TTDs commonly applied in hydrologic systems: the exponential, linear, exponential-piston flow, linear-piston flow, advection-dispersion (Maloszewski and Zuber, 1996; Cook and Böhlke, 2000), and the gamma model (Kirchner et al., 2000). While the exponential-piston flow and advection-dispersion models have been used in riverbank infiltration studies (e.g., Stichler et al., 1986; Maloszewski et al., 1992; Stichler et al., 2008; Kármán et al., 2014) and in groundwater studies (e.g., Cartwright and Morgenstern, 2016; Stewart et al., 2017), the exponential and gamma models have been widely applied for catchment mTT modeling (cf. McGuire and McDonnell, 2006; Hrachowitz et al., 2010).

Identifying TTDs that best describe the subsurface flow conditions requires both theoretical and experimental considerations (McGuire and McDonnell, 2006). Theoretically, the exponential distribution can only be applied for unconfined aquifers, while the combinations of exponential (or linear) and piston flow distributions or the advection-dispersion distribution are more applicable for partly confined aquifers (Małoszewski and Zuber, 1982; Maloszewski and Zuber, 1996). Considering the hydrogeological setting of the Holocene aquifer, characterized by the upper low-permeable aquitard and the lower high-permeable aquifer, the exponential

distribution (exhibiting flow lines with extremely short mTTs) seems therefore inappropriate for precipitation infiltration to wells screened at depth, but more adequate for riverbank infiltration to shallow groundwater (see Zuber et al., 2011). Hence, the optimization of two-component LPMs can be considered as an experimental approach to test the application of the selected TTDs.

Table 3.2: The TTD functions and their parameter ranges (assumed uniform distribution) for the GLUE analysis

Model	Transit time distribution $g(\tau)$	Parameter(s) range
Exponential distribution (E)	$\frac{1}{\tau_m} exp\left(\frac{-\tau}{\tau_m}\right)$	$\tau_m\ [1-250]$
Linear distribution (L)	$\frac{1}{2\tau_m}\ for\ \tau \le 2\tau_m$ $0\ for\ \tau > 2\tau_m$	$\tau_m\ [1-250]$
Exponential piston flow distribution (EPF)	$\frac{\eta}{\tau_m}\ exp\left(-\frac{\eta\tau}{\tau_m}+\eta-1\right)\ for\ \tau \ge\ \tau_m(1-\eta^{-1})$ $0\ for\ \tau <\ \tau_m(1-\eta^{-1})$	$\tau_m\ [1-250]$ $\eta\ [1-4]$
Linear piston flow distribution (LPF)	$\frac{\eta}{2\tau_m}\ for\ \tau_m-\frac{\tau_m}{\eta} \le \tau \le \tau_m+\frac{\tau_m}{\eta}$ $0\ for\ other\ \tau$	$\tau_m\ [1-250]$ $\eta\ [1-4]$
Advection – dispersion distribution (AD)	$(4\pi P_D\tau/\tau_m)^{-\frac{1}{2}}\frac{1}{\tau}exp\left[-\frac{(1-\tau/\tau_m)^2}{4P_D\tau/\tau_m}\right]$	$\tau_m\ [1-250]$ $P_D\ [0-1]$
Gamma distribution (G)	$\frac{\tau^{\alpha-1}}{\beta^{\alpha}\Gamma(\alpha)}exp(-\tau/\beta)$	$\tau_m\ [1-250]$ $\alpha\ [0.001-10]$ $\beta=\tau_m/\alpha$

Note: τ_m = subsurface mTT (weeks); η = parameter indicating the contribution of each flow type (dimensionless), expressed as the total volume/volume with exponential (or linear) TTD; P_D = dispersion parameter (dimensionless); α = shape parameter (dimensionless) and β = scale parameter (dimensionless). Γ is the Gamma function.

Typically, each TTD function requires one or two fitting parameters. Table 3.2 summarizes the equations, the fitting parameters, and the pre-defined parameter ranges of TTDs used. The initial parameter ranges were assumed to be bounded, uniform distributions:

(1) The range of the mTT (τ_m) was limited to a maximum of 250 weeks, equivalent to approximately the maximum 5 years that mTTs can be determined using stable isotopes of water (Maloszewski and Zuber, 1996; McGuire and McDonnell, 2006; Stewart et al., 2010).

(2) The range of the parameter η was set to [1-4]. This parameter indicates the contribution of the different flow types, expressed as the ratio of the total volume to the volume with an exponential (or linear) distribution. When η is equal to 1, the mixed model becomes the pure exponential (or linear) model. When η approaches infinity, the mixed model is a close approximation of the well-

known but unrealistic piston-flow model represented by a Dirac function. We limited the upper bound of η to 4 (equivalent to a maximum of 75% of piston flow in the TTD) to improve the convergence of the Monte Carlo simulations.

(3) The dispersion parameter (P_D) in the advection-dispersion model should not exceed 2 for a constant tracer input (Maloszewski and Zuber, 1996). To improve the convergence of Monte Carlo simulations, we limited P_D to 1 (cf. Cartwright and Morgenstern, 2016), which is appropriate for kilometer-scale flow systems (Mook and Rozanski, 2000).

(4) The range of the shape parameter (α) in the gamma model was limited to 10, following Timbe et al. (2014) and Stewart et al. (2017).

To set up the two-component LPMs, the free combination of two TTDs (e.g., the exponential combined with the dispersion model) would yield a large number of possible setups. This approach would require a multitude of assumptions, increase computational cost, and model uncertainties. For computational reasons, as well as to keep the model as simple as possible, we assumed that the TTDs of precipitation and river infiltration are of the same type (e.g. exponential or linear piston-flow TTDs). The number of models to be tested is thus equal to the number of selected TTDs. Theoretically unreasonable models, as e.g. the double exponential model, which includes an exponential TTD for precipitation, are also included in order to test the theoretical limitations with observations in the model fitting. The hypothesis is that theoretically unreasonable models should be rejected during the model fitting.

3.3.5 Model performance and uncertainty analysis

Monte Carlo experiments were used to find the best parameter sets. The generalized likelihood uncertainty estimation (GLUE) methodology (Beven and Binley, 1992) was applied to determine behavioral solutions (i.e., parameter sets giving acceptable predictions) and parameter identifiability. Due to the high number of fitting parameters, the analysis consisted of 10^6 iterations. For each model setup, the model performance was evaluated using the Kling–Gupta efficiency (KGE) (Gupta et al., 2009) for describing the model performance and the root mean square error (RMSE) for describing the mass balance. While the model performance based on KGE can be classified as good (KGE>0.75), intermediate (0.75>KGE>0.5), weak (0.5>KGE>0), and very poor (KGE<0), following Thiemig et al. (2013), there is no standard criterion to classify the performance based on RMSE. The model performance was therefore classified as satisfactory for KGE > 0.5. We finally used the solution with the Euclidean distance (D_E) between (1 - KGE) and RMSE as likelihood measures (see Eq. 3.6). The best 5% solutions in terms of D_E were selected as behavioral models, from which we constructed 90% confidence intervals of the estimated mTTs (see Timbe et al., 2014; Mosquera et al., 2016). We also examined the dotty plots to check that the selected solution provides a reasonably wide range of behavioral parameter set. In this study, D_E =1 indicates a perfect fit.

$$D_E = 1 - \sqrt{(1 - KGE)^2 + (RMSE)^2} \quad (3.6)$$

3.3.6 Data preparation

Since data were collected at different temporal resolutions, from fortnightly to sub-weekly, all data were aggregated to weekly-mean values for consistency. The early fortnightly river water samples were repeated in order to obtain a weekly time series. This simplification does not affect the mTT analysis, as these data were used for model warm-up only. The actual model fitting was performed for the period of sub-weekly sampling of both river water and precipitation.

Considering the different length of the input time series (nine years of river water and three years of precipitation, cf. Table 3.1), the time series of precipitation was repeated back to January 2009 using monthly weighted means from the three years of available data. This procedure implies a stable inter-annual variation of precipitation isotopes, a reasonable assumption in the VMD (see Duy et al., 2018). The approach does not change the results of the mTT estimation while giving the models more room to find stable results (Hrachowitz et al., 2011).

3.3.7 Modification of the input function

The isotopic fractionation of precipitation before infiltration (e.g., due to evaporation or mixing processes) should be considered during the calibration of LPMs. Precipitation falling on the ground likely mixes with local surface water (e.g., ponds, rice paddies, and irrigated, inundated, or wetland areas) and partly evaporates before infiltrating. We considered the vertical infiltration as a mix of local surface waters and precipitation, both affected by evaporation. This assumption is in line with the suggestion that both river and evaporated-surface-water sources recharge groundwater along the Mekong river (Lawson et al., 2013; Lawson et al., 2016; Richards et al., 2018). Therefore, the input of precipitation infiltration was corrected, considering isotopic enrichment caused by evaporation.

We modified the input functions by adding a correction factor (Δ) to the isotopic composition of precipitation. This factor accounts for the isotopic enrichment due to the evaporation and mixing processes before the infiltration. This value was assumed to be constant and was derived by accounting for the potential evaporation in the region. However, in order to quantify the uncertainty that is introduced by a constant correction factor, a sensitivity analysis of the model results to the isotopic correction of precipitation infiltration was conducted (cf. Section 3.3.8). All modified input functions are referred to as precipitation infiltration. The input of river infiltration was not isotopically corrected, implying no isotopic fractionation before and during the infiltration process.

3.3.8 Model setup

In order to get deeper insights into the model behavior, parameter identifiability, and uncertainties, three LPM setups were defined (Test 1, 2, and 3). The uncertainties were attributed to errors:

(1) the modified input functions (correction factor Δ),

(2) the mass balance analysis (value of *p* integrated into the two-component LPMs), and

(3) the assumed non-stationary or steady-state conditions during the calibration.

We assumed steady-state conditions to be dominant in the groundwater system and estimated time-invariant mTTs in Test 1 and 2. For Test 3, the two-component LPMs were applied in a moving-window approach (e.g., Hrachowitz et al., 2009; Heidbüchel et al., 2012) to examine the time-variant TTDs and their corresponding mTTs. The detailed setups of these tests are:

Test 1: Modified input functions

We varied the correction values (Δ^{var}) in the range between 0‰ and 5‰ (with increments of 0.2) to create 26 modified input functions. Δ^{var} = 0‰ indicates no isotopic enrichment and Δ^{var} = 5‰ (mean value + standard deviation) represents the likely maximum isotopic enrichment before infiltration. The upper limit is derived from the distribution of differences between isotopic content of rainfall and pond water. It represents the mean value + 1 standard deviation, i.e., the 84% quantile. Because we could not use another tracer (e.g., Cl) to independently assess the uncertainties of the mass balance analysis, the fraction of river infiltration was considered a fitting parameter (p^{cal}) and calibrated accordingly. Depending on the assumed TTD function, three or five parameters were fitted during the calibration with each of the 26 modified input functions. In this test, 9-year records of $\delta^{18}O$ were used (the first six years for a warm-up and the last three years for analysis).

Test 2: Mass balance

We fixed a correction value (Δ^{fix} = 1.81‰), defined by the isotopic difference between the arithmetic mean value of the pond water and the weighted mean value of precipitation. The aim was to match the mean values of the modified input function and the pond water, implying that the precipitation ponding on the ground is mixed with preexisting local surface water and partly evaporates before infiltrating to the groundwater. In this test, the fraction of river infiltration was pre-defined by Equation 3.5 and used as a fixed parameter (p^{fix}). The motivation for this test was that the contribution of river (or precipitation) infiltration should be identical independent of the selected TTDs. This was tested with this approach. Consequently, two or four fitting parameters (depending on the assumed TTD) were fitted with the modified input function created by Δ^{fix}. Similar to Test 1, we used 9-year records of $\delta^{18}O$.

Test 3: Non-stationarity

Non-stationarity is implicitly considered by the weighing according to discharge (Eq. 3.3), and the alpha coefficient determining the seasonal variation between losing and gaining stream conditions. However, possible additional non-stationarity caused by changes in the state of the surface-groundwater system were investigated. This was performed by a moving windows approach. Windows of 2-year length (adding previous six years for warm-up) were applied with a 2-week increment to create overall 29 sliding-window sequences of the isotopic time series. The window length was defined sufficiently long to accommodate the identified mTTs in Test 1 and 2, which vary up to almost two years (cf. Section 4.3). In this analysis, [Δ^{fix}, p^{fix}] were used to calibrate the two-component LPMs in order to avoid over-parametrization. For computational reasons, only the best-suited TTD identified in Test 1 and 2 was used to estimate the time-variant mTTs. The Bayesian information criteria (BIC) was selected as a parsimoniousness metric (Birkel et al., 2010; Hrachowitz et al., 2010) to identify the best-suited TTD. A lower BIC value suggests a better model, considering the model performance in relation to the number of fitting parameters.

$$BIC = n \ln\left(\frac{SSE}{n}\right) + k \ln(n) \tag{7}$$

where n is the number of observations, k is the number of fitting parameters, and SSE is the sum of squared errors.

3.4 Results

3.4.1 Surface-groundwater interaction

Considerable dynamics of surface-groundwater interaction were observed at the study site, as depicted by the similar water level variations up to 2 m annually in the river and groundwater (Figure 3.2). Seasonal changes in groundwater levels observed between Well A and Well B mostly lay between those found in Well C and the river. The groundwater level observed at wells closer to the river (Well A and Well B) exhibited a higher seasonal variation than the site farther from the river (Well C).

Gaining or losing stream conditions were defined as river water penetrating into the groundwater system, or groundwater seeping out into the river, respectively (Fetter, 2001). Losing stream periods (higher monthly river water level than groundwater level) were detected mainly during the flood season from July to November, whereas gaining stream periods were observed primarily during the end of the dry season from April to June (Figure 3.2). From December to February, the differences between river water and groundwater levels were insignificant. These months were considered as the transition period between losing and gaining stream conditions.

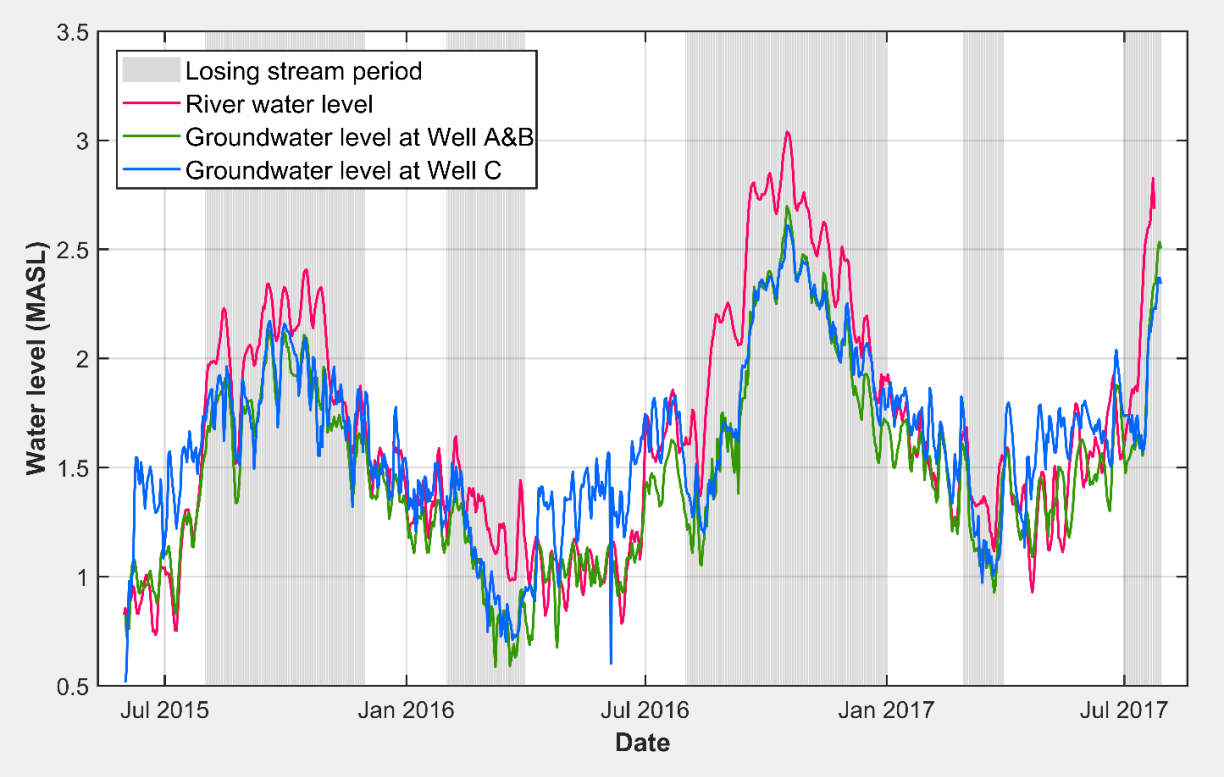

Figure 3.2: The daily groundwater and river water levels at An Long. Grey background indicates losing stream periods when the monthly river water level is higher than the monthly groundwater level

3.4.2 Stable isotope ratios

Figure 3.3 shows the isotopic datasets of precipitation, river, pond water, and groundwater on a dual-isotope plot of $\delta^{18}O$ and $\delta^{2}H$. The isotopic compositions vary between the dry and rainy seasons with more negative values during the rainy seasons. The precipitation $\delta^{18}O$ ranges between -13.7‰ and -1.0‰, with an arithmetic mean value and a standard deviation of -6.0‰ ± 2.5‰. The precipitation $\delta^{2}H$ varies between -98.7‰ and 0.9‰, with a mean and standard deviation of -38.6‰ ± 19.3‰.

The isotopic composition of river water showed a variation from -9.6‰ to -5.3‰ and -70.3‰ to -40.2‰ for $\delta^{18}O$ and $\delta^{2}H$, respectively. The arithmetic mean values and standard deviations for $\delta^{18}O$ and $\delta^{2}H$ were -7.6‰ ± 0.8‰ and -55.6‰ ± 5.9‰, respectively. The river samples plotted below the local meteoric water line (LMWL) and exhibited a regression line with a less steep slope than the LMWL.

The isotopic composition of pond water showed considerable variability ranging from -9.4‰ to 3.6‰ and -66.6‰ to 5.3‰ for $\delta^{18}O$ and $\delta^{2}H$, respectively. The arithmetic mean values and standard deviations for $\delta^{18}O$ and $\delta^{2}H$ were -4.6‰ ± 3.0‰ and -37.3‰ ± 15.8‰, respectively. The pond water exhibited an evaporation trend with a slope of 5.3, suggesting that the isotopic

enrichment is likely caused by evaporation taking place at 70–85% humidity (Clark and Fritz, 1997), comparable to the range of average annual relative humidity (77-88%) in the VMD.

All groundwater samples plot below the LMWL and are distinctly separated corresponding to the sampling wells. According to the distances from Well A (140 m), Well B (190 m), and Well C (660 m) to the river, more negative isotopic values were observed at the wells located closer to the river. The arithmetic mean values (± standard deviation) for $\delta^{18}O$ of Well A, Well B, and Well C were -6.1‰ ± 0.3‰, -5.5‰ ± 0.2‰, and -5.2‰ ± 0.6‰, respectively.

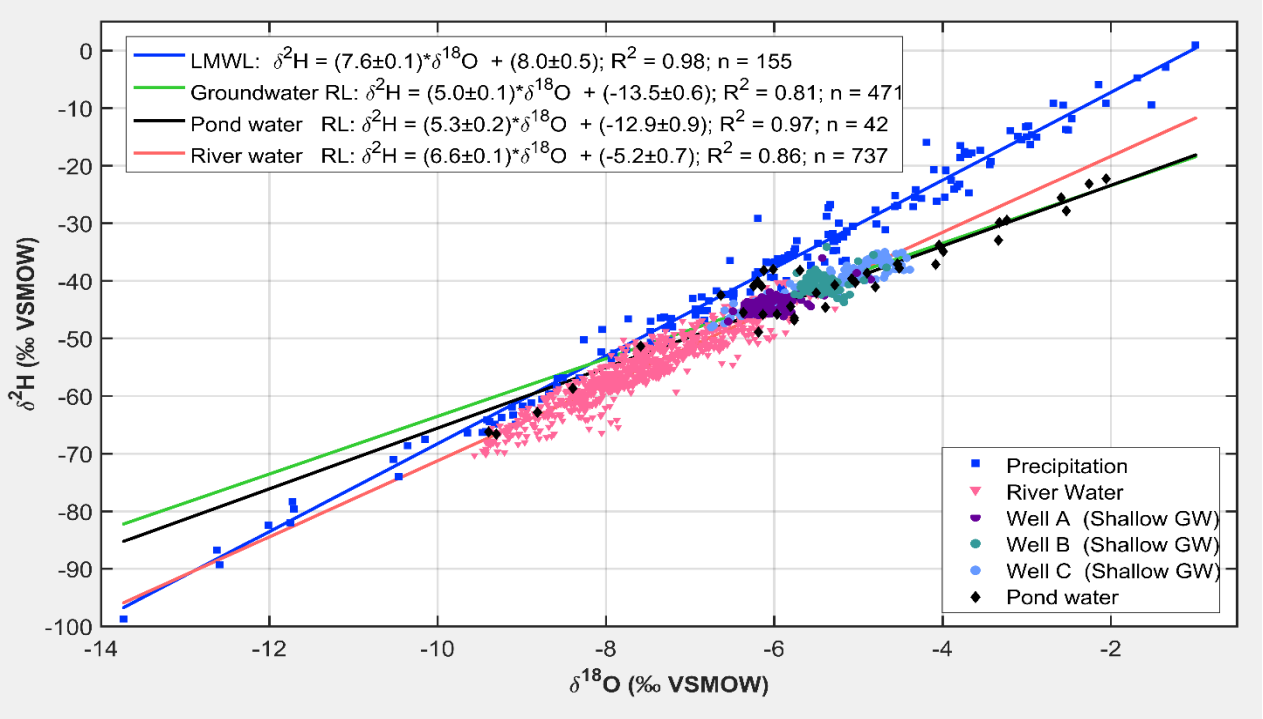

Figure 3.3: The isotopic data at An Long in a dual isotope plot. The regression line (RL) for groundwater is derived using all groundwater samples from all the wells. GW, groundwater; LMWL, local meteoric water line; VSMOW, Vienna Standard Mean Ocean Water

3.4.3 Stationary transit time modeling

Figure 3.4 shows the results of Test 1 for the three investigated wells considering the sensitivity of model performances and parameter identifiability to the isotopic correction (based on the likelihood measure D_E). The model performances based on KGE and RMSE statistics are shown in the Appendix B1. The fitting accuracy generally increased with an increasing correction factor (Δ^{var}) up to 1.4‰, remained stable around the peak for Δ^{var} between 1.4‰ and 2.6‰, and decreased slightly after that. The best performances were identified for the linear-piston flow (LPF) model (Figure 3.4d), followed by the advection-dispersion model (Figure 3.4e). Notably, the optimum correction value (Δ^{var} = 1.8‰), providing the best LPF model performance, was very close to the isotopic difference between the arithmetic mean value of the pond water and the weighted mean

value of precipitation (Δ^{fix} = 1.81‰). This supports the validity of the assumed fixed correction factor.

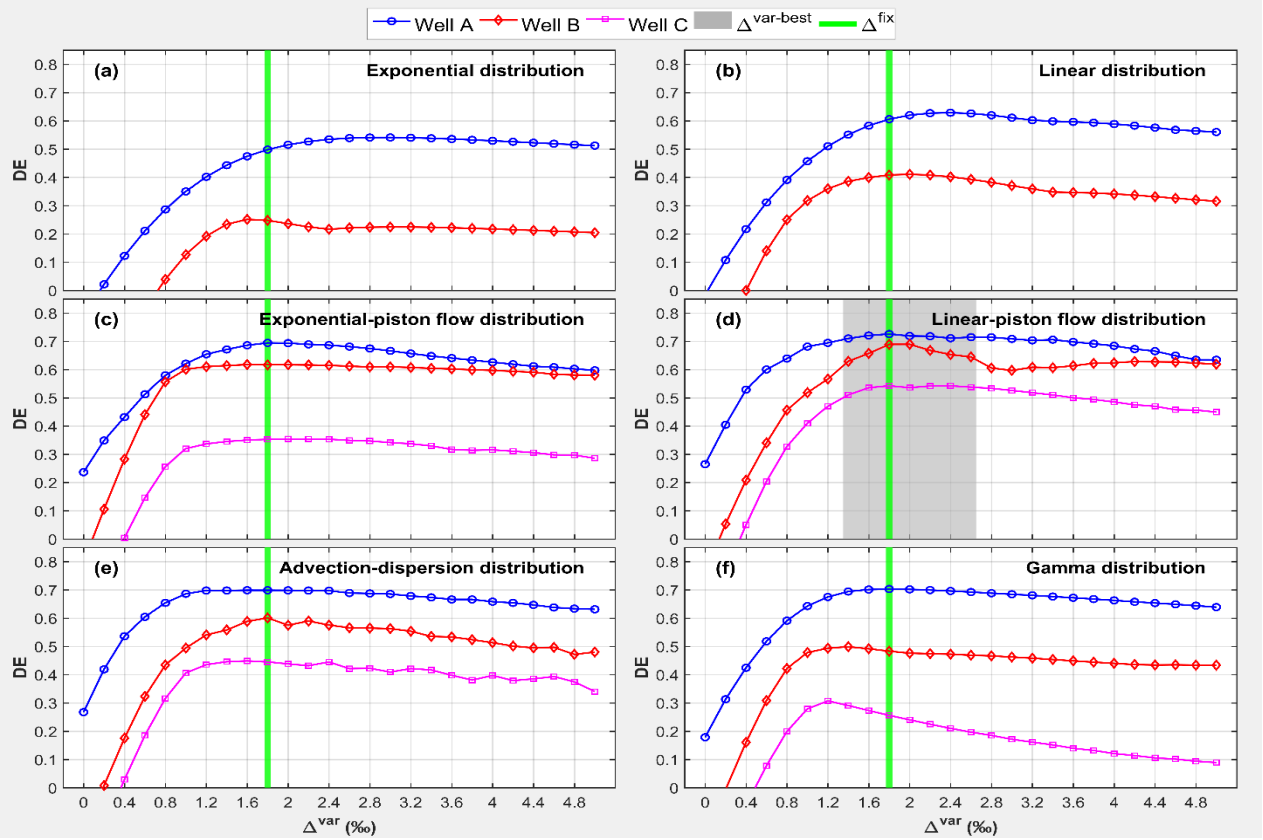

Figure 3.4: Sensitivity of the efficiency of two-component lumped parameter models to isotopic correction values (Δ^{var}) measured by using the Euclidean distance (DE) between (1 – Kling–Gupta efficiency [KGE]) and root mean square error values. The green reference line indicates the isotopic difference (Δ^{fix}) between the arithmetic mean value of the pond water and the weighted mean value of precipitation. $\Delta^{var\text{-}best}$ corresponds to the best-possible model performance and reasonable parameter identifiability (see Figure 3.5). Negative likelihood measures (DE < 0) are not shown

To evaluate the sensitivity of the parameter identifiability to the isotopic input correction, we focused on the LPF models providing the best-fit accuracies. The behavioral solutions (90% confidence bound of the GLUE analysis) corresponding to a threshold of 5% of the best predictions by LPF models are shown in Figure 3.5. For other TTDs, results of optimized behavioral solutions are shown in the Appendix B2.

Isotopic correction factors between 1.4‰ and 2.6‰ ($\Delta^{var\text{-}best}$ in Figure 3.4d and Figure 3.5a,b,c) provided both acceptable fitting accuracies (D_E> 0.5) and reasonable identifiability of mTTs. Therefore only the estimated mTTs obtained with these correction factors were considered for further analysis and discussion below.

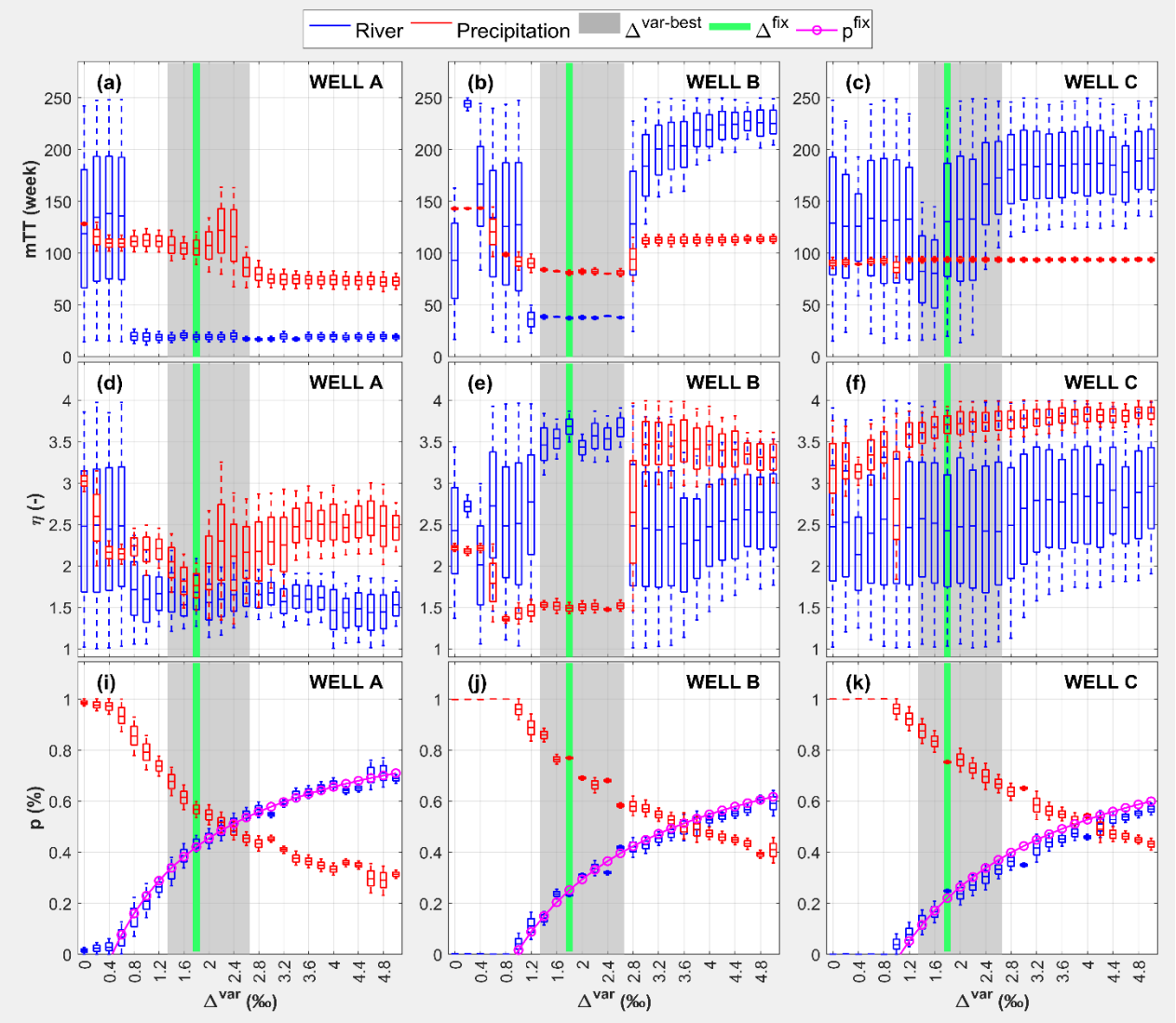

Figure 3.5: Sensitivity of the parameter identifiability of the linear piston flow model (i.e., the best-performing model) to the correction values (Δ^{var}) for all tested wells. The box plots indicate the 90% confidence intervals of fitting parameters given by the generalized likelihood

Considering each investigated well, the estimations of river mTTs were identical for the identified range of acceptable isotopic corrections (Figure 3.5 a,b,c, blue boxes in the gray shaded areas). Shorter mTTs of river infiltration were determined consistently for sites closer to the river. The optimized river mTTs ranged approximately from 15 to 20 weeks for Well A, from 35 to 40 weeks for Well B, and from 25 to 240 weeks for Well C. The parameter identifiability of river mTTs was better for the sites close to the river (e.g., Well A and B).

The behavioral solutions of precipitation mTTs were identical for wells B and C, independent of the isotopic correction and the distance of wells to the river. For Well A the behavioral mTTs were also very similar, with a tendency to a larger range for higher acceptable correction factors. Compared to river-bank infiltration, the precipitation infiltration exhibited longer mTTs. Optimized precipitation mTTs were between 75 and 110 weeks with low uncertainties for all tested sites

(Figure 3.5 a,b,c). However, the LPF model provided poor constraints of parameter η, indicating different ratios of linear or piston flows at different investigated sites (Figure 3.5 d,e,f). The uncertainty bounds of river infiltration fraction (p^{cal}) were quite narrow and increased with higher Δ^{var} (Figure 3.5 i,j,k). Analogously, the fraction of precipitation infiltration ($1-p^{cal}$) decreased with higher Δ^{var}.

Results in Test 2 were compared to the best-fit results in Test 1 (e.g., using Δ^{var} = 1.8‰), considering the model efficiency (Figure 3.6), the fractions of water components contributing to the shallow groundwater (Figure 3.5 i,j,k), and the behavioral solutions of optimized mTTs (Figure 3.7). The best-fit results (LPF models) of the tests are reported in Table 3.3. The model performances (corresponding to the best-matching likelihood measures) of these tests were comparable (Figure 3.6a,b,d,e) and relatively good (>0.7) in terms of the KGE statistic for all investigated wells. Although the model parsimoniousness is slightly better within the setups in Test 2, illustrated by lower BIC values (see Figure 3.6 c,f and Table 3.3), the dotty plots indicate that the parameter identifiability of two of these tests is comparable (see Appendix B3). Better parameter identifiability of river mTTs is observed for sites close to the river (e.g., Well A). Conversely, parameter identifiability of precipitation mTTs is much better for sites farther from the river (e.g., Well C).

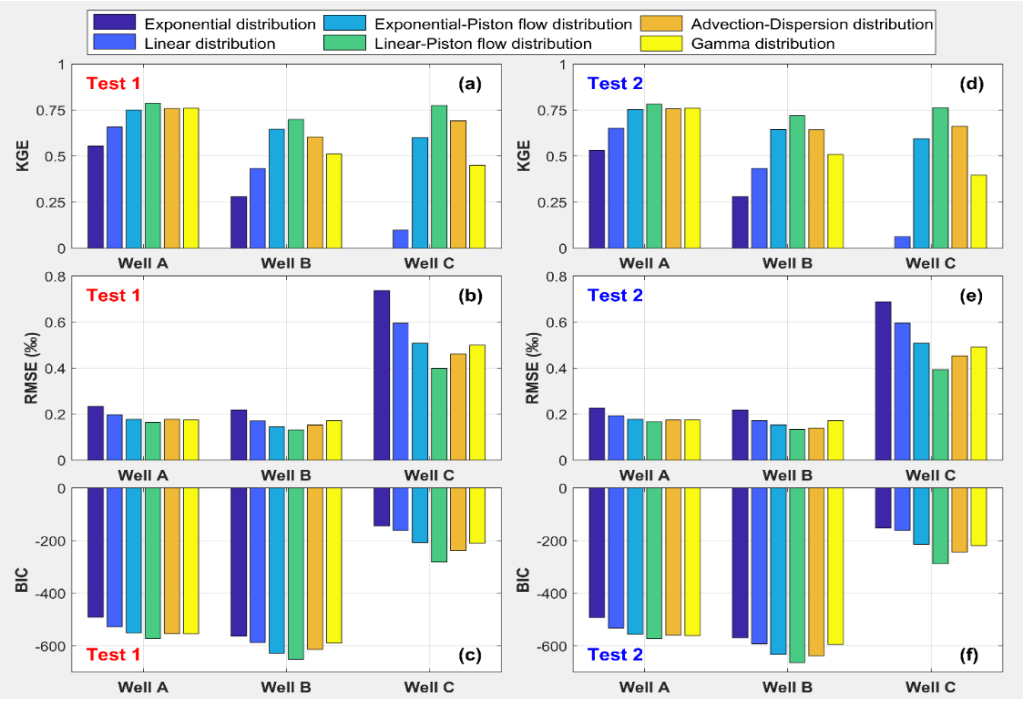

Figure 3.6: Comparison of Tests 1 (left) and 2 (right) for model efficiencies (the best performing models according to best likelihood measures). The two-component lumped parameter models were calibrated with [Δ^{var}, p^{cal}] and [Δ^{fix}, p^{fix}] for Tests 1 and 2, respectively. Negative Kling–Gupta efficiency (KGEs) are not shown. RMSE, root mean square error; BIC, Bayesian information criteria

Table 3.3: Statistical parameters of the observed and simulated δ18O time series by LPF models for Wells A, B, and C within the three model set-ups (Tests 1, 2, 3).

Test case	Observed[b]	Simulated[b]		Model efficiency[c]			Parameter[d]	Units	River			Precipitation		
	Mean ± σ (‰)	Mean ± σ (‰)	Bias (‰)	KGE (-)	RMSE (‰)	BIC			Best - fit	Behavioral solution		Best - fit	Behavioral solution	
										low	up		low	up
WELL A														
Test 1	-6.07 ± 0.26	-6.07 ± 0.25	0.004	0.79	0.16	-572	τ_m η p	week (-) %	17.5 1.83 41.9	14.5 1.36 37.9	18.8 1.98 46.0	94.4 1.86 58.1	92.1 1.62 54.0	109.9 1.95 62.1
Test 2	-6.07 ± 0.26	-6.08 ± 0.25	0.010	0.78	0.17	-573	τ_m η p	week (-) %	17.1 1.82 42.1	13.6 1.26	23.9 2.07	95.0 1.90 57.9	87.6 1.40	121.3 2.03
Test 3[a]	-6.10 ± 0.23	-6.10 ± 0.22	0.00	0.74	0.16	-392	τ_m η p	week (-) %	18.2 1.71 43.2	15.6 1.28	22.3 1.91	107.0 1.98 56.8	83.9 1.39	135.9 2.60
WELL B														
Test 1	-5.45 ± 0.18	-5.46 ± 0.17	0.01	0.70	0.13	-651	τ_m η p	week (-) %	38.3 3.44 24.7	35.3 3.44 21.0	39.5 3.88 27.8	83.0 1.55 75.3	78.8 1.45 79.0	86.1 1.56 72.2
Test 2	-5.45 ± 0.18	-5.47 ± 0.18	0.02	0.72	0.13	-664	τ_m η p	week (-) %	36.8 3.77 25.1	35.5 3.26	40.0 3.78	82.3 1.52 74.9	78.9 1.42	85.9 1.61
Test 3[a]	-5.47 ± 0.15	-5.48 ± 0.15	0.01	0.72	0.12	-472	τ_m η p	week (-) %	41.4 2.97 25.7	32.9 1.97	67.4 3.73	88.1 1.68 74.3	80.4 1.44	96.6 1.87
WELL C														
Test 1	-5.25 ± 0.63	-5.22 ± 0.58	-0.03	0.78	0.40	-282	τ_m η p	week (-) %	58.0 2.90 20.0	17.2 1.06 24.7	240.7 3.91 26.0	93.7 3.75 80.0	91.0 3.50 75.3	96.4 3.96 74.0
Test 2	-5.25 ± 0.63	-5.27 ± 0.57	0.02	0.76	0.39	-287	τ_m η p	week (-) %	62.3 3.62 22.0	15.5 1.00	169.8 4.00	93.5 3.75 78.0	91.1 3.49	96.4 4.00
Test 3[a]	-5.43 ± 0.65	-5.59 ± 0.59	0.17	0.72	0.47	-162	τ_m η p	week (-) %	38.3 2.86 27.1	27.0 1.41	57.0 3.81	93.7 3.78 72.9	91.1 3.46	96.2 3.97

Note: [a]Mean values of the 29 best-fit LPF models are reported; [b]σ: standard deviation; [c]KGE: Kling–Gupta efficiency; RMSE: Root mean square error; BIC: Bayesian information criteria; [d]τm: tracer's mTT; η: parameter indicating the ratio of total volume/volume with exponential (or linear) TTD; p: fraction of recharge from river (or precipitation) infiltration; (−): dimensionless.

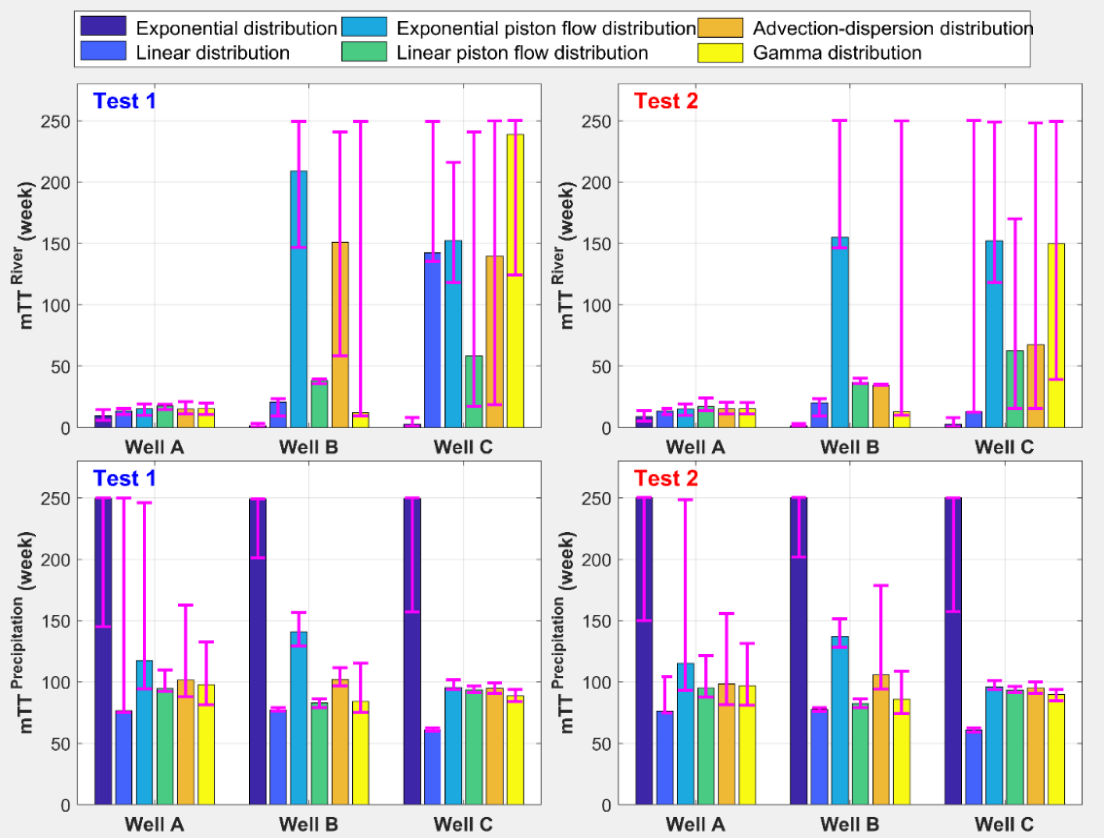

Figure 3.7: Estimated mean transit times (mTTs) of river (top) and precipitation (bottom) infiltration in Tests 1 (left) and 2 (right). The error bars indicate the 90% confidence intervals of mTT given by the generalized likelihood uncertainty estimation analysis

3.4.4 Identification of best-suited TTD

Out of all 18 models (three tested sites and six models per site), the threshold of model acceptance (KGE > 0.5) was fulfilled in 13 cases (Figure 3.6a,d). The five poor models with KGE < 0.5 were the exponential (E), the linear (L), and the gamma (G) models at two sites located farther from the river (Well B and Well C). The exponential-piston flow (EPF), the linear-piston flow (LPF), and the advection-dispersion (AD) models provided satisfactory performances for all sites. Unsurprisingly, the more complex models (EPF, LPF, AD, and G) performed better than the simpler models (E and L), depicted by higher KGE and lower RMSE values. However, a better fit obtained with a higher number of adjustable parameters does not necessarily mean that an adequate model was found. Based on the model selection criterion (the lowest BIC), the best performing model type for all sites was the LPF model (Figure 3.6c,f). The other goodness-of-fit measures (KGE and RMSE, Figure 3.6a,b,d,e) confirmed this ranking. Although the LPF model can better constrain the behavioral solutions of optimized mTTs (Figure 3.7), the dotty plots illustrate comparable parameter identifiability for all tested models (see Appendix B3). Figure 3.8 shows the best-fit modeled $\delta^{18}O$ of LPF models and the uncertainty interval (90 % confidence bound of the GLUE analysis).

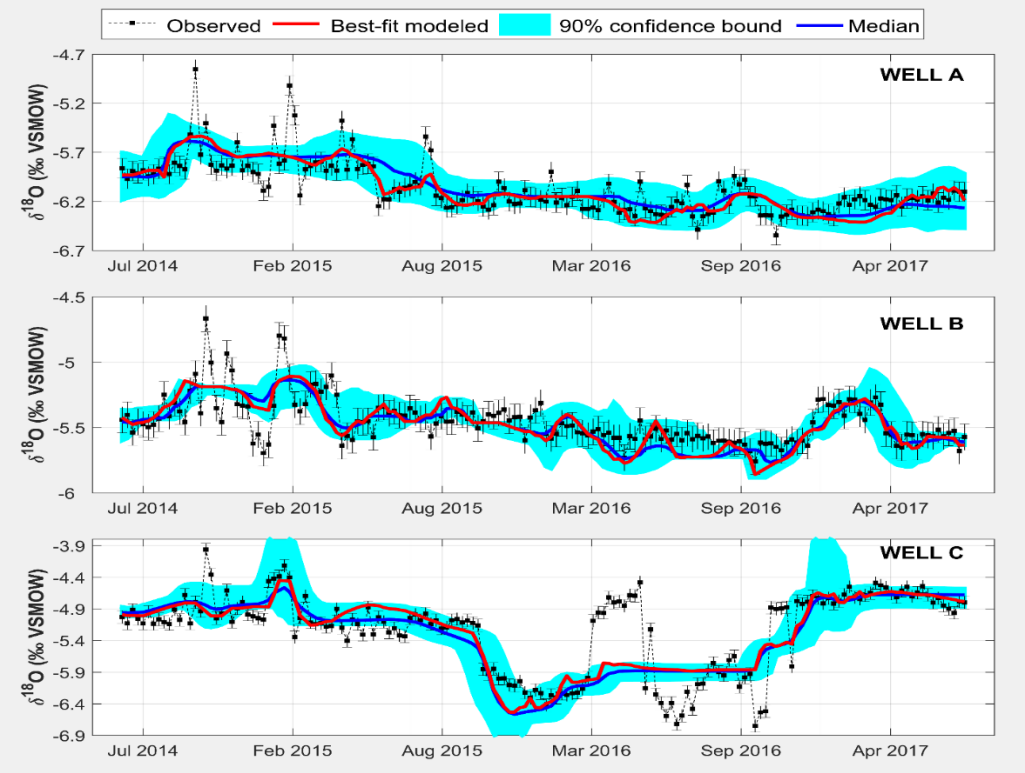

Figure 3.8: The observed and modelled $\delta^{18}O$ plotted with the behavioural solutions (90% confidence bound of generalized likelihood uncertainty estimation analysis) corresponding to a threshold of 5% of the best prediction by the linear-piston flow models. Error bars indicate the analytical reproducibility of the $\delta^{18}O$ measurements. VSMOW, Vienna Standard Mean Ocean Water

3.4.5 Time-variant transit time modeling

Following the identification of the best-suited TTD, we calibrated the LPF model within the moving window approach (Test 3) to estimate time-variant mTTs. The 2-year moving window with 2-week increments resulted in 29 best-fit LPF models for the study period from June 2014 to July 2017. Figure 3.9 shows varying model performance, a wide range of mTTs, and their associated parameter uncertainties (90% confidence limits) derived from the GLUE analysis. For all 29 models, the goodness of fit measured by the KGE statistic were reasonable (>0.5), suggesting reliable estimations of time-variant mTTs.

Considering each investigated well, the best-fit mTTs of river infiltration were identical (stable in time) with acceptable parameter uncertainties (Figure 3.9). The best-fit mTTs of river infiltration were approximately between 16 and 24 weeks for Well A, between 36 and 48 weeks for Well B, and between 17 and 55 weeks for Well C. The uncertainties of river mTT were better constrained for sites close to the river. Regarding precipitation infiltration, the best-fit mTTs were relatively similar (mainly around between 85 and 125 weeks) for all investigated wells. However, the uncertainties of precipitation mTTs were poorly constrained for the Well A close to the river

compared to Well C farther from the river. In general, the uncertainty of river mTTs increased with distance to the river, while the uncertainties for precipitation infiltration mTTs decreased with distance to the river. Also, stationary and time-variant mTTs estimated by LPF models were comparable, both in terms of best-fit and behavioral solutions (Table 3.3).

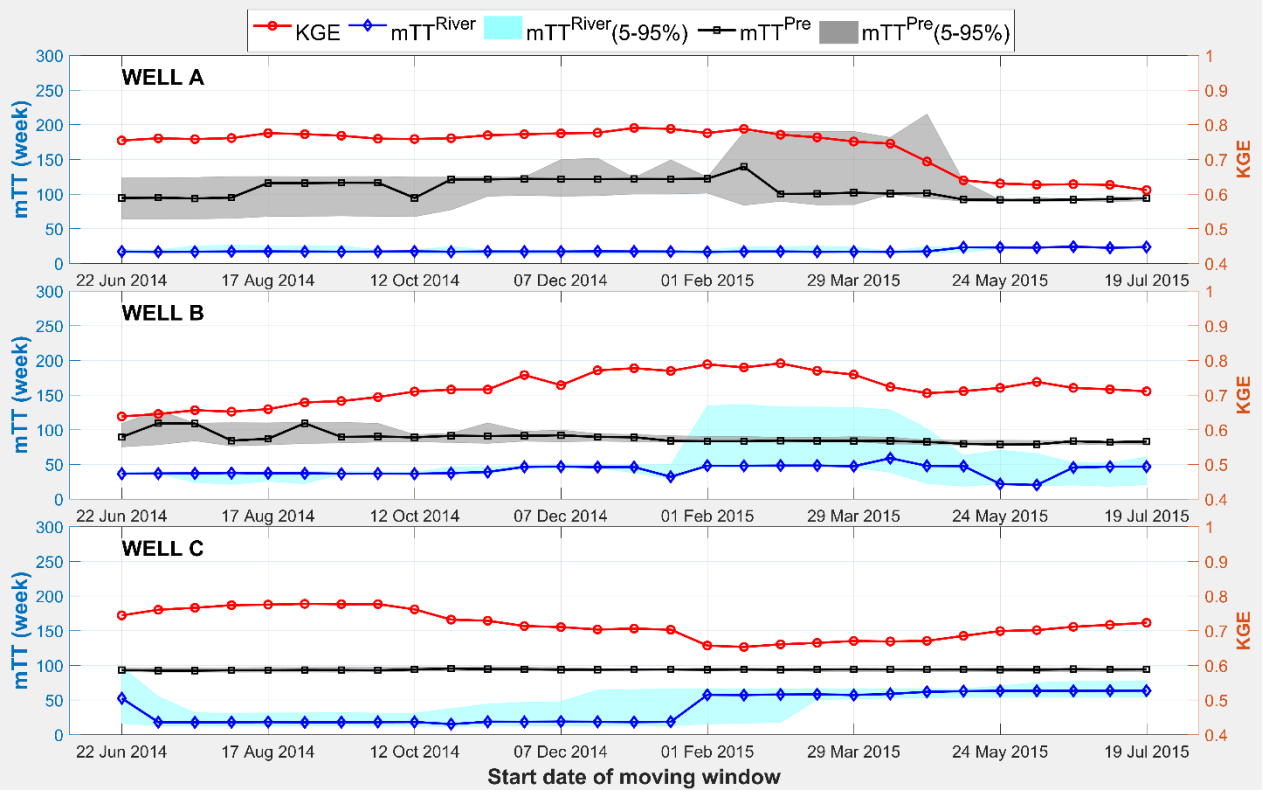

Figure 3.9: Model efficiencies (Kling–Gupta efficiency [KGE]) and the mean transit times (mTTs) of river and precipitation infiltration corresponding to the best-matching linear-piston flow models. The shaded areas represent the best behavioural solutions (90% confidence) of mTT predictions by generalized likelihood uncertainty estimation analysis. Results of time-variant mTTs are shown for every 2 weeks

3.5 Discussion

3.5.1 Mechanisms and sources of groundwater recharge

Similar seasonal fluctuations between groundwater and river levels over the monitoring period (Figure 3.2) suggested a good hydraulic connection between surface water and groundwater along the Mekong River. The semi-annual reversal of gradients between the river and the groundwater indicates groundwater recharge, i.e. that the river loses water to bank infiltration and recharges the Holocene aquifer during flooding. In contrast, groundwater is released from the aquifer to compensate for the small amount of river water at the end of the dry season. Considering the difference of the hydraulic conductivity and the elevation of the aquitard and aquifer layers, the

shallow groundwater is mainly in horizontal hydraulic contact with the river via bank infiltration at the highly permeable aquifer (characterized by the medium and coarse sand layer), instead of the low-permeable aquitard (characterized by the silt and clay layers).

Compared to precipitation and river water, groundwater showed strong damping of the isotopic signals, reflecting water storage systems dominated by subsurface flow paths (Dunn et al., 2008) with relatively long transit times (Hrachowitz et al., 2013). The unique step-wise increase in heavy isotopes observed in the groundwater with increasing distance from the river (Figure 3.3) might be explained by the mixing of river-bank infiltration with a more significant contribution from an evaporated recharge source to the shallow groundwater. The isotopic signatures indicate the different importance of the two sources for the groundwater recharge at the investigated sites, as one would also expect from a hydraulic point of view due to the different distances to the river. With increasing distance, the exchange between groundwater and river is usually dampened due to infiltration length and associated longer transit times.

The groundwater regression line deviated significantly from the LMWL exhibiting a less steep slope while it compared well to the regression line of the pond water (Figure 3.3). This indicates that the local surface water, being affected by evaporative fractionation processes, is likely a second source recharging the shallow groundwater. The slopes derived from the regression lines of groundwater and pond water in our study are comparable to those in (Lawson et al., 2013; Lawson et al., 2016; Richards et al., 2018), who also suggested an evaporated source of surface recharge (e.g., from the wetland and ponds) to the groundwater in Cambodia. Such comparable results support the assumption that the precipitation is mixed with preexisting local surface water and evaporates before infiltrating down the unsaturated zone towards the shallow groundwater in the VMD. Considering the offset of isotopic samples of the river from the local precipitation (Figure 3.3), it is unlikely that the river was recharged by the local precipitation, but is preferably sourced from upstream of the VMD (i.e., its runoff stems almost exclusively from the Mekong basin).

Generally, the analysis of water level fluctuations and isotopic signatures suggests that the shallow groundwater is recharged by two distinct water components via different flow pathways, justifying the use of two-component LPMs, beyond simple fitting considerations.

3.5.2 Sensitivity of modeling results to isotopic correction

The sensitivity analysis (Test 1) illustrates that using modified input functions within the calibration of two-component LPMs can provide better fitting accuracies (Figure 3.4) without altering the estimated mTTs (Figure 3.5). Better performance was also reported when LPMs were calibrated with input functions modified by canopy interception (e.g., Stockinger et al., 2014), evapotranspiration (e.g., Stumpp et al., 2009), or the correction of the isotopic mass balance (e.g., Viville et al., 2006). In this study, the correction was necessary because of a) isotope enrichment

in ponding water, and b) theoretical preconditions for the application of the mixing models, specifically the assumption that the water at the wells is the product of mixing of both river water and precipitation. Therefore, the $\delta^{18}O$ content of the well must range between the $\delta^{18}O$ content of the sources. This precondition is not fulfilled if the original $\delta^{18}O$ values of precipitation are used. Mass balance analysis indicates an unrealistic situation that there is no contribution of river infiltration to groundwater when the correction values are lower than 1.0‰ (Figure 3.5i,j,k), and hence justifies the isotopic correction. However, it has to be noted that the quantification of contributions from the two sources is sensitive to the isotopic correction of precipitation, depicted by the increase of p^{cal} with higher Δ^{var}.

A comparison between Test 1 and Test 2 illustrates that the pre-defined mixing process (e.g., using Eq. 3.5) and fixed correction for the $\delta^{18}O$ precipitation (e.g., Δ^{fix} = 1.81‰ to produce the same mean value of precipitation infiltration as the ponding water) provide reasonable modeling results. In this context, it is noteworthy that the best model results are obtained with Δ^{var} = 1.8‰, which is almost identical to Δ^{fix}. This similarity supports the validity of the definition of Δ^{fix} by the mean difference between precipitation and ponding water isotopic content. The fixing of the correction factor not only fulfills real-world and theoretical constraints, but it also improves the parsimoniousness of the applied model. A similar correction of $\delta^{18}O$ of precipitation (1.4‰) was applied by (Calderon and Uhlenbrook, 2016) for a hydrograph separation in Nicaragua, a climatic environment somewhat similar to this study.

3.5.3 Dominant subsurface flow conditions

The relatively high performance (KGE>0.7 and RMSE<0.4‰, Table 3.3), better parsimoniousness (Figure 3.6c,f), reasonable parameter identifiability of mTT (Figure 3.7), and low fitting uncertainty (Figure 3.8) of the LPF model suggest that the linear-piston flow distribution likely represents the subsurface flow conditions at the study site. Other evidence supporting the dominance of linear and piston flow distributions and justifying the best performance of the LPF model are the poor performances of (i) the exponential model compared to the linear model, and (ii) the related non-linear models (exponential-piston flow or gamma model) compared to the related linear models (e.g., LPF model) (see Figure 3.6). This suggests that the subsurface transport of water is better characterized by a linear distribution rather than by an exponential distribution. This confirms that the exponential model is inadequate to represent recharge to groundwater collected at larger depths below the ground surface (Zuber et al., 2011). Secondly, mTT modeling results suggest a considerable fraction of piston flow in the TTDs. For example, considering the results of Test 2 from the LPF model for Well A (see Table 3.3), the best-fit value of η = 1.82 for river water implies that 55% of the volume of the river water infiltration passes through the aquifer as linear flow, while 45% can be characterized by piston flow behavior. Accordingly, the value of η = 1.90 for

precipitation implies a 53% of volume portion of linear flow and a 47% volume of piston flow in the TTD of precipitation infiltration.

The statistical findings indicate that the subsurface flow condition at the study site is likely best described with a linear distribution accounting for the infiltration along the river followed by the hydraulic replacement of groundwater caused by pressure gradients which adds the piston flow component to the model. The explanation is consistent with the hydrogeological setting at the study site characterized as a partially confined aquifer which does not create a phreatic system. This situation can be represented by a linear-piston model or a dispersion model according to the five hydrogeological settings described in Małoszewski and Zuber (1982). The accordance of the statistical finding with these theoretical considerations serves as a corroboration of the ranking of models (see Section 3.4.4) by the model fitting and the GLUE analysis.

Compared to the gamma model, the exponential-piston flow and advection-dispersion models provide better performances (Figure 3.6). The results agree well with the dominance of these TTDs in riverbank infiltration studies (e.g., Stichler et al., 1986; Maloszewski et al., 1992; Stichler et al., 2008; Kármán et al., 2014) and/or in groundwater studies (e.g., Cartwright and Morgenstern, 2016; Stewart et al., 2017), whereas, the gamma model has been frequently used in catchment studies (cf. McGuire and McDonnell, 2006; Hrachowitz et al., 2010). Although the linear-piston flow distribution has been introduced early (see Małoszewski and Zuber, 1982; Maloszewski and Zuber, 1996), it has rarely been tested, to our best knowledge, within the lumped parameter approach. Our study agrees well with Timbe et al. (2014), who suggested that the linear-piston flow model could be a reliable method to determine water transit times in southern Ecuador.

3.5.4 Two-component LPM reveals recharge mechanism

Comparisons of the results (e.g., estimated mTT, parameter identifiability, and model efficiency) of three tests suggest that two-component LPMs can be applied to investigate mTTs and TTDs of different water components in tracer studies. We combine theoretical considerations and measurements of the hydrogeological setting with the best-fit LPF models (reported in Table 3.3) to develop a conceptual model of surface-groundwater interaction at the study site. The conceptual model (Figure 3.10) shows the spatial variation of mTTs, the different recharge contributions, and the subsurface flow conditions.

The contributions of the two recharge sources change with distance to the river. The mTTs of river bank infiltration increase with the length of the horizontal flow path and the decreasing flow path gradient between river and groundwater. The mTTs of river infiltration are relatively short (approximately 13-40 weeks) for locations close to the river (Well A and B), but cannot be constrained for sites farther from the river (Well C). Notably, using stable isotopes alone cannot provide reliable longer mTTs, despite the used LPMs (Seeger and Weiler, 2014; Kirchner, 2016a), indicating the contribution of older water (> 5 years) to the groundwater system of the VMD. The

mTTs of precipitation infiltration were independent of the distance to the river, depicted by the relative similarity of mTTs (82-95 weeks) for all investigated wells. The fact that the estimated mTTs of precipitation infiltration are longer than the ones of river infiltration is attributable to the hydraulic conductivity of the soil. The horizontal infiltration from the river takes place mainly via the highly permeable aquifer, resulting in short mTTs (<40 weeks) for the investigated wells located close to the river (e.g., <200 m). Meanwhile, the vertical infiltration of precipitation (after ponding on the surface) takes place primarily via a low-permeable overlying aquitard, resulting in considerably longer mTTs (>80 weeks) for all investigated wells.

Overall, the results follow the general understanding of groundwater hydraulics and are reasonable from physical and hydrological points of view, corroborating the applicability of two-component LPMs to identify groundwater mTTs at riverbank infiltration systems. However, in the given lithological setting the predictive skill and particularly the reliability of the models decrease for locations farther from the river, where recharge by precipitation dominates and a low-permeable aquitard layer above the aquifer is present. This specific setting impairs the identifiability of model parameters in this case. In other settings, e.g. without an overlying aquitard, better model performance and parameter identifiability can be expected even for larger distances to the river.

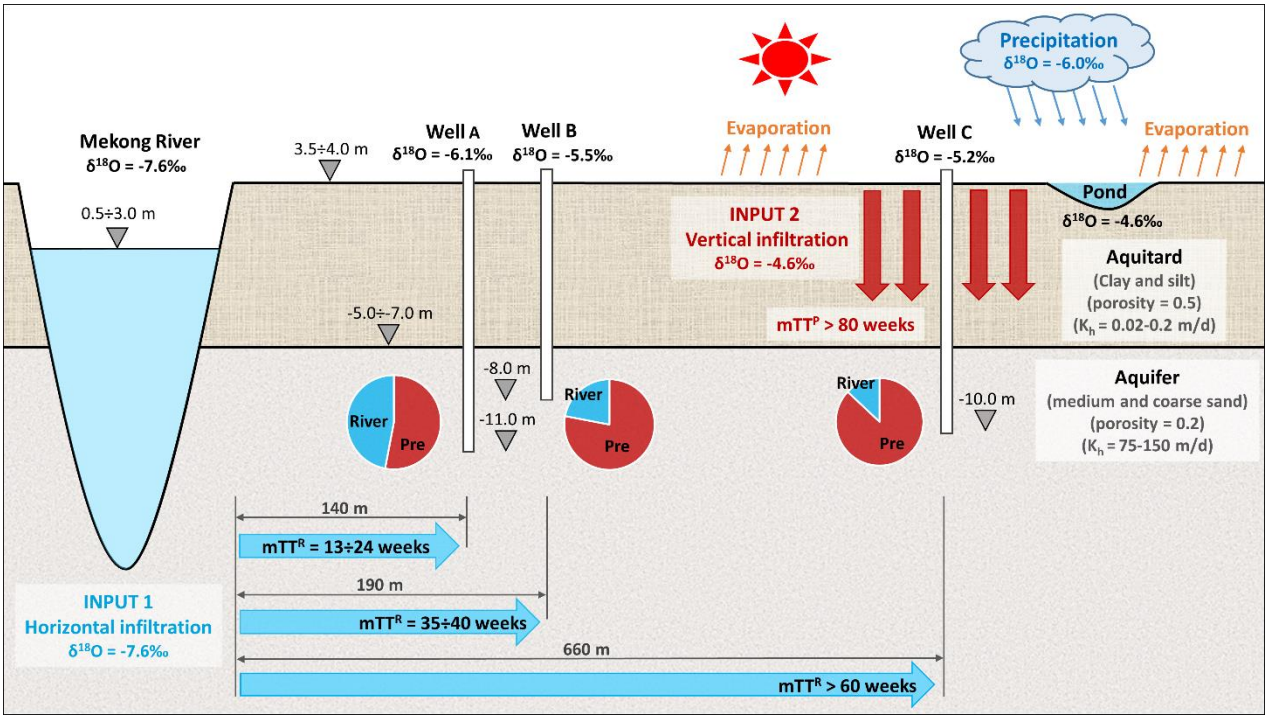

Figure 3.10: Conceptual model of subsurface flow conditions at the study site. The mean transit times (mTTs; arrows) and recharge contributions (pie charts) of river water and precipitation shown here result from the linear-piston flow model. The characteristics of the aquitard and aquifer layers (e.g., the thickness, type of soil, porosity, and vertical hydraulic conductivity) are referenced from (Boehmer, 2000; Benner et al., 2008; Minderhoud et al., 2017).

3.5.5 Limitations and wider implications

Although the identified results are hydrologically plausible, corroborating the validity of the model concept, we acknowledge the limitations of this study. Here we point out possible reasons related to the inevitable errors of two-component LPMs and shortcomings of data that could add uncertainties to the mTT analysis.

First, the lumped convolution modeling approaches rely on steady-state conditions and assumed nonstationary TTDs (Test 1 and 2). Such assumptions are probably less problematic for groundwater than they are for surface water systems (Birkel et al., 2016), yet they are rarely met in any real hydrologic setting (Rinaldo et al., 2011). Although time-variance was introduced to the TTDs and their corresponding mTTs (Test 3), within each 2-year time frame of the moving window steady-state conditions prevailed. The limitation of the time series by a moving window resulted in a somewhat poorer description of the groundwater system because the moving window was hardly larger than the mTT of precipitation infiltration. Consequently, our results concerning time-variable TTDs and mTTs should be considered a first step towards an analysis of non-stationary in surface-groundwater interaction.

Second, potential aggregation biases might lead to an underestimation of the mTTs in the heterogeneous system (see Kirchner, 2016b; Stewart et al., 2017). The mixing between vertical and horizontal recharge might not be correctly described with the LPMs, thus the resulting mTTs could be biased by the selection of the method. To what extent this theoretical restriction applies to the presented results cannot, however, be determined.

Third, this work relying solely on stable isotopes cannot provide the ages of water older than five years (Stewart et al., 2010), which could result in the truncation of water transit time and skew the understanding of how the system stores and transmits water (Stewart et al., 2012). Consequently, the identified mTTs should be considered partial transit times with preference for young waters contributing to shallow groundwater in the VMD. To evaluate potential contributions of older water fraction, environmental isotopes (e.g., tritium) have been frequently used (e.g., Stewart et al., 2010; Morgenstern et al., 2015; Cartwright and Morgenstern, 2016; Duvert et al., 2016).

Fourth, the study would have benefited from higher sampling frequencies (e.g., daily) to provide better insights into short term system responses (see Hrachowitz et al., 2010; Birkel et al., 2016). Higher sampling resolution could also improve model conceptualization and calibration (e.g., Birkel et al., 2010), reduce potentially misleading insights (Hrachowitz et al., 2011), and uncertainties of mTT modeling (Timbe et al., 2015). However, given the practical constraints and costs of isotope sampling, higher sampling frequencies are difficult to realize in general.

Fifth, the reconstruction of the precipitation record (see Section 3.3.6) could be a potential source of error. However, the approach of looping precipitation isotopic signature has been common

practice when input time series are too short to constrain mTT estimates adequately (e.g., Timbe et al., 2014; Birkel et al., 2016; Mosquera et al., 2016; Muñoz-Villers et al., 2016). For more reliable paleoclimate reconstructions of precipitation isotopes in Asian monsoon regions, model-based statistical approaches (e.g., the combination of global climate models with statistical analyses) could be applied (see Duy et al., 2018 and references therein).

Sixth, choosing the same types of TTDs to combine in the two-component LPMs cannot provide an entire picture of all possible combination of selected TTDs. Although mixing different kinds of TTDs (e.g., the combination of AD model for precipitation infiltration and LPF model for river infiltration) could improve the model performance, we expect that this approach invalidates the estimated mTTs, since most of the TTD types are relatively flexible and tend to accommodate themselves to the data. However, this approach should be considered in further study.

Finally, although the isotopic correction due to the evaporation process is in line with the hydrological setting (discussed in Section 3.3.7) and essential to fulfilling the theoretical constraints (discussed in Section 3.5.2), adding a constant value to the isotopic signature of rainfall to estimate the isotopic signature of vertical recharge unavoidably introduces uncertainties. This approach assumes a stable isotopic fractionation process for the whole study period, which is probably quite unrealistic. The sensitivity analysis revealed that although the mTTs are relatively insensitive to the correction factor, the identifiability of the contribution of the different sources to recharge is impaired by the correction factor. Moreover, if the water does pond on the surface before it infiltrates, the isotopic signature may be attenuated prior to recharge. This will result in mTTs being overestimated, because the presented approach does not account for the time required for evaporative changes in isotopic composition, but not for the time required for this. With the available data, it is impossible to analyze the isotopic enrichment of local surface water (e.g., Skrzypek et al., 2015), or independently assess actual contributions of infiltrated water components in this study. This could e.g. be achieved by using another tracer (e.g., Cl).

Despite these limitations, our results underline the usefulness of two-component LPMs in describing subsurface water movement at locations with different flow-path configurations and two groundwater recharge sources, for example, at riverbank infiltration areas. The concept could be further developed by utilizing two-component LPMs in conjunction with both stable and environmental isotopes (e.g., $\delta^{18}O$ and tritium). This could provide insights into the dynamics of both younger and older waters (e.g., <5 years and up to 200 years) contributing to the groundwater system. Generally, the model concept (integrating different TTDs of water components into LPMs) could be a powerful tool for better understanding the hydrological functioning of mixing processes and water movement in groundwater studies.

3.6 Conclusions

This study investigated groundwater transit times and subsurface flow conditions at the riverbank infiltration areas in the VMD. Precipitation, river, groundwater, and local surface water were sampled on a sub-weekly to weekly basis for different periods between 2009 and 2017 and analyzed for stable isotopes. The applicability of two-component LPMs (allowing different TTDs for different recharge components) in conjunction with hydrological and isotopic measurements to identify subsurface flow conditions and the contribution to groundwater mixing was tested. The proposed method proved to be able to identify the TTDs and their corresponding mTTs of both river and precipitation infiltration to shallow groundwater using $\delta^{18}O$ records.

LPMs based on the linear-piston flow distribution were able to capture isotopic variations in shallow groundwater in response to the modified input function. Although the exact contribution of the water components infiltrating to the groundwater system remains uncertain, the dynamics of the surface-groundwater interaction could be identified. River water infiltrates horizontally mainly via the highly permeable aquifer, resulting in short mTTs (<40 weeks) for locations close to the river (<200 m). The vertical infiltration from precipitation takes place primarily via a low-permeable overlying aquitard, resulting in considerably longer mTTs (>80 weeks). The outcomes are hydrologically plausible, corroborating the validity of the applied approach. Our findings enhance the understanding of the shallow groundwater recharge dynamics and may serve as a baseline for future groundwater studies using environmental isotopes in the VMD. Groundwater resources management needs to consider the different recharge mechanisms and mTTs (mainly controlled by the distance to the river), resulting in different management options for different areas in the delta.

Our study suggests that the highly complex mechanism of surface-groundwater interaction and subsurface mixing processes at riverbank infiltration systems can be conceptualized by exploiting two-component LPMs. Regardless of the restrictions associated with certain errors of LPMs and the use of stable isotopes, the model concept can be transferred to other locations. Therefore, the proposed model concept with the associated model selection procedure could provide a comprehensive hydrological tool for the analysis and understanding of groundwater recharge by different sources.

Chapter 4 Groundwater Dynamics in the Vietnamese Mekong Delta: Trends, Memory Effects, and Response Times

This is part of the publication:
Duy, N. L., Nguyen, T. V. K., Nguyen, D. V., Tran, A. T., Nguyen, H. T., Heidbüchel, I., Merz, B., Apel, H., 2021. Groundwater dynamics in the Vietnamese Mekong Delta: Trends, memory effects, and response times. Journal of Hydrology: Regional Studies, 33: 100746.
DOI: https://doi.org/10.1016/j.ejrh.2020.100746.

Abstract

This study investigates the trends of groundwater levels (GWLs), the memory effect of alluvial aquifers, and the response times between surface water and groundwater across the Vietnamese Mekong Delta (VMD). Trend analysis, auto- and cross-correlation, and time-series decomposition were applied within a moving window approach to examine non-stationary behavior.

Our study revealed an effective connection between the shallowest aquifer unit (Holocene) and surface water, and a high potential for shallow groundwater recharge. However, low-permeable aquicludes separating the aquifers behave as low-pass filters that reduce the high-frequency signals in the GWL variations, and limit the recharge to the deep groundwater. Declining GWLs (0.01-0.55 m/year) were detected for all aquifers throughout the 22 years of observation, indicating that the groundwater abstraction exceeds groundwater recharge. Stronger declining trends were detected for deeper groundwater. The dynamic trend analysis indicates that the decrease of GWLs accelerated continuously. The groundwater memory effect varies according to the geographical location, being shorter in shallow aquifers and flood-prone areas and longer in deep aquifers and coastal areas. Variation of the response time between the river and alluvial aquifers is controlled by groundwater depth and season. The response time is shorter during the flood season, indicating that the bulk of groundwater recharge occurs in the late flood season, particularly in the deep aquifers.

4.1 Introduction

Alluvial aquifers play an important role in sustaining agricultural activities and the livelihood of the population in river deltas. In areas where rainfall is not uniformly distributed throughout the year (e.g., tropical or arid regions), they are primary sources for good quality freshwater, as they are less vulnerable to contamination or climate variability than surface water bodies. However, accurate estimates of groundwater recharge and the response between surface water and alluvial aquifers can be difficult to obtain, and significant uncertainties exist in groundwater storage in alluvial settings. Under impacts of climate change and human activities (Syvitski et al., 2009; Vörösmarty et al., 2009; Hirabayashi et al., 2013), which challenge national to global food security (Kummu et al., 2012), understanding the mechanisms of alluvial aquifers is fundamental.

The Vietnamese Mekong Delta (VMD), an alluvial delta forming the southern tip of Vietnam, is home to 18 million people and plays a vital role in the country's food security and economy (Renaud and Kuenzer, 2012). Groundwater resources management is one of the prerequisites for living and livelihood in the VMD. The extensive hydrological manipulation of the delta has a direct impact on groundwater resources, mainly through the disruption of natural flood regimes, groundwater exploitation and artificial groundwater recharge, and salt intrusion in the alluvial aquifers (Renaud and Kuenzer, 2012). Since the 1990s, groundwater has been increasingly utilized for irrigation, domestic, and industrial purposes (Danh and Khai, 2015), while the extraction has been poorly managed (Wagner et al., 2012). Unsustainable groundwater abstraction causes declining groundwater levels (Erban et al., 2014) and land subsidence (Minderhoud et al., 2017) in the delta.

The dynamics of surface water have been continuously highlighted in a number of publications denoting increasing trends in water level (Dang et al., 2016; Fujihara et al., 2016), sedimentation (Hung et al., 2014b; Hung et al., 2014a; Manh et al., 2015) and floodplain inundation (Dung et al., 2011; Triet et al., 2017). Analyses on groundwater dynamics are, however, scarce in the VMD. Instead, groundwater studies have focused on the arsenic contamination of aquifers (e.g., Shinkai et al., 2007; Buschmann et al., 2008; Kocar et al., 2008; Erban et al., 2013; Huang et al., 2016), groundwater quality (e.g., Wilbers et al., 2014; An et al., 2018; Tran et al., 2019), groundwater recharge sources (Ho et al., 1991; An et al., 2014), or shallow groundwater transit time (Duy et al., 2019). Notably, these studies mostly focused on local areas (e.g., provinces or cities) rather than the whole delta. At the larger scale, groundwater has been reported to be considerably controlled by the river system (Wagner et al., 2012) and closely connected to the surface water in the floodplains (Kazama et al., 2007). However, information on water flow processes in the multi-layered alluvial aquifer system based on numerical modeling (e.g., Vermeulen et al., 2013; Shrestha et al., 2016; Hung Van et al., 2019) is scarce due to the complexity of the hydrogeological subsurface system (Wagner et al., 2012) and the sparsity of groundwater level and lithological data (Johnston and Kummu, 2012). To our best knowledge, groundwater dynamics focusing on

the recent trend of groundwater levels, the “memory effect” (Mangin, 1984; Massei et al., 2006; Duvert et al., 2015) (representing the time that an aquifer holds water), and the response time between surface water and alluvial aquifers have not been quantified for the VMD.

Time-series analysis (e.g., Box et al., 2011; Box et al., 2015) can be applied to study the dynamics of a groundwater system (Bakker and Schaars, 2019). In this context, trend analysis and correlation analysis have been frequently applied. Decomposition analysis (e.g., Shamsudduha et al., 2009; Lafare et al., 2016; Wunsch et al., 2018) and/or predefined response functions (e.g., von Asmuth et al., 2002) can be additional tools to characterize the hydrologic behavior of a groundwater system. For trend analysis, the nonparametric Mann-Kendall test (Mann, 1945; Kendall, 1948) and Sen's slope estimator (Sen, 1968) are commonly applied in hydrological studies (see Madsen et al., 2014 and references therein). This estimator evaluates the median values of all pairwise slopes. The method does not require normality of the residuals; hence it is insensitive to outliers (Helsel and Hirsch, 2002). To examine the memory effect and the impulse response of an aquifer, the pioneering work of Mangin (1984) demonstrates that correlation analysis (auto-correlation and cross-correlation) can be used. Aquifers can act as filters to transform input signals into output signals by transfer functions (Labat et al., 2000), which can be interpreted to gain insight into the function and structure of aquifers (Delbart et al., 2014). Following the methodology of Mangin (1984), numerous studies have reported the memory effect and response of groundwater in karst systems (e.g., Larocque et al., 1998; Massei et al., 2006; Mayaud et al., 2014; Delbart et al., 2016). In alluvial systems, however, these concepts have found limited application and need further testing (Imagawa et al., 2013; Duvert et al., 2015).

In this study, groundwater flow processes in the alluvial aquifers of the VMD are investigated by trend and correlation analysis, as well as time-series decomposition. All these analyses are incorporated into a moving window approach to identify non-stationary responses. We investigate (1) trends in groundwater levels, (2) the memory effect of alluvial aquifers, and (3) the time-variant response between surface water and groundwater throughout the VMD. The results are essential for groundwater resource management and livelihoods in the region, and highlight the general mechanisms of sub-surface water transport in alluvial settings.

4.2 Study area

The study area is the VMD covering an area of 4 million hectares between 8.5–11.5 ºN and 104.5–106.8 ºE (Figure 4.1). The delta has an extremely low mean elevation (~0.8m above sea level) (Minderhoud et al., 2019). During the flood season (July-November), 35–50% of the delta is flooded, mainly by river discharge exceeding bank level. The resulting inundation reaches depths of up to 4.0 m for 3 to 6 months (Toan, 2014), constituting inundation areas that recharge water to alluvial aquifers. In this study, the inundation areas were adapted from Triet et al. (2017). These areas cover a territory of approximately 2.0 million hectares in the northern part of the VMD.

According to Danh and Khai (2015), groundwater in the VMD is typically accessed via private tube-wells (more than 1 million shallow tube-wells across the delta) at depths of 80-120 m, and groundwater abstraction wells of water supply plants, reaching depths of 200-450 m. The total groundwater abstraction was estimated at approximately 2.5 million m^3 per day in 2015 (Minderhoud et al., 2017).

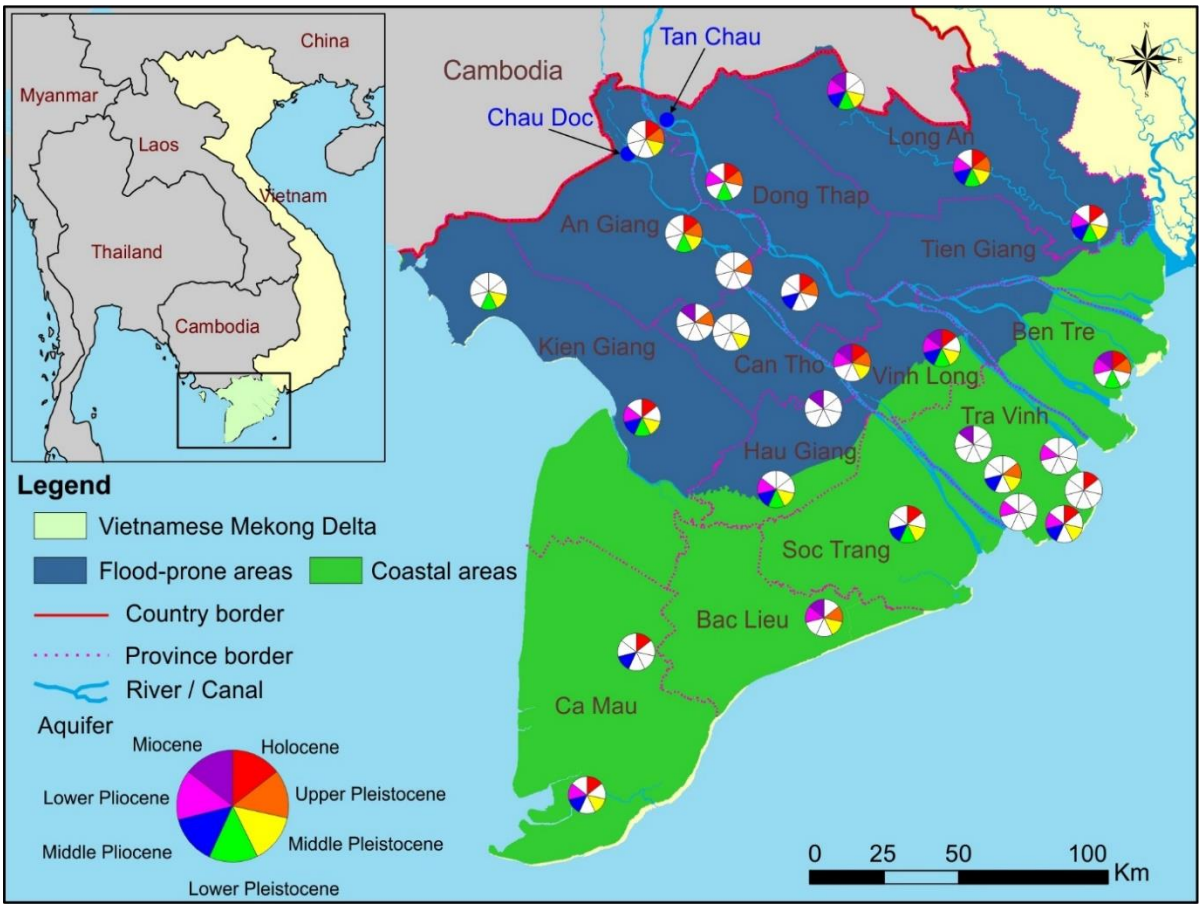

Figure 4.1: Study site in the Vietnamese Mekong Delta. The pie charts indicate the location of national stations monitoring groundwater levels within seven aquifers. Color/white pie segments denote that a monitoring borehole is available/unavailable at a given aquifer, respectively.

The multi-layered aquifer system in the VMD has an alluvial basin structure. The deepest area of the basement is located below the Mekong and Bassac Rivers and rises to the Northeast, North, and Northwest borders (Anderson, 1978; Wagner et al., 2012). Sediments were deposited during transgression and regression events around 6,000–5,000 yr BP (Lap Nguyen et al., 2000), resulting in a highly complex stratigraphy. The subsurface structure and hydrogeological units in the VMD are classified according to geological formations: Holocene, Pleistocene, Pliocene, and Miocene aquifer systems (Wagner et al., 2012). These aquifers are located below ground level around 0-49 m, 31-193 m, 153-381 m, and 275-550 m, respectively (cf. Appendix C1). These age units can be sub-divided into eight hydrogeological aquifer systems: Holocene (qh), Upper Pleistocene (qp_3),

Middle Pleistocene (qp_{2-3}), Lower Pleistocene (qp_1), Middle Pliocene (n_2^2), Lower Pliocene (n_2^1), Upper Miocene (n_1^3), and Middle Miocene (n_1^{2-3}). Generally, each unit consists of two layers: (i) a low-permeable aquitard layer composed of silt and clay; and (ii) a high-permeable aquifer layer composed of fine to coarse sand and gravel. The horizontal hydraulic conductivities of the aquitards and aquifers are in the range of $(3\text{-}40)*10^{-8}$ m/s and $(1\text{-}20)*10^{-4}$ m/s, respectively. The hydrogeological characterization of these semi-confined aquifers is given in (Wagner et al., 2012), and their lithological nature and hydraulic properties are described in (Minderhoud et al., 2017) and summarised in (Hung Van et al., 2019). In this study, the Middle Miocene (n_1^{2-3}) was not considered due to a lack of data.

4.3 Methods

4.3.1 Datasets

Groundwater levels (GWL) in the VMD have been recorded starting from the mid-1990s at multiple temporal resolutions (from daily to monthly) and with different monitoring duration (8-22 years). We collected GWL time series between 1996 and 2017 from 88 boreholes (see Appendix C1) at 27 distributed well nests (Figure 4.1). From these data sets the borehole data series with temporal resolutions higher than weekly and monitoring durations longer than ten years were selected. The datasets were supported by the project "Research on improvement for the efficiency of water resources monitoring system for early warning of depletion and saline intrusion in the Mekong Delta plain – No. ĐTĐL.CN-46/18", which is funded by Ministry of Science and Technology (MOST). An hourly discharge time series from 1996 to 2017 at Chau Doc was also collected to represent the variability of surface water in the VMD in the analysis. The discharge data was provided by the Southern Institute of Water Resources Research (SIWRR). For consistency, all collected data were aggregated to weekly mean values.

4.3.2 Time-series decomposition

We applied a nonparametric time-series decomposition approach known as "STL: Seasonal-Trend decomposition procedure based on LOESS" (Cleveland et al., 1990). The STL method uses locally weighted regression (LOESS) operations with different moving window lengths to separate a time series into three distinct components. Equation 4.1 shows the additive decomposition of the trend (T_t), seasonal (S_t), and remainder (R_t) components from the original signal (Y_t).

$$Y_t = T_t + S_t + R_t \quad (4.1)$$

Typically, each component can be related to different processes acting during the generation of the time series. In the case of GWL time series, the role of each component was classified by (Lafare et al., 2016) as follows: (1) T_t represents the long-term processes operating over the period of the entire time series; (2) S_t represents a cyclical process, e.g., the annual cycles resulting from

recharge periods; (3) R_t represents local processes that cause variability between cycles and can thus be attributed to shorter-term events or impacts (e.g., the local recharge and/or abstraction) on the groundwater system.

There is no unique choice for selecting the smoothing parameter (e.g., the length of the moving window) within the STL algorithm. In many applications, the decision should be based on the goals of the analysis and the knowledge about the mechanisms generating the time series (Cleveland et al., 1990). While a large value can result in similar components in all years, a small value can track the observations more closely (Shamsudduha et al., 2009). In this study, we selected a 10-years window for the trend component and 1-year window for the seasonal component. In this way we were able to highlight decadal trends and annual cycles.

4.3.3 Identification of GWL variability

We calculated the ratio between the variance of decomposed components and the original signal (Eq. 4.2) to measure the relative importance of the variance associated with each component in comparison to the original signal. Graphical comparison of these ratios (Lafare et al., 2016) and the boxplot of seasonal variation of normalized time series were used to characterize the relative variability of GWL in the VMD.

$$\text{Ratio}^{\text{Trend}} = \text{Variance}(T_t)/\text{Variance}(Y_t) \quad (4.2a)$$

$$\text{Ratio}^{\text{Seasonal}} = \text{Variance}(S_t)/\text{Variance}(Y_t) \quad (4.2b)$$

$$\text{Ratio}^{\text{Remainder}} = \text{Variance}(R_t)/\text{Variance}(Y_t) \quad (4.2c)$$

4.3.4 Trend analysis

We applied the Mann–Kendall (MK) nonparametric trend test (Mann, 1945; Kendall, 1948) with Sen's slope (Sen, 1968) to investigate recent changes (1996-2017) of the groundwater system in the VMD. The trend magnitude was reported as Sen's slope considering a significance level of 95%. Trends were calculated by a moving-window approach (10-year window with 1-year increment of the original groundwater level time series) to investigate the time-variations of trends. Spatial patterns of Sen's slope were mapped at the regional scale using GIS built-in interpolation models and geostatistical Kriging techniques in ArcGIS version 10.4. Time-series were analyzed using MATLAB R2019b with the Statistics Toolbox version 11.6.

4.3.5 Auto-correlation

Auto-correlation analysis was used to identify the memory effect (Mangin, 1984; Massei et al., 2006; Duvert et al., 2015) of alluvial aquifers in the VMD. We applied the auto-correlation to the remainder component (R_t), because it represents the local effects and short-term events (Lafare

et al., 2016), while the trend and seasonal components are by definition significantly auto-correlated. The auto-correlation of a time-series *x* is defined as (Box et al., 2015):

$$r_x(k) = \frac{N^{-1}\sum_{i=1}^{N-k}(\mathrm{x}_i - \bar{x})(\mathrm{x}_{i+k} - \bar{x})}{{\sigma_x}^2} \quad (4.3)$$

Where $r_x(k)$ is the autocorrelation coefficient at lag *k,* and $\bar{x}$ is the arithmetic mean of the time series with *N* observations. σ_x is the standard deviation of the time series. The value of *k* was selected smaller than the cutting point (*N*/3) to avoid stability problems. The memory effect of the signal was defined as the time lag when $r_x(k)$ reached a value of 0.2, as frequently applied in GWL studies (Mangin, 1984). The value was termed as the de-correlation time lag ($k_{0.2}$) here. Alternatively, the memory effect was also characterized by the overall shape and magnitude of the auto-correlogram (Massei et al., 2006). We quantified the slope of the auto-correlogram by logarithmic fits, following (Massei et al., 2006; Duvert et al., 2015):

$$r_x(k) = \alpha \log(k) + \beta \quad (4.4)$$

where α (week^{-1}) and β (dimensionless) are slope and intercept of the logarithmic function, respectively. Typically, α describes the rate at which the correlation decreases during the study period, and β corresponds to the loss of correlation for a unit lag *k*.

4.3.6 Cross-correlation

Cross-correlation, represented by a cross-correlogram, identifies the relationship between two signals. The cross-correlation between two time series *x* and *y* with *N* observations is defined as (Box et al., 2015):

$$R_{xy}(k) = \frac{N^{-1}\sum_{i=1}^{N-k}(\mathrm{x}_i - \bar{x})(\mathrm{y}_{i+k} - \bar{y})}{\sigma_x \sigma_y} \quad (4.5)$$

Where $R_{xy}(k)$ is the cross-correlation coefficient at lag time *k*, $\bar{x}$ and $\bar{y}$ are the arithmetic means of the two time series and σ_x and σ_y are the standard deviations.

The cross-correlation analysis was applied in a moving-window approach (1-year window with 1-week increment) to highlight the inter-annual variability of the response time of groundwater levels to changes in discharge. For each window, the cross-correlogram function between input and output was calculated, and the response time τ (the lag time *k* corresponding to the maximum correlation) was identified, following Delbart et al. (2014) and Duvert et al. (2015). Only a cross-correlation coefficient higher than the standard error of $2/N^{0.5}$ (corresponding to 95% confidence level) was accepted. *N* is the number of observations in the moving window (Diggle, 1990). Readers are referred to Delbart et al. (2014) for a graphical example of the sliding cross-correlation method.

The response time evaluated by the cross-correlation analysis alone can be less accurate if the autocorrelation of the input signal is high (e.g., close to 1) (Bailly-Comte et al., 2011). In order to reduce this effect, the autocorrelation of the input is removed by prefiltering the input signal (e.g., removing all serial dependencies such as trend, seasonal, and autoregressive components). By this pre-whitening procedure, white noise residuals are obtained (Watts and Jenkins, 1968). The analyses of time-series decomposition in this study can be considered as an appropriate approach to prefilter the input signal. Therefore, we used the remainder component of river discharge (at Chau Doc) as an input signal in the cross-correlation analysis. We assumed that the selected input signal represents random, un-correlated processes in surface water (e.g., unaffected by the trend, seasonal, and autoregressive components). The output signal was the remainder component of the GWL time-series. It is noted that groundwater recharge in the VMD is considered to stem mainly from surface water (Wagner et al., 2012). We assumed that the precipitation ponding on the ground is mixed with preexisting surface water (e.g., river water and/or floodwater) before infiltrating to the groundwater. This means that all types of recharge sources were summed up in the "surface water" component. In this context, the time-series of τ gives information about the impulse response that transfers surface water into the aquifers of the VMD.

4.4 Results

4.4.1 Variability of GWL time series

Figure 4.2 shows an example of the decomposition of weekly discharge (at Chau Doc) and the GWL time series (at borehole No. 14) using the STL algorithm. The plot highlights both seasonality and long-term trends in GWLs. The results of the time-series decomposition analysis showed that the relative magnitude of each component varies considerably across the delta. Therefore, the relative variability of the GWL was assessed based on the variances of the trend, seasonal, and remainder components along with the variance of the original time series. This relative variability (represented by the variance ratios defined by Eq. 4.2) was plotted in Figure 4.3.

The decomposition of the time-series revealed a higher variability of the seasonal component in the shallow aquifers (e.g., Holocene), and the dominant variability of the trend component in the deep aquifers (e.g., Pliocene and Miocene). For example, the trend component represented more than 90 % and less than 55 % of the variance of the original time series for deep and shallow aquifers, respectively (Figure 4.3). For the Pleistocene aquifer, the GWL time series were separated into two distinct clusters dominated by the seasonal and trend components (Figure 4.3). However, there was no apparent relationship between the borehole depth and the variance of components in the Pleistocene aquifers, as indicated by the wide scatter without any grouping of the "Pleistocene" symbols in Figure 4.3.

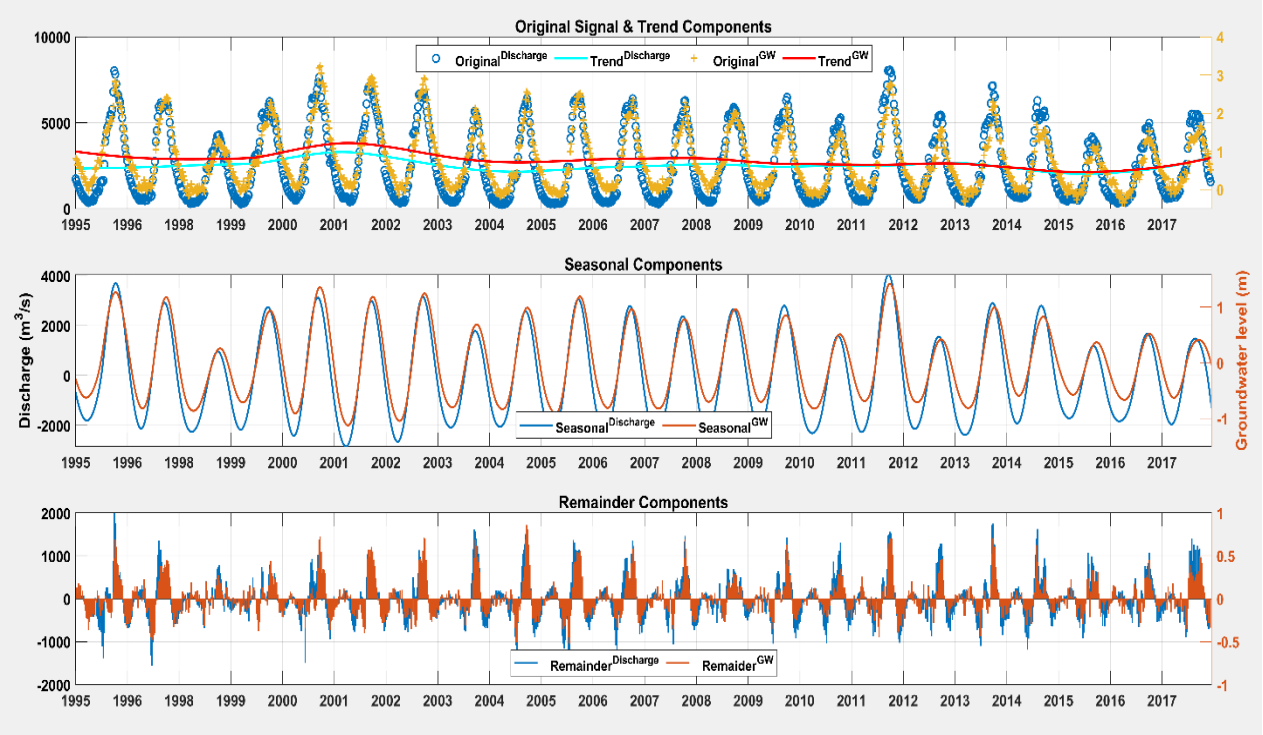

Figure 4.2: STL decomposition of weekly discharge (at Chau Doc) and GWL time series (borehole No. 14). Trends T_t (top), seasonal components S_t (middle) and remainder components R_t (bottom). Left and right axes denote for discharge (m3/s) and groundwater level (m), respectively

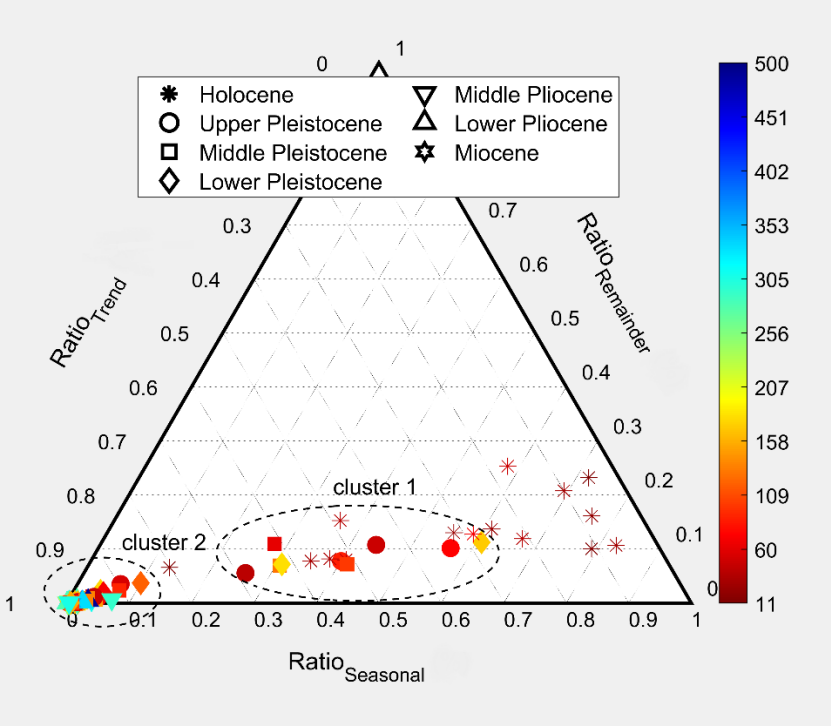

Figure 4.3: Variability ratios (defined by Eq. 4.2) associated with each time series component for the different aquifers. The color bar indicates the depth of the borehole (m).

To highlight the seasonal variation, each time-series was normalized to values between 0 and 1 by subtracting the minimum value and dividing by the total range. Figure 4.4 is a boxplot of the normalized time series of GWLs and river discharge. Higher GWLs were observed in the flood season. The amplitude of the seasonal variation of GWLs decreases with increasing borehole depth, from substantial seasonal variation in the Holocene to no seasonal variation in the Pliocene and Miocene aquifers. Comparing between flood and coastal areas for shallow groundwater, a similar seasonal pattern was observed for the Holocene aquifer. In contrast, the GWLs in flood-prone areas varied slightly more than those in coastal areas for the Pleistocene aquifers.

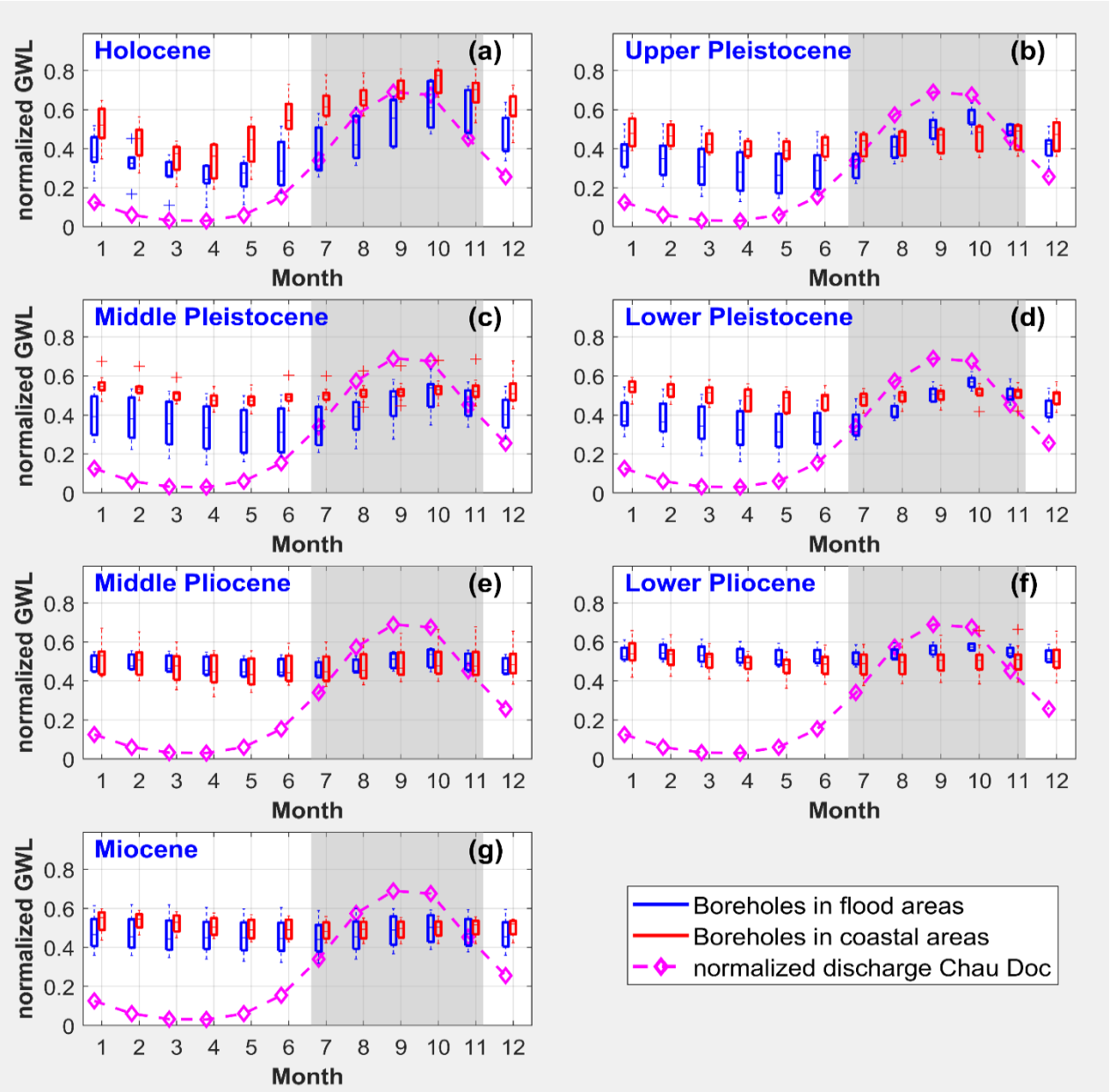

Figure 4.4: Seasonal variation of normalized GWL and discharge at Chau Doc station. The box-whisker plots show the interquartile ranges; the whiskers show the min/max values associated with 1.5 times the interquartile range. The grey areas mark the monsoon/flood season.

4.4.2 Trend of groundwater levels

Figure 4.5 shows the results for recent (1996–2017) trends of GWLs across the VMD. The GWL in all aquifers showed various magnitudes of decreasing trends from 0.01-0.55 m/year (all significant at the 95% level). The strongest negative trends were observed mainly in areas around major cities and major industrial areas (e.g., Tan An, Cao Lanh, Long Xuyen, Can Tho, and Ca Mau). Moreover, stronger declining trends were detected in deeper aquifers with the highest decrease (0.30-0.55 m/year) in the Pliocene and Miocene aquifers. The weakest declining trends (0.01-0.11 m/year) were observed in the Holocene aquifer. The medium depth Pleistocene aquifers showed decreasing trends in-between the trends of the deep and shallow aquifers, with values of 0.05-0.28 m/year and 0.22-0.41 m/year for boreholes located at flood and coastal areas, respectively. An increasing trend was not found for any of the investigated boreholes.

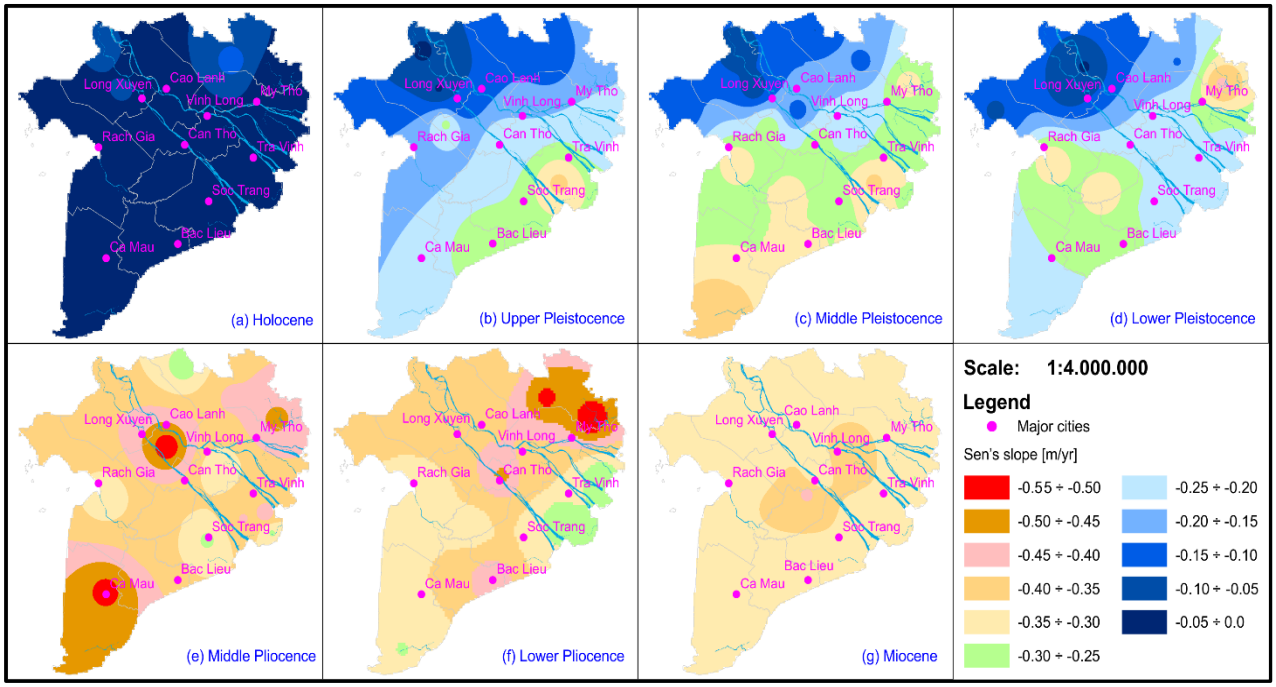

Figure 4.5: Spatially interpolated recent (1996–2017) trends of GWLs of the different aquifers in the VMD.

A comprehensive analysis of the time-variant trends (10-year periods with 1-year increments) is presented in Figure 4.6. Similar to the previous analysis, we observed declining trends in GWLs at all aquifers with higher magnitudes in deeper aquifers. However, no significant trends were detected for some short-term periods for the Holocene aquifer. For other aquifers (e.g., Pleistocene, Pliocene, and Miocene), all declining trend patterns are significant at the 95% level. Except for the Holocene aquifer, the magnitude of the declining trend for almost all boreholes was considerably higher in later periods (e.g., after 2007) than in early periods. For example, the declining trend before 2006 was around 0.1-0.35 m/year but increased up to 0.6-0.75 m/year after 2007 (Figure 4.6). Hence, the decrease of GWL accelerated over the last two decades. The

strongest declining time-variant trends were observed in the Pliocene aquifer, particularly close to big cities such as Ca Mau (borehole No. 22), Can Tho (borehole No. 40), Dong Thap (borehole No. 36), and Long An (borehole No. 65). In line with the overall trends (Figure 4.5), the GWLs in coastal areas decreased more strongly than in flood-prone areas for the Pleistocene aquifers. For the Holocene and Miocene aquifers, the magnitude of the declining GWL trends was not significantly different between flood-prone and coastal areas.

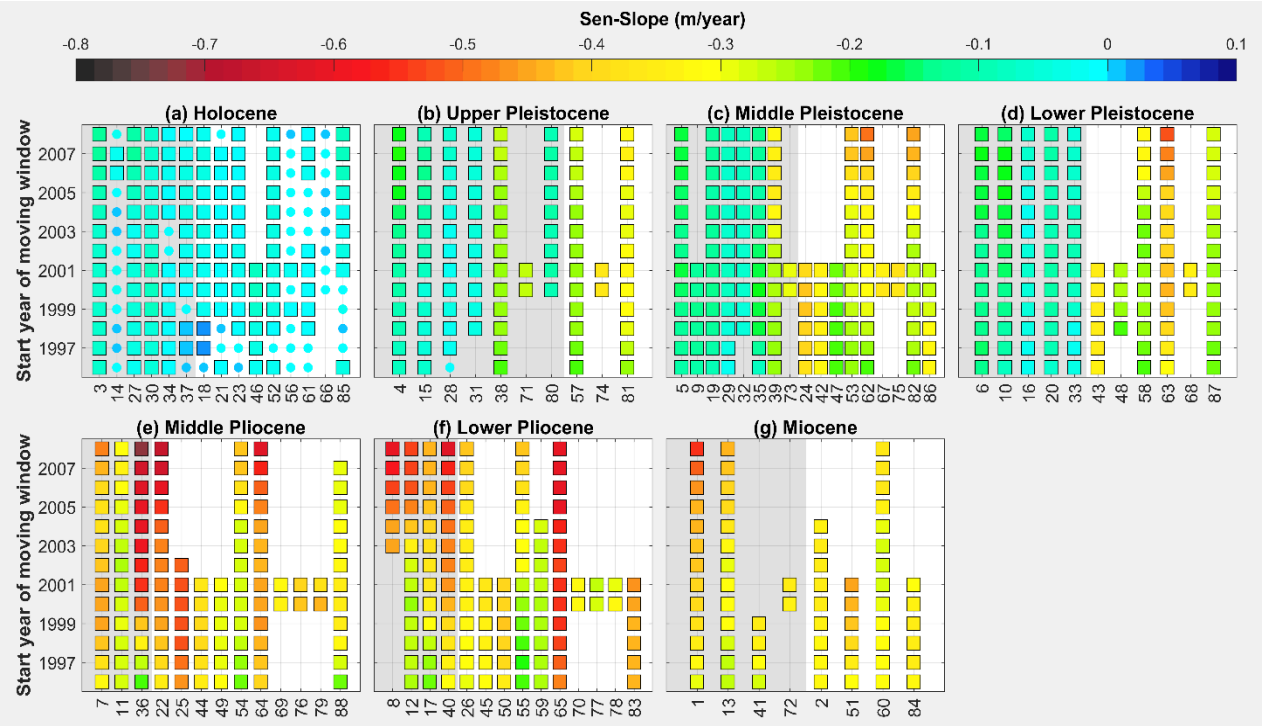

Figure 4.6: Time-variant trends (reported as Sen's slope) calculated for ten-year periods in different aquifers in the VMD. The y-axis shows the start year of the moving window, while the x-axis shows the borehole number (see Appendix C1). The values of Sen's slope (m/year) correspond to the color bar. The squares and circles indicate that the trends are significant or insignificant at the 95% level, respectively. Grey (or white) backgrounds indicate that the location of a borehole is at flood-prone (or coastal) areas. Blank areas indicate no available GWL data.

4.4.3 Memory effect of alluvial aquifers

From the remainder component of each GWL time series, an auto-correlation function was derived. Distinct behaviors were observed among the 88 auto-correlograms, with various degrees of groundwater memory effect. Figure 4.7 shows the rate of decrease of the auto-correlation function (α), together with the de-correlation time lag ($k_{0.2}$) when the auto-correlation coefficient (r_x) of 0.2 was reached. Both methods (logarithmic fit and de-correlation time lag) highlighted similar results. Typically, a stronger memory effect was detected for deeper aquifers, as depicted by more negative α and higher $k_{0.2}$ (Figure 4.7). Stronger memory effects were also identified for

boreholes located in coastal areas compared to those in flood-prone areas; this behavior was, however, not apparent for Holocene aquifers. The de-correlation time lag of the Holocene aquifer was between 5 and 17 weeks. The time lag of the Pleistocene aquifer was between 6 and 26 weeks, showing two distinct groups of flood-prone and coastal areas. The range of the time lag of Pliocene and Miocene aquifers was 11-27 weeks and 13-33 weeks, respectively.

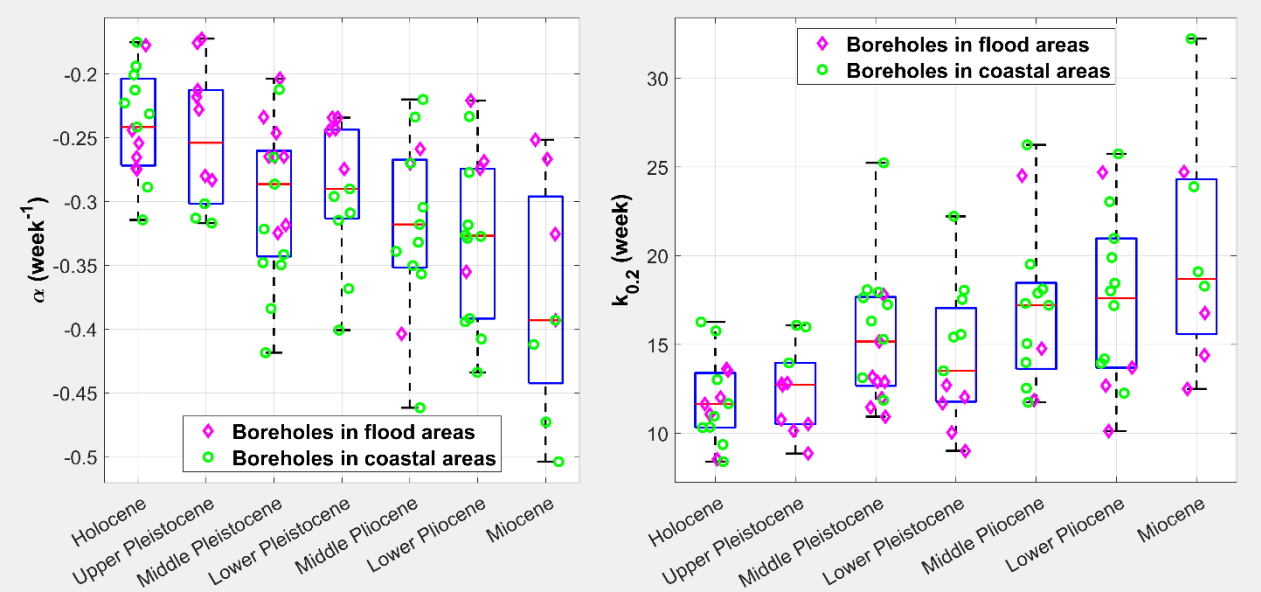

Figure 4.7: Memory effect of aquifers in the VMD, characterized by (α) the rate of decrease of the autocorrelation function (left), and ($k_{0.2}$) the lag time (week) to reach the autocorrelation coefficient of 0.2 (right).

4.4.4 Response time analysis

The moving-window cross-correlation analysis was performed between the remainder component of discharge at Chau Doc gauging station and of GWLs at 88 boreholes. Depending on the length of each GWL time series, 523 to 1,098 moving windows were obtained applying a window length of one year and moving in one-week increments. For example, a borehole with 10-year monitoring GWL will result in a sequence of 523 one-year moving windows. Consequently, we obtained 88 time-series of response time τ with different time lengths (e.g., 523-1,098 values per time series of τ depending on the number of moving windows detected for each borehole). Each time series of τ was then averaged by calculating the arithmetic means of the τ values falling in the month of the year. This analysis is meant to highlight seasonal differences in water level response. It is noted that the shape of the cross-correlogram varied considerably between boreholes. Only cross-correlation coefficients higher than the standard error of 0.28 (corresponding to the 95% confidence level) were accepted. The variability of the response time was reported for every month in Figure 4.8, showing the seasonal variation of the time required for the pulse of surface water to reach the alluvial aquifers. Long-term changes of the response

time within the individual boreholes were analysed by the Mann–Kendall nonparametric trend test, applied on the moving time windows. Results of Sen's slope (considering a significance level of 95%) are reported for 88 boreholes in Figure 4.9. Long-term changes in response time were found to be negligible. Only 20 boreholes showed minor significant changes in Sen's slope of less than 0.3 weeks per year. No significant long-term change was observed for all other wells.

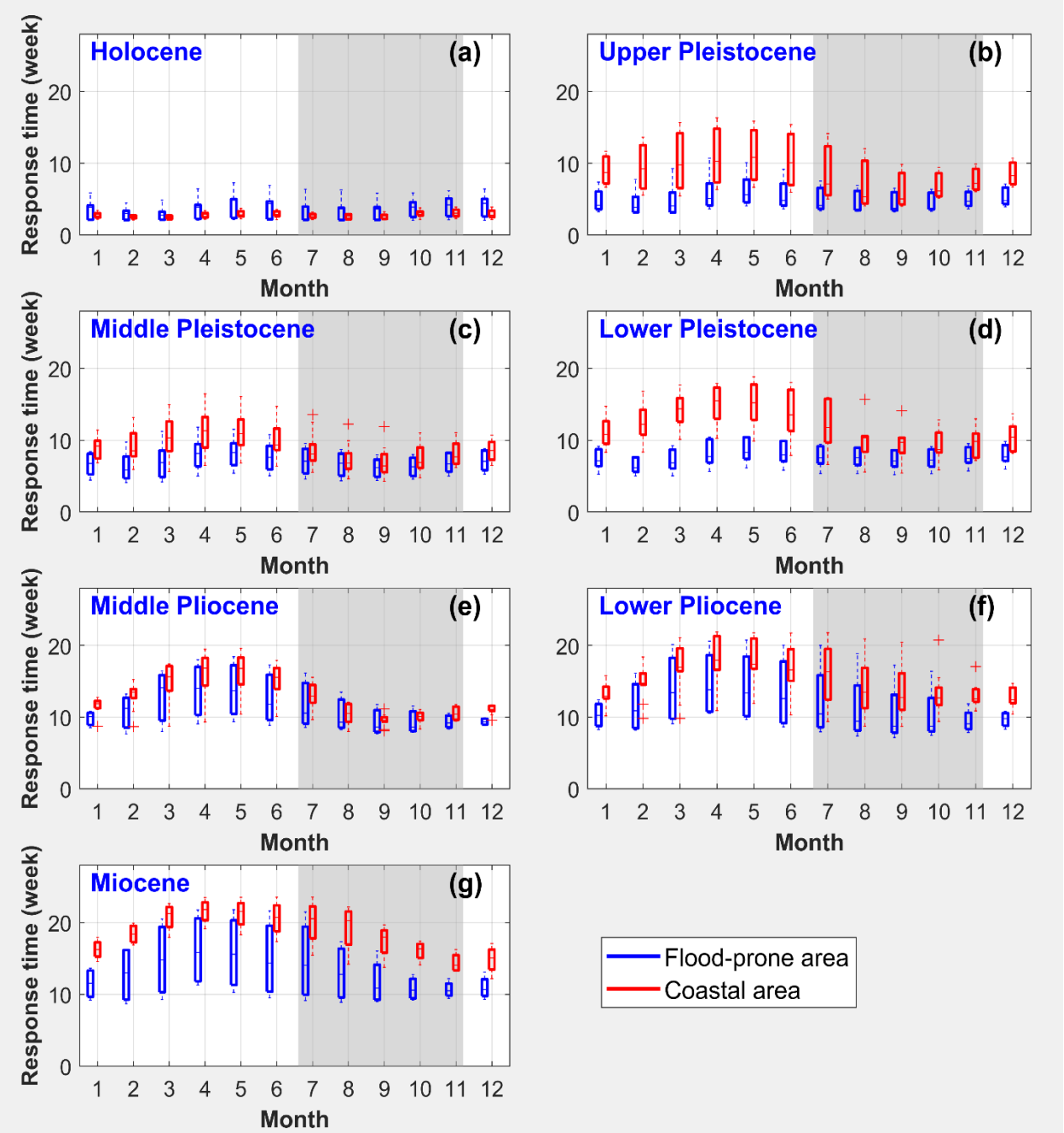

Figure 4.8: Response time, averaged for each month, between surface water and groundwater for different aquifers in both flood-prone and coastal areas in the VMD. Grey areas indicate flood season

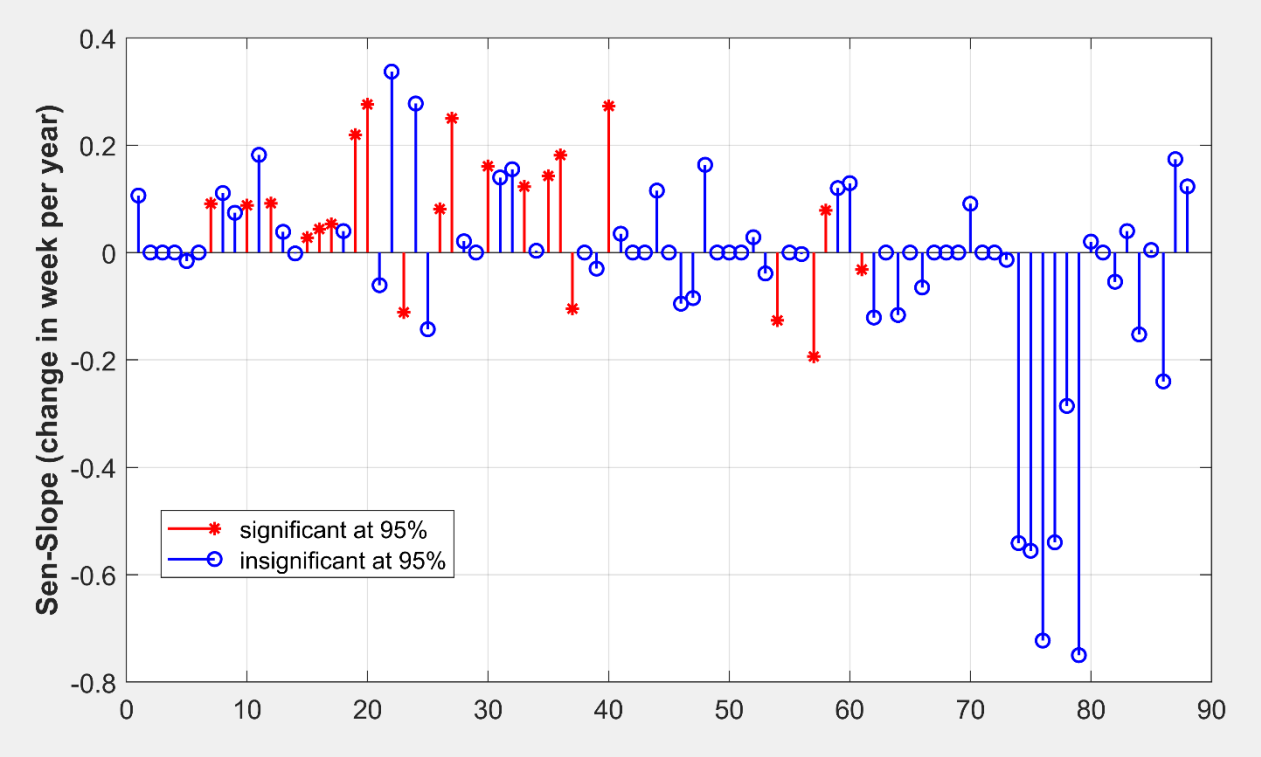

Figure 4.9: Long-term changes of the response times (reported as Sen's slope in the y-axis) relative to the monthly mean response time for the 88 boreholes (x-axis) in the VMD.

Generally, we observed high variability in response time in the alluvial multi-aquifer system. Shorter response time was observed for shallow groundwater compared to deep groundwater (Figure 4.8). The response time range increased from the Holocene (1.9-7.3 weeks) to the Pleistocene (3.7-18.9 weeks), the Pliocene (7.5-22.5 weeks), and the Miocene aquifers (9.1-23.8 weeks). Except for the Holocene aquifer, apparent seasonal variation of response time was observed for all aquifers, and the response times in the flood-prone areas were shorter compared to those in the coastal areas.

The variability of response time in both flood and dry seasons for the Holocene aquifer was insignificant. For other aquifers, response time varied seasonally, with lower values during the flood season. The shortest response time was detected mainly in the peak flood period (e.g., September or October), with the longest response time at the end of the dry season (e.g., May). Most likely this was caused by the higher hydraulic head in the surface water during the flood season. Notably, due to a low number of monitoring boreholes in the Pliocene and Miocene aquifers (3-4 boreholes in each aquifer, cf. Figure 4.7), the identification of response-time variations in these aquifers in the flood-prone areas might be impaired.

4.5 Discussion

4.5.1 Potential of groundwater recharge and role of alluvial aquifers in the VMD

The decreasing magnitude of seasonal variation from shallow to deep groundwater (Figure 4.4) suggests that the alluvial aquifers act as low-pass filters during the transformation of input signals (e.g., river discharge or water levels) into output signals (e.g., groundwater water levels), resulting in increasing memory effects (Figure 4.7) and response times (Figure 4.8) with aquifer depth in the VMD. The role of aquifers as a low-pass filter in the frequency domain has also been reported in other alluvial settings (e.g., Imagawa et al., 2013; Duvert et al., 2015).

Regarding shallow aquifers, the dominance of the seasonal variability (Figure 4.3) and similar patterns of seasonal fluctuations between GWLs and surface water (Figure 4.4) suggest a good hydraulic connection between river water and shallow aquifers (i.e. Holocene and Pleistocene) across the delta. This result is in line with the findings of Wagner et al. (2012) that shallow groundwater is effectively connected to surface water (e.g., rivers, irrigation channels, or floodplains) in the area. This connectivity, as expressed by higher seasonal variabilities (Figure 4.4b, c, d), is more pronounced in the flood-prone areas compared to the coastal areas. Such effective connection suggests a high potential for groundwater recharge from surface water to shallow aquifers, particularly for locations in the flood-prone areas, where long-lasting and widespread inundations occur regularly. The inundations create a strong hydraulic head and provide sufficient water volume for shallow GW recharge, which is missing in the coastal region. Therefore, the seasonal signal observed in the coastal shallow aquifers has to be attributed to different sources or causes. The most plausible reason and the source are likely lateral inflow in the shallow coastal aquifers from the upstream region, i.e. from the inundated areas, as suggested by Hoang and Bäumle (2019). During the flood season, the hydraulic head in the shallow aquifers underneath the inundated areas rise and creates a head for lateral downstream flow within the aquifers towards the coastal region. The seasonal signal is thus dampened because of the flow time and distance and available volume. This seasonal component is additionally dampened in the coastal region by the permanent head caused by the ocean.

For deep groundwater, low permeable aquicludes appear to limit the recharge to the deeper aquifers (Pliocene and Miocene aquifers) both in flood-prone and coastal areas. The dominance of trend components (Figure 4.3) and the low variation of GWLs in the Pliocene and Miocene aquifers (Figure 4.4e,f,g) corroborate these findings. Significant increasing memory effect and response time within the well depth (Figure 4.7 and Figure 4.8) also indicate that the recent recharge to deep aquifers, if there is any, is very limited. Hence the deeper aquifers may be hardly replenished by surface water sources including precipitation sources in the VMD. Hung Van et al. (2019) pointed out that the freshwater from the upper system cannot infiltrate deeper than about 350 m; hence saline water could also not enter the deep groundwater system. Considering the

presented results and the literature sources, any potential recharge of the deeper aquifers is very unlikely to originate from vertical infiltration through the aquiclude layers, but rather from the lateral flow within the aquifers from upstream areas. Considering the morphological development of the Mekong Delta, the deeper aquifers are located closer to the surface in the highland areas of southern Vietnam (e.g. Binh Phuoc) or Cambodia (Ha et al., 2019). The presented analysis, in combination with literature findings, implies that the vertical recharge pathway via aquiclude layers and the inter-aquifer connectivity in the multi-aquifer system is insignificant in the VMD. This, in turn, means that a natural replenishment of the over-exploited deeper aquifers as the primary freshwater sources in the VMD cannot be achieved locally by natural pathways. Instead, the recharge could depend on the infiltration processes and management and exploitation of the deeper aquifers in the neighboring regions, particularly Cambodia. This also means that recovery of GW levels in the deeper aquifers by natural sources requires a substantial amount of time.

Additionally, the operation of all planned dams in the Mekong basin will most likely reduce flood season flow. It will thus also reduce the recharge to the aquifers in the VMD, both the shallow aquifers (recharge within the VMD) and deeper aquifers (recharge from the inundated areas in the Cambodian part of the delta). This finding is in line with Kazama et al. (2007), who stated that a 44% reduction in flooding areas could result in a 42% decline of shallow groundwater storage in the Mekong delta. Weighing the potential impacts of climate change and reservoir operation on the Mekong hydrology on groundwater recharge, the negative impacts of reservoir operation will more likely overwrite the possible positive effects of increased flood season flow under climate change projections (Lauri et al., 2012). Although a quantitative assessment of the effects of dam development on groundwater recharge has not been carried yet, the presented results imply that any substantial negative changes in flood volume and floodplain inundation could impair the recharge of groundwater in all aquifers in the VMD. This aspect should be considered in long term strategic planning of the management of the groundwater resources, next to the urgently needed short-term limitation of current GW exploitation.

4.5.2 Drivers of GWL declines

Extending the findings of previous studies (e.g., Wagner et al., 2012; Erban et al., 2014), this work uses more recent data to confirm the previously observed decrease of GWLs in deeper aquifers in the VMD by time-variant trend analysis based on high-frequency groundwater observations considering both shallow and deep aquifers. The overall variabilities of the declining trends of GWLs confirm the decrease rate of 9-78 cm/year reported in Erban et al. (2014), i.e. indicate that GW over-exploitation continued in the last decade. Our results indicate that groundwater abstractions highly exceeded groundwater recharge, resulting in a considerable decrease of GWLs and groundwater storage in the VMD over the last 22 years.

The minor changes in GWL in the shallow aquifers, however, are a result of the interplay between the good connectivity to and recharge from surface water, the compaction of the young sediment composing the aquifers (Wagner et al., 2012), and the comparatively low abstraction from the aquifers. These factors compensate each other, resulting in the observed overall low decline in the shallow aquifers. On the contrary, the significant decrease of GWLs in the deeper aquifers can be linked to the limited potential recharge (section 4.5.1) and to the high amount of groundwater abstraction. The groundwater in the Pliocene and Miocene aquifers has good drinking water quality and is thus heavily used. The highest decreasing trends were identified mainly for urban areas with high population densities (Figure 4.5), and thus indicate that human activities are very likely the dominant driver of this GWL decline. Moreover, in coastal regions saltwater intrusion in surface water poses impedes the use of shallow groundwater as a drinking water source or for irrigation (cf. Fig.2 Smajgl et al., 2015). Therefore groundwater is the key source of freshwater for domestic uses and agricultural production in the coastal regions (Wagner et al., 2012). The pronounced decreasing trend of GWLs in the coastal areas compared to the flood-prone areas in the Pleistocene aquifers (Figure 4.5b, c, d) thus provides evidence for a significant and non-sustainable groundwater abstraction in the coastal areas. For example, groundwater is highly exploited for domestic freshwater supply in Ca Mau peninsula. The results presented in this study indicate that the high demands for groundwater resources cannot be compensated by the limited recharge. According to Danh and Khai (2015), groundwater in the VMD is typically accessed via private tube-wells (more than one million over the whole delta) at depths of 80-120 m (corresponding to Pleistocene aquifers), and abstraction wells of freshwater supply plants, reaching depths of 200-450 m (corresponding to the Pliocene and Miocene aquifers). Therefore the decline of GWLs in the Pleistocene aquifers can be attributed to household demand. In contrast, the decrease in the Pliocene or Miocene aquifers can be linked to the demand of water supply plants, and thus the general water demand of the population and economy.

The acceleration of the decrease of GWLs (Figure 4.6) can be linked to the increasing trend in groundwater exploitation, and the consequent widespread land subsidence for the VMD (Erban et al., 2013; Erban et al., 2014; Minderhoud et al., 2017), similar to many deltas and coastal areas around the world (see Gambolati and Teatini, 2015). Our study suggests that the current groundwater exploitation already exceeds aquifer recharge capacities in the VMD. Due to the demand for socio-economic and industrial development, groundwater exploitation is forecasted to further increase in the future (Danh and Khai, 2015). A further severe decline of GWLs would, however, accelerate saltwater intrusion into the alluvial aquifers, groundwater contamination, land subsidence, and thus threaten sustainable development in the entire delta (Minderhoud et al., 2017).

4.5.3 Groundwater memory effect in alluvial settings

The analysis of the auto-correlation with the logarithmic fits and the de-correlation time provides insights into the memory effects in the different aquifers. For shallow groundwater, the short memory effect indicates a good hydraulic connection to surface water, and thus a high potential for groundwater recharge. This was to be expected from the geological setting. Following the same logic, long memory effects in the deeper aquifers, indicate a poor hydraulic connection to surface water and thus limited groundwater recharge. Because groundwater storage can be attributed to structural factors that are difficult to assess (e.g., the change in grain size of the aquifer material or its degree of compaction, which can change the hydraulic conductivities and groundwater outflow) (Duvert et al., 2015), the presented analysis of the memory effects might serve as a proxy-information on potential groundwater storage. In the VMD, the memory effect of alluvial aquifers varies according to the geographical location (Figure 4.7). Groundwater memory increases in both vertical and horizontal directions: (1) from shallow to deep aquifer, and (2) from upstream (i.e., flood-prone regions) to downstream (i.e., coastal areas). The vertical increase of the memory effect from shallow to deep aquifer can be attributed to the existence of low-permeable aquicludes between aquifers. The aquicludes between deep aquifers (Pliocene and Miocene) are thicker and characterized by lower hydraulic conductivities compared to the shallow aquifer (Holocene and Pleistocene) (Hung Van et al., 2019). These aquicludes act thus as low-pass filters in the frequency domain weakening the variation of GWLs at the deep groundwater in the VMD. This behavior was also reported for similar geological settings, e.g. for alluvial aquifers in the Shiga Prefecture, Japan (Imagawa et al., 2013) and southeast Queensland, Australia (Duvert et al., 2015) –. Similarly, the horizontal spatial differences of the memory effect may be caused by the spatial variation of physical properties (e.g., hydraulic conductivity and thickness) of the aquifers (Zhang and Schilling, 2004). In this context, an explanation for the generally higher memory effect from upstream to downstream in the VMD could be the higher thickness of the aquicludes in coastal areas compared to flood-prone areas, cf. to Figure 2 in Hung Van et al. (2019).

Generally, longer memory effects indicate higher water storage capacities, particularly in the case of the deep alluvial aquifers in the VMD. The longer the groundwater memory, i.e. the persistence of a signal in an aquifer, the larger is the storage capacity because the comparatively large storage dampens the signal. A similar explanation for longer memory effects and groundwater storage was given by Mangin (1984) and Imagawa et al. (2013). This means that the potential for groundwater storage and restoration is higher in the deeper aquifers. This comes, however, at the cost of longer natural recharge times, which has to be considered in any sustainable GW management plan.

4.5.4 Factors controlling the impulse response between surface water and alluvial aquifers

The moving window cross-correlation analysis shows that the interaction between surface water and groundwater is highly dynamic and exhibiting strong seasonality. The differences in impulse response between the river and the different alluvial aquifers can be attributed to (1) groundwater depth, (2) seasonal variability, (3) location (i.e., flood-prone or coastal areas), and (4) existence of aquicludes. Shorter response times were detected for shallow groundwater, the flood season, and flood-prone regions (Figure 4.8). Except for Holocene aquifer, the response time of boreholes in flood-prone areas in the dry season are still shorter than those in coastal are in flood season, indicating that the response time is more controlled by location than seasonal variability. This result supports the assumption that the deeper aquifers might be recharged from upstream areas of the VMD (see Section 4.5.1). These findings are in line with the expected behaviour based on general hydrological and hydraulic reasoning, thus confirming the validity of the approach. During the flood season (July-November), inundation is up to 4.0 m high and lasts for 3 to 6 months in flood-prone areas (Toan, 2014). River water levels, inundation depths and soil saturation are higher during the flood period; thus the pressure pulse is transmitted more rapidly and directly to aquifers compared to the dry period, and sufficient amounts of water (ponding water on inundated floodplains) are available to recharge the GW. The response times of the deeper aquifers (Lower Pliocene and Miocene) are in the range of the duration of the flood season. This does not mean that these aquifers are recharged at the end of the flood season because the response might be lagged in time. Because the response time is calculated by mathematical relations (correlations) between time series; it is not the residence time that water particles travel from the surface water to aquifers (an actual recharge of freshwater). Instead, it should be considered as an indicator for the hydraulic response of the alluvial aquifers in the VMD. Although the response time does not reveal much about the actual rate of recharge, it can provide an initial "threshold" about the actual rate of recharge. For example, the response time of Pliocene is about 5-7 times longer than of Holocene (Figure 4.8). If the residence time of Holocene is identified from 35-40 weeks (see Duy et al., 2019), it can be estimated that residence time from surface water to Pliocene aquifer should be longer than 200 weeks. Any shortening of the flood season and reduction of flood season flow, as e.g. caused by strong El Niño events (Ruiz-Barradas and Nigam, 2018) or by the operation of reservoirs in the Mekong basin (Lauri et al., 2012), would thus indicate that the deeper aquifers will likely receive less recharge during the flood season. However, as climate change scenarios predict an intensification of the Southeast Asian monsoon and an increase in flood season discharge (Hoang et al., 2016), there are also chances of increasing recharge of the deeper aquifers in the VMD in the future, provided that the reservoir operation does not diminish this effect.

4.5.5 Limitations and wider implications

The time series analysis we are applying is in principle a black-box model, and can only determine mathematical relations (correlations) between time series, not causal relationships (Bakker and Schaars, 2019). The approach is thus only suitable to highlight and visualize the behavior of a groundwater system without an explicit analysis of the underlying physics and/or drivers of system behavior. Therefore, this study should be considered as the first step towards a characterization of the previously unstudied behaviors of alluvial aquifers in the VMD. Future research should thus aim at a quantitative investigation of the drivers of the memory effect and response time in the VMD. To understand the physical processes of a groundwater system, a physical-based or at least conceptual groundwater model is required, which is out of the scope of this study.

In this study, time series analysis can provide valuable information about time-variant trends of GWLs, the memory effect, and the response time for the whole VMD. The visualization of these groundwater dynamics provides an overview on how long an aquifer stores water (memory effect), how fast an aquifer responds to variations in surface water (response time), and the recently accelerating decline of GWLs in the VMD. These findings should be considered as initial contributions to the hydrogeological literature of a little-known groundwater system in alluvial settings. Due to simplicity and ease of interpretation, the applied time series analysis can be an additional tool, for example, to process data and quickly provide efficient alternatives to calibrate groundwater models (Bakker and Schaars, 2019). Also, the approach has direct implications for the initial investigations of an understudied groundwater system where data and/or resources (e.g., human or financial) are insufficient to develop a dynamic groundwater model.

4.6 Conclusions

This study provides hydrogeological storage characteristics of the alluvial aquifers in the VMD. We examined the groundwater dynamics focusing on (1) the recent trend of groundwater levels in order to indicate GW over-exploitation, (2) the memory effect of alluvial aquifers for an assessment of the GW storage, and (3) the response time between surface water and groundwater as a proxy for GW recharge. GWL time series between 1996 and 2017 from 88 boreholes at 27 national stations were collected, selecting time series with a sampling resolution higher than once per week and monitoring periods longer than ten years.

The time-series decomposition of GWLs highlights the large seasonal variability in the shallow aquifers and the dominance of the trend component in the deep aquifers. This indicates an effective connection between the shallow Holocene aquifer and surface water, and a high potential for shallow groundwater recharge. The low permeable aquicludes separating the aquifers behave as low-pass filters that reduce the high-frequency signals in the GWL variations, and limit the recharge to the deeper aquifers.

The trend analysis indicates that both shallow and deep aquifers are currently over-exploited and not fully recharged, resulting in a considerable decrease of GWLs (0.01-0.55 m/year) and groundwater storage over the last 22 years. Significant downward trends were detected in the deep aquifers, which is the primary source of GW used for drinking water purposes, compared to weak declining trends in shallow aquifers, which has a higher potential for groundwater recharge and is much less exploited due to water quality issues. This study leads to the conclusion that the groundwater abstraction has accelerated the GWL declines. These findings are evidenced by a stronger declining time-variant trend observed for almost all boreholes in later periods (i.e., after 2007) compared to early periods (i.e., before 2006). While the slight decline of GWLs in the Holocene aquifer (0.01-0.11 m/year) is likely caused by natural variations and effects (e.g., the compaction of the delta), the significantly declining GWLs of the Pliocene and Miocene aquifers (0.25-0.55 m/year) can be attributed to the groundwater over-exploitation particularly around urban and industrial areas in the VMD.

The groundwater memory varies according to the geographical location, being shorter from shallow to deep aquifers, and from flood to coastal areas. The memory effects of shallow and deep groundwater are in the range of 5-17 weeks and 10-33 weeks, respectively. Interpreting longer memory as higher storage, it can be concluded that the deeper aquifers have a higher storage capacity than the shallow aquifers.

The moving cross-correlation analysis highlights the highly dynamic interaction between surface water and groundwater. The response time between the river and alluvial aquifers depends on groundwater depth, seasonal variability, and location. Shorter response times were detected in the flood season compared to the dry season. The seasonal variability of response time was influenced by the flood period and the flood timing. Higher water levels during the flood season likely transmit the pressure pulse more rapidly and directly. Moreover, the response times of the deeper and heavily used aquifers are in the range of the duration of the flood season. This finding is relevant for any estimation of the recharge to the most important aquifer (i.e., the Pliocene aquifer) of the VMD during the flood season. It essentially means that this aquifer most likely receives hardly any recharge during shortened flood seasons (like, e.g., during the frequently occurring El Niño events).

More generally, our study illustrates the usefulness of time-series techniques to understand the mechanisms of groundwater recharge, discharge and storage in alluvial settings. The findings on the variabilities of GWL trends, the memory effect of alluvial aquifers, and the response time between surface water and groundwater are primarily highlighted for the VMD. The information is crucial for groundwater resource management in the VMD. Due to its simplicity, the applied time-series analysis can be easily reproduced to provide insights on groundwater behavior in other alluvial settings.

Chapter 5 Discussion and Conclusions

5.1 Main findings

The main objectives of this thesis were to advance existing methodologies for a better understanding of hydrological processes in the VMD. The assessment was mainly based on statistical analyses of the isotopic data of GNIP stations (IAEA/WMO, 2016), the meteorological and hydrological data from Vietnamese agencies, and of the stable water isotopes and monitoring data collected as part of this work. The component studies, presented as three stand-alone publications, have together provided insights into the controlling processes of precipitation (Chapter 2), the mechanism of surface–groundwater interaction (Chapter 3), and the groundwater dynamics (Chapter 4) in the VMD. The main achievements in relation to the research questions framed in the beginning are summarized in the following.

1. Where do the moisture sources of precipitation in the VMD origin from?

Backward trajectory computations by the HYSPLIT model (section 2.3.5) provided a rough indication of potential moisture sources of precipitation (section 2.4.1). The precipitation in the dry season likely originates from the moisture sources of the Asian continent and the equatorial easterlies; meanwhile, the precipitation in the rainy season might arises from the moisture sources of tropical Indian Ocean and the South Pacific Ocean (Figure 2.5 and Figure 2.6). The analysis of transport durations indicates that the moisture-producing precipitation reaching the study area likely travels about 4–6 days from its source, as the best regressions are obtained for these travel durations (Figure 2.11). For longer travel durations, the moisture can be recycled (e.g., precipitated and evaporated again) when the travel time exceeds six days.

2. Which factors control the precipitation isotopes in the VMD?

Simultaneous testing of multi-factor linear regression (section 2.3.6) combined with relative importance analysis (section 2.3.7) were used to identify factors controlling the precipitation isotopes as well as their contributions (section 2.4.3 and 2.4.4). The study showed that regional and local climatic factors vary in importance over the seasons and that the source regions and transport pathways have a considerable influence on the isotopic composition of rainfall. The multiple linear regression can better explain the total variation in $\delta^{18}O$ precipitation (up to 80%) compared to single-factor linear regression (30%) (Figure 2.12). The relative importance analysis indicated that precipitation isotopes were dominantly controlled by regional moisture regimes ($\sim$ 70 %) compared to local climatic conditions ($\sim$ 30 %) (Table 2.4). The most important factor was the upstream rainfall along the trajectories of air mass movement. It is also suggested that regional and local climatic factors vary in importance over the seasons (Figure 2.13), and the source regions and transport pathways have a significant influence on the precipitation isotopes in the VMD.

This work also indicated that the variability in the isotopic signature and the developed LMWL (see section 2.4.2) could be representative of the southern continental part of the Indochinese Peninsula. The results have direct implications for the interpretation of paleo records of stable water isotopes in terms of past climate conditions for Southeast Asia. The factors controlling the isotopic signature of precipitation in tropical areas are changing between and even within seasons, and regional factors have substantial impacts on the local isotopic composition of rainfall. This needs to be considered in the reconstruction of past climates based on isotopic records.

3. What are the subsurface flow conditions in riverbank infiltration areas in the VMD?

Two-component LPMs (section 3.3.3) in conjunction with hydrological and isotopic measurements (section 3.3.1 and 3.3.2) could identify subsurface flow conditions in riverbank infiltration system. The statistical analysis of best-suited TTDs (section 3.4.4) indicated that the linear piston flow (LPF) distribution likely represents the subsurface flow conditions in the VMD. Remarkably, the subsurface flow condition was probably best described with a linear distribution accounting for the infiltration along the river followed by the hydraulic replacement of groundwater caused by pressure gradients that adds the piston flow component to the model (see discussion in section 3.5.3). In the hydrogeological setting characterized by a partially confined aquifer that does not create a phreatic system, the subsurface transport of water can be better described by a linear distribution rather than by an exponential distribution. It is suggested that the LPF model could be a reliable method to examine the subsurface flow condition in the riverbank infiltration system.

4. What is the level of infiltration of river water and precipitation to shallow groundwater and their age variations in riverbank areas in the VMD?

Transit time modelling (section 3.4.3 and section 3.4.5) indicated that the mTTs of riverbank infiltration increase with the length of the horizontal flow path and the decreasing flow path gradient between river and groundwater. River water infiltrates horizontally mainly via the highly permeable aquifer, resulting in short mTTs (<40 weeks) for locations close to the river (<200 m). For sites farther from the river (>750m), the mTTs of river infiltration cannot be constrained. The infiltration of precipitation is independent of the distance to the river and takes place vertically mainly via a low-permeable overlying aquitard, resulting in considerably longer mTTs (>80 weeks). It is noted that the identified mTTs should be considered partial transit times with preference for young waters contributing to shallow groundwater in the VMD.

The findings on the spatial variation of mTTs, the different recharge contributions, and the subsurface flow conditions are useful to develop a conceptual model of surface–groundwater interaction in riverbank areas (see section 3.5.4). Groundwater resources management needs to consider the different recharge mechanisms and mTTs (mainly controlled by the distance to the river), resulting in different management options for other areas in the alluvial delta.

5. What changes in groundwater levels in the VMD can be detected over the last two decades? (Chapter 4)

Time-variant trend analysis (section 4.3.4) highlighted both temporal and spatial changes of GWLs in the VMD (section 4.4.2). Both shallow and deep aquifers exhibited a considerable decrease of GWLs (0.01-0.55 m/year), as a result of over-exploitation and partial recharge over the last 22 years. Significant declining trends were detected in deeper aquifers (e.g., the Pliocene and Miocene), while slightly declining trends (0.01-0.11 m/year) are observed in the shallow aquifer (e.g., the Holocene). The medium depth Pleistocene aquifers showed decreasing trends (0.05-0.41 m/year) in-between the detected trends of the deep and shallow aquifers. The strongest negative trends were observed mainly in areas around major cities (e.g., Tan An, Cao Lanh, Long Xuyen, Can Tho, and Ca Mau) (Figure 4.5). Significant downward trends were also detected in deep aquifers, which is the primary source of GW used for drinking water purposes. Whereas weak declining trends were observed in shallow aquifers, which is a higher potential of groundwater recharge and much less exploited due to water quality issues. Detected trends do not only vary depending on spatial variability but also on the considered time period. For example, the magnitude of the declining trend for almost all boreholes has been considerably higher since post-2007 (Figure 4.6), indicating that the recent groundwater abstraction has accelerated the GWL declines in the VMD. These findings are in line with declining trends in groundwater levels expected in other Asian mega-deltas influenced by groundwater abstraction and global sea-level rise.

6. What is the length of groundwater memory effect (the time that an aquifer holds water) in the VMD?

Auto-correlation analysis (section 4.3.5) highlighted a stronger memory effect for deep aquifers (e.g., Pliocene and Miocene) compared to shallow aquifers (e.g., Holocene and Pleistocene) (section 4.4.3). Stronger memory effects are also identified for boreholes located in coastal areas compared to those in flood-prone areas. However, this behaviour is not apparent for Holocene aquifers. The memory effect of alluvial aquifers varies according to the geographical location (Figure 4.7), increasing from shallow to deep groundwater and from upstream to downstream. An explanation for the increasing memory effect can be attributed to the physical properties (e.g., hydraulic conductivity and thickness) of the low-permeable aquicludes which act as low-pass filters in the frequency domain between alluvial aquifers (see discussion in section 4.5.3). The findings on memory effect can serve as a proxy-information on potential groundwater storage in the VMD.

7. What is the response of alluvial aquifers to surface water in the VMD?

The sliding window cross-correlation analysis (section 4.3.6) revealed a highly dynamic response between surface water and alluvial aquifers in the VMD (section 4.4.4). The response time between the river and alluvial aquifers were mainly controlled by the groundwater depth, season,

location, and existence of aquicludes. Except for the Holocene aquifer, faster responses were observed for shallow groundwater compared to deep groundwater and in the flood-prone areas compared to the coastal regions (Figure 4.8). The seasonal variability of response time was also influenced by the flood period and the flood timing. Higher water levels during the flood season likely transmitted the pressure pulse more rapidly and directly. Moreover, the response times of the deeper and heavily used aquifers were in the range of the duration of the flood season indicating that these aquifers most likely received hardly any recharge during shortened flood seasons (like, e.g., during the frequently occurring El Niño events). These findings provided a sound basis for any estimation of the seasonal recharge from the surface water to alluvial aquifers in the VMD.

5.2 Methodological implications

The thesis not only adds to the conceptual understanding of hydrological processes, but it also contributed to methodologies applicable in alluvial regions in the VMD. Specifically, the methodological implications of component chapters are highlighted in the following.

Chapter 2 indicated that model-based statistical approaches (e.g., the combination of trajectory analysis, multi-factor linear regression, and relative importance analysis) could be a powerful tool to detect the relevant factors controlling the precipitation isotopes as well as their contributions. The approach is easily reproducible and contains a rigorous quantitative analysis of the interplay of different driving factors, without the requirement of setting up or in-depth knowledge about running complex numerical atmospheric circulation models. If applied to seasonal data subsets, the quantification can be improved, and the seasonal differences in controlling factors and processes can be identified. The validity of the approach is confirmed by similar, but mainly qualitative results obtained in other studies. It is argued that the method constitutes an advancement in the statistical analysis of isotopic records in precipitation that can supplement or precede more complex studies utilizing atmospheric models. Due to the simplicity, the method can be easily transferred to investigate factors controlling the isotopic composition of precipitation at similar tropical and monsoon-region settings.

Chapter 3 suggested a novel concept of two-component LPMs that are solved using $\delta^{18}O$ records to investigate the young water transit times and subsurface flow conditions. Based on different model setups (see section 3.3.8), insights into the model behaviour, parameter identifiability, and uncertainties can be examined. The concept could be further developed by utilizing two-component LPMs in conjunction with both stable and environmental isotopes (e.g., $\delta^{18}O$ and tritium) to investigate the subsurface flow of both younger and older water contributing to a groundwater system. However, the inevitable errors of two-component LPMs and shortcomings of isotopic data that could add uncertainties to the transit time analysis should be acknowledged (see section 3.5.5). Despite these limitations, this work underlines the power of two-component

LPMs in describing subsurface water movement at locations with different flow-path configurations and two groundwater recharge sources (e.g., at riverbank infiltration areas).

Chapter 4 illustrated the usefulness of time-series techniques to understand the groundwater dynamics in alluvial settings. In this work, time series analysis can reveal valuable information about time-variant trends of GWLs, the memory effect, and the response time of multi-layer alluvial aquifers. It is noted that the approach is suitable to highlight and visualize the behaviour of a groundwater system without an explicit analysis of underlying physics and drivers of system behaviour. Hence, it should be used as a first step towards behaviours of an understudied groundwater system where data and/or resources (e.g., human or financial) are insufficient to develop a regular groundwater model. Due to its simplicity, the applied time-series analysis can be easily reproduced to investigate unstudied behaviours of a groundwater system in other alluvial settings.

5.3 Limitations and recommendations for future studies

This thesis provides practical methodologies to answer research questions with respect to the specific hydrological processes (e.g., controls on precipitation, surface-groundwater interaction, and behaviours of alluvial aquifers) in the VMD. Regarding the validation and reproducibility of the suggested methods, a number of questions still need to be addressed, in part due to a range of limitations in the original research design. These limitations are briefly discussed below, and some recommendations should be considered to expand the implications of suggested methods to examine hydrological processes in similar settings.

5.3.1 Model-based statistical approaches to reconstruct paleoclimate based on isotopic records

An intrinsic limitation of the approach is that physical phenomenon (e.g., the moisture sources of precipitation) that occur in the real world cannot be adequately simulated within a climate model (here the HYSPLIT model and the underlying climate model). Despite the ongoing improvement, the HYSPLIT model parameterizations are still far from perfect, and this work cannot cover the known uncertainties in climate models. For example, the horizontal uncertainty of the trajectory calculations by HYSPLIT has been estimated to be 10–20 % of the travel distance (Draxler and Hess, 1998). To reduce the uncertainty in the trajectory analysis, grouping trajectories that share some commonalities in space and time can be applied (Fleming et al., 2012). Considering these uncertainties, the model-based statistical approaches should be tested in large-scale circulation studies.

The approach was based on the hypothesis that using multiple factors in a single linear model can explain a significant share of the observed variance in isotopic composition. A substantial limitation of this assumption is that climatic factors control the isotopic signal and the relationship

(e.g., linear regression) should remain valid over the entire proxy record. These assumptions are rarely fulfilled and often unrealistic because of the changes in seasonality and atmospheric circulation patterns, hence adding more uncertainties to the simulation of isotopic composition in precipitation. Findings of the factors controlling precipitation isotopes in this work might thus be valid for the studied time period only. Future studies should rely on high sampling resolution (e.g., daily) and long-term monitoring periods (e.g., more than five years) to improve the model validation, as well as reduce potentially misleading insights and uncertainties in the reconstruction of past climates based on isotopic records.

5.3.2 Two-component LPMs in conjunction with stable water isotopes to evaluate the groundwater transit time

The limitations and broader implications of two-component LPMs in conjunction with stable water isotopes to evaluate the groundwater transit time were well discussed in section 3.5.5. They are briefly summarized in the following.

The findings of TTDs and mTTs should be considered as the first step towards an analysis of nonstationary in surface-groundwater interaction. Future studies should focus mainly on time-variant transit time to highlight short-term system responses. Moreover, the long sequence and high resolution of samples should be made to improve the model calibration (Birkel et al., 2010) and reduce the uncertainties of mTT modelling (Timbe et al., 2015).

Studies relying solely on stable isotopes cannot provide the water ages older than 5 years (Stewart et al., 2010). Consequently, the identified mTTs should be considered partial transit times with preference for young waters contributing to a groundwater system. To evaluate contributions of older water fraction, environmental isotopes (e.g., tritium) can be used (e.g., Stewart et al., 2010; Morgenstern et al., 2015; Duvert et al., 2016).

The present two-component LPMs based on the same types of TTDs cannot provide an entire picture of all possible combination of selected TTDs. Future studies should consider the different mixing kinds of TTDs (e.g., Duvert et al., 2016) to examine other flow-path conditions of subsurface water in a groundwater system.

The isotopic enrichment due to the evaporation process could introduce uncertainties. With the available data, the present study cannot analyse the isotopic enrichment of local surface water, neither independently assess actual contributions of infiltrated water components. This should be achieved by using another tracer (e.g., Cl) in future studies.

5.3.3 Time series analysis to examine groundwater behaviours in alluvial settings

In this work, the time series analysis is, in principle a black-box model, and can only determine mathematical relations (correlations) between time series, not causal relationships. Without an

explicit analysis of the underlying physics or drivers of system behaviour, the approach is more appropriate to highlight and visualize the behaviour of a groundwater system. Therefore, this method should be used as the first step to understand the initial unstudied behaviours of alluvial aquifers. To explain the physical processes of a groundwater system, a physical-based or at least conceptual groundwater model is required, which is out of the scope of this study.

5.4 Concluding remarks

This thesis indicated that the statistical analyses of stable isotope and monitoring data is a powerful tool to gain insights in the hydrological processes in the VMD. Based on the application of model-based statistical approaches, two-component LPMs, and time series analysis, a number of research questions concerning the controls on precipitation, the surface-groundwater interaction, and the behaviours of alluvial aquifers can be answered. While the thesis focused on the studied areas in the VMD, the findings and the suggested methodologies in this work could apply to other tropical environments worldwide, particularly those experiencing alluvial settings.

Bibliography

Aggarwal, P.K., Fröhlich, K., Kulkarni, K.M., Gourcy, L.L., 2004. Stable isotope evidence for moisture sources in the Asian summer monsoon under present and past climate regimes. Geophysical Research Letters, 31(8).

An, T.D., Tsujimura, M., Le Phu, V., Kawachi, A., Ha, D.T., 2014. Chemical Characteristics of Surface Water and Groundwater in Coastal Watershed, Mekong Delta, Vietnam. Procedia Environmental Sciences, 20: 712-721.

An, T.D., Tsujimura, M., Phu, V.L., Ha, D.T., Hai, N.V., 2018. Isotopic and Hydrogeochemical Signatures in Evaluating Groundwater Quality in the Coastal Area of the Mekong Delta, Vietnam. Advances and Applications in Geospatial Technology and Earth Resources. Springer International Publishing, Cham, pp. 293-314.

Anderson, H.R., 1978. Hydrogeologic reconnaissance of the Mekong Delta in South Vietnam and Cambodia. 1608R. DOI:10.3133/wsp1608R

Anthony, E.J. et al., 2015. Linking rapid erosion of the Mekong River delta to human activities. Scientific Reports, 5: 14745. DOI:10.1038/srep14745

Apel, H., Hung, N., Long, T., Tri, V., 2012. Flood Hydraulics and Suspended Sediment Transport in the Plain of Reeds, Mekong Delta. In: Renaud, F.G., Kuenzer, C. (Eds.), The Mekong Delta System. Springer Environmental Science and Engineering. Springer Netherlands, pp. 221-232. DOI:10.1007/978-94-007-3962-8_8

Araguás-Araguás, L., Froehlich, K., Rozanski, K., 1998. Stable isotope composition of precipitation over southeast Asia. Journal of Geophysical Research: Atmospheres, 103(D22): 28721-28742.

Arias, M.E. et al., 2014. Impacts of hydropower and climate change on drivers of ecological productivity of Southeast Asia's most important wetland. Ecological Modelling, 272: 252-263. DOI:https://doi.org/10.1016/j.ecolmodel.2013.10.015

Bailly-Comte, V., Martin, J.B., Screaton, E., 2011. Time variant cross correlation to assess residence time of water and implication for hydraulics of a sink-rise karst system. Water Resources Research, 47(5).

Baker, A.J. et al., 2015. Seasonality of westerly moisture transport in the East Asian summer monsoon and its implications for interpreting precipitation δ18O. Journal of Geophysical Research: Atmospheres, 120(12): 5850-5862.

Bakker, M., Schaars, F., 2019. Solving Groundwater Flow Problems with Time Series Analysis: You May Not Even Need Another Model. Groundwater, 57(6): 826-833. DOI:10.1111/gwat.12927

Benner, S.G. et al., 2008. Groundwater flow in an arsenic-contaminated aquifer, Mekong Delta, Cambodia. Applied Geochemistry, 23(11): 3072-3087. DOI:https://doi.org/10.1016/j.apgeochem.2008.06.013

Bethke, C.M., Johnson, T.M., 2008. Groundwater Age and Groundwater Age Dating. Annual Review of Earth and Planetary Sciences, 36(1): 121-152. DOI:10.1146/annurev.earth.36.031207.124210

Beven, K., Binley, A., 1992. The future of distributed models: model calibration and uncertainty prediction. Hydrological processes, 6(3): 279-298.

Birkel, C., Dunn, S.M., Tetzlaff, D., Soulsby, C., 2010. Assessing the value of high-resolution isotope tracer data in the stepwise development of a lumped conceptual rainfall–runoff model. Hydrological Processes, 24(16): 2335-2348. DOI:10.1002/hyp.7763

Birkel, C. et al., 2016. Hydroclimatic controls on non-stationary stream water ages in humid tropical catchments. Journal of Hydrology, 542: 231-240. DOI:https://doi.org/10.1016/j.jhydrol.2016.09.006

Birkmann, J., Garschagen, M., Van Tuan, V., Binh, N.T., 2012. Vulnerability, coping and adaptation to water related hazards in the Vietnamese Mekong Delta, The Mekong delta system. Springer, pp. 245-289.

Blasch, K.W., Bryson, J.R., 2007. Distinguishing sources of ground water recharge by using δ2H and δ18O. Groundwater, 45(3): 294-308.

Boehmer, W., 2000. Ground Water Study Mekong Delta. HASKONING B. V. Consulting Engineers and Architects, in association with Division of Hydro-Geology and Engineering Geology for the South of Vietnam and ARCADIS Euroconsult, 136.

Bonell, M., Bruijnzeel, L.A., 2005. Forests, water and people in the humid tropics: past, present and future hydrological research for integrated land and water management. Cambridge University Press.

Bowen, G.J., 2008. Spatial analysis of the intra-annual variation of precipitation isotope ratios and its climatological corollaries. Journal of Geophysical Research: Atmospheres, 113(D5).

Bowen, G.J., Kennedy, C.D., Liu, Z., Stalker, J., 2011. Water balance model for mean annual hydrogen and oxygen isotope distributions in surface waters of the contiguous United States. Journal of Geophysical Research: Biogeosciences, 116(G4).

Box, G.E., Jenkins, G.M., Reinsel, G.C., 2011. Time series analysis: forecasting and control, 734. John Wiley & Sons.

Box, G.E., Jenkins, G.M., Reinsel, G.C., Ljung, G.M., 2015. Time series analysis: forecasting and control. John Wiley & Sons.

Breitenbach, S.F. et al., 2010. Strong influence of water vapor source dynamics on stable isotopes in precipitation observed in Southern Meghalaya, NE India. Earth and Planetary Science Letters, 292(1): 212-220.

Budescu, D.V., 1993. Dominance analysis: A new approach to the problem of relative importance of predictors in multiple regression. Psychological bulletin, 114(3): 542.

Buschmann, J. et al., 2008. Contamination of drinking water resources in the Mekong delta floodplains: Arsenic and other trace metals pose serious health risks to population. Environment International, 34(6): 756-764. DOI:https://doi.org/10.1016/j.envint.2007.12.025

Cabello, M., Orza, J., Galiano, V., Ruiz, G., 2008. Influence of meteorological input data on backtrajectory cluster analysis? a seven-year study for southeastern Spain. Advances in Science and Research, 2: 65-70.

Calderon, H., Uhlenbrook, S., 2016. Characterizing the climatic water balance dynamics and different runoff components in a poorly gauged tropical forested catchment, Nicaragua. Hydrological Sciences Journal, 61(14): 2465-2480. DOI:10.1080/02626667.2014.964244

Cartwright, I., Morgenstern, U., 2016. Contrasting transit times of water from peatlands and eucalypt forests in the Australian Alps determined by tritium: implications for vulnerability and the source of water in upland catchments. Hydrol Earth Syst Sc, 20(12): 4757-4773.

Chakraborty, S. et al., 2016. Atmospheric controls on the precipitation isotopes over the Andaman Islands, Bay of Bengal. Scientific reports, 6.

Clark, I.D., Fritz, P., 1997. Environmental isotopes in hydrogeology. CRC press.

Cleveland, R.B., Cleveland, W.S., McRae, J.E., Terpenning, I., 1990. STL: a seasonal-trend decomposition. Journal of official statistics, 6(1): 3-73.

Conroy, J.L., Cobb, K.M., Noone, D., 2013. Comparison of precipitation isotope variability across the tropical Pacific in observations and SWING2 model simulations. Journal of Geophysical Research: Atmospheres, 118(11): 5867-5892.

Cook, P.G., Böhlke, J.-K., 2000. Determining timescales for groundwater flow and solute transport, Environmental tracers in subsurface hydrology. Springer, pp. 1-30.

Craig, H., 1961. Isotopic variations in meteoric waters. Science, 133(3465): 1702-1703.

Crawford, J., Hollins, S.E., Meredith, K.T., Hughes, C.E., 2017. Precipitation stable isotope variability and subcloud evaporation processes in a semi-arid region. Hydrological Processes, 31(1): 20-34. DOI:10.1002/hyp.10885

Crawford, J., Hughes, C.E., Lykoudis, S., 2014. Alternative least squares methods for determining the meteoric water line, demonstrated using GNIP data. Journal of Hydrology, 519: 2331-2340.

Dang, T.D., Cochrane, T.A., Arias, M.E., Tri, V.P.D., 2018. Future hydrological alterations in the Mekong Delta under the impact of water resources development, land subsidence and sea level rise. Journal of Hydrology: Regional Studies, 15: 119-133. DOI:https://doi.org/10.1016/j.ejrh.2017.12.002

Dang, T.D., Cochrane, T.A., Arias, M.E., Van, P.D.T., de Vries, T.T., 2016. Hydrological alterations from water infrastructure development in the Mekong floodplains. Hydrological Processes, 30(21): 3824-3838. DOI:10.1002/hyp.10894

Danh, V.T., Khai, H.V., 2015. Household demand and supply for clean groundwater in the Mekong Delta, Vietnam. Renewables: Wind, Water, and Solar, 2(1): 4. DOI:10.1186/s40807-014-0004-7

Dansgaard, W., 1964. Stable isotopes in precipitation. Tellus, 16(4): 436-468.

Darby, S.E. et al., 2016. Fluvial sediment supply to a mega-delta reduced by shifting tropical-cyclone activity. Nature, 539(7628): 276-279. DOI:10.1038/nature19809

Darling, W., Morris, B., Stuart, M., Gooddy, D., 2005. Groundwater age indicators from public supplies tapping the Chalk aquifer of Southern England. Water and Environment Journal, 19(1): 30-40.

Dayem, K.E., Molnar, P., Battisti, D.S., Roe, G.H., 2010. Lessons learned from oxygen isotopes in modern precipitation applied to interpretation of speleothem records of paleoclimate from eastern Asia. Earth and Planetary Science Letters, 295(1): 219-230.

Delbart, C., Valdes, D., Barbecot, F., Tognelli, A., Couchoux, L., 2016. Spatial organization of the impulse response in a karst aquifer. Journal of hydrology, 537: 18-26.

Delbart, C. et al., 2014. Temporal variability of karst aquifer response time established by the sliding-windows cross-correlation method. Journal of Hydrology, 511: 580-588. DOI:https://doi.org/10.1016/j.jhydrol.2014.02.008

Delgado, J.M., Merz, B., Apel, H., 2012. Monsoon variability and the Mekong flood regime, The Mekong Delta System. Springer, pp. 233-244.

Diggle, P.J., 1990. Time series : a biostatistical introduction. Oxford : Clarendon press.

Draxler, R.R., Hess, G., 1998. An overview of the HYSPLIT_4 modelling system for trajectories. Australian meteorological magazine, 47(4): 295-308.

Draxler, R.R., Rolph, G., 2003. HYSPLIT (HYbrid Single-Particle Lagrangian Integrated Trajectory) model access via NOAA ARL READY website (http://ready.arl.noaa.gov/HYSPLIT.php). NOAA Air Resources Laboratory, Silver Spring. Md.

Dung, N.V., Merz, B., Bárdossy, A., Thang, T.D., Apel, H., 2011. Multi-objective automatic calibration of hydrodynamic models utilizing inundation maps and gauge data. Hydrol Earth Syst Sc, 15(4): 1339-1354.

Dunn, S.M. et al., 2008. Interpretation of homogeneity in δ18O signatures of stream water in a nested sub-catchment system in north-east Scotland. Hydrological Processes, 22(24): 4767-4782. DOI:doi:10.1002/hyp.7088

Duvert, C., Jourde, H., Raiber, M., Cox, M.E., 2015. Correlation and spectral analyses to assess the response of a shallow aquifer to low and high frequency rainfall fluctuations. Journal of Hydrology, 527: 894-907. DOI:https://doi.org/10.1016/j.jhydrol.2015.05.054

Duvert, C., Stewart, M., Cendón, D., Raiber, M., 2016. Time series of tritium, stable isotopes and chloride reveal short-term variations in groundwater contribution to a stream. Hydrol Earth Syst Sc, 20(1): 257-277.

Duy, N.L. et al., 2019. Identification of groundwater mean transit times of precipitation and riverbank infiltration by two-component lumped parameter models. Hydrological Processes, 0(ja). DOI:10.1002/hyp.13549

Duy, N.L., Heidbüchel, I., Meyer, H., Merz, B., Apel, H., 2018. What controls the stable isotope composition of precipitation in the Mekong Delta? A model-based statistical approach. Hydrol Earth Syst Sc, 22(2): 1239-1262.

Eberts, S.M., Böhlke, J.K., Kauffman, L.J., Jurgens, B.C., 2012. Comparison of particle-tracking and lumped-parameter age-distribution models for evaluating vulnerability of production wells to contamination. Hydrogeology Journal, 20(2): 263-282. DOI:10.1007/s10040-011-0810-6

Erban, L.E., Gorelick, S.M., Zebker, H.A., 2014. Groundwater extraction, land subsidence, and sea-level rise in the Mekong Delta, Vietnam. Environmental Research Letters, 9(8): 084010.

Erban, L.E., Gorelick, S.M., Zebker, H.A., Fendorf, S., 2013. Release of arsenic to deep groundwater in the Mekong Delta, Vietnam, linked to pumping-induced land subsidence. Proceedings of the National Academy of Sciences, 110(34): 13751-13756. DOI:10.1073/pnas.1300503110

Eslami, S. et al., 2019. Tidal amplification and salt intrusion in the Mekong Delta driven by anthropogenic sediment starvation. Scientific Reports, 9(1): 18746. DOI:10.1038/s41598-019-55018-9

Farrick, K.K., Branfireun, B.A., 2015. Flowpaths, source water contributions and water residence times in a Mexican tropical dry forest catchment. Journal of Hydrology, 529: 854-865. DOI:https://doi.org/10.1016/j.jhydrol.2015.08.059

Fekete, B.M., Gibson, J.J., Aggarwal, P., Vörösmarty, C.J., 2006. Application of isotope tracers in continental scale hydrological modeling. Journal of Hydrology, 330(3): 444-456.

Fetter, C., 2001. Applied Hydrogeology. 4th ed. Upper Saddle River, NJ: Prentice Hall: 598.

Fleming, Z.L., Monks, P.S., Manning, A.J., 2012. Untangling the influence of air-mass history in interpreting observed atmospheric composition. Atmospheric Research, 104: 1-39.

Froehlich, K., 2001. Deuterium excess in precipitation and its climatological significance. International Atomic Energy Agency, C&S Papers Series 13: 54-66.

Fujihara, Y. et al., 2016. Analysis and attribution of trends in water levels in the Vietnamese Mekong Delta. Hydrological Processes, 30(6): 835-845.

Gambolati, G., Teatini, P., 2015. Geomechanics of subsurface water withdrawal and injection. Water Resources Research, 51(6): 3922-3955.

Gat, J.R., 1996. Oxygen and hydrogen isotopes in the hydrologic cycle. Annual Review of Earth and Planetary Sciences, 24(1): 225-262.

Genereux, D.P., Hooper, R.P., 1998. Oxygen and hydrogen isotopes in rainfall-runoff studies. Isotope tracers in catchment hydrology: 319-346.

Gonfiantini, R., Fröhlich, K., Araguas-Araguas, L., Rozanski, K., 1998. Isotopes in groundwater hydrology. Isotope tracers in catchment hydrology: 203-246.

Grabczak, J., Różański, K., Maloszewski, P., Zuber, A., 1984. Estimation of the tritium input function with the aid of stable isotopes. CATENA, 11(2): 105-114. DOI:https://doi.org/10.1016/0341-8162(84)90001-8

GSO, 2016. Statistical Yearbook of Vietnam 2016. Hanoi: General Statistics Office (GSO) Vietnam.

Guan, H., Zhang, X., Skrzypek, G., Sun, Z., Xu, X., 2013. Deuterium excess variations of rainfall events in a coastal area of South Australia and its relationship with synoptic weather systems and atmospheric moisture sources. Journal of Geophysical Research: Atmospheres, 118(2): 1123-1138.

Gupta, H.V., Kling, H., Yilmaz, K.K., Martinez, G.F., 2009. Decomposition of the mean squared error and NSE performance criteria: Implications for improving hydrological modelling. Journal of Hydrology, 377(1): 80-91. DOI:https://doi.org/10.1016/j.jhydrol.2009.08.003

Ha, K., Ngoc, N.T.M., Lee, E., Jayakumar, R., 2015. Current Status and Issues of Groundwater in the Mekong River Basin. Korea Institute of Geoscience and Mineral Resources (KIGAM): Bangkok, Thailand: 121.

Heidbüchel, I., Troch, P.A., Lyon, S.W., Weiler, M., 2012. The master transit time distribution of variable flow systems. Water Resources Research, 48(6).

Helsel, D.R., Hirsch, R.M., 2002. Statistical methods in water resources, 323. US Geological survey Reston, VA.

Hirabayashi, Y. et al., 2013. Global flood risk under climate change. Nature Climate Change, 3(9): 816-821. DOI:10.1038/nclimate1911

Hiscock, K.M., Grischek, T., 2002. Attenuation of groundwater pollution by bank filtration. Journal of Hydrology, 266(3): 139-144. DOI:https://doi.org/10.1016/S0022-1694(02)00158-0

Ho, H.D. et al., 1991. Environmental isotope study related to the origin, salinization and movement of groundwater in the Mekong Delta (Viet Nam). Isotopes techniques in Water Resource Development: 415-428.

Hoang, L.P. et al., 2016. Mekong River flow and hydrological extremes under climate change. Hydrol. Earth Syst. Sci., 20(7): 3027-3041. DOI:10.5194/hess-20-3027-2016

Hoang, T.H., Bang, S., Kim, K.-W., Nguyen, M.H., Dang, D.M., 2010. Arsenic in groundwater and sediment in the Mekong River delta, Vietnam. Environmental Pollution, 158(8): 2648-2658. DOI:https://doi.org/10.1016/j.envpol.2010.05.001

Hrachowitz, M., Savenije, H., Bogaard, T.A., Tetzlaff, D., Soulsby, C., 2013. What can flux tracking teach us about water age distribution patterns and their temporal dynamics? Hydrol. Earth Syst. Sci., 17(2): 533-564. DOI:10.5194/hess-17-533-2013

Hrachowitz, M. et al., 2009. Using long-term data sets to understand transit times in contrasting headwater catchments. Journal of Hydrology, 367(3): 237-248. DOI:https://doi.org/10.1016/j.jhydrol.2009.01.001

Hrachowitz, M., Soulsby, C., Tetzlaff, D., Malcolm, I.A., 2011. Sensitivity of mean transit time estimates to model conditioning and data availability. Hydrological Processes, 25(6): 980-990. DOI:10.1002/hyp.7922

Hrachowitz, M., Soulsby, C., Tetzlaff, D., Malcolm, I.A., Schoups, G., 2010. Gamma distribution models for transit time estimation in catchments: Physical interpretation of parameters and implications for time-variant transit time assessment. Water Resources Research, 46(10): n/a-n/a. DOI:10.1029/2010WR009148

Huang, Y. et al., 2016. Arsenic contamination of groundwater and agricultural soil irrigated with the groundwater in Mekong Delta, Vietnam. Environmental Earth Sciences, 75(9): 757. DOI:10.1007/s12665-016-5535-3

Hughes, C.E., Crawford, J., 2012. A new precipitation weighted method for determining the meteoric water line for hydrological applications demonstrated using Australian and global GNIP data. Journal of Hydrology, 464: 344-351.

Hung, N.N. et al., 2014a. Sedimentation in the floodplains of the Mekong Delta, Vietnam Part II: deposition and erosion. Hydrological Processes, 28(7): 3145-3160. DOI:10.1002/hyp.9855

Hung, N.N. et al., 2014b. Sedimentation in the floodplains of the Mekong Delta, Vietnam. Part I: suspended sediment dynamics. Hydrological Processes, 28(7): 3132-3144.

Hung, N.N. et al., 2012. Floodplain hydrology of the Mekong Delta, Vietnam. Hydrological Processes, 26(5): 674-686. DOI:10.1002/hyp.8183

Hung Van, P., Van Geer, F.C., Bui Tran, V., Dubelaar, W., Oude Essink, G.H.P., 2019. Paleo-hydrogeological reconstruction of the fresh-saline groundwater distribution in the Vietnamese Mekong Delta since the late Pleistocene. Journal of Hydrology: Regional Studies, 23: 100594. DOI:https://doi.org/10.1016/j.ejrh.2019.100594

IAEA, 1992. Statistical treatment of data on environmental isotopes in precipitation. . IAEA: 781.

IAEA, 2014. IAEA/GNIP precipitation sampling guide. International Atomic Energy Agency.

IAEA/WMO, 2016. Global Network of Isotopes in Precipitation. The GNIP Database. Accessible at: http://www.iaea.org/water.

Ichiyanagi, K., Yamanaka, M.D., 2005. Interannual variation of stable isotopes in precipitation at Bangkok in response to El Niño Southern Oscillation. Hydrological processes, 19(17): 3413-3423.

Imagawa, C., Takeuchi, J., Kawachi, T., Chono, S., Ishida, K., 2013. Statistical analyses and modeling approaches to hydrodynamic characteristics in alluvial aquifer. Hydrological processes, 27(26): 4017-4027.

Ingraham, N.L., 1998. Isotopic variations in precipitation. Isotope Tracers in Catchment Hydrology: 87-118.

Ishizaki, Y. et al., 2012. Interannual variability of H218O in precipitation over the Asian monsoon region. Journal of Geophysical Research: Atmospheres, 117(D16).

Jacob, H., Sonntag, C., 1991. An 8-year record of the seasonal variation of 2H and 18O in atmospheric water vapour and precipitation at Heidelberg, Germany. Tellus B, 43(3): 291-300.

Jacobs, S.R. et al., 2018. Assessment of hydrological pathways in East African montane catchments under different land use. Hydrol. Earth Syst. Sci., 22(9): 4981-5000. DOI:10.5194/hess-22-4981-2018

Johnson, J.W., 2000. A heuristic method for estimating the relative weight of predictor variables in multiple regression. Multivariate behavioral research, 35(1): 1-19.

Johnson, K.R., Ingram, B.L., 2004. Spatial and temporal variability in the stable isotope systematics of modern precipitation in China: implications for paleoclimate reconstructions. Earth and Planetary Science Letters, 220(3): 365-377.

Johnston, R., Kummu, M., 2012. Water Resource Models in the Mekong Basin: A Review. Water Resources Management, 26(2): 429-455. DOI:10.1007/s11269-011-9925-8

Kabeya, N., Katsuyama, M., Kawasaki, M., Ohte, N., Sugimoto, A., 2007. Estimation of mean residence times of subsurface waters using seasonal variation in deuterium excess in a small headwater catchment in Japan. Hydrological Processes, 21(3): 308-322.

Kabeya, N. et al., 2008. Isotopic investigation of river water mixing around the confluence of the Tonle Sap and Mekong rivers. Hydrological Processes, 22(9): 1351-1358. DOI:Doi 10.1002/Hyp.6944

Kármán, K., Maloszewski, P., Deák, J., Fórizs, I., Szabó, C., 2014. Transit time determination for a riverbank filtration system using oxygen isotope data and the lumped-parameter model. Hydrological Sciences Journal, 59(6): 1109-1116.

Kazama, S., Hagiwara, T., Ranjan, P., Sawamoto, M., 2007. Evaluation of groundwater resources in wide inundation areas of the Mekong River basin. Journal of Hydrology, 340(3): 233-243. DOI:https://doi.org/10.1016/j.jhydrol.2007.04.017

Kendall, C., Caldwell, E.A., 1998. Fundamentals of isotope geochemistry. Isotope tracers in catchment hydrology: 51-86.

Kendall, C., McDonnell, J.J., 2012. Isotope tracers in catchment hydrology. Elsevier.

Kendall, M.G., 1948. Rank correlation methods. Rank correlation methods. Griffin, Oxford, England.

Kirchner, J.W., 2016a. Aggregation in environmental systems–Part 1: Seasonal tracer cycles quantify young water fractions, but not mean transit times, in spatially heterogeneous catchments. Hydrol Earth Syst Sc, 20(1): 279-297. DOI:https://doi.org/10.5194/hess-20-279-2016

Kirchner, J.W., 2016b. Aggregation in environmental systems – Part 1: Seasonal tracer cycles quantify young water fractions, but not mean transit times, in spatially heterogeneous catchments. Hydrol. Earth Syst. Sci., 20(1): 279-297. DOI:10.5194/hess-20-279-2016

Kirchner, J.W., Feng, X., Neal, C., 2000. Fractal stream chemistry and its implications for contaminant transport in catchments. Nature, 403(6769): 524.

Klaus, J., McDonnell, J., 2013. Hydrograph separation using stable isotopes: Review and evaluation. Journal of Hydrology, 505: 47-64.

Klaus, J., McDonnell, J., Jackson, C., Du, E., Griffiths, N., 2014. Where does streamwater come from in low relief forested watersheds? A dual isotope approach. Hydrology and Earth System Sciences Discussions, 11(3): 2613-2638.

Kocar, B.D. et al., 2008. Integrated biogeochemical and hydrologic processes driving arsenic release from shallow sediments to groundwaters of the Mekong delta. Applied Geochemistry, 23(11): 3059-3071. DOI:https://doi.org/10.1016/j.apgeochem.2008.06.026

Koeniger, P., Gaj, M., Beyer, M., Himmelsbach, T., 2016. Review on soil water isotope-based groundwater recharge estimations. Hydrological Processes, 30(16): 2817-2834. DOI:10.1002/hyp.10775

Kraha, A., Turner, H., Nimon, K., Zientek, L., Henson, R., 2012. Tools to Support Interpreting Multiple Regression in the Face of Multicollinearity. Frontiers in Psychology, 3: 44.

Kummu, M. et al., 2012. Lost food, wasted resources: Global food supply chain losses and their impacts on freshwater, cropland, and fertiliser use. Science of The Total Environment, 438: 477-489. DOI:https://doi.org/10.1016/j.scitotenv.2012.08.092

Kummu, M., Varis, O., 2007. Sediment-related impacts due to upstream reservoir trapping, the Lower Mekong River. Geomorphology, 85(3): 275-293. DOI:https://doi.org/10.1016/j.geomorph.2006.03.024

Kurita, N., Fujiyoshi, Y., Nakayama, T., Matsumi, Y., Kitagawa, H., 2015. East Asian Monsoon controls on the inter-annual variability in precipitation isotope ratio in Japan. Climate of the Past, 11(2): 339-353.

Kurita, N., Ichiyanagi, K., Matsumoto, J., Yamanaka, M.D., Ohata, T., 2009. The relationship between the isotopic content of precipitation and the precipitation amount in tropical regions. Journal of Geochemical Exploration, 102(3): 113-122.

Labat, D., Ababou, R., Mangin, A., 2000. Rainfall–runoff relations for karstic springs. Part I: convolution and spectral analyses. Journal of Hydrology, 238(3): 123-148. DOI:https://doi.org/10.1016/S0022-1694(00)00321-8

Lachniet, M.S., 2009. Sea surface temperature control on the stable isotopic composition of rainfall in Panama. Geophysical Research Letters, 36(3).

Lafare, A.E.A., Peach, D.W., Hughes, A.G., 2016. Use of seasonal trend decomposition to understand groundwater behaviour in the Permo-Triassic Sandstone aquifer, Eden Valley, UK. Hydrogeology Journal, 24(1): 141-158. DOI:10.1007/s10040-015-1309-3

Lamontagne, S. et al., 2015. River infiltration to a subtropical alluvial aquifer inferred using multiple environmental tracers. Water Resources Research, 51(6): 4532-4549.

Landais, A. et al., 2010. Combined measurements of 17 O excess and d-excess in African monsoon precipitation: Implications for evaluating convective parameterizations. Earth and Planetary Science Letters, 298(1): 104-112.

Lap Nguyen, V., Ta, T.K.O., Tateishi, M., 2000. Late Holocene depositional environments and coastal evolution of the Mekong River Delta, Southern Vietnam. Journal of Asian Earth Sciences, 18(4): 427-439. DOI:https://doi.org/10.1016/S1367-9120(99)00076-0

Larocque, M., Mangin, A., Razack, M., Banton, O., 1998. Contribution of correlation and spectral analyses to the regional study of a large karst aquifer (Charente, France). Journal of Hydrology, 205(3): 217-231. DOI:https://doi.org/10.1016/S0022-1694(97)00155-8

Lauri, H. et al., 2012. Future changes in Mekong River hydrology: impact of climate change and reservoir operation on discharge. Hydrol. Earth Syst. Sci., 16(12): 4603-4619. DOI:10.5194/hess-16-4603-2012

Lawson, M., Polya, D.A., Boyce, A.J., Bryant, C., Ballentine, C.J., 2016. Tracing organic matter composition and distribution and its role on arsenic release in shallow Cambodian groundwaters. Geochimica et Cosmochimica Acta, 178: 160-177. DOI:https://doi.org/10.1016/j.gca.2016.01.010

Lawson, M. et al., 2013. Pond-derived organic carbon driving changes in arsenic hazard found in Asian groundwaters. Environmental science & technology, 47(13): 7085-7094.

Le Luu, T., 2017. Remarks on the current quality of groundwater in Vietnam. Environmental Science and Pollution Research. DOI:10.1007/s11356-017-9631-z

LeBreton, J.M., Hargis, M.B., Griepentrog, B., Oswald, F.L., Ployhart, R.E., 2007. A multidimensional approach for evaluating variables in organizational research and practice. Personnel Psychology, 60(2): 475-498.

Lee, J.E. et al., 2012. Asian monsoon hydrometeorology from TES and SCIAMACHY water vapor isotope measurements and LMDZ simulations: Implications for speleothem climate record interpretation. Journal of Geophysical Research: Atmospheres, 117(D15).

Lee, K.-S. et al., 2003. Climatic controls on the stable isotopic composition of precipitation in Northeast Asia. Climate Research, 23(2): 137-148.

LeGrande, A.N., Schmidt, G.A., 2009. Sources of Holocene variability of oxygen isotopes in paleoclimate archives. Clim. Past, 5(3): 441-455. DOI:10.5194/cp-5-441-2009

Leibundgut, C., Maloszewski, P., Külls, C., 2011. Tracers in hydrology. John Wiley & Sons.

Levene, H., 1960. Robust tests for equality of variances. Contributions to probability and statistics, 1: 278-292.

Liu, Z. et al., 2014. Chinese cave records and the East Asia summer monsoon. Quaternary Science Reviews, 83: 115-128.

Madsen, H., Lawrence, D., Lang, M., Martinkova, M., Kjeldsen, T.R., 2014. Review of trend analysis and climate change projections of extreme precipitation and floods in Europe. Journal of Hydrology, 519: 3634-3650. DOI:https://doi.org/10.1016/j.jhydrol.2014.11.003

Maloszewski, P., 2000. Lumped-parameter models as a tool for determining the hydrological parameters of some groundwater systems based on isotope data. IAHS Publication(International Association of Hydrological Sciences)(262): 271-276.

Maloszewski, P., Rauert, W., Trimborn, P., Herrmann, A., Rau, R., 1992. Isotope hydrological study of mean transit times in an alpine basin (Wimbachtal, Germany). Journal of Hydrology, 140(1): 343-360. DOI:https://doi.org/10.1016/0022-1694(92)90247-S

Maloszewski, P., Stichler, W., Zuber, A., Rank, D., 2002. Identifying the flow systems in a karstic-fissured-porous aquifer, the Schneealpe, Austria, by modelling of environmental 18O and 3H isotopes. Journal of Hydrology, 256(1): 48-59. DOI:https://doi.org/10.1016/S0022-1694(01)00526-1

Maloszewski, P., Zuber, A., 1996. Lumped parameter models for the interpretation of environmental tracer data. International Atomic Energy Agency, 28(6): 9-58.

Małoszewski, P., Zuber, A., 1982. Determining the turnover time of groundwater systems with the aid of environmental tracers: 1. Models and their applicability. Journal of hydrology, 57(3): 207-231.

Mangin, A., 1984. Pour une meilleure connaissance des systèmes hydrologiques à partir des analyses corrélatoire et spectrale. Journal of Hydrology, 67(1): 25-43. DOI:https://doi.org/10.1016/0022-1694(84)90230-0

Manh, N.V. et al., 2015. Future sediment dynamics in the Mekong Delta floodplains: Impacts of hydropower development, climate change and sea level rise. Global and Planetary Change, 127: 22-33.

Manh, N.V., Dung, N.V., Hung, N.N., Merz, B., Apel, H., 2014. Large-scale suspended sediment transport and sediment deposition in the Mekong Delta. Hydrol Earth Syst Sc, 18(8): 3033.

Mann, H.B., 1945. Nonparametric tests against trend. Econometrica: Journal of the Econometric Society: 245-259.

Massei, N. et al., 2006. Investigating transport properties and turbidity dynamics of a karst aquifer using correlation, spectral, and wavelet analyses. Journal of Hydrology, 329(1): 244-257. DOI:https://doi.org/10.1016/j.jhydrol.2006.02.021

Mayaud, C., Wagner, T., Benischke, R., Birk, S., 2014. Single event time series analysis in a binary karst catchment evaluated using a groundwater model (Lurbach system, Austria). Journal of Hydrology, 511: 628-639. DOI:https://doi.org/10.1016/j.jhydrol.2014.02.024

McGuffie, K., Henderson-Sellers, A., 2004. Stable water isotope characterization of human and natural impacts on land-atmosphere exchanges in the Amazon Basin. Journal of Geophysical Research: Atmospheres, 109(D17).

McGuire, K., DeWalle, D., Gburek, W., 2002. Evaluation of mean residence time in subsurface waters using oxygen-18 fluctuations during drought conditions in the mid-Appalachians. Journal of Hydrology, 261(1): 132-149.

McGuire, K., McDonnell, J., 2008. Stable Isotope Tracers in Watershed Hydrology, Stable Isotopes in Ecology and Environmental Science. Blackwell Publishing Ltd, pp. 334-374. DOI:10.1002/9780470691854.ch11

McGuire, K.J., McDonnell, J.J., 2006. A review and evaluation of catchment transit time modeling. Journal of Hydrology, 330(3): 543-563.

Merlivat, L., Jouzel, J., 1979. Global climatic interpretation of the deuterium-oxygen 18 relationship for precipitation. Journal of Geophysical Research: Oceans, 84(C8): 5029-5033.

Merola, R.B., Hien, T.T., Quyen, D.T.T., Vengosh, A., 2015. Arsenic exposure to drinking water in the Mekong Delta. Science of The Total Environment, 511: 544-552. DOI:https://doi.org/10.1016/j.scitotenv.2014.12.091

Meyer, H., Schönicke, L., Wand, U., Hubberten, H.-W., Friedrichsen, H., 2000. Isotope studies of hydrogen and oxygen in ground ice-experiences with the equilibration technique. Isotopes in Environmental and Health Studies, 36(2): 133-149.

Minderhoud, P. et al., 2017. Impacts of 25 years of groundwater extraction on subsidence in the Mekong delta, Vietnam. Environmental Research Letters, 12(6): 064006.

Minderhoud, P.S.J., Coumou, L., Erkens, G., Middelkoop, H., Stouthamer, E., 2019. Mekong delta much lower than previously assumed in sea-level rise impact assessments. Nature Communications, 10(1): 3847. DOI:10.1038/s41467-019-11602-1

Mook, W., Rozanski, K., 2000. Environmental isotopes in the hydrological cycle. IAEA Publish, 39.

Morgenstern, U. et al., 2015. Using groundwater age and hydrochemistry to understand sources and dynamics of nutrient contamination through the catchment into Lake Rotorua, New Zealand. Hydrol. Earth Syst. Sci., 19(2): 803-822. DOI:10.5194/hess-19-803-2015

Mosquera, G.M. et al., 2016. Insights into the water mean transit time in a high-elevation tropical ecosystem. Hydrol. Earth Syst. Sci., 20(7): 2987-3004. DOI:10.5194/hess-20-2987-2016

Muñoz-Villers, L.E., Geissert, D.R., Holwerda, F., McDonnell, J.J., 2016. Factors influencing stream baseflow transit times in tropical montane watersheds. Hydrol. Earth Syst. Sci., 20(4): 1621-1635. DOI:10.5194/hess-20-1621-2016

Muñoz-Villers, L.E., McDonnell, J.J., 2012. Runoff generation in a steep, tropical montane cloud forest catchment on permeable volcanic substrate. Water Resources Research, 48(9).

Nam, N.D.G., Goto, A., Osawa, K., 2017. Groundwater Modeling for Groundwater Management in the Coastal Area of Mekong Delta, Vietnam. Transactions of The Japanese Society of Irrigation, Drainage and Rural Engineering, 85(1): I_93-I_103.

Nguyen, A.D., Savenije, H.H., 2006. Salt intrusion in multi-channel estuaries: a case study in the Mekong Delta, Vietnam. Hydrol. Earth Syst. Sci., 10(5): 743-754. DOI:10.5194/hess-10-743-2006

Nguyen, V.L., Ta, T.K.O., Tateishi, M., 2000. Late Holocene depositional environments and coastal evolution of the Mekong River Delta, Southern Vietnam. Journal of Asian Earth Sciences, 18(4): 427-439. DOI:https://doi.org/10.1016/S1367-9120(99)00076-0

Noone, D., Simmonds, I., 2002. Associations between δ 18O of Water and Climate Parameters in a Simulation of Atmospheric Circulation for 1979-95. Journal of Climate, 15(22): 3150-3169.

Nuber, T., Van Nam, V., Stolpe, H., 2009. VI-4: Modelling the groundwater dynamics of Can Tho City–challenges, approaches, solutions. Closing Nutrient Cycles in Decentralised Water Treatment Systems in the Mekong Delta: 236.

Okazaki, A., Yoshimura, K., 2017. Development and evaluation of a system of proxy data assimilation for paleoclimate reconstruction. Climate of the Past, 13(4): 379.

Peng, T.-R. et al., 2010. Stable isotopic characteristic of Taiwan's precipitation: A case study of western Pacific monsoon region. Earth and Planetary Science Letters, 289(3): 357-366.

Pfahl, S., Sodemann, H., 2014. What controls deuterium excess in global precipitation? Climate of the Past, 10(2): 771-781.

Pfahl, S., Wernli, H., 2008. Air parcel trajectory analysis of stable isotopes in water vapor in the eastern Mediterranean. Journal of Geophysical Research: Atmospheres, 113(D20).

Raksmey, M., Jinno, K., Tsutsumi, A., 2009. Effects of river water on groundwater in Cambodia. Memoirs of the Faculty of Engineering, Kyushu University, 69(3): 95-115.

Renaud, F.G., Kuenzer, C., 2012. The Mekong Delta system: Interdisciplinary analyses of a river delta. Springer Science & Business Media.

Renaud, F.G., Le, T.T.H., Lindener, C., Guong, V.T., Sebesvari, Z., 2015. Resilience and shifts in agro-ecosystems facing increasing sea-level rise and salinity intrusion in Ben Tre Province, Mekong Delta. Climatic Change, 133(1): 69-84. DOI:10.1007/s10584-014-1113-4

Richards, L.A. et al., 2018. Delineating sources of groundwater recharge in an arsenic-affected Holocene aquifer in Cambodia using stable isotope-based mixing models. Journal of Hydrology, 557: 321-334. DOI:https://doi.org/10.1016/j.jhydrol.2017.12.012

Rinaldo, A. et al., 2011. Catchment travel time distributions and water flow in soils. Water resources research, 47(7).

Risi, C., Bony, S., Vimeux, F., 2008a. Influence of convective processes on the isotopic composition (δ18O and δD) of precipitation and water vapor in the tropics: 2. Physical interpretation of the amount effect. Journal of Geophysical Research: Atmospheres, 113(D19).

Risi, C., Bony, S., Vimeux, F., Chong, M., Descroix, L., 2010a. Evolution of the stable water isotopic composition of the rain sampled along Sahelian squall lines. Quarterly Journal of the Royal Meteorological Society, 136(S1): 227-242.

Risi, C. et al., 2008b. What controls the isotopic composition of the African monsoon precipitation? Insights from event-based precipitation collected during the 2006 AMMA field campaign. Geophysical Research Letters, 35(24).

Risi, C., Bony, S., Vimeux, F., Jouzel, J., 2010b. Water-stable isotopes in the LMDZ4 general circulation model: Model evaluation for present-day and past climates and applications to climatic interpretations of tropical isotopic records. Journal of Geophysical Research: Atmospheres, 115(D12).

Roa-García, M.C., Weiler, M., 2010. Integrated response and transit time distributions of watersheds by combining hydrograph separation and long-term transit time modeling. Hydrol. Earth Syst. Sci., 14(8): 1537-1549. DOI:10.5194/hess-14-1537-2010

Rozanski, K., Araguas-Araguas, L., Gonfiantini, R., 1992. Relation between long-term trends of oxygen-18 isotope composition of precipitation and climate. Science, 258(5084): 981-985.

Ruiz-Barradas, A., Nigam, S., 2018. Hydroclimate Variability and Change over the Mekong River Basin: Modeling and Predictability and Policy Implications. Journal of Hydrometeorology, 19(5): 849-869. DOI:10.1175/jhm-d-17-0195.1

Seeger, S., Weiler, M., 2014. Reevaluation of transit time distributions, mean transit times and their relation to catchment topography. Hydrol Earth Syst Sc, 18(12): 4751-4771.

Sen, P.K., 1968. Estimates of the regression coefficient based on Kendall's tau. Journal of the American statistical association, 63(324): 1379-1389.

Shamsudduha, M., Chandler, R.E., Taylor, R.G., Ahmed, K.M., 2009. Recent trends in groundwater levels in a highly seasonal hydrological system: the Ganges-Brahmaputra-Meghna Delta. Hydrol. Earth Syst. Sci., 13(12): 2373-2385. DOI:10.5194/hess-13-2373-2009

Shinkai, Y., Truc, D.V., Sumi, D., Canh, D., Kumagai, Y., 2007. Arsenic and Other Metal Contamination of Groundwater in the Mekong River Delta, Vietnam. Journal of Health Science, 53(3): 344-346. DOI:10.1248/jhs.53.344

Shrestha, S., Bach, T.V., Pandey, V.P., 2016. Climate change impacts on groundwater resources in Mekong Delta under representative concentration pathways (RCPs) scenarios. Environmental science & policy, 61: 1-13.

SIWRP, 2014. Flood Planning in Vietnamese Mekong Delta until 2020.

Skrzypek, G. et al., 2015. Estimation of evaporative loss based on the stable isotope composition of water using Hydrocalculator. Journal of Hydrology, 523: 781-789.

Smajgl, A. et al., 2015. Responding to rising sea levels in the Mekong Delta. Nature Climate Change, 5(2): 167-174. DOI:10.1038/nclimate2469

Sodemann, H., Schwierz, C., Wernli, H., 2008. Interannual variability of Greenland winter precipitation sources: Lagrangian moisture diagnostic and North Atlantic Oscillation influence. Journal of Geophysical Research: Atmospheres, 113(D3).

Stanger, G., Truong, T.V., Ngoc, K.S.L.T.M., Luyen, T.V., Thanh, T.T., 2005. Arsenic in groundwaters of the Lower Mekong. Environmental Geochemistry and Health, 27(4): 341-357. DOI:10.1007/s10653-005-3991-x

Stein, A. et al., 2015. NOAA's HYSPLIT atmospheric transport and dispersion modeling system. Bulletin of the American Meteorological Society, 96(12): 2059-2077.

Stewart, M., Morgenstern, U., McDonnell, J., Pfister, L., 2012. The 'hidden streamflow'challenge in catchment hydrology: a call to action for stream water transit time analysis. Hydrological Processes, 26(13): 2061-2066.

Stewart, M., Thomas, J., 2008. A conceptual model of flow to the Waikoropupu Springs, NW Nelson, New Zealand, based on hydrometric and tracer (18 O, Cl, 3 H and CFC) evidence. Hydrology and Earth System Sciences Discussions, 12(1): 1-19.

Stewart, M.K., 1975. Stable isotope fractionation due to evaporation and isotopic exchange of falling waterdrops: Applications to atmospheric processes and evaporation of lakes. Journal of Geophysical Research, 80(9): 1133-1146.

Stewart, M.K., McDonnell, J.J., 1991. Modeling Base Flow Soil Water Residence Times From Deuterium Concentrations. Water Resources Research, 27(10): 2681-2693. DOI:10.1029/91WR01569

Stewart, M.K., Mehlhorn, J., Elliott, S., 2007. Hydrometric and natural tracer (oxygen-18, silica, tritium and sulphur hexafluoride) evidence for a dominant groundwater contribution to Pukemanga Stream, New Zealand. Hydrological Processes, 21(24): 3340-3356. DOI:10.1002/hyp.6557

Stewart, M.K., Morgenstern, U., Gusyev, M.A., Małoszewski, P., 2017. Aggregation effects on tritium-based mean transit times and young water fractions in spatially heterogeneous catchments and groundwater systems. Hydrol Earth Syst Sc, 21(9): 4615.

Stewart, M.K., Morgenstern, U., McDonnell, J.J., 2010. Truncation of stream residence time: how the use of stable isotopes has skewed our concept of streamwater age and origin. Hydrological Processes, 24(12): 1646-1659.

Stichler, W., Maloszewski, P., Bertleff, B., Watzel, R., 2008. Use of environmental isotopes to define the capture zone of a drinking water supply situated near a dredge lake. Journal of Hydrology, 362(3): 220-233. DOI:https://doi.org/10.1016/j.jhydrol.2008.08.024

Stichler, W., Maloszewski, P., Moser, H., 1986. Modelling of river water infiltration using oxygen-18 data. Journal of Hydrology, 83(3-4): 355-365.

Stockinger, M.P. et al., 2014. Seasonal soil moisture patterns: Controlling transit time distributions in a forested headwater catchment. Water Resources Research, 50(6): 5270-5289. DOI:10.1002/2013WR014815

Stohl, A., 1998. Computation, accuracy and applications of trajectories—a review and bibliography. Atmospheric Environment, 32(6): 947-966.

Stumpp, C., Stichler, W., Maloszewski, P., 2009. Application of the environmental isotope δ18O to study water flow in unsaturated soils planted with different crops: Case study of a weighable lysimeter from the research field in Neuherberg, Germany. Journal of Hydrology, 368(1): 68-78. DOI:https://doi.org/10.1016/j.jhydrol.2009.01.027

Sturm, C., Zhang, Q., Noone, D., 2010. An introduction to stable water isotopes in climate models: benefits of forward proxy modelling for paleoclimatology. Climate of the Past, 6(1): 115-129.

Syvitski, J.P.M. et al., 2009. Sinking deltas due to human activities. Nature Geoscience, 2(10): 681-686. DOI:10.1038/ngeo629

Tan, M., 2009. Circulation effect: climatic significance of the short term variability of the oxygen isotopes in stalagmites from monsoonal China—dialogue between paleoclimate records and modern climate research. Quaternary Sciences, 29(5): 851-862.

Tan, M., 2014. Circulation effect: response of precipitation δ18O to the ENSO cycle in monsoon regions of China. Climate Dynamics, 42(3-4): 1067-1077.

Tetzlaff, D., Birkel, C., Dick, J., Geris, J., Soulsby, C., 2014. Storage dynamics in hydropedological units control hillslope connectivity, runoff generation, and the evolution of catchment transit time distributions. Water resources research, 50(2): 969-985.

Thiemig, V., Rojas, R., Zambrano-Bigiarini, M., De Roo, A., 2013. Hydrological evaluation of satellite-based rainfall estimates over the Volta and Baro-Akobo Basin. Journal of Hydrology, 499: 324-338. DOI:https://doi.org/10.1016/j.jhydrol.2013.07.012

Thu, N.T., 2017. Groundwater and surface water cycle system in Mekong Delta, Vietnam. 171. DOI:https://tsukuba.repo.nii.ac.jp/?action=repository_uri&item_id=43117&file_id=17&file_no=1

Timbe, E. et al., 2015. Sampling frequency trade-offs in the assessment of mean transit times of tropical montane catchment waters under semi-steady-state conditions. Hydrol. Earth Syst. Sci., 19(3): 1153-1168. DOI:10.5194/hess-19-1153-2015

Timbe, E. et al., 2014. Understanding uncertainties when inferring mean transit times of water trough tracer-based lumped-parameter models in Andean tropical montane cloud forest catchments. Hydrol. Earth Syst. Sci., 18(4): 1503-1523. DOI:10.5194/hess-18-1503-2014

Tindall, J., Valdes, P., Sime, L.C., 2009. Stable water isotopes in HadCM3: Isotopic signature of El Niño–Southern Oscillation and the tropical amount effect. Journal of Geophysical Research: Atmospheres, 114(D4).

Toan, T.Q., 2014. 9 - Climate Change and Sea Level Rise in the Mekong Delta: Flood, Tidal Inundation, Salinity Intrusion, and Irrigation Adaptation Methods. In: Thao, N.D., Takagi, H., Esteban, M. (Eds.), Coastal Disasters and Climate Change in Vietnam. Elsevier, Oxford, pp. 199-218. DOI:https://doi.org/10.1016/B978-0-12-800007-6.00009-5

Tonidandel, S., LeBreton, J.M., 2011. Relative importance analysis: A useful supplement to regression analysis. Journal of Business and Psychology, 26(1): 1-9.

Tonidandel, S., LeBreton, J.M., Johnson, J.W., 2009. Determining the statistical significance of relative weights. Psychological methods, 14(4): 387.

Tran, D.A., Tsujimura, M., Kambuku, D., Dang, T.D., 2019. Hydrogeochemical characteristics of a multi-layered coastal aquifer system in the Mekong Delta, Vietnam. Environmental geochemistry and health: 1-20.

Tri, V.K., 2012. Hydrology and hydraulic infrastructure systems in the Mekong Delta, Vietnam, The Mekong Delta System. Springer, pp. 49-81.

Triet, N.V.K. et al., 2020. Future projections of flood dynamics in the Vietnamese Mekong Delta. Science of The Total Environment, 742: 140596. DOI:https://doi.org/10.1016/j.scitotenv.2020.140596

Triet, N.V.K. et al., 2017. Has dyke development in the Vietnamese Mekong Delta shifted flood hazard downstream? Hydrol Earth Syst Sc, 21(8): 3991.

Tu, L.X. et al., 2019. Sediment transport and morphodynamical modeling on the estuaries and coastal zone of the Vietnamese Mekong Delta. Continental Shelf Research, 186: 64-76. DOI:https://doi.org/10.1016/j.csr.2019.07.015

Uemura, R., Matsui, Y., Yoshimura, K., Motoyama, H., Yoshida, N., 2008. Evidence of deuterium excess in water vapor as an indicator of ocean surface conditions. Journal of Geophysical Research: Atmospheres, 113(D19).

Vermeulen, P. et al., 2013. Groundwater modeling for the Mekong Delta using iMOD, MODSIM2013, 20th International Congress on Modelling and Simulation. Modelling and Simulation Society of Australia and New Zealand, pp. 2499-2505.

Viville, D., Ladouche, B., Bariac, T., 2006. Isotope hydrological study of mean transit time in the granitic Strengbach catchment (Vosges massif, France): application of the FlowPC model with modified input function. Hydrological Processes: An International Journal, 20(8): 1737-1751.

von Asmuth, J.R., Bierkens, M.F.P., Maas, K., 2002. Transfer function-noise modeling in continuous time using predefined impulse response functions. Water Resources Research, 38(12): 23-1-23-12. DOI:10.1029/2001wr001136

Vörösmarty, C.J. et al., 2009. Battling to Save the World's River Deltas. Bulletin of the Atomic Scientists, 65(2): 31-43. DOI:10.2968/065002005

Vuille, M., Bradley, R., Werner, M., Healy, R., Keimig, F., 2003. Modeling δ18O in precipitation over the tropical Americas: 1. Interannual variability and climatic controls. Journal of Geophysical Research: Atmospheres, 108(D6).

Vuille, M., Werner, M., Bradley, R., Keimig, F., 2005. Stable isotopes in precipitation in the Asian monsoon region. Journal of Geophysical Research: Atmospheres, 110(D23).

Wagner, F., Tran, V.B., Renaud, F.G., 2012. Groundwater resources in the Mekong Delta: availability, utilization and risks, The Mekong Delta System. Springer, pp. 201-220.

Wang, B., Wu, R., Lau, K., 2001. Interannual variability of the Asian summer monsoon: contrasts between the Indian and the Western North Pacific-East Asian Monsoons*. Journal of climate, 14(20): 4073-4090.

Wassmann, R., Hien, N.X., Hoanh, C.T., Tuong, T.P., 2004. Sea level rise affecting the Vietnamese Mekong Delta: water elevation in the flood season and implications for rice production. Climatic Change, 66(1-2): 89-107.

Watts, D.G., Jenkins, G., 1968. Spectral analysis and its applications. San Francisco.

Weiler, M., McGlynn, B.L., McGuire, K.J., McDonnell, J.J., 2003a. How does rainfall become runoff? A combined tracer and runoff transfer function approach. Water Resources Research, 39(11): n/a-n/a. DOI:10.1029/2003WR002331

Weiler, M., McGlynn, B.L., McGuire, K.J., McDonnell, J.J., 2003b. How does rainfall become runoff? A combined tracer and runoff transfer function approach. Water Resources Research, 39(11).

Wenninger, J., Beza, D.T., Uhlenbrook, S., 2010. Experimental investigations of water fluxes within the soil–vegetation–atmosphere system: Stable isotope mass-balance approach to partition evaporation and transpiration. Physics and Chemistry of the Earth, Parts A/B/C, 35(13): 565-570.

Wentworth, C.K., 1922. A Scale of Grade and Class Terms for Clastic Sediments. The Journal of Geology, 30(5): 377-392. DOI:10.1086/622910

Weyhenmeyer, C.E., Burns, S.J., Waber, H.N., Macumber, P.G., Matter, A., 2002. Isotope study of moisture sources, recharge areas, and groundwater flow paths within the eastern Batinah coastal plain, Sultanate of Oman. Water Resources Research, 38(10): 2-1-2-22.

Wilbers, G.-J., Sebesvari, Z., Renaud, F., 2014. Piped-Water Supplies in Rural Areas of the Mekong Delta, Vietnam: Water Quality and Household Perceptions. Water, 6(8): 2175.

Wunsch, A., Liesch, T., Broda, S., 2018. Forecasting groundwater levels using nonlinear autoregressive networks with exogenous input (NARX). Journal of Hydrology, 567: 743-758. DOI:https://doi.org/10.1016/j.jhydrol.2018.01.045

Yang, H., Johnson, K., Griffiths, M., Yoshimura, K., 2016. Interannual controls on oxygen isotope variability in Asian monsoon precipitation and implications for paleoclimate reconstructions. Journal of Geophysical Research: Atmospheres, 121(14): 8410-8428.

Yoshimura, K., Kanamitsu, M., Noone, D., Oki, T., 2008. Historical isotope simulation using reanalysis atmospheric data. Journal of Geophysical Research: Atmospheres, 113(D19).

Yoshimura, K., Miyoshi, T., Kanamitsu, M., 2014. Observation system simulation experiments using water vapor isotope information. Journal of Geophysical Research: Atmospheres, 119(13): 7842-7862.

Yoshimura, K., Oki, T., Ohte, N., Kanae, S., 2003. A quantitative analysis of short-term 18O variability with a Rayleigh-type isotope circulation model. Journal of Geophysical Research: Atmospheres, 108(D20).

Zhang, Y.-K., Schilling, K., 2004. Temporal scaling of hydraulic head and river base flow and its implication for groundwater recharge. Water Resources Research, 40(3). DOI:10.1029/2003wr002094

Zuber, A., Różański, K., Kania, J., Purtschert, R., 2011. On some methodological problems in the use of environmental tracers to estimate hydrogeologic parameters and to calibrate flow and transport models. Hydrogeology journal, 19(1): 53-69.

Appendix A

Supplement to chapter 2

This is part of the publication:

Duy, N. L., Heidbüchel, I., Meyer, H., Merz, B., & Apel, H. (2018). What controls the stable isotope composition of precipitation in the Mekong Delta? A model-based statistical approach. Hydrology and Earth System Sciences, 22(2), 1239–1262. https://doi.org/10.5194/hess-22-1239-2018

A.1 Sensitivity of LMWL to regression techniques

The sensitivity of the LMWL to different regression techniques was tested applying three methods of linear regression between $\delta^{18}O$ and $\delta^{2}H$ values:

1) ordinary least squares regression (OLSR),

2) reduced major axis (RMA) regression,

3) precipitation amount weighted least squares regression (PWLSR).

OLSR and RMA give equal weight to all data points regardless of their precipitation amount, while PWLSR minimizes the effect of smaller precipitation amounts (Hughes and Crawford, 2012), which are more likely to have a lower d-excess due to re-evaporation of raindrops below the cloud base (Jacob and Sonntag, 1991), or biases in the sampling method (Froehlich, 2001). OLSR tends to be more useful when investigating the interaction between hydro-climatic processes and stable isotope signatures in precipitation, whereas PWLSR is adequate in studying surface and groundwater hydrology (Hughes and Crawford, 2012). For a more detailed discussion, the reader is referred to IAEA (1992); Hughes and Crawford (2012); Crawford et al. (2014).

The quality of fit of the three LMWLs resulting from OLSR, RMA, and PWLSR was evaluated based on the coefficient of determination R^2, also referred to as explained variance, the standard error SE and the statistical significance value (p-value). The regression model indicates a good fit to the data when R^2 is close to 1.0, the standard error is small in relation to the magnitude of the data, and the p-value is smaller than 0.0001 (Helsel and Hirsch, 2002).

The resulting regressions are:

1) Ordinary least squares regression (OLSR):

$\delta^{2}H = (7.56 \pm 0.11)* \delta^{18}O + (7.26 \pm 0.67)$

(SE = 2.26; $r^2 = 0.99$; $p < 0.0001$; n = 74),

2) Reduced major axis regression (RMA):

$\delta^{2}H = (7.61 \pm 0.11)* \delta^{18}O + (7.58 \pm 0.68)$

(SE = 2.27; $r^2 = 0.99$; $p < 0.0001$; n = 74),

3) Precipitation amount weighted least squares regression (PWLSR):

$\delta^{2}H = (7.61 \pm 0.11)* \delta^{18}O + (7.87 \pm 0.73)$

(SE = 2.29; $r^2 = 0.99$; $p < 0.0001$; n = 74).

A.2 Multiple linear regression analysis of δ^2H

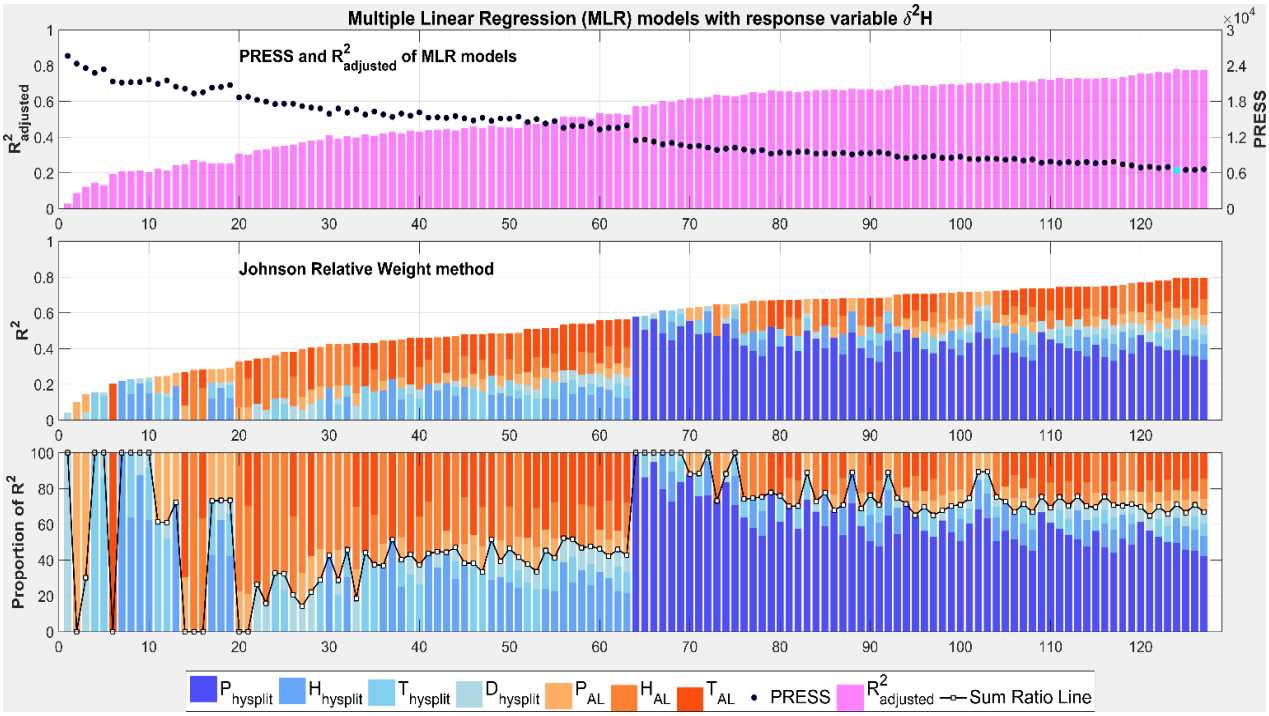

Figure A1: MLR with response variable δ^2H and relative importance analysis applied for all possible subsets. The 127 MLR models are sorted according to their R^2 values in ascendant order. Colors represent the relative contribution (in %) of the predictors. The sum ratio line separates the role of local (in red and orange) and regional (in blue) factors. PRESS and adjusted R^2 values indicate the quality of the MLR model. The best MLR model depicted by the lowest PRESS (model 124, highlighted by the cyan dot) explains 79% of the δ^2H variation (R^2 = 0.79).

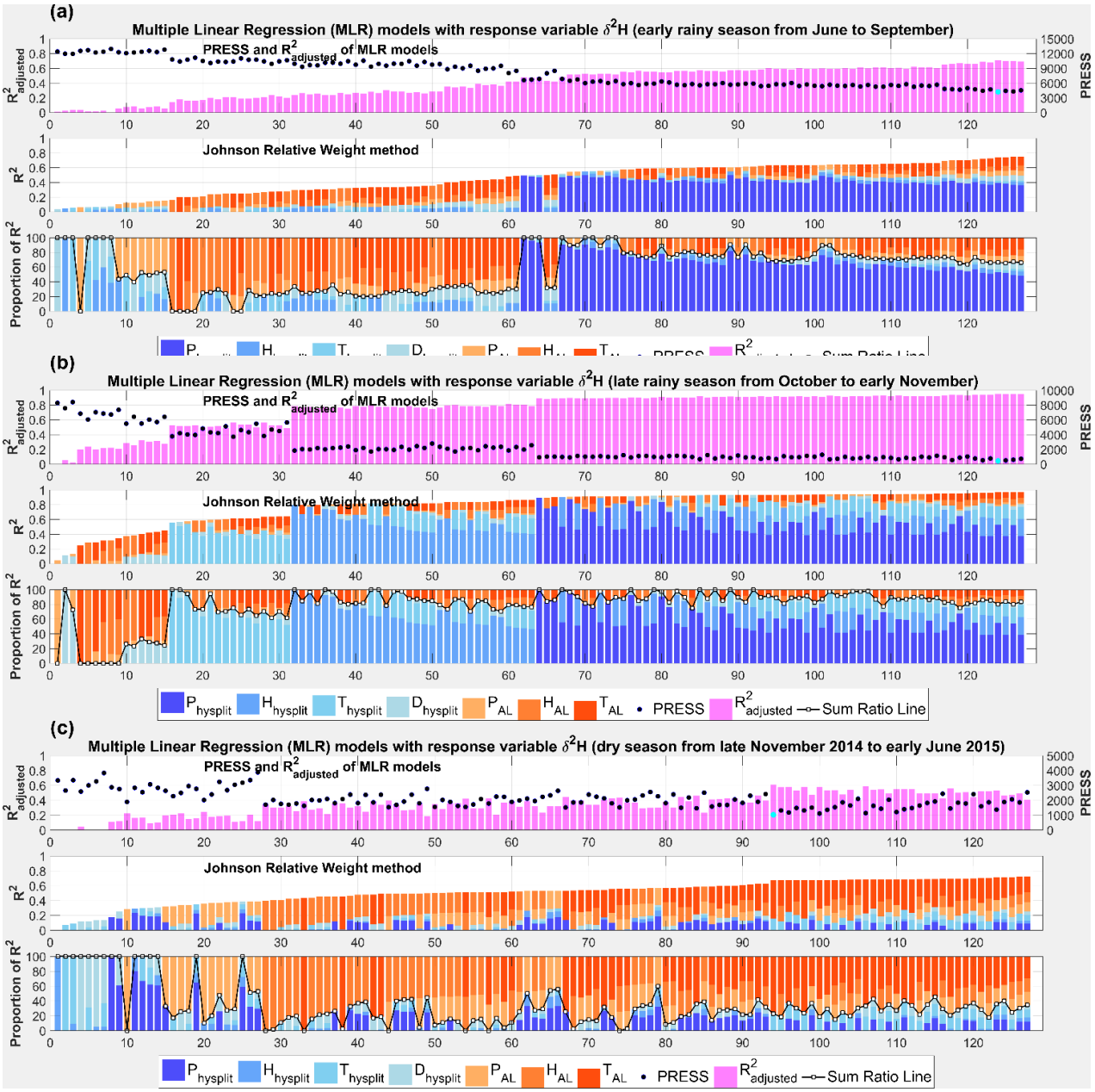

Figure A2: MLR with response variable δ^2H and relative importance analysis applied for all possible subsets (127 MLR models) for different seasons: a) early monsoon from June to September, b) late monsoon from October to mid-November, and c) the dry season from mid-November to mid-June.

A.3 Multiple linear regression analysis of d-excess

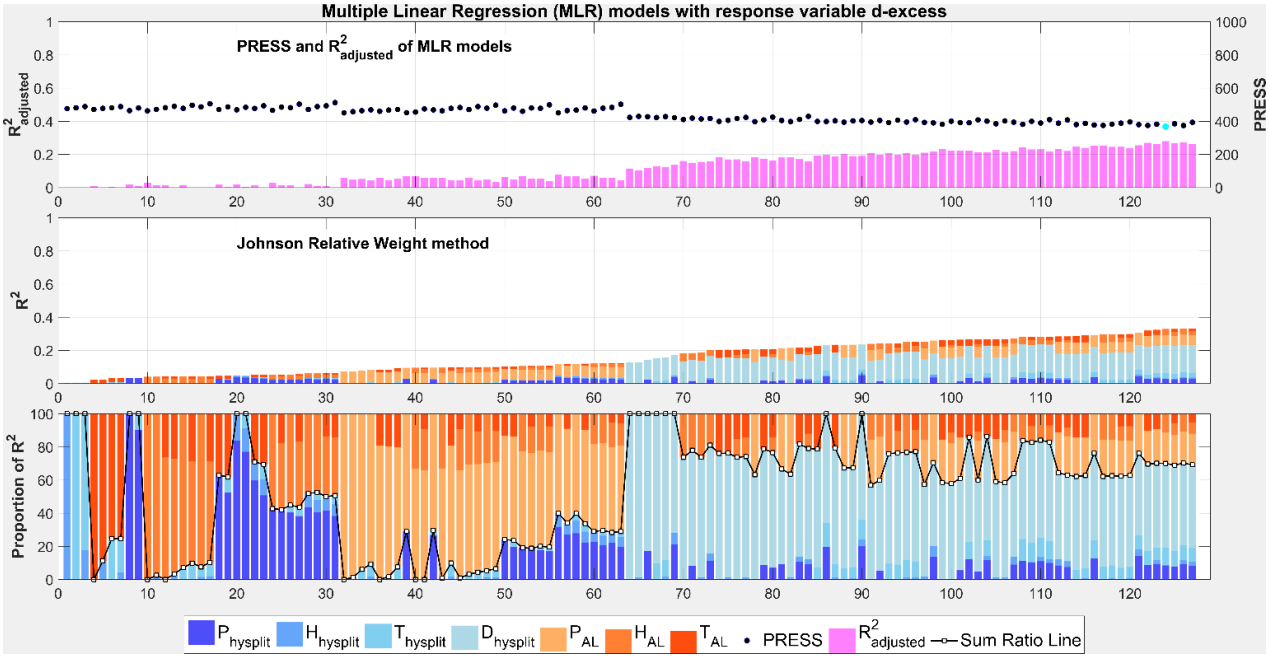

Figure A3: MLR with response variable d-excess and relative importance analysis applied for all possible subsets. The 127 MLR models are sorted according to their R^2 values in ascendant order. Colors represent the relative contribution (in %) of the predictors. The sum ratio line separates the role of local (in red and orange) and regional (in blue) factors. PRESS and adjusted R^2 values indicate the quality of the MLR model. The best MLR model depicted by the lowest PRESS (model 124, highlighted by the cyan dot) explains 30% of the d-excess variation (R^2 = 0.3).

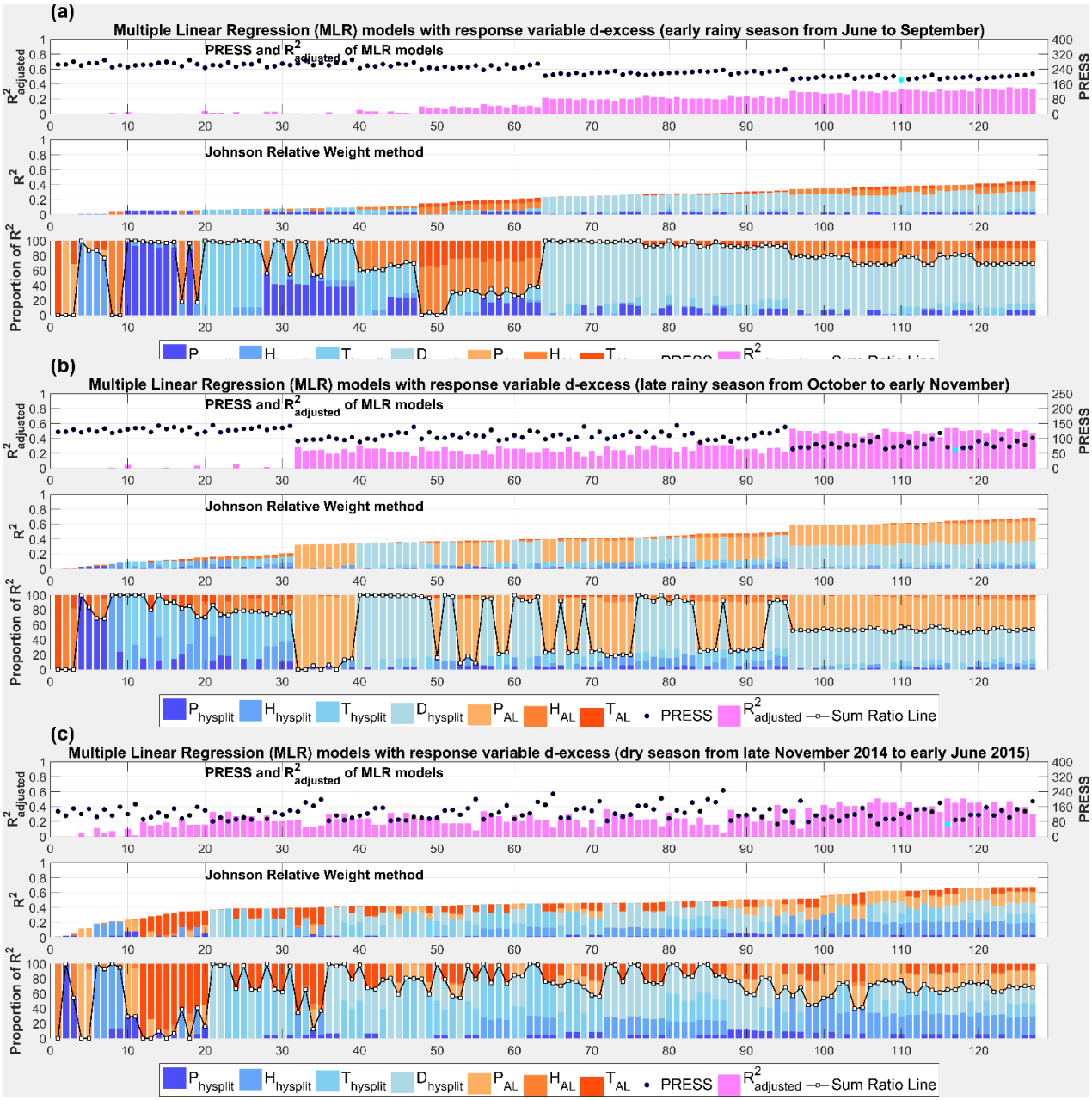

Figure A4: MLR with response variable d-excess and relative importance analysis applied for all possible subsets (127 MLR models) for different seasons: a) early monsoon from June to September, b) late monsoon from October to mid-November, and c) the dry season from mid-November to mid-June.

Appendix B

Supplement to chapter 3

This is part of the publication:

Le Duy, N., Dung, N. V., Heidbüchel, I., Meyer, H., Weiler, M., Merz, B., & Apel, H. (2019). Identification of groundwater mean transit times of precipitation and riverbank infiltration by two-component lumped parameter models. Hydrological Processes, 33(24), 3098-3118.

B.1 Sensitivity of the efficiency of two-component lumped parameter models to isotopic correction values

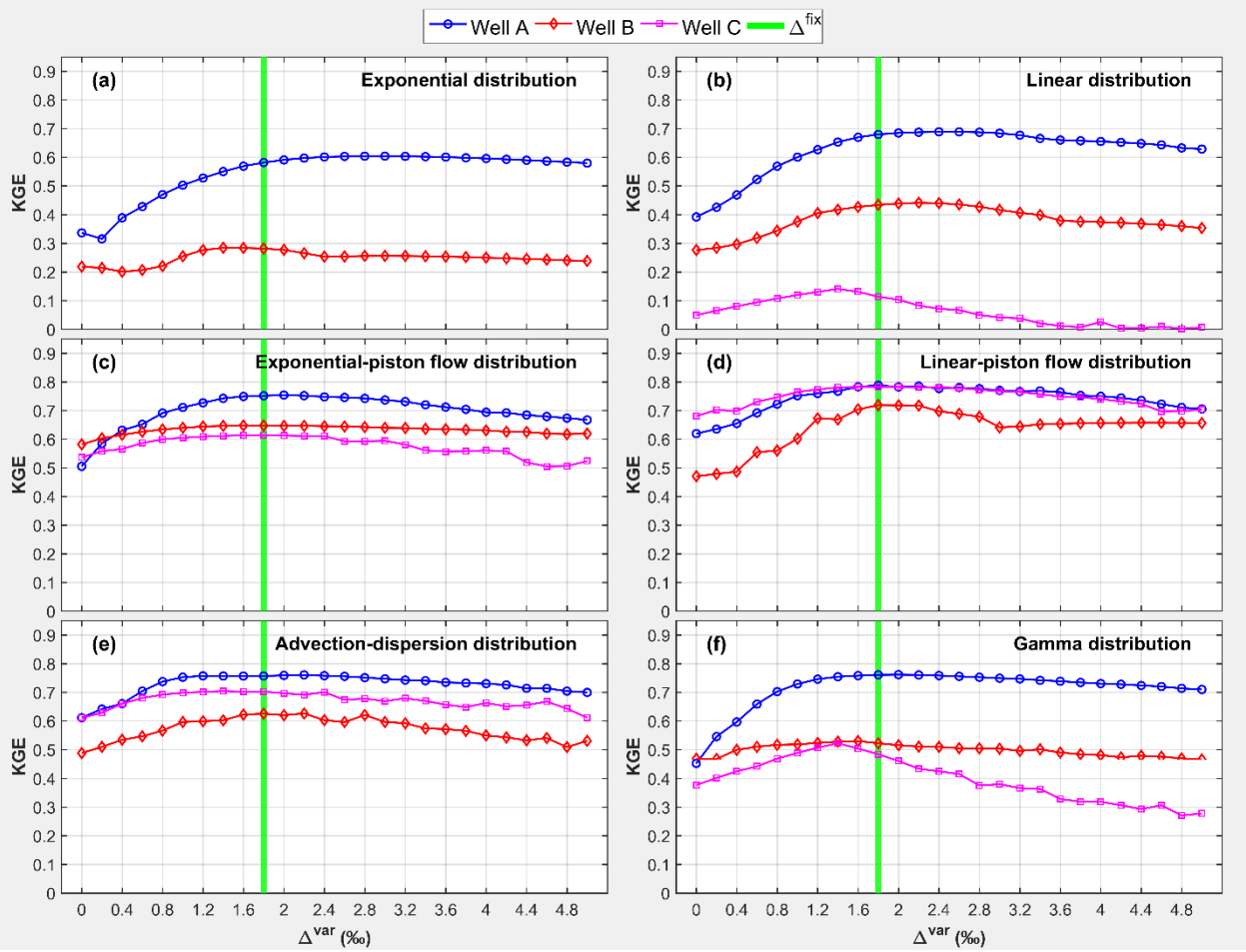

Figure B1: Sensitivity of the efficiency of two-component lumped parameter models to isotopic correction values (Δ^{var}) measured by KGE statistic. The green reference line indicates the isotopic difference (Δ^{fix}) between the arithmetic mean value of the pond water and the weighted mean value of precipitation. $\Delta^{var\text{-}best}$ corresponds to the best-possible model performance and reasonable parameter identifiability.

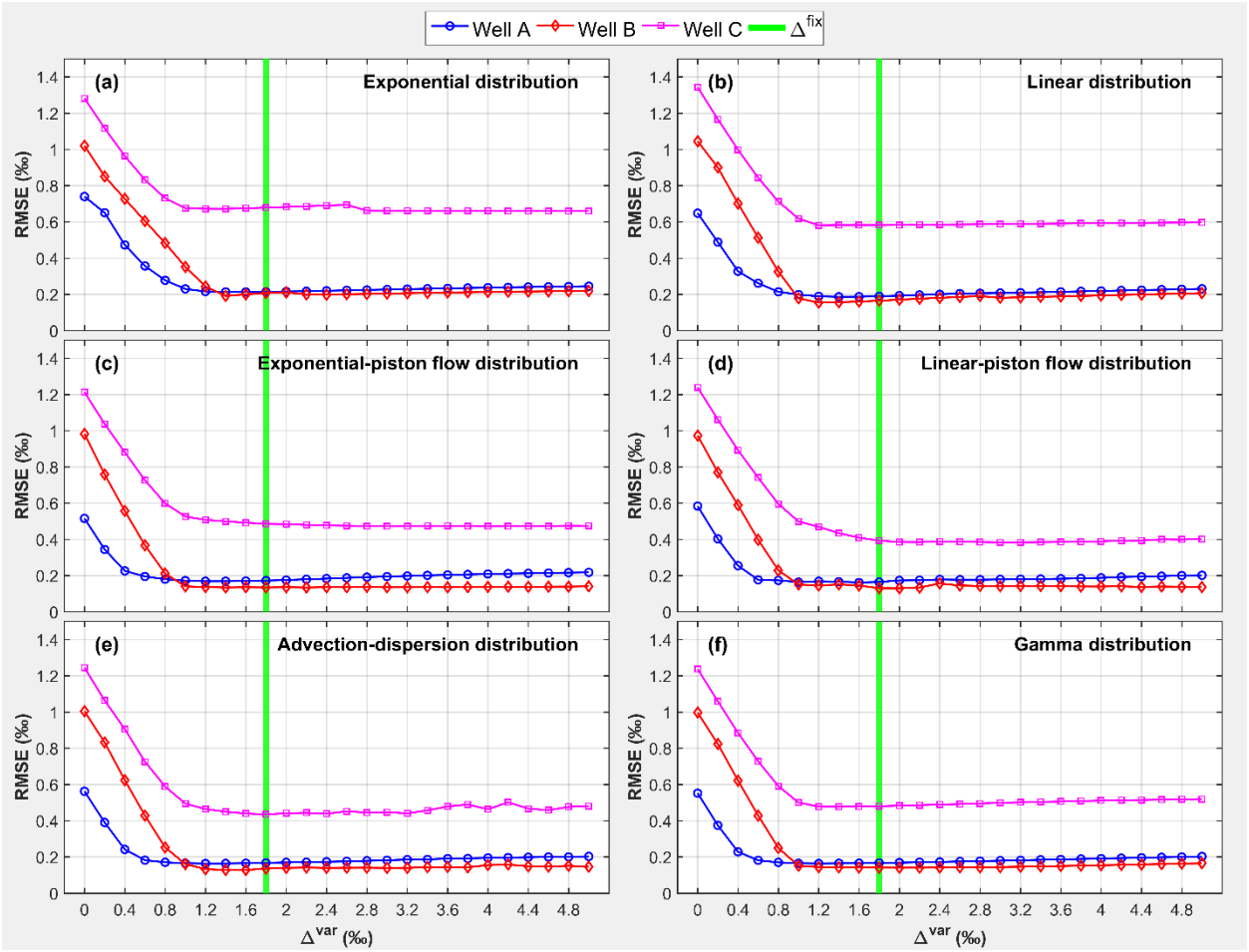

Figure B2: Sensitivity of the efficiency of two-component lumped parameter models to isotopic correction values (Δ^{var}) measured by RMSE statistic. The green reference line indicates the isotopic difference (Δ^{fix}) between the arithmetic mean value of the pond water and the weighted mean value of precipitation. $\Delta^{var\text{-}best}$ corresponds to the best-possible model performance and reasonable parameter identifiability.

B.2 Sensitivity of the parameter identifiability of two-component LPMs to the isotopic correction values

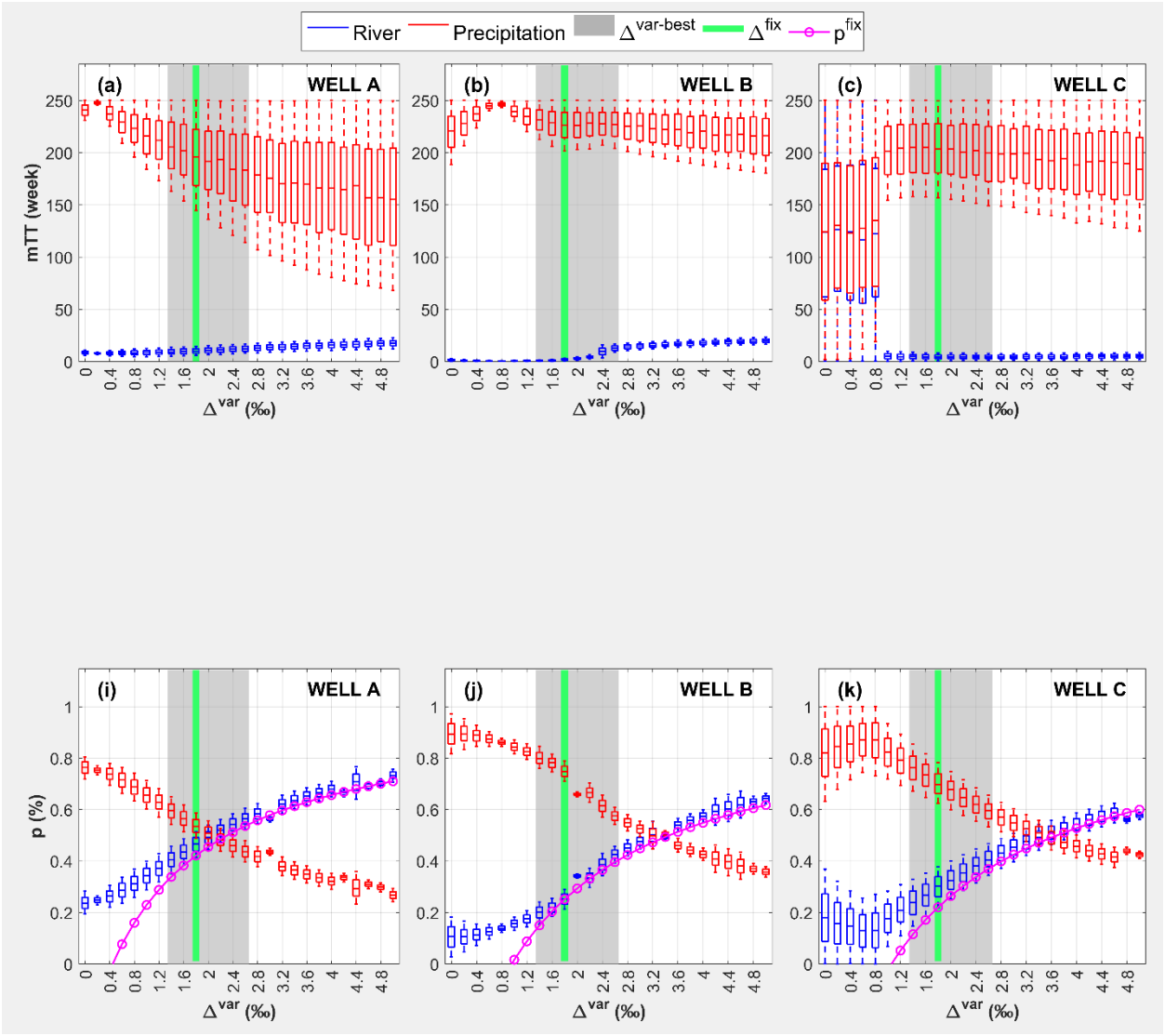

Figure B3: Sensitivity of the parameter identifiability of the exponential model to the correction values (Δ^{var}) for all tested wells. The box plots indicate the 90% confidence intervals of fitting parameters given by the generalized likelihood.

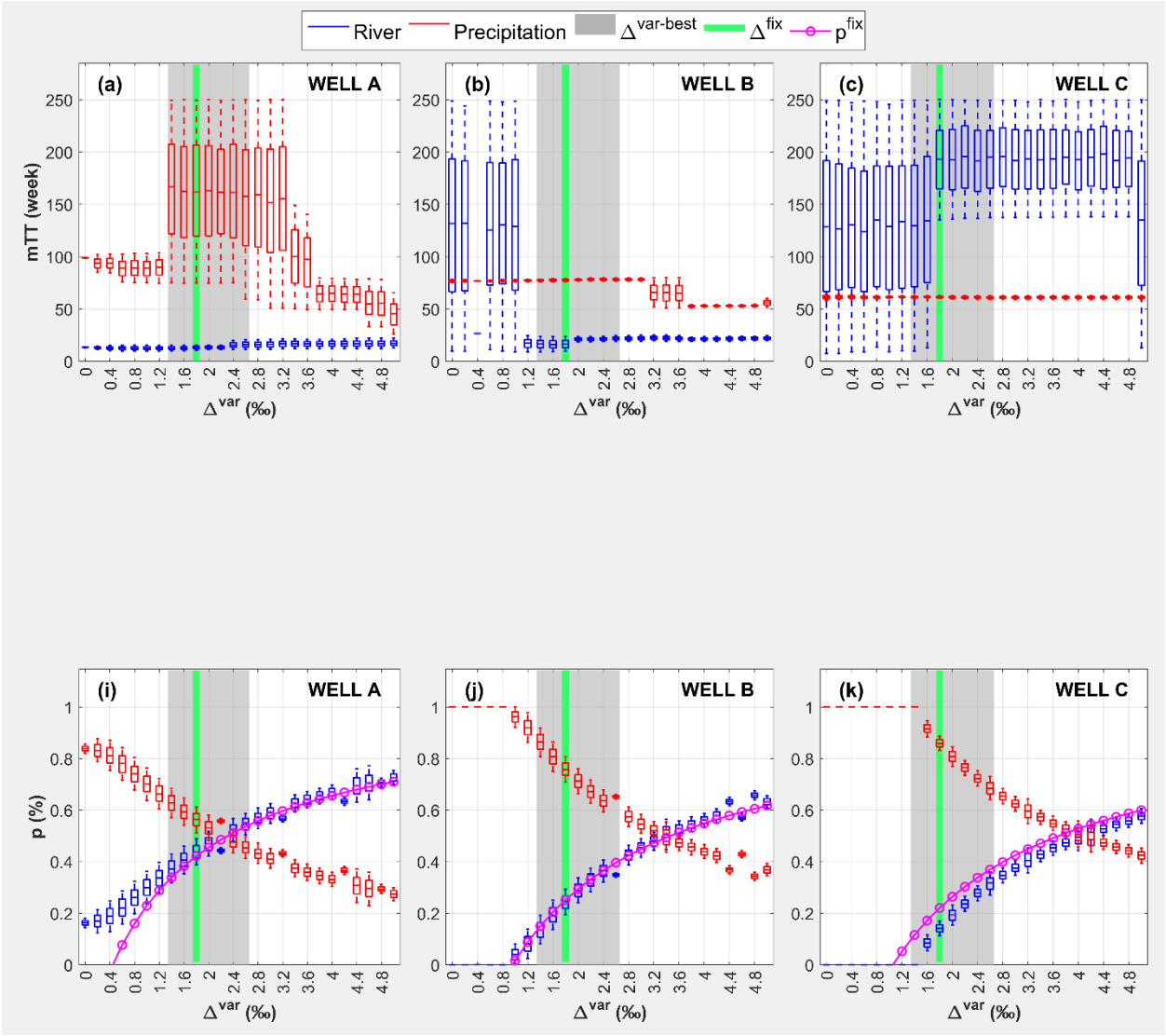

Figure B4: Sensitivity of the parameter identifiability of the linear model to the correction values (Δ^{var}) for all tested wells. The box plots indicate the 90% confidence intervals of fitting parameters given by the generalized likelihood.

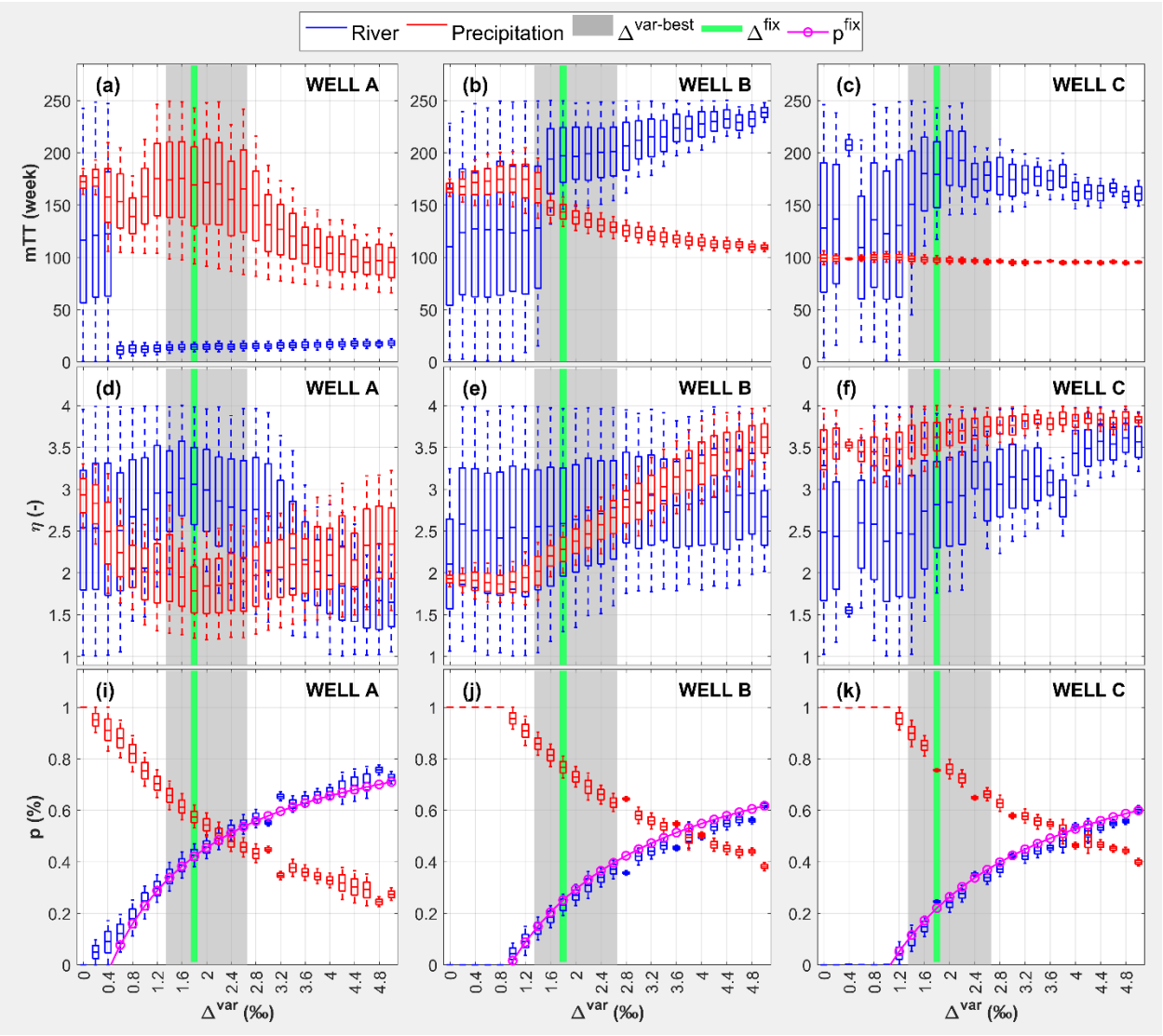

Figure B5: Sensitivity of the parameter identifiability of the exponential-piston flow model to the correction values (Δ^{var}) for all tested wells. The box plots indicate the 90% confidence intervals of fitting parameters given by the generalized likelihood.

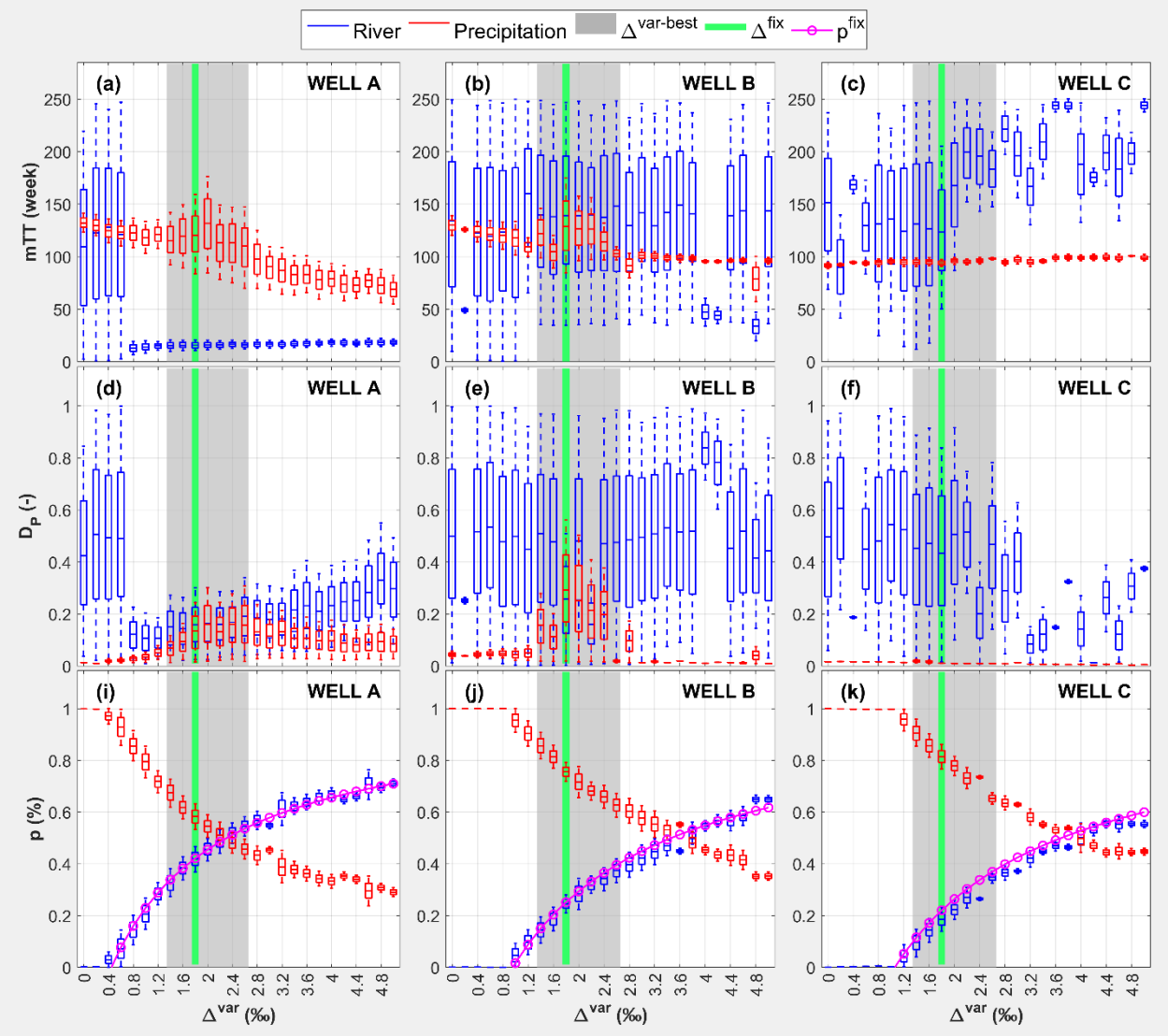

Figure B6: Sensitivity of the parameter identifiability of the advection-dispersion model to the correction values (Δ^{var}) for all tested wells. The box plots indicate the 90% confidence intervals of fitting parameters given by the generalized likelihood.

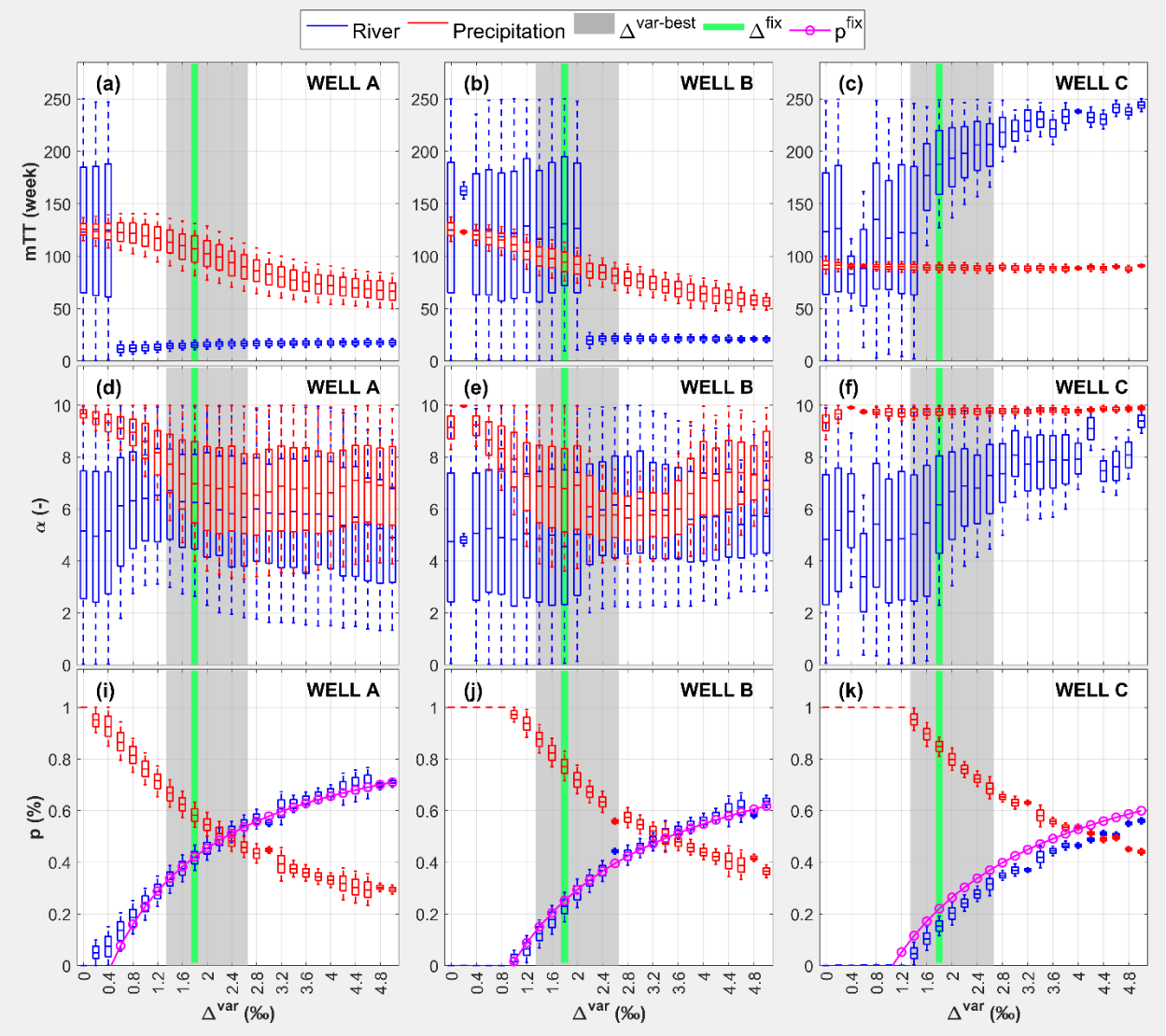

Figure B7: Sensitivity of the parameter identifiability of the gamma model to the correction values (Δ^{var}) for all tested wells. The box plots indicate the 90% confidence intervals of fitting parameters given by the generalized likelihood.

B.3 Dotty plots of likelihood measures against fitted parameters tested with six different TTDs

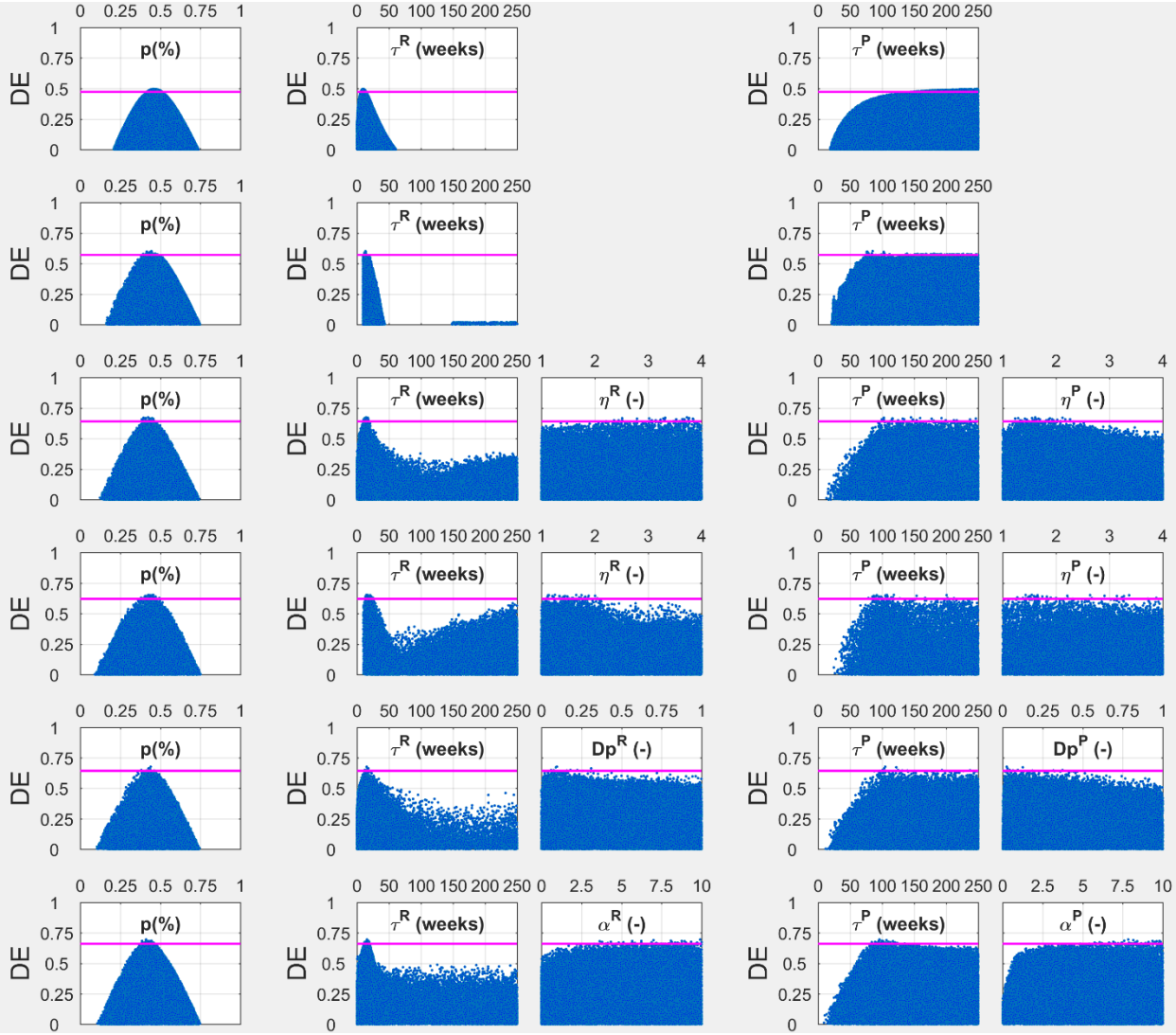

Figure B8: Dotty plots of likelihood measures against fitted parameters from 10^6 Monte Carlo simulations tested with six different TTDs for Well A. The results correspond to Test 1 in Figure 3.6 and Figure 3.7. Shown from top to bottom are the exponential, linear, exponential-piston flow, linear-piston flow, advection-dispersion, and gamma distributions. Magenta lines indicate the thresholds of 5% of the best predictions. p is the fraction of recharge from river (or precipitation) infiltration; τ_m is the tracer's mTT; η is a parameter indicating the ratio of total volume/volume with exponential (or linear) TTD; D_P is the dispersion parameter; α is the shape parameter. The superscripts R and P indicate infiltration from river water and precipitation, respectively.

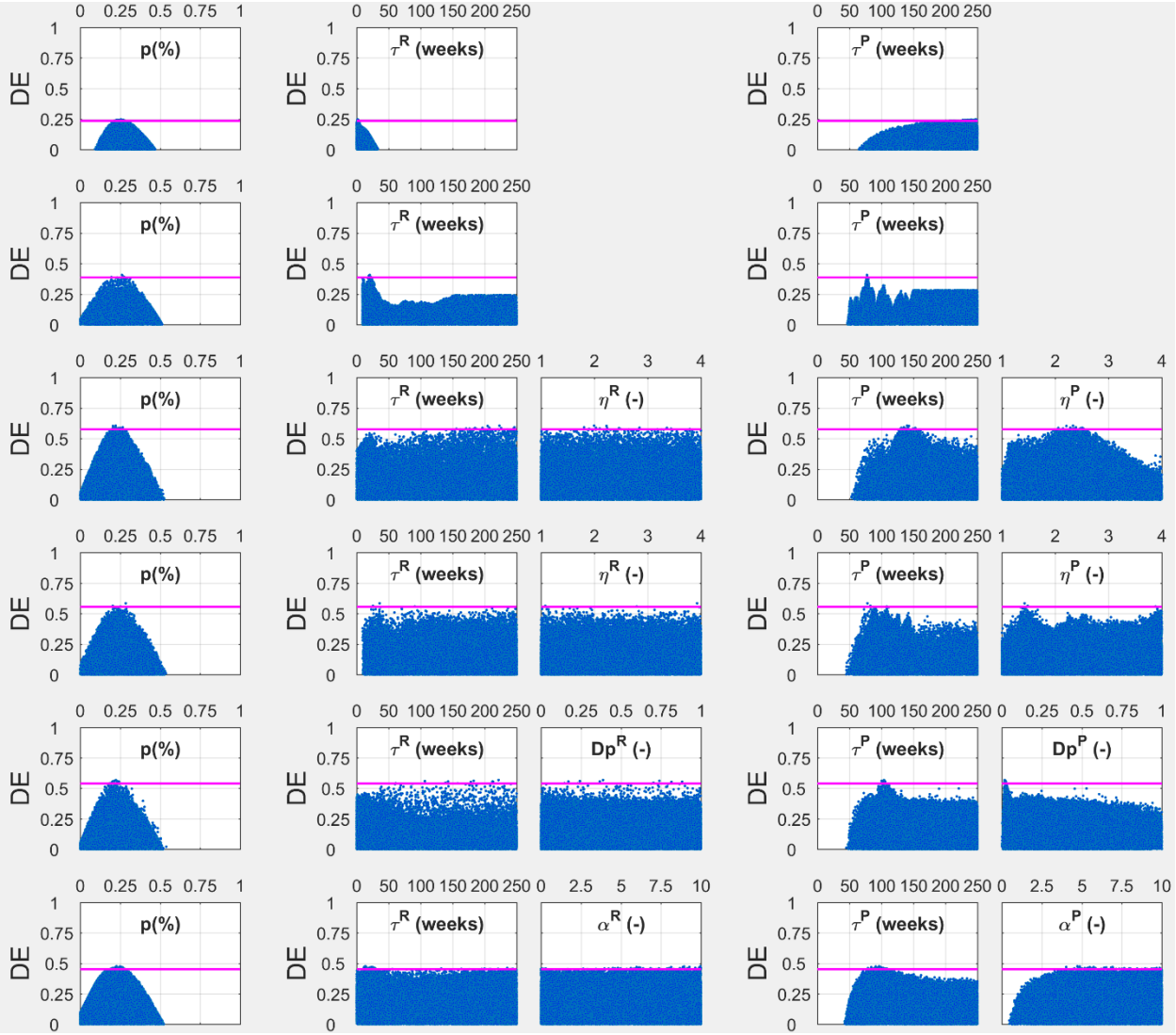

Figure B9: Dotty plots of likelihood measures against fitted parameters from 10^6 Monte Carlo simulations tested with six different TTDs for Well B. The results correspond to Test 1 in Figure 3.6 and Figure 3.7. Shown from top to bottom are the exponential, linear, exponential-piston flow, linear-piston flow, advection-dispersion, and gamma distributions. Magenta lines indicate the thresholds of 5% of the best predictions. p is the fraction of recharge from river (or precipitation) infiltration; τ_m is the tracer's mTT; η is a parameter indicating the ratio of total volume/volume with exponential (or linear) TTD; D_P is the dispersion parameter; α is the shape parameter. The superscripts R and P indicate infiltration from river water and precipitation, respectively.

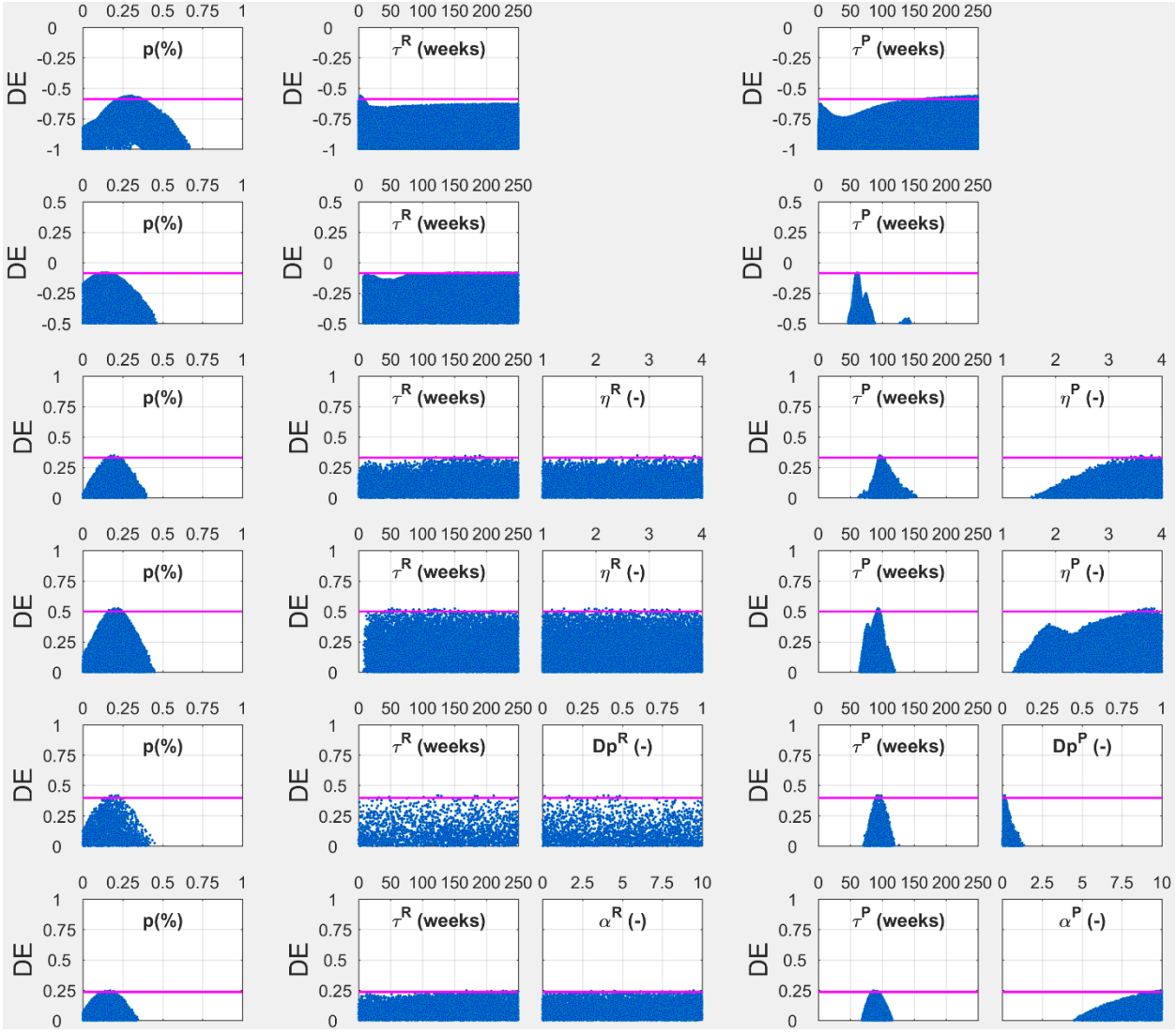

Figure B10: Dotty plots of likelihood measures against fitted parameters from 10^6 Monte Carlo simulations tested with six different TTDs for Well C. The results correspond to Test 1 in Figure 3.6 and Figure 3.7. Shown from top to bottom are the exponential, linear, exponential-piston flow, linear-piston flow, advection-dispersion, and gamma distributions. Magenta lines indicate the thresholds of 5% of the best predictions. p is the fraction of recharge from river (or precipitation) infiltration; τ_m is the tracer's mTT; η is a parameter indicating the ratio of total volume/volume with exponential (or linear) TTD; D_P is the dispersion parameter; α is the shape parameter. The superscripts R and P indicate infiltration from river water and precipitation, respectively.

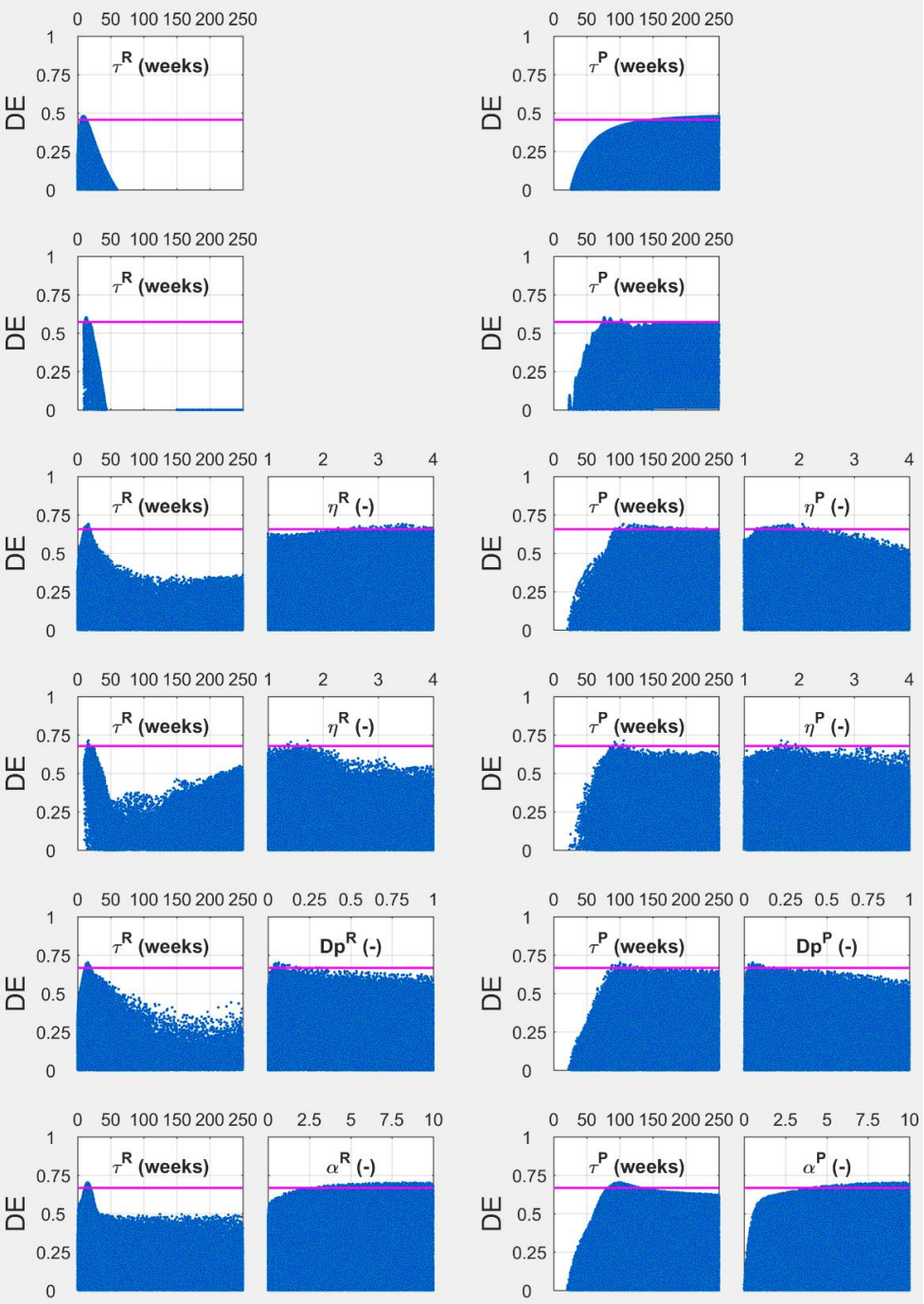

Figure B11: Dotty plots of likelihood measures against fitted parameters from 10^6 Monte Carlo simulations tested with six different TTDs for Well A. The results were corresponding to Test 2 with fixed p. Shown from top to bottom are the exponential, linear, exponential-piston flow, linear-piston flow, advection-dispersion, and gamma distributions. Magenta lines indicate the thresholds of 5% of the best predictions. τ_m is the tracer's mTT; η is a parameter indicating the ratio of total volume/volume with exponential (or linear) TTD; D_P is the dispersion parameter; α is the shape parameter. The superscripts R and P indicate infiltration from river water and precipitation, respectively.

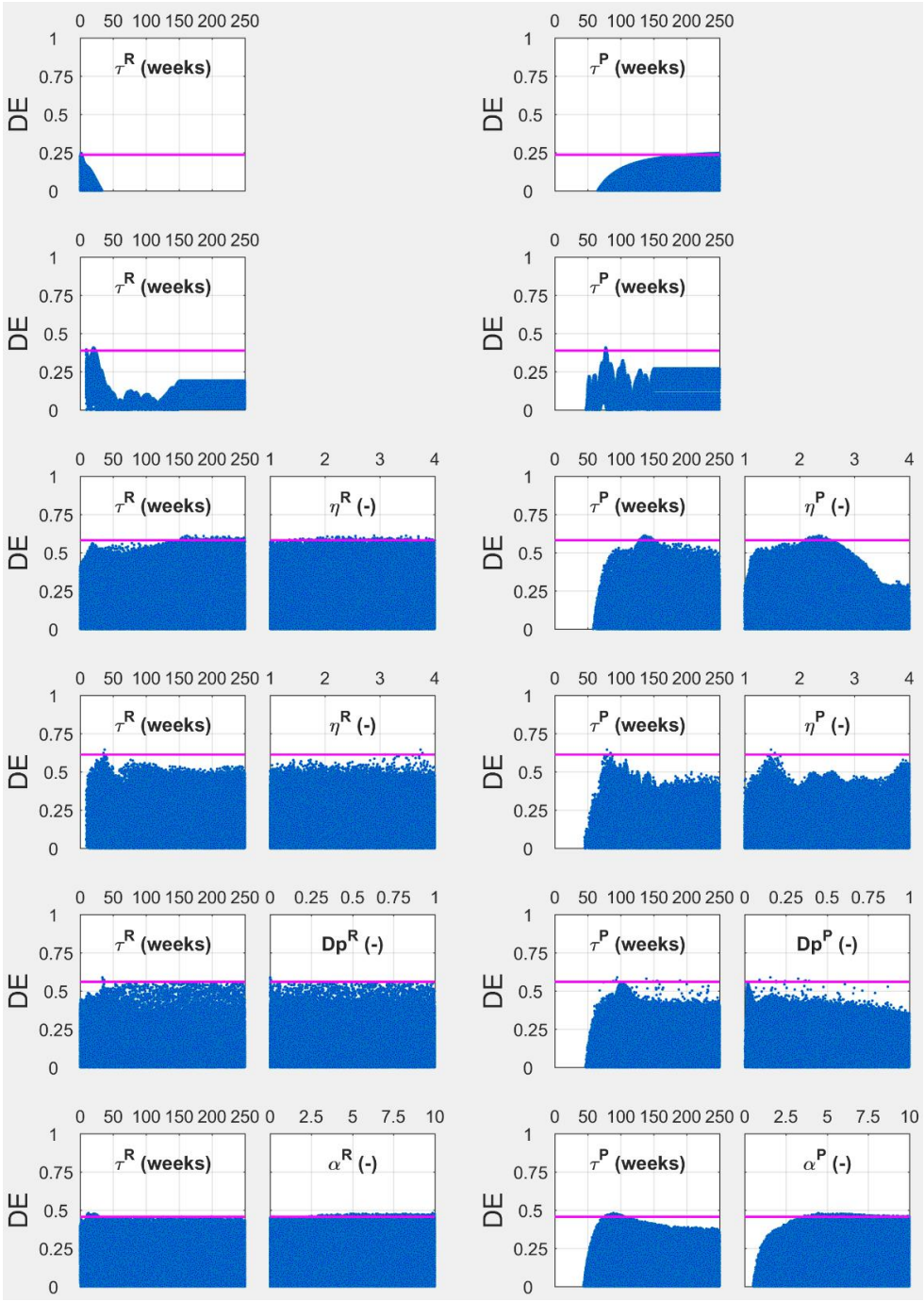

Figure B12: Dotty plots of likelihood measures against fitted parameters from 10^6 Monte Carlo simulations tested with six different TTDs for Well B. The results were corresponding to Test 2 with fixed p. Shown from top to bottom are the exponential, linear, exponential-piston flow, linear-piston flow, advection-dispersion, and gamma distributions. Magenta lines indicate the thresholds of 5% of the best predictions. τ_m is the tracer's mTT; η is a parameter indicating the ratio of total volume/volume with exponential (or linear) TTD; D_P is the dispersion parameter; α is the shape parameter. The superscripts R and P indicate infiltration from river water and precipitation, respectively.

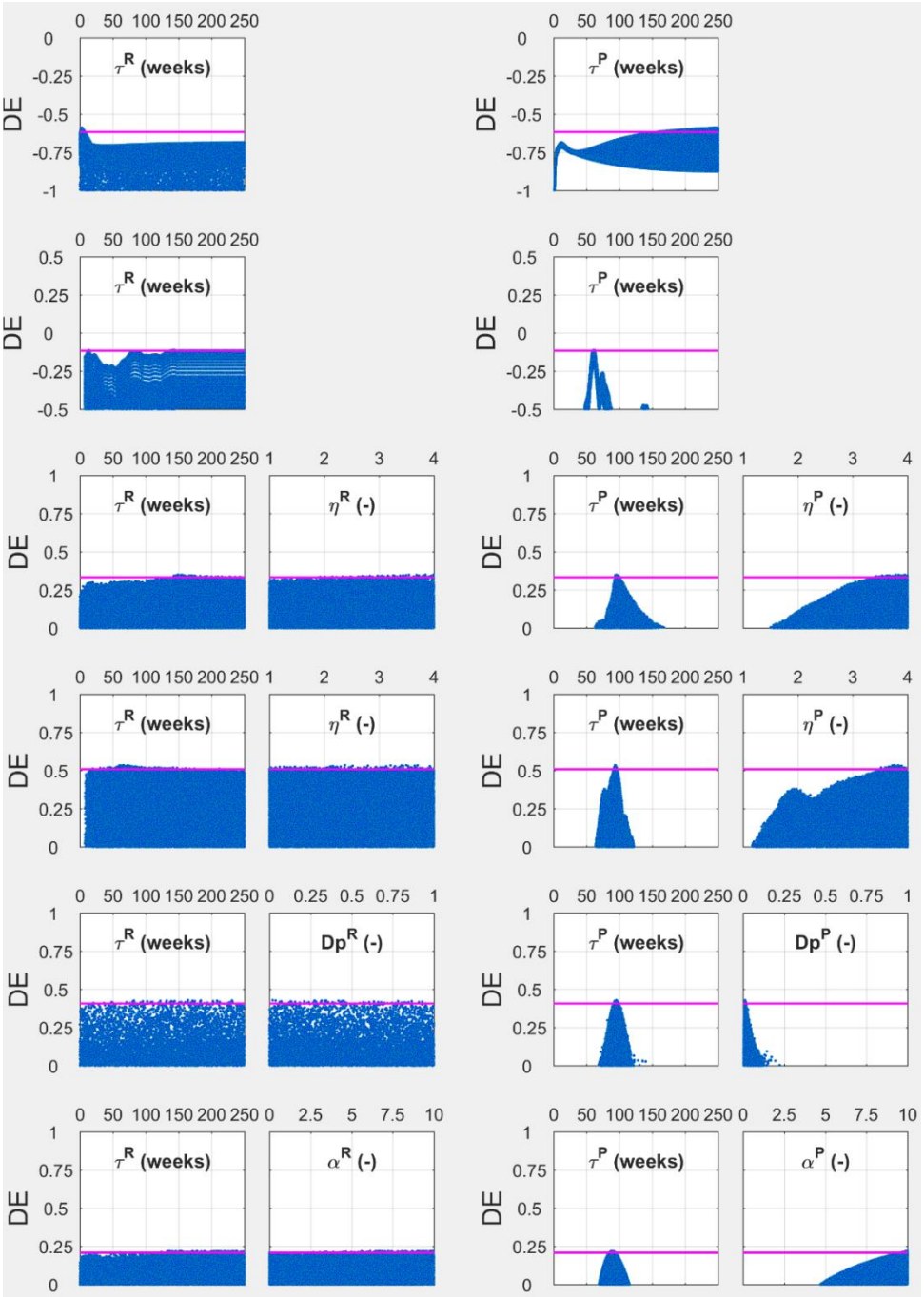

Figure B13: Dotty plots of likelihood measures against fitted parameters from 10^6 Monte Carlo simulations tested with six different TTDs for Well A. The results were corresponding to Test 2 with fixed p. Shown from top to bottom are the exponential, linear, exponential-piston flow, linear-piston flow, advection-dispersion, and gamma distributions. Magenta lines indicate the thresholds of 5% of the best predictions. τ_m is the tracer's mTT; η is a parameter indicating the ratio of total volume/volume with exponential (or linear) TTD; D_P is the dispersion parameter; α is the shape parameter. The superscripts R and P indicate infiltration from river water and precipitation, respectively.

Appendix C

Supplement to chapter 4

This is part of the publication:
Duy, N. L., Nguyen, T. V. K., Nguyen, D. V., Tran, A. T., Nguyen, H. T., Heidbüchel, I., Merz, B., Apel, H., 2021. Groundwater dynamics in the Vietnamese Mekong Delta: Trends, memory effects, and response times. Journal of Hydrology: Regional Studies, 33: 100746.
DOI: https://doi.org/10.1016/j.ejrh.2020.100746.

C.1 Information about 88 monitoring boreholes in the VMD

C.2 Results of memory effect, trend analysis, and response time of alluvial aquifers in the VMD

C.1 Information about 88 monitoring boreholes in the VMD

Table C.1 Information about 88 monitoring boreholes in the VMD

No	Borehole name	Aquifer	Province	Coodinate			Monitoring period		Depth (m)	
				Lat.	Lon.	Elev.	from	to	from	to
1	Q017050	Miocene	Hau Giang	9.93	105.72	1.73	1996	2017	393	468
2	Q021050	Miocene	Tra Vinh	9.81	106.19	1.82	1996	2014	430	476.5
3	Q022010	Holocene	Long An	10.66	106.17	2.50	1996	2017	5	14
4	Q02202T	Upper Pleistocene	Long An	10.66	106.17	2.48	1996	2017	31	55.2
5	Q02202ZM1	Middle Pleistocene	Long An	10.66	106.17	2.72	1996	2017	61.5	91.5
6	Q02204T	Lower Pleistocene	Long An	10.66	106.17	2.61	1996	2017	136.9	178
7	Q02204Z	Middle Pliocene	Long An	10.66	106.17	2.78	1996	2017	191	246
8	Q022050	Lower Pliocene	Long An	10.66	106.17	2.87	2003	2017	266	287.8
9	Q02702Z	Middle Pleistocene	Long An	10.89	105.78	3.60	1996	2010	32	63
10	Q027030	Lower Pleistocene	Long An	10.89	105.78	3.65	1996	2017	79	121
11	Q02704T	Middle Pliocene	Long An	10.89	105.78	3.71	1996	2017	153	195
12	Q02704Z	Lower Pliocene	Long An	10.89	105.78	3.66	1996	2017	207	266
13	Q027050M1	Miocene	Long An	10.89	105.78	3.71	1996	2017	275	320
14	Q031010	Holocene	Dong Thap	10.62	105.41	4.45	1996	2017	5	31
15	Q031020	Upper Pleistocene	Dong Thap	10.62	105.41	3.93	1996	2017	46	88.5
16	Q031030	Lower Pleistocene	Dong Thap	10.62	105.41	3.92	1996	2017	134	171.5
17	Q031040	Lower Pliocene	Dong Thap	10.62	105.41	4.01	1996	2017	243	285
18	Q07701A	Holocene	Tra Vinh	9.67	106.51	1.83	1996	2017	0	15
19	Q104020	Middle Pleistocene	Kien Giang	10.29	104.70	1.77	1996	2017	35	58
20	Q104030	Lower Pleistocene	Kien Giang	10.29	104.70	1.77	1996	2017	58	70
21	Q17701T	Holocene	Ca Mau	9.19	105.15	1.11	1996	2017	1.2	30.5
22	Q17704TM1	Middle Pliocene	Ca Mau	9.19	105.15	1.11	1996	2017	191	231
23	Q199010	Holocene	Ca Mau	8.76	105.00	1.12	1996	2017	0	40
24	Q199020	Middle Pleistocene	Ca Mau	8.76	105.00	1.12	1996	2013	115	145.9
25	Q19904T	Middle Pliocene	Ca Mau	8.76	105.00	1.12	1996	2013	224	240
26	Q19904ZM1	Lower Pliocene	Ca Mau	8.76	105.00	1.12	1996	2017	294.5	324.5
27	Q203010M1	Holocene	An Giang	10.74	105.17	5.06	1996	2017	3.5	38
28	Q20302ZM1	Upper Pleistocene	An Giang	10.74	105.17	5.06	1996	2017	45	75
29	Q203040M1	Middle Pleistocene	An Giang	10.74	105.17	5.07	1996	2017	77	102
30	Q204010	Holocene	An Giang	10.46	105.29	3.44	1996	2017	23.5	32.8
31	Q20402T	Upper Pleistocene	An Giang	10.46	105.29	3.40	1998	2017	42	49
32	Q20402Z	Middle Pleistocene	An Giang	10.46	105.29	3.44	1998	2017	76.2	130
33	Q204040	Lower Pleistocene	An Giang	10.46	105.29	3.47	1996	2017	162	182
34	Q206010M1	Holocene	Dong Thap	10.28	105.65	2.54	1996	2017	0	40
35	Q206020M1	Middle Pleistocene	Dong Thap	10.28	105.65	2.53	1996	2017	111	140

No	Borehole name	Aquifer	Province	Coodinate			Monitoring period		Depth (m)	
				Lat.	Lon.	Elev.	from	to	from	to
36	Q206030M1	Middle Pliocene	Dong Thap	10.28	105.65	2.47	1996	2017	192	271.5
37	Q209010	Holocene	Vinh Long	10.07	105.80	2.56	1996	2017	1	71
38	Q209020	Upper Pleistocene	Vinh Long	10.07	105.80	2.37	1996	2017	88.7	132.5
39	Q209030	Middle Pleistocene	Vinh Long	10.07	105.80	2.32	1996	2017	142	207
40	Q20904T	Lower Pliocene	Vinh Long	10.07	105.80	2.44	1996	2017	285	328.2
41	Q20904Z	Miocene	Vinh Long	10.07	105.80	2.19	1996	2009	355	400
42	Q211020	Middle Pleistocene	Hau Giang	9.68	105.57	1.75	1996	2017	52	96.7
43	Q211030	Lower Pleistocene	Hau Giang	9.68	105.57	1.76	1996	2017	96.7	193.5
44	Q21104T	Middle Pliocene	Hau Giang	9.68	105.57	1.77	1996	2017	198.5	238
45	Q21104ZM1	Lower Pliocene	Hau Giang	9.68	105.57	1.78	1996	2010	284	345
46	Q214010M1	Holocene	Vinh Long	10.11	106.07	1.63	1996	2010	0	36.2
47	Q21402TM1	Middle Pleistocene	Vinh Long	10.11	106.07	1.66	1996	2010	73	119.6
48	Q21402ZM1	Lower Pleistocene	Vinh Long	10.11	106.07	1.64	1998	2010	122.3	167
49	Q214030M1	Middle Pliocene	Vinh Long	10.11	106.07	1.65	1996	2010	215	281
50	Q214040M1	Lower Pliocene	Vinh Long	10.11	106.07	1.66	1996	2010	306	367
51	Q214050M1	Miocene	Vinh Long	10.11	106.07	1.67	1996	2010	393	470.5
52	Q217010	Holocene	Tra Vinh	9.63	106.49	1.85	1996	2017	0	26
53	Q217020	Middle Pleistocene	Tra Vinh	9.63	106.49	1.86	1996	2017	100	152
54	Q217030	Middle Pliocene	Tra Vinh	9.63	106.49	1.87	1996	2017	229.5	313
55	Q217040	Lower Pliocene	Tra Vinh	9.63	106.49	1.88	1996	2017	322	381
56	Q219010	Holocene	Ben Tre	10.05	106.60	1.68	1996	2017	0	22
57	Q219020M1	Upper Pleistocene	Ben Tre	10.05	106.60	1.69	1996	2017	41	98
58	Q219030	Lower Pleistocene	Ben Tre	10.05	106.60	1.70	1996	2017	148	219
59	Q219040	Lower Pliocene	Ben Tre	10.05	106.60	1.71	1996	2013	290	330
60	Q219050	Miocene	Ben Tre	10.05	106.60	1.72	1996	2017	407	500.2
61	Q326010	Holocene	Long An	10.49	106.53	1.40	1996	2017	24	49
62	Q326020M1	Middle Pleistocene	Long An	10.49	106.53	1.55	1996	2017	86	101
63	Q326030M1	Lower Pleistocene	Long An	10.49	106.53	1.55	1996	2017	130	159
64	Q32604TM1	Middle Pliocene	Long An	10.49	106.53	1.54	1996	2017	168	204
65	Q32604Z	Lower Pliocene	Long An	10.49	106.53	1.42	1996	2017	250	306
66	Q40101T	Holocene	Kien Giang	9.90	105.16	1.20	2000	2017	0	11
67	Q40102Z	Middle Pleistocene	Kien Giang	9.90	105.16	1.18	2000	2010	54	90
68	Q401030	Lower Pleistocene	Kien Giang	9.90	105.16	1.18	2000	2010	104	164
69	Q40104T	Middle Pliocene	Kien Giang	9.90	105.16	1.18	2000	2010	197	210
70	Q40104Z	Lower Pliocene	Kien Giang	9.90	105.16	1.18	2000	2010	218	282
71	Q402020M1	Upper Pleistocene	Can Tho	10.19	105.35	1.79	2000	2010	33	48
72	Q402040M1	Miocene	Can Tho	10.19	105.35	1.80	2000	2010	317	350
73	Q403020	Middle Pleistocene	Can Tho	10.17	105.41	1.81	2000	2010	53	138.5

No	Borehole name	Aquifer	Province	Coodinate			Monitoring period		Depth (m)	
				Lat.	Lon.	Elev.	from	to	from	to
74	Q404020	Upper Pleistocene	Tra Vinh	9.74	106.26	1.89	2000	2010	56	128
75	Q40403T	Middle Pleistocene	Tra Vinh	9.74	106.26	1.90	2000	2010	128	174
76	Q40403Z	Middle Pliocene	Tra Vinh	9.74	106.26	1.91	2000	2010	237	285
77	Q40404TM1	Lower Pliocene	Tra Vinh	9.74	106.26	1.92	2000	2010	306	377
78	Q405050M1	Lower Pliocene	Tra Vinh	9.63	106.30	1.94	2000	2010	372	492
79	Q406040	Middle Pliocene	Tra Vinh	9.77	106.44	1.95	2000	2010	244	294.9
80	Q408020	Upper Pleistocene	An Giang	10.35	105.47	2.49	2000	2017	29	42.5
81	Q597020M1	Upper Pleistocene	Bac Lieu	9.30	105.72	1.11	1996	2017	36	56
82	Q597030M1	Middle Pleistocene	Bac Lieu	9.30	105.72	1.11	1996	2017	71	138
83	Q59704TM1	Lower Pliocene	Bac Lieu	9.30	105.72	1.11	1996	2010	268	335
84	Q59704ZM1	Miocene	Bac Lieu	9.30	105.72	1.11	1996	2010	340	355
85	Q59801T	Holocene	Soc Trang	9.58	105.97	1.99	1996	2017	0	26
86	Q598020M1	Middle Pleistocene	Soc Trang	9.58	105.97	1.10	1996	2010	62	105
87	Q598030	Lower Pleistocene	Soc Trang	9.58	105.97	1.10	1996	2017	105	157.5
88	Q59804T	Middle Pliocene	Soc Trang	9.58	105.97	1.10	1996	2016	160.5	307.5

C.2 Results of memory effect, trend analysis, and response time of alluvial aquifers in the VMD

Table C.2 Results of memory effect, declining trend (reported by Sen's Slope)

No	Borehole name	Aquifer	Memorry effect		Sen's Slope
			$K_{0.2}$ (week)	Logarit	(m/year)
1	Q017050	Miocene	16.77	-0.25	-0.41
2	Q021050	Miocene	18.28	-0.41	-0.33
3	Q022010	Holocene	8.53	-0.18	-0.08
4	Q02202T	Upper Pleistocene	8.86	-0.18	-0.13
5	Q02202ZM1	Middle Pleistocene	11.98	-0.25	-0.14
6	Q02204T	Lower Pleistocene	9.01	-0.23	-0.15
7	Q02204Z	Middle Pliocene	14.77	-0.27	-0.41
8	Q022050	Lower Pliocene	13.69	-0.27	-0.51
9	Q02702Z	Middle Pleistocene	12.91	-0.26	-0.10
10	Q027030	Lower Pleistocene	10.03	-0.23	-0.13
11	Q02704T	Middle Pliocene	11.86	-0.26	-0.28
12	Q02704Z	Lower Pliocene	12.69	-0.27	-0.35
13	Q027050M1	Miocene	14.40	-0.33	-0.34
14	Q031010	Holocene	13.63	-0.27	-0.02
15	Q031020	Upper Pleistocene	12.78	-0.28	-0.09
16	Q031030	Lower Pleistocene	12.71	-0.27	-0.05
17	Q031040	Lower Pliocene	10.12	-0.22	-0.36
18	Q07701A	Holocene	16.27	-0.31	-0.02
19	Q104020	Middle Pleistocene	13.18	-0.26	-0.12
20	Q104030	Lower Pleistocene	11.69	-0.24	-0.09
21	Q17701T	Holocene	15.76	-0.29	-0.01
22	Q17704TM1	Middle Pliocene	17.31	-0.36	-0.48
23	Q199010	Holocene	10.35	-0.20	-0.01
24	Q199020	Middle Pleistocene	17.63	-0.35	-0.39
25	Q19904T	Middle Pliocene	12.54	-0.23	-0.48
26	Q19904ZM1	Lower Pliocene	18.45	-0.33	-0.34
27	Q203010M1	Holocene	11.65	-0.24	-0.06
28	Q20302ZM1	Upper Pleistocene	12.83	-0.28	-0.04
29	Q203040M1	Middle Pleistocene	12.90	-0.26	-0.07
30	Q204010	Holocene	12.02	-0.27	-0.06
31	Q20402T	Upper Pleistocene	10.77	-0.22	-0.04
32	Q20402Z	Middle Pleistocene	11.47	-0.23	-0.07
33	Q204040	Lower Pleistocene	12.04	-0.24	-0.06
34	Q206010M1	Holocene	11.06	-0.25	-0.01
35	Q206020M1	Middle Pleistocene	15.17	-0.32	-0.13
36	Q206030M1	Middle Pliocene	24.50	-0.40	-0.53
37	Q209010	Holocene	13.52	-0.27	-0.01

No	Borehole name	Aquifer	Memorry effect		Sen's Slope
			$K_{0.2}$ (week)	Logarit	(m/year)
38	Q209020	Upper Pleistocene	10.14	-0.17	-0.23
39	Q209030	Middle Pleistocene	17.80	-0.32	-0.27
40	Q20904T	Lower Pliocene	24.69	-0.36	-0.46
41	Q20904Z	Miocene	24.71	-0.39	-0.31
42	Q211020	Middle Pleistocene	25.23	-0.42	-0.32
43	Q211030	Lower Pleistocene	22.21	-0.40	-0.33
44	Q21104T	Middle Pliocene	19.51	-0.33	-0.35
45	Q21104ZM1	Lower Pliocene	19.89	-0.33	-0.33
46	Q214010M1	Holocene	10.96	-0.21	-0.05
47	Q21402TM1	Middle Pleistocene	17.94	-0.32	-0.21
48	Q21402ZM1	Lower Pleistocene	17.54	-0.31	-0.23
49	Q214030M1	Middle Pliocene	26.24	-0.46	-0.30
50	Q214040M1	Lower Pliocene	25.73	-0.43	-0.37
51	Q214050M1	Miocene	32.22	-0.50	-0.38
52	Q217010	Holocene	11.67	-0.23	-0.03
53	Q217020	Middle Pleistocene	11.86	-0.21	-0.30
54	Q217030	Middle Pliocene	11.74	-0.22	-0.29
55	Q217040	Lower Pliocene	12.26	-0.23	-0.29
56	Q219010	Holocene	10.32	-0.22	-0.01
57	Q219020M1	Upper Pleistocene	16.08	-0.32	-0.23
58	Q219030	Lower Pleistocene	18.05	-0.37	-0.24
59	Q219040	Lower Pliocene	17.19	-0.33	-0.25
60	Q219050	Miocene	19.10	-0.39	-0.30
61	Q326010	Holocene	8.40	-0.18	-0.01
62	Q326020M1	Middle Pleistocene	18.08	-0.35	-0.32
63	Q326030M1	Lower Pleistocene	15.42	-0.31	-0.41
64	Q32604TM1	Middle Pliocene	17.20	-0.34	-0.46
65	Q32604Z	Lower Pliocene	20.97	-0.39	-0.54
66	Q40101T	Holocene	9.36	-0.19	0.00
67	Q40102Z	Middle Pleistocene	15.28	-0.29	-0.34
68	Q401030	Lower Pleistocene	15.57	-0.30	-0.34
69	Q40104T	Middle Pliocene	18.12	-0.32	-0.32
70	Q40104Z	Lower Pliocene	14.18	-0.32	-0.31
71	Q402020M1	Upper Pleistocene	10.52	-0.21	-0.26
72	Q402040M1	Miocene	12.50	-0.27	-0.33
73	Q403020	Middle Pleistocene	10.94	-0.20	-0.28
74	Q404020	Upper Pleistocene	15.98	-0.31	-0.36
75	Q40403T	Middle Pleistocene	17.24	-0.34	-0.36
76	Q40403Z	Middle Pliocene	17.89	-0.35	-0.40
77	Q40404TM1	Lower Pliocene	13.94	-0.28	-0.27
78	Q405050M1	Lower Pliocene	23.04	-0.39	-0.30

No	Borehole name	Aquifer	Memorry effect		Sen's Slope
			$K_{0.2}$ (week)	Logarit	(m/year)
79	Q406040	Middle Pliocene	13.98	-0.30	-0.42
80	Q408020	Upper Pleistocene	12.69	-0.23	-0.10
81	Q597020M1	Upper Pleistocene	13.96	-0.30	-0.29
82	Q597030M1	Middle Pleistocene	13.13	-0.27	-0.30
83	Q59704TM1	Lower Pliocene	18.01	-0.41	-0.43
84	Q59704ZM1	Miocene	23.88	-0.47	-0.30
85	Q59801T	Holocene	13.02	-0.24	-0.04
86	Q598020M1	Middle Pleistocene	16.32	-0.38	-0.29
87	Q598030	Lower Pleistocene	13.51	-0.29	-0.24
88	Q59804T	Middle Pliocene	15.05	-0.27	-0.29

Table C.3 Results of response time of alluvial aquifers in the VMD

No	Borehole name	Monthly response time (week)											
		Jan	Feb	Mar	Apr	May	Jun	Jul	Aug	Sep	Oct	Nov	Dec
1	Q017050	15.78	17.80	21.11	23.30	23.51	23.54	23.54	23.12	20.83	17.61	14.28	13.69
2	Q021050	6.35	5.12	4.43	5.58	7.11	7.15	6.65	6.35	5.91	5.87	6.00	6.33
3	Q022010	6.98	5.98	6.00	7.22	8.17	7.96	7.37	7.00	6.63	6.39	6.63	6.93
4	Q02202T	8.50	7.65	7.57	8.78	9.72	9.61	9.26	8.80	8.09	8.04	8.09	8.53
5	Q02202ZM1	9.07	8.05	8.11	9.07	10.38	10.20	9.35	9.07	8.65	8.57	8.76	8.98
6	Q02204T	10.04	10.33	13.13	13.84	14.21	12.65	11.11	10.04	8.54	8.72	8.80	9.60
7	Q02204Z	10.84	12.10	14.90	16.69	16.42	16.00	13.40	10.83	9.00	8.97	9.03	9.90
8	Q022050	5.97	4.90	4.70	5.63	7.19	6.71	6.39	6.07	5.77	5.70	6.09	6.26
9	Q02702Z	7.54	6.51	6.57	7.09	8.26	8.09	7.72	7.67	7.20	7.17	7.39	7.58
10	Q027030	8.93	7.85	7.84	8.41	9.40	9.09	8.73	8.45	7.82	7.68	8.20	8.55
11	Q02704T	9.50	8.72	9.74	10.71	10.87	10.11	9.41	9.11	8.52	8.50	8.61	9.09
12	Q02704Z	10.41	9.81	10.53	11.84	12.64	11.63	10.96	10.63	9.59	9.65	9.96	10.18
13	Q027050M1	2.04	2.00	2.00	2.02	2.15	2.09	2.05	2.02	2.00	2.02	2.07	2.12
14	Q031010	3.52	3.07	3.04	3.33	3.91	3.87	3.50	3.30	3.22	3.20	3.41	3.98
15	Q031020	5.65	5.07	5.04	5.31	5.98	6.07	5.52	5.37	5.24	5.24	5.52	5.89
16	Q031030	8.37	8.07	8.79	9.80	10.19	9.02	8.50	7.43	7.24	7.28	7.59	8.18
17	Q031040	3.02	2.51	2.43	2.69	3.23	3.40	3.20	3.00	2.70	2.77	3.36	3.36
18	Q07701A	8.54	7.19	7.11	8.73	9.45	9.04	8.28	7.80	7.30	7.63	7.96	8.31
19	Q104020	9.74	8.30	8.17	10.13	10.55	10.09	9.78	9.20	8.67	9.04	9.24	9.76
20	Q104030	2.60	2.54	2.51	2.49	2.55	2.63	2.67	2.62	2.62	2.83	2.76	2.53
21	Q17701T	11.93	12.54	14.11	15.59	15.79	14.84	13.55	12.68	10.80	9.86	10.30	10.95
22	Q17704TM1	3.65	3.09	2.81	3.13	3.66	3.67	3.28	3.13	3.07	3.63	3.83	3.89
23	Q199010	7.87	7.66	8.63	10.67	10.53	9.71	9.16	7.17	6.57	6.87	6.41	7.10
24	Q199020	11.13	12.32	16.06	17.78	18.26	17.85	16.27	12.41	11.28	10.55	11.18	10.97
25	Q19904T	14.89	16.98	20.06	21.80	21.66	21.11	21.30	21.07	18.39	14.74	13.98	13.71
26	Q19904ZM1	4.24	3.65	3.23	3.71	4.64	4.54	4.02	3.76	3.76	4.02	4.22	4.47
27	Q203010M1	3.98	3.23	3.26	3.71	4.26	4.22	3.70	3.43	3.46	3.46	3.78	4.13
28	Q20302ZM1	4.89	4.19	4.11	4.60	5.28	5.30	4.80	4.41	4.35	4.50	4.80	5.24
29	Q203040M1	4.24	2.95	2.72	3.33	4.64	4.67	4.24	3.87	3.61	3.50	3.83	4.31
30	Q204010	5.07	4.00	4.05	4.49	5.74	5.86	5.19	4.79	4.64	4.67	5.00	5.37
31	Q20402T	6.09	5.05	4.68	5.49	6.64	6.67	6.12	5.72	5.38	5.40	5.80	6.42
32	Q20402Z	7.28	6.09	6.17	6.69	7.72	7.63	7.39	7.13	6.80	6.52	6.98	7.47
33	Q204040	2.30	2.09	2.13	2.13	2.34	2.33	2.13	2.11	2.04	2.30	2.57	2.69
34	Q206010M1	8.78	8.02	8.70	9.18	9.51	9.24	8.85	8.09	7.37	7.22	7.89	8.60
35	Q206020M1	10.09	11.72	15.15	17.38	18.64	17.61	17.13	14.46	12.17	11.76	11.54	9.24
36	Q206030M1	4.70	3.67	2.83	3.04	4.62	4.91	4.17	3.78	3.63	4.22	4.87	5.07
37	Q209010	7.37	7.33	8.55	10.22	10.51	9.57	8.17	7.02	6.59	6.15	6.24	6.71
38	Q209020	7.80	8.91	10.62	11.76	11.60	11.28	10.00	9.48	7.15	6.91	6.85	7.60
39	Q209030	11.30	14.44	18.28	20.53	20.94	20.09	20.43	19.48	17.50	17.04	14.20	10.89
40	Q20904T	12.85	14.88	17.50	19.15	19.31	17.81	17.59	16.69	13.23	11.77	11.65	13.07

No	Borehole name	Monthly response time (week)											
		Jan	Feb	Mar	Apr	May	Jun	Jul	Aug	Sep	Oct	Nov	Dec
41	Q20904Z	7.13	7.59	9.47	11.23	11.44	9.71	8.48	7.73	7.13	7.07	6.91	6.35
42	Q211020	9.03	9.93	12.10	13.97	14.28	12.94	11.74	10.57	10.30	9.47	7.78	7.48
43	Q211030	10.53	12.10	15.63	18.67	18.88	16.94	15.77	13.23	10.57	10.00	9.41	10.10
44	Q21104T	12.43	13.21	16.53	18.63	17.84	16.19	16.52	16.87	16.80	16.77	13.50	12.65
45	Q21104ZM1	3.20	2.83	2.63	2.93	3.16	3.42	3.00	2.80	2.53	2.73	3.13	3.58
46	Q214010M1	10.13	11.66	14.17	15.93	16.53	14.81	14.39	12.80	12.50	11.03	10.22	9.87
47	Q21402TM1	10.79	12.00	14.38	16.88	18.33	18.43	17.36	12.45	9.48	8.71	9.96	10.64
48	Q21402ZM1	11.90	13.97	16.03	19.00	19.97	18.48	17.19	13.20	10.73	9.43	10.19	10.26
49	Q214030M1	11.93	14.90	18.00	21.00	21.31	19.97	19.68	18.03	13.93	12.90	12.38	11.81
50	Q214040M1	13.40	16.41	19.30	21.43	21.47	20.19	20.87	21.00	19.27	17.47	14.28	12.68
51	Q214050M1	2.20	2.16	2.15	2.21	2.23	2.22	2.13	2.13	2.11	2.13	2.26	2.21
52	Q217010	9.74	8.70	8.36	8.18	9.15	9.65	8.67	7.54	7.35	8.46	9.07	9.67
53	Q217020	11.70	10.81	10.96	11.04	11.98	11.96	10.96	9.63	9.52	10.59	11.24	11.60
54	Q217030	12.98	12.16	11.53	11.91	12.64	12.85	11.98	10.65	10.54	11.41	11.96	12.56
55	Q217040	2.41	2.16	2.11	2.20	2.47	2.54	2.50	2.33	2.26	2.43	2.50	2.56
56	Q219010	11.17	12.60	14.66	16.33	16.00	15.87	14.72	13.13	10.63	9.41	9.57	10.38
57	Q219020M1	14.22	15.81	17.34	17.98	17.96	17.33	16.50	15.80	14.85	13.20	13.07	13.11
58	Q219030	13.08	13.69	16.16	17.43	17.90	15.89	13.76	11.67	10.86	10.55	11.05	11.86
59	Q219040	17.57	18.80	21.07	22.00	22.04	21.68	20.60	20.10	18.67	17.70	16.45	16.71
60	Q219050	2.54	2.51	2.45	2.40	2.64	2.76	2.48	2.13	2.11	2.41	3.04	2.82
61	Q326010	11.17	12.19	13.98	14.80	15.13	14.61	13.35	11.22	9.02	9.09	10.72	10.51
62	Q326020M1	12.30	13.28	15.40	16.27	16.66	15.78	13.48	11.22	10.50	10.74	10.85	11.40
63	Q326030M1	12.11	13.58	16.15	17.64	18.11	17.57	15.13	11.98	10.09	10.59	11.43	11.44
64	Q32604TM1	12.54	14.02	15.94	18.18	18.49	17.65	15.07	13.52	12.87	11.98	12.61	11.67
65	Q32604Z	2.73	2.71	2.72	2.73	2.82	2.84	2.89	2.89	2.91	3.05	3.08	2.82
66	Q40101T	7.33	7.10	7.82	8.91	9.32	7.74	6.32	4.95	4.29	4.43	5.38	7.04
67	Q40102Z	8.43	8.40	9.14	10.23	10.41	8.83	7.18	6.05	5.33	5.61	6.43	8.04
68	Q401030	11.57	12.50	15.14	17.32	18.68	17.43	14.00	9.59	8.24	8.09	8.86	10.39
69	Q40104T	10.57	12.90	17.91	21.68	21.77	21.71	21.79	21.60	20.43	20.65	19.86	12.87
70	Q40104Z	4.57	3.65	3.82	5.23	5.82	5.09	4.27	3.73	3.67	3.65	3.86	4.65
71	Q402020M1	9.29	8.90	8.64	10.82	10.86	9.70	9.27	8.95	9.00	9.13	9.14	9.52
72	Q402040M1	5.38	4.55	5.41	6.82	6.59	5.87	5.09	4.64	4.48	4.57	4.67	5.39
73	Q403020	8.43	9.05	9.36	9.95	10.91	11.00	8.18	5.82	5.05	5.57	6.71	7.83
74	Q404020	9.38	10.15	10.18	11.00	11.91	11.52	9.36	7.00	6.24	6.70	7.86	8.96
75	Q40403T	11.33	12.25	13.00	14.18	14.68	15.04	14.36	10.18	9.52	9.70	9.90	10.30
76	Q40403Z	15.14	15.70	16.41	16.77	17.55	17.26	17.09	15.18	11.95	12.52	12.81	14.26
77	Q40404TM1	14.38	14.35	15.68	16.59	17.00	16.35	16.41	14.55	13.14	13.17	13.86	14.39
78	Q405050M1	9.14	8.65	8.50	8.91	10.14	10.52	10.11	8.25	8.05	8.77	10.10	9.96
79	Q406040	4.32	3.21	3.08	3.54	4.92	4.95	4.42	3.78	3.57	3.45	4.27	4.85
80	Q408020	6.91	6.02	5.36	5.84	6.66	6.35	5.46	4.46	3.91	4.50	5.67	6.38
81	Q597020M1	6.91	6.02	5.36	5.84	6.66	6.35	5.46	4.46	3.91	4.5	5.67	6.38

No	Borehole name	Monthly response time (week)											
		Jan	Feb	Mar	Apr	May	Jun	Jul	Aug	Sep	Oct	Nov	Dec
82	Q597030M1	7.17	6.28	5.77	5.98	6.77	6.67	5.93	5.04	4.43	5.26	6.37	6.87
83	Q59704TM1	10.33	10.03	9.5	10.47	11.78	10.87	9.84	9.03	8.57	8.97	10.41	10.68
84	Q59704ZM1	15.73	16.34	17.33	18.8	18.69	17.97	16.32	14.67	13.83	13.9	14.34	15.13
85	Q59801T	3.34	2.71	2.29	2.35	2.98	3.07	2.89	2.7	2.59	3.16	3.64	3.79
86	Q598020M1	8.9	9.86	11.27	12.37	12.72	11.26	8.71	7.47	5.73	5.93	7.09	8.16
87	Q598030	10.33	11.05	12.02	12.8	13.15	11.93	10.43	9	8.18	8.07	9.04	9.67
88	Q59804T	11.84	12.95	14.4	15.09	15.78	15.41	13	10.98	9.45	9.86	11.38	11.51